THE
PHYSICAL REVIEW

A journal of experimental and theoretical physics established by E. L. Nichols in 1893

SECOND SERIES, VOL. 73, NO. 6 MARCH 15, 1948

Yields of Neutrons from Photo-Neutron Sources*

B. RUSSELL, D. SACHS, A. WATTENBERG, AND R. FIELDS
Agonne National Laboratory, Chicago, Illinois

(Received December 15, 1947)

The number of neutrons emitted per second per curie from ten photo-neutron sources was determined, and they are listed in Table I. Absolute values of yields and cross sections may be in error by 27 percent, but relative values are more reliable. The photo-disintegration cross section for deuterium, $\sigma_D(\gamma,n)$, is found to be 16×10^{-28} cm² at 2.76 Mev. $\sigma_{Be}(\gamma,n)$ is found to be 7×10^{-28} cm² at 2.76 Mev, and is greater than 9.7×10^{-28} cm² at 1.67 Mev. The more reliable ratios of $\sigma_{Be}(\gamma,n)/\sigma_D(\gamma,n)$ are found to be 0.43 at 2.76 Mev and 0.30 at 2.50 Mev.

The curve of $\sigma_{Be}(\gamma,n)$ *versus* energy must pass through at least one maximum and one minimum in the range 1.63 Mev to 2.76 Mev.

The number of 2.7-Mev photons per disintegration of Mn^{56} is estimated to be about 1 percent. These photons are probably due to direct transitions to the ground state from the known excited levels of Fe^{56}.

1. INTRODUCTION

IN order to facilitate the planning of experiments employing photo-neutron sources, measurements were undertaken to determine the yield of neutrons from some of the sources employed at the Argonne National Laboratory.[1,2] As no further work is being done along these lines at the present time, it was considered desirable to make these data available to others despite the fact that more refined measurements should be made.

The number of neutrons produced per curie of radio-isotope was observed to vary by large factors in the photo-disintegration of beryllium and deuterium.[1] One cause of this variation is that the cross section for the (γ,n) reaction depends upon the energy of the photons. A detailed discussion of the theoretical dependence of the deuterium cross section, $\sigma_D(\gamma,n)$, is given by Bethe and Bacher.[3] A more recent calculation at one energy is given by Rarita and Schwinger.[4] However, previous experimental determinations[5–7] have yielded values lower than that calculated by Rarita and Schwinger.[4]

The only theoretical prediction that has been made of the dependence of $\sigma_{Be}(\gamma,n)$ on the energy of the photons is that of Mamasachlisow.[8] Determinations of $\sigma_{Be}(\gamma,n)$ using the γ-rays from the radium chain and from ThC″ are summarized by Houtermans and Bartz.[9]

* This document is based on work performed under Contract Number W-31-109-eng-38 for the Atomic Energy Project at the Argonne National Laboratory.

[1] Wattenberg, Fields, Russell, and Sachs, Phys. Rev. 71, 497, 508 (1947).

[2] D. J. Hughes and C. Eggler, Phys. Rev. 72, 902 (1947).

[3] H. Bethe and R. Bacher, Rev. Mod. Phys. 8, 125 (1936).

[4] W. Rarita and J. Schwinger, Phys. Rev. 59, 436 (1941).

[5] H. Halban, Comptes rendus 206, 1170 (1938).

[6] G. A. R. Graham and H. Halban, Rev. Mod. Phys. 17, 297 (1945).

[7] Chadwick and Goldhaber, Proc. Roy. Soc. A151, 479 (1935).

[8] V. I. Mamasachlisow, Physik. Zeits. Sowjetunion 10, 214 (1936).

[9] F. G. Houtermans and I. Bartz, Physik. Zeits. 44, 167 (1943).

A second cause for the variation of the number of neutrons emitted per second per curie of radio-isotope is that the majority of radio-isotopes employed have complex decay schemes. Na^{24} was the only radio isotope used that seemed to have a reliably established simple disintegration scheme.[10,11] According to this scheme one 2.76-Mev photon is emitted per disintegration. Therefore the yields of neutrons from sources employing Na^{24} are the only ones that can be readily converted into cross sections for photo-disintegration.

2. YIELDS

Experiment

The sources employed in these measurements were of the same shape and size as those previously described[1,2] and are shown in Fig. 1. The photon emitting radio-isotopes were activated in the Heavy Water Pile of the Argonne National Laboratory.

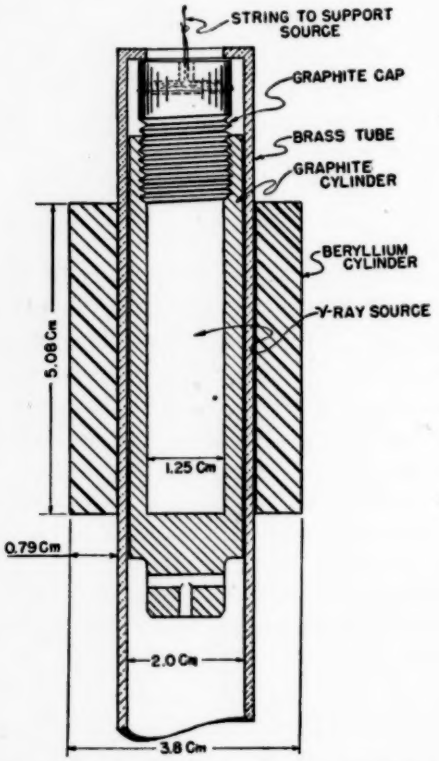

FIG. 1. Photo-neutron sources used in determining yields. For sources employing deuterium, an identically shaped thin-walled brass cylinder of heavy water was substituted for the beryllium.

To determine the absolute number of neutrons emitted by these sources, a comparison was made with a Ra-(α,n)-Be source whose neutron yield had been determined.[12] The comparison was made with the aid of a "long counter" (i.e., a BF_3 counter embedded in a large cylinder of paraffin). The "long counter" was constructed in the same manner as the one studied by A. O. Hanson and designated as type No. 3.[13] Hanson's work indicated that such a "long counter" had a neutron detecting efficiency that was approximately independent of the energy of the neutrons above 0.1 Mev.

The number of neutrons emitted by the photo sources was compared with that from the Ra-(α,n)-Be source with the sources at a distance of one meter from the face of the "long counter." The apparatus was six feet above the floor in a large room; the room scattering and counter background were determined. Measurements were made in cycles at counting rates between 200 and 1000 counts per minute. A total of at least 10,000 counts was taken in each measurement.

In order to determine the number of curies of radio-isotope, the activity of the γ-ray sources was calculated from the isotopic neutron activation cross sections given in column 3 of Table I and measurements of the neutron flux in which the photon sources were irradiated. The neutron flux was measured by means of small gold foils.[14]

3. RESULTS

The results obtained with the sources shown in Fig. 1 are listed in the fifth column of Table I. Corrections have been applied to take account of the following: (a) the time of irradiation and the decay of the sources; (b) the self-shielding of the sources during their activation in the Pile; (c) the room scattering and background present during the "long counter" measurements; (d) the distribution of the neutrons from the sources not being spherically symmetrical because of shape and finite thickness of the sources (this correction was determined experimentally); (e) the known

[10] L. G. Elliott, M. Deutsch, and A. Roberts, Phys. Rev. 63, 386 (1943).
[11] K. Siegbahn, Phys. Rev. 70, 127 (1946).
[12] F. Seidl and S. Harris, Rev. Sci. Inst. (in press).
[13] A. O. Hanson, Los Alamos Declassified Report No. 59.
[14] A. Wattenberg and D. Sachs, to be published in the Plutonium Project Record.

TABLE I. Yields of neutrons from photo-neutron sources.

Sources	½ life	Neutron activation cross section* (in barns)	γ-rays energies[1,2] (in Mev)	Number of neutrons second—curie sources shown in Fig. 1	Number of neutrons second—curie "standard sources"**
$Na^{24}+D_2O$	14.8 hrs.	0.41	2.76	2.7×10^6	29.0×10^4
$Na^{24}+Be$	14.8 hrs.	0.41	2.76	2.4×10^6	14.0×10^4
$Mn^{56}+D_2O$	2.6 hrs.	10.7	2.7 ± 0.2	0.029×10^6	0.31×10^4
$Mn^{56}+Be$	2.6 hrs.	10.7	1.81, 2.13, 2.7	0.50×10^6	2.9×10^4
$Ga^{72}+D_2O$	14 hrs.	1.3	2.50	0.64×10^6	6.9×10^4
$Ga^{72}+Be$	14 hrs.	1.3	2.50 and ?	1.04×10^6	5.9×10^4
$In^{116}+Be$	54 min.	150.0	1.8, 2.1	0.14×10^6	0.82×10^4
$Sb^{124}+Be$	60 days	1.1	1.67	3.2×10^6	19.0×10^4
$La^{140}+D_2O$	40 hrs.	7.0	2.50	0.062×10^6	0.68×10^4
$La^{140}+Be$	40 hrs.	7.0	2.50	0.041×10^6	0.23×10^4

* These are activation cross sections for the periods indicated in column 2 for the energy distribution of neutrons that exists in a Pile. The cross sections for Mn, Ga, In, and Sb are from L. Seren, Phys. Rev. **72**, 881 (1947); the cross sections for Na and La are from A. Wattenberg and G. Thomas, to be published in the Plutonium Project Record. The method employed is that described by Anderson, Fermi, Wattenberg, Weil, and Zinn, Phys. Rev. **72**, 16 (1947).
** See section on Results for description of "standard source."

variation of the efficiency of the "long counter" below 0.1 Mev.[13]

In order to calculate cross sections and to make the data more useful to others who will undoubtedly use sources of a different size and shape, the number of neutrons per second per curie has been calculated for a "standard source" (that is, a source of one curie of activity placed at a distance of one centimeter from one gram of target material). The values obtained for the "standard sources" are listed in column 6 of Table I. In order to perform this calculation, it was necessary to determine the average path length of a γ-ray through the target material. The average path length was first estimated graphically and later checked by a numerical integration by A. V. Martin of the Theoretical Division of the Argonne Laboratory. The average path length was 0.74 cm.**

4. UNCERTAINTIES

The largest uncertainties in these measurements are those concerned with the determination of the strength of the photon sources employed. The relative "pile neutron" flux measurements are good to about 2 percent, but the absolute values of the flux may be in error by 15 percent. The activation cross sections are considered to be reliable to 20 percent. The next largest error is probably that of the number of neutrons emitted by the Ra(α,n)Be source with which the other sources were compared. Seidl and Harris[12] estimate a 7 percent probable error for this value. The known variation of the efficiency of the long counter is probably reliable to 5 percent. The errors in the comparison of the sources are estimated to be less than 5 percent.

These known uncertainties, if they are subject to the theory of errors, would give an uncertainty of about 27 percent in the absolute values. The relative values are not subject to the uncertainties in the absolute flux measurement and in the Ra(α,n)Be source calibration. The relative values are therefore considered to be more reliable. Ratios of the photo-disintegration cross sections for beryllium and deuterium for the same γ-ray source will suffer only from errors in the intercomparison of the sources and the uncertainty in the efficiency of the "long counter." Therefore, ratios of σ_{Be}/σ_D given in Section 6 are good to about 7 percent.

5. THE PHOTO-DISINTEGRATION CROSS SECTION OF DEUTERIUM

In the case of Na^{24}, since one photon of 2.76 Mev is emitted per disintegration,[10,11] each curie of radio-isotope emits 3.7×10^{10} of the desired γ-rays per second, and the data of column 6 can be used directly to calculate $\sigma_D(\gamma,n)$. The value so obtained is 16.4×10^{-28} cm² for 2.76-Mev γ-rays.

Rarita and Schwinger[4] have calculated that $\sigma_D=15.3\times10^{-28}$ cm² for 2.62-Mev γ-rays, and

** This average path length for the γ-rays includes those γ-rays that escape from the end of the source without ever passing through any target material.

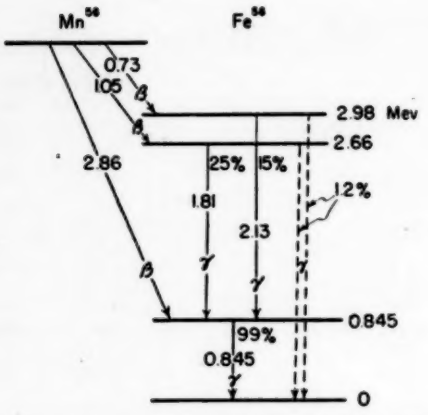

FIG. 2. The disintegration scheme of Mn^{56}. The solid lines and associated data are from Elliott and Deutsch (reference 20). The broken lines indicate the transition (or transitions) which give rise to the 2.7-Mev γ-ray.

Halban[5] observed 10×10^{-28} cm^2 for 2.62-Mev γ-rays.

S. Moskowski has used the curves and formulae of Rarita and Schwinger to calculate $\sigma_D(\gamma,n)$ at several other energies. Moskowski's value at 2.76 Mev is $\sigma_D=18.7\times10^{-28}$ cm^2. The value obtained in this experiment of 16.4×10^{-28} cm^2 seems to be in slightly better agreement with the theory than the previously obtained values. Unfortunately the large uncertainty of 27 percent raises the possibility of this agreement being merely fortuitous.

6. THE PHOTO-DISINTEGRATION CROSS SECTION OF Be

$\sigma_{Be}(\gamma,n)$ can be calculated in the same manner as $\sigma_D(\gamma,n)$, using the data of column 6, and the value so obtained is $\sigma_{Be}=7\times10^{-28}$ cm^2 at 2.76 Mev. From the discussion of the uncertainties, the ratio of $\sigma_{Be}(\gamma,n)/\sigma_D(\gamma,n)$ is a more reliable quantity than the individual cross sections. This ratio is 0.43 for 2.76-Mev γ-rays from the Na^{24} data, and is 0.30 at 2.50 Mev from the La^{140} data.

From Moskowski's calculations σ_D at 2.50 Mev is estimated to be $0.67\times\sigma_D$ at 2.76 Mev. Using this factor and the ratios for σ_{Be}/σ_D at 2.50 and at 2.76 Mev we obtained σ_{Be} at 2.50 Mev $=0.47\times\sigma_{Be}$ at 2.76 Mev. The slope of the curve of σ_{Be} *versus* photon energy is seen to be steeper in this energy region than the curve for σ_D.

It will be noticed in column six that the Sb+Be source has a larger yield than any other source using Be. This was unexpected as the γ-rays from Sb^{124} are only 0.04 Mev above the threshold for the (γ,n) reaction in Be. There was some question as to whether Sb^{124} might not emit in each disintegration two γ-rays whose energies are so close that they have not been resolved.[15] However, the most recent studies on γ—γ coincidences[16] indicate that there is only one photon emitted that is sufficiently energetic to disintegrate beryllium, and this photon is emitted in approximately half of the disintegrations. If one uses the data of column six and just assumes that less than one 1.67-Mev photon is emitted per disintegration, one gets a lower limit for σ_{Be} of 9.7×10^{-28} cm^2 at 1.67 Mev.

σ_{Be} is thus greater at 1.67 Mev than at 2.76 Mev, and its value at 2.50 Mev is lower than both of these values. Therefore the curve of σ_{Be} *versus* energy must pass through at least one maximum and one minimum between 1.63 Mev and 2.76 Mev.

These results are not in agreement with the theoretical conclusions of Mamasachlisow.[8] Snell and co-workers,[17] at Oak Ridge, independently and concurrently with the work reported here, measured yields of photo-neutrons from sodium, antimony, and lanthanum sources. They employed differently shaped sources and entirely different techniques. The above conclusions concerning the energy variation of $\sigma_{Be}(\gamma,n)$ are consistant with Snell's results.

7. THE 2.7-MEV γ-RAYS FROM Mn^{56}

The decay scheme for Mn^{56} has been studied by Elliott and Deutsch[18] and K. Siegbahn[19]; their result are essentially in agreement, and the decay scheme as given by Elliott and Deutsch is shown in Fig. 2. The solid lines indicate the transitions which were observed. The 2.66-Mev and 2.98-Mev levels were both observed to decay by the emission of two quanta in cascade. The 2.7 ± 0.2-Mev photons found in previous photo-neutron work[1] fit into this decay scheme as

[15] W. E. Meyerhoff and G. Scharff-Goldhaber, Phys. Rev. **72**, 164A (1947).
[16] W. E. Meyerhoff and G. Scharff-Goldhaber, Phys. Rev. **72**, 273 (1947).
[17] Snell *et al.*, to be published in the Plutonium Project Record.
[18] L. G. Elliott and M. Deutsch, Phys. Rev. **64**, 321 (1943).
[19] K. Siegbahn, Arkiv F. Mat. Astro. o Fys. **33A**, No. 10 (1946).

direct transitions to the ground state of Fe^{56} of the 2.66-Mev and/or the 2.98-Mev levels. (The uncertainty of ± 0.2 Mev does not permit a decision as to whether solely the 2.66-Mev level or the 2.98-Mev level or some combination of the two is involved.) These direct transitions are indicated by the dotted line in Fig. 2. By taking the ratio of the data in column 6 for $Na+D_2O$ and $Mn+D_2O$ one gets (neglecting a small energy correction) an estimate of the frequency of occurrence of the direct transitions to the ground state. The number of such transitions is 0.011 per disintegration. Compared to the probabilities for the transition to the 0.845 level, the low probability of 0.011 would indicate that the transition to the ground state is of a higher electric or magnetic multipolarity than the transitions to the 0.84-Mev level.

It is the experience of the authors that the photo-neutron techniques can be extended to measurements of γ-rays that are emitted with a probability as low as 0.0001 per disintegration.

ACKNOWLEDGMENT

The authors wish to express their appreciation to E. Fermi and S. M. Dancoff for their active interest in this work. Thanks are also due A. V. Martin for his calculations on the effective thickness of the target materials, and to S. Moskowski for his calculations of the deuterium cross section.

PHYSICAL REVIEW VOLUME 73, NUMBER 6 MARCH 15, 1948

On the Mobility of Electrons in Pure Non-Polar Insulators

FREDERICK SEITZ
Carnegie Institute of Technology, Pittsburgh, Pennsylvania

(December 8, 1947)

It is pointed out that Peierls' condition for the validity of time-dependent perturbation theory in the determination of the mobility μ of electrons in crystals can be transformed to the form

$$\mu > 30 \text{ cm}^2/\text{volt-sec. (at room temperature)}$$

in the case in which the electrons are distributed classically. Since the recent investigations of the mobility of electrons in diamond, silicon, and germanium indicate that the mobility in these materials is at least several times greater than the foregoing limit, it would appear that perturbation methods may be used to discuss the mobility in these materials and possibly in other non-polar insulating materials, such as sulfur.

An expression is derived for the collision frequency for conduction electrons having velocity v as a result of collisions with the acoustical modes of oscillation. It is pointed out that these modes will be the only ones of interest in diamond at room temperature because the characteristic temperature is in the vicinity of 1800°K. The collision time τ is found to satisfy the equation

$$1/\tau = (4/9\pi)(C^2 k_0 T/\hbar^3 c^2 n_0)(m^{*2}/M)k, \qquad \text{(A)}$$

where C is a constant, having the dimensions of energy, that measures the interaction between the lattice and the electron, k_0 is Boltzmann's constant, T is the absolute temperature, c is the acoustical velocity, n_0 is the density of atoms, m^* is the effective electron mass, M is the mass of the atoms in the crystal, and k is the wave number vector of the electron. Since the mean free path is proportional to k, it follows that the mean free path is independent of velocity in the approximation in which (A) is valid. The conditions for validity of the equation, all of which are normally well satisfied in diamond at room temperature, are: (1) The temperature be sufficiently low that the principal inelastic collisions involve only one lattice vibrational quantum; (2) only the acoustical modes of vibration be excited; (3) the temperature of the electrons be sufficiently high that their mean energy be large compared with m^*c^2, in which c is the acoustical velocity; (4) the electrostatic field be sufficiently low that only linear terms are important. The second of these conditions is usually not satisfied in materials such as silicon, germanium, or sulfur near room temperature, although it will be satisfied at lower temperatures. The temperature m^*c^2/k_0 is near 10°K for diamond, but is much less than this for most other materials, so that (A) should be applicable for determining the mobility of conduction electrons in a large number of pure non-polar insulators at low temperatures not too close to 1°K.

In the case of diamond, the mobility at room temperature is found to have the value

$$\mu = (1.46/C^2)10^5 \text{ cm}^2/\text{volt-sec.}$$

if m^* is taken as the free electron mass. This leads to a mobility of about 156 cm²/volt-sec. if C is assumed to have a value of 30.6 ev obtained from the relation $C(\text{ev}) = 1.7 \cdot 10^{-2}\Theta$ that seems to be obeyed for the electrons in the simpler metals. In a range of temperature in which

only acoustical modes of vibration are excited the relative mobilities of two different substances μ_a and μ_b should satisfy the relation

$$\mu_a/\mu_b=(\Theta_a/\Theta_b)^2(n_a/n_b)^{\frac{1}{3}}(C_b/C_a)^2(M_a/M_b),$$

in which the subscripts refer to the two different substances, Θ is the characteristic temperature, n is the atomic density, C is the interaction constant appearing in (A), and M is the atomic mass. Since C and Θ are probably roughly proportional to one another, this relationship suggests that the mobilities of various insulators should have similar values in a range of temperature where only the acoustical modes cause excitation.

The influence of non-acoustical modes in non-polar materials are discussed. It is pointed out that two interesting cases can occur and the case of diamond is discussed and clarified with use of group theory. It is found that the scattering from non-acoustical modes contributes to the collision frequency to about the same degree as the non-acoustical modes when the crystal temperature is not too far below the characteristic temperature.

The implications of the foregoing work for the problem of crystal counters is discussed. It is pointed out that the mobility is probably sufficiently large at room temperature in any of the non-polar crystalline insulators that they would make satisfactory counters if mobility were the only determining factor. It is shown that the concentration of trapping centers in a give specimen is probably the greatest limitation on the use of the material for purposes of a counter.

I. INTRODUCTION*

THE development of crystalline microwave rectifiers[1] and crystal counters[2] during recent years has given stimulus to the study of the mobilities of conduction electrons in non-metallic materials, particularly non-polar insulators and semi-conductors such as diamond, silicon, and germanium. Ionic materials[3] had been subject to a great deal of experimental and theoretical investigation prior to the war by a large number of investigators, both in this country and in Europe, because of the wide interest in the colored alkali halides, photo-conducting luminescent crystals, such as zinc sulfide, and rectifier materials such as cuprous oxide.

Fröhlich and Mott[4] have shown that when the temperature of a polar crystal is near or above the characteristic temperature, the mobility of conduction electrons that are at equilibrium with the lattice is determined primarily by the optical branch of the vibrational spectrum, the greatest electron-lattice interaction being that involving the polarization waves of long wave-length. As the crystal is cooled to a temperature well below the characteristic temperature, the conduction electrons can no longer interact with the optical modes of vibration having long wave-length, if they remain in temperature equilibrium, and the mobility increases. In the range of temperature just below the characteristic temperature in which the collisions involving the optical branch still determine the collision time τ of the conduction electrons, this quantity depends upon temperature through the equation

$$1/\tau=(1/\tau_0)\exp(-h\nu_0/kT) \qquad (1)$$

* A large fraction of this manuscript was prepared while the writer was guest lecturer at the Berkeley campus of the University of California during the summer of 1947. He is indebted to the Department of Physics for a very pleasant and stimulating period of work.

[1] The study of crystalline microwave rectifiers was sponsored in this country during the war by Division 14 of NDRC. Particular emphasis was placed on silicon and germanium to which controlled amounts of additional agents were added to obtain desired electrical properties. No comprehensive survey of the fundamental aspects of this research has apparently appeared as yet in print in the standard journals, although such surveys have been presented at meetings of the American Physical Society (see paper by V. Johnson and K. Lark-Horovitz, Phys. Rev. **72**, 153 (1947)). The institutions and laboratories which contributed to this work are as follows: Radiation Laboratory of the Massachusetts Institute of Technology, Randal Morgan Laboratory of the University of Pennsylvania, Department of Physics of Purdue University, The Bell Laboratories, Westinghouse Research Laboratories, Sylvania Electric Corporation, RCA Laboratories. The following references have bearing on the study of these rectifiers: V. Johnson and K. Lark-Horovitz, Phys. Rev. **71**, 374 (1947); **71**, 709 (1947); E. Conwell and V. F. Weisskopf, Phys. Rev. **69**, 258 (1946); G. L. Pearson and W. Shockley, Phys. Rev. **71**, 142 (1947); B. Goodman, A. W. Lawson, and L. I. Schiff, Phys. Rev. **71**, 191 (1947); I. Estermann, A. Foner, and J. A. Randall, Phys. Rev. **71**, 484 (1947).

[2] P. J. Van Heerden, *The Crystal Detector* (Thesis. Utrecht, 1945); D. E. Wooldridge, A. J. Ahearn, and J. A, Burton, Phys. Rev. **71**, 913 (1947); R. Hofstadter, J. C. D. Milton, and S. L. Ridgway, Phys. Rev. **72**, 977 (1947); The writer desires to express appreciation to the group at the Bell Laboratories, Professor Hofstadter, Dr. Wouters of the Radiation Laboratory of the University of California, and Commander P. S. Johnson of the Bureau of Ships for very informative discussions of the properties of crystal counters.

[3] This work is surveyed in several books and review articles. See, for example, N. F. Mott and Gurney, *Electrical Processes in Ionic Crystals* (Oxford University Press, New York, 1940); F. Seitz, *Modern Theory of Solids* (McGraw-Hill Book Company, New York, 1941), Rev. Mod. Phys. **18**, 384 (1946).

[4] H. Fröhlich, Proc. Roy. Soc. **160**, 230 (1937); **188**, 521 (1947); H. Fröhlich and N. F. Mott, Proc. Roy. Soc. **171**, 496 (1939).

in which τ_0 is practically independent of temperature and ν_0 is the frequency associated with the longest polarization wave in the optical branch. At sufficiently low temperatures, however, the collisions involving the optical branch become unimportant and the collisions involving acoustical modes determine the collision frequency. In particular, the selection rules involving conservation of energy and momentum show that only acoustical waves of fairly long wave-length are involved in these collisions.

The pure non-polar insulating crystals differ from the polar crystals in the sense that the optical modes of vibration of highest frequency are not of the polar type because the atoms are electrically neutral. In the case of diamond, for example, which possesses two atoms per unit cell and has a lattice structure similar to that of Sphalerite (ZnS), the mode of highest frequency is that in which the two atoms in a given cell move in opposite directions at the same time and in which corresponding atoms in different cells derived by pure translation from the first cell move in phase with atoms in the first cell. The crystal does not become polarized during this motion because the carbon atoms in diamond are uncharged. The crystal would become polarized for the corresponding mode of vibration in Sphalerite, however, because the zinc and sulfur atoms have a divalent change. Since polarization is absent, the interaction between the electron and lattice vibrations may be expected to be smaller in the non-polar than in the polar insulators when the temperature is near the characteristic temperature. Moreover, it may be expected that the influence of the optical modes in non-polar materials will not necessarily obliterate the influence of the acoustical modes when the former are excited.

The purpose of the present paper is to discuss the electron mobility in the non-polar insulators, using diamond, silicon, and germanium as prototypes since the values of the mobilities of these materials seem to be known, at least in order of magnitude, at room temperature. A group of investigators at the Bell Telephone Laboratories[5] has demonstrated that electrons liberated in diamond can possess a long mean free path. The experiments carried out to date indicate, in fact, that the mobility at room temperature probably is 100 cm²/volt-sec. or larger. Similarly, the work[6] of the Bell Laboratories, of Estermann and of Lark-Horowitz on combined measurements of conductivity and the Hall effect shows that the mobility of free electrons in pure silicon and germanium at room temperature is about 300 and 1300 cm² per volt-sec., respectively. In this work, use is made of the relation

$$R\sigma = 3\pi\mu/8c,$$

in which R is the Hall constant, σ the electrical conductivity, c the ratio of electromagnetic to electrostatic unit of charge, and μ is the mobility (see Eqs. (39) and (42) below). Since the characteristic temperature of diamond is in the vicinity of 1800°K, it follows that the optical modes are scarcely excited at temperatures near room temperature and below, so that the collision time is determined primarily by interaction with the acoustical modes of vibration. This simplification cannot be expected to hold in other non-polar insulators, such as silicon, germanium, or sulfur, for which the characteristic temperatures are much nearer to room temperature.

The following discussion will have only minor bearing on the mobility of electrons in the non-polar semi-conductors such as silicon and germanium in the form in which they are ordinarily employed as rectifiers, for in such cases the materials usually are intentionally contaminated with impurity agents which have a substantial influence on the mobility. The results do have bearing, however, on the mobility in pure specimens.

II. DISCUSSION OF PERTURBATION THEORY

In accordance with conventional procedure, we shall consider an electron having a wave number vector $\mathbf{k}$ that is moving through a crystal lattice whose normal modes of vibration are

[5] D. E. Wooldridge, A. J. Ahearn, and J. A. Burton, Phys. Rev. **71**, 913 (1947). This work has not actually yielded quantitative values of the mobility to date.

[6] This work is unpublished for the most part (see reference 1). The writer is grateful to the various investigators for the opportunity of discussing their results. Dr. G. L. Pearson and his associates at the Bell Laboratories have found that the mobility in silicon can be expressed in the form $AT^{-\frac{3}{2}}$ at sufficiently high temperatures. A is $5.0 \cdot 10^{5}$ (cm²-deg$^{\frac{3}{2}}$/volt-cm), respectively, for silicon conducting by means of holes and electrons (p-type and n-type).

traveling waves having wave number vectors σ extending through as many Brillouin zones as there are atoms in the unit cell of the lattice. Three polarization waves are associated with each value of σ. We shall designate the circular frequencies associated with σ by $\omega_i(\sigma)(i=1, 2, 3)$. In the most highly symmetric crystals the three modes of vibration may be separated into two transverse and one longitudinal mode, as for an isotropic medium. The modes of vibration having frequency near zero satisfy the relation

$$\omega_i(\sigma)=c_i\sigma, \tag{2}$$

in which c_i is the constant acoustical velocity for long waves having the appropriate polarization and σ is the absolute value of the wave number vector.

The electron under consideration will possess an energy of the order of magnitude of k_0T, where k_0 is Boltzmann's constant and T is the absolute temperature. As a result it will lie near the bottom of the conduction band. For this reason, the relation between the energy ϵ and wave number k can be expressed in the manner

$$\epsilon(k)=\hbar^2k^2/2m^*, \tag{3}$$

in which $\hbar$ is Planck's constant divided by 2π, k is the absolute value of k, and m^* is the effective electron mass which may differ from the true electron mass by a factor substantially different from unity.

As long as the lattice is treated as if completely rigid and perfect the electrons will not be deflected; however, transitions actually will take place even if the lattice contains no impurities, vacancies, or interstitial atoms because of inelastic encounters between the electrons and the lattice vibrations. According to conventional time-dependent perturbation theory, the probability that a transition will take place in time t between two states of the total system having energy E_1 and E_2, respectively, is

$$P_{12}(t)=(1/\hbar^2)\,|\,V_{12}\,|^2t^2(\sin^2x/x^2). \tag{4}$$

Here V_{12} is the matrix component of the potential representing the interaction between the electron and the lattice waves and

$$x=(E_1-E_2)t/2\hbar. \tag{5}$$

If the average time τ in which an electron changes its state from energy ϵ_1 to ϵ_2 is sufficiently long that the condition

$$\tau(\epsilon_1-\epsilon_2)/\hbar>1 \tag{6}$$

is satisfied, the function $\sin^2x/x^2$ can be replaced by a delta function for values of the argument of practical interest. Thus P_{12} can be written

$$P_{12}(t)=(2\pi t/\hbar)\,|\,V_{12}\,|^2\delta(E_1-E_2) \tag{7}$$

when (6) is satisfied.

Peierls[7] has shown that the results of perturbation theory can be used in the determination of the statistical distribution function at temperature T in the presence of an electric field even when the delta function approximation (7) is not completely valid provided the following two conditions are satisfied:

(a) The matrix components of the interaction potential connecting an initial state and those states to which transitions are possible do not vary too greatly over the range of states to which transitions are allowed.

(b) The statistical distribution function does not vary too widely over the range of energy in which (4) takes its principal value when t is of the order of magnitude of the collision time. The distribution function usually involves energy E and temperature through a factor E/k_0T and changes its value appreciably. Therefore, when E changes by an amount k_0T, in electrons of interest for conduction the second condition takes the form,

$$\tau k_0T/\hbar>1. \tag{8}$$

The condition (8) can be placed in a very convenient form if the mobility can be expressed simply in terms of the collision time. This can be done, for example, when the distribution function has the Maxwell-Boltzmann form, as is true for semi-conductors in which the electron density is not too high. In this case

$$\mu\cong e/m\tau, \tag{9}$$

where e and m are the electronic charge and mass. Hence, (8) may be written

$$\mu>e\hbar/mk_0T, \tag{10}$$

which is about 30 cm²/volt-sec. when T is

[7] R. Peierls, Zeits. f. Physik **88**, 786 (1934).

300°K. Van Vleck[8] has shown that this condition is too stringent in metals. In this case the parameter T appearing in (9) is the average collision time for one of the electrons at the top of the Fermi distribution, which is smaller than the average collision time for all conduction electrons by a factor of the order k_0T/ϵ_0, where ϵ_0 is the kinetic energy of an electron at the top of the Fermi distribution which is about 100 times larger than k_0T.

III. SELECTION RULES GOVERNING TRANSITIONS

As long as the amplitude of oscillation of the lattice vibrations is sufficiently small—a condition that is well satisfied at temperatures of normal interest—the potential representing the interaction between the conduction electrons and the lattice vibrations depends linearly upon the amplitude of the normal modes. In this case the first order transitions described by perturbation theory are those in which only one quantum of vibrational energy is emitted or absorbed in each step. Under the conditions in which the delta-function approximation (7) can be used, we may expect the following equation to be valid:

$$\epsilon(\mathbf{k}')=\epsilon(\mathbf{k})\pm\hbar\omega_i(\sigma), \tag{11}$$

in which $\mathbf{k}'$ is the wave number vector of the electron after the transition, $\mathbf{k}$ that before, and $\omega_i(\sigma)$ is the frequency of the mode of vibration having wave number σ that has gained or lost one quantum of energy. The positive sign is valid in the case in which vibrational energy is lost, whereas the negative sign is valid in the opposite case.

In the case in which the electron interacts with only one mode of vibration at a time, the condition of conservation of wave number is expressible in the form

$$\mathbf{k}'=\mathbf{k}+\sigma+\mathbf{K}, \tag{12}$$

$$\cos\theta=-|\sigma+\mathbf{K}|/2k\pm m\omega_i(\sigma)/\hbar k|\sigma+\mathbf{K}|, \tag{13}$$

in which the plus sign corresponds to the case in which the scattered electron gains one quantum of energy and the negative sign corresponds to the reverse case. We shall consider separately the two cases in which $\mathbf{K}=0$ and $\mathbf{K}\neq 0$.

[8] J. H. Van Vleck, Revista de la Universidad Nacional de Tecuman, 1, 81 (1940).

(1) $\mathbf{K}=0$.—In this case we are only interested in values of σ near the origin of wave number space since k is very near the origin. Hence, the approximation (3) is valid and Eq. (13) may be written

$$\cos\theta=-\sigma/2k\pm m^*c_i/\hbar k. \tag{14}$$

The ratio $m^*c_i/\hbar k$ may also be written $(m^*c_i^2/2\epsilon(k))^{\frac{1}{2}}$. The quantity $m^*c_i^2$ corresponds to an energy of the order of 0.001 ev or less for the acoustical velocities met with in all solids. Thus $m^*c_i^2/k_0$ corresponds to a temperature of 10°K for the case of diamond and usually is much smaller for other materials. It follows that the absolute value of the second term on the right-hand side of (14) is less than unity as long as the temperature of motion of the electron is not too close to absolute zero. When $\epsilon(k)$ becomes less than $m^*c_i^2/2$ for all values of i, θ becomes imaginary for all values of σ in Eq. (14) if the negative sign prevails before the second term on the right-hand side. Thus, the electron cannot lose energy in collisions for which $\mathbf{K}=0$ if its energy becomes sufficiently small. Such electrons are equivalent to the "cold neutrons" which have a very long mean free path for scattering in crystalline substances. The "cold electron" can still be scattered by collisions for $\mathbf{K}=0$ in which it gains energy, provided the lattice vibrations having energy $2m^*c_i^2$ are appreciably excited. It is evident that at very low energies $(T<m^*c_i^2/k_0)$ the electrons will have difficulty coming to temperature equilibrium[8] with the lattice through inelastic collisions with the perfect lattice for which $K=0$.

When the electron temperature is near room temperature, the electron will be able to exchange energy with modes of vibration for which $\sigma<2k\pm 2m^*c_i/\hbar\cong 2k$. Equation (14) cannot be satisfied for larger values of σ with real values of θ. Now the energy $\hbar c_i\sigma\cong 2\hbar c_i k$ of the lattice quanta associated with the uppermost value of σ is equal to $\epsilon(k)(8m^*c_i^2/\epsilon)^{\frac{1}{2}}$, which is generally much smaller than $\epsilon(k)$. It follows that if the electron and the lattice are at the same temperature, not too close to the absolute zero, the distribution of energy among the lattice vibrational quanta with which the electron can interact (when $\mathbf{K}=0$) is classical since $\hbar c_i\sigma/kT$ will be small compared with unity for these lattice

vibrations. This fact was apparently first pointed out by Fröhlich.[9]

(2) $\mathbf{K}\neq 0$.—It follows from Eq. (13) that $\boldsymbol{\sigma}$ must be comparable to $\mathbf{K}$, for if $\boldsymbol{\sigma}$ is very small, of the same order of magnitude as $\mathbf{k}$ or less, the absolute value of the first term on the right of (13) is very large compared with unity and the corresponding value of the second term is unity or less for reasonable values of $\mathbf{k}$. These values of $\boldsymbol{\sigma}$ are just those which would lie near the origin of wave number space if the "reduced" zone scheme is employed in which all permissible values of $\boldsymbol{\sigma}$ are taken in the first zone. Since $\omega_t(\boldsymbol{\sigma})$ has zero gradient near $\boldsymbol{\sigma}=0$ for branches other than the three acoustical branches, it follows that the corresponding values of $\omega_t(\boldsymbol{\sigma})$ can be taken to be constant in the range of $\boldsymbol{\sigma}$ that is of interest to us.

A straightforward analysis of Eq. (13) shows that the electron can always be scattered by collisions involving the umklapp process in transitions in which it gains vibrational energy; however, transitions in which the electron loses energy are permitted only when the energy of the electron is larger than the energy of the uppermost vibrational quanta. In general, ϵ must be larger than $k\Theta$ where Θ is the characteristic temperature of the lattice. It follows that transitions involving the umklapp process will not occur if the electron and lattice are at equilibrium at a temperature well below the characteristic temperature, for collisions in which the electron gains energy will be prevented by the fact that the lattice waves which can produce the transitions are not excited, whereas collisions in which the electron loses energy are prevented by the fact that Eq. (13) cannot be satisfied with real values of θ. This probably is the situation in diamond at room temperature for the available data on specific heat and inelastic constants indicate that Θ is about 1800°K. On the other hand, umklapp processes will play a role at room temperature in materials such as silicon, germanium, and sulfur, for which $\Theta\sim 300$°K.

IV. THE INTERACTION POTENTIAL

To begin with, we shall consider the case in which umklapp processes can be neglected. In lieu of more exact information we shall determine the interaction potential between electrons and lattice vibrations on the assumption that the deformable atom hypothesis first introduced by Bloch[10] for the case of metals is valid. According to this assumption, the electronic potential V_d in the displaced lattice is related to the potential V_n in the normal lattice by the equation

$$V_d(\mathbf{r}+\mathbf{R})=V_n(\mathbf{r}). \tag{15}$$

Here $\mathbf{r}$ is the coordinate of the electron in the undeformed lattice and

$$\mathbf{R}(\mathbf{r})=\frac{1}{(N)^{\frac{1}{2}}}\sum_{\sigma,t}\frac{a_t(\boldsymbol{\sigma})}{M}\xi_t(\boldsymbol{\sigma})\exp(i\boldsymbol{\sigma}\cdot\mathbf{r}), \tag{16}$$

in which N is the number of unit cells in the specimen of crystal under consideration, $a_t(\boldsymbol{\sigma})$ is the complex amplitude of the mode of vibration having wave number $\boldsymbol{\sigma}$ and polarization index t, $\xi_t(\boldsymbol{\sigma})$ is the polarization vector for this mode of vibration, and M is the mass of the atoms of the lattice. Corresponding to this assumption, the perturbing potential satisfies the equation

$$V_p=-\mathbf{R}\cdot\operatorname{grad}V_n(\mathbf{r}). \tag{17}$$

The use of (16) and (17) in the form given implies that we are dealing with a crystal in which the directions of polarization of the elastic waves are the same for all atoms and that the phase relations for the various atoms can be expressed in terms of a continuous function. The first of these conditions is always satisfied for crystals in which all of the atoms are at positions where a point center of symmetry (or inversion center) exists. The second condition also can usually be satisfied in these cases. The atoms in diamond, silicon, and germanium are not at positions of inversion symmetry so that the directions of polarization are usually not the same for all atoms. We shall see later that the conditions corresponding to the use of (16) and (17) can be met for the interesting modes of vibration even in these cases.

Peterson and Nordheim[11] have shown that the

[9] H. Fröhlich, *Theorie der Metalle* (Julius Springer, Berlin, 1939).

[10] F. Bloch, Zeits. f. Physik **52**, 555 (1928); A. Sommerfeld and H. Bethe, *Handbuch der Physik*, Vol. XXIV 1; A. H. Wilson, *The Theory of Metals* (Cambridge University Press, Teddington, England, 1936).

[11] E. L. Peterson and L. W. Nordheim, Phys. Rev. **51**, 355 (1937).

hypothesis of deformable atoms is only of semi-quantitative value in the case of the simple metals. On the other hand, Bardeen[12] has found that the more accurate interaction potential is very similar to (17) for alkali metals. It is possible that Nordheim's approximation[13] of "rigid atoms" which replaces (15) by the condition

$$V_a(\mathbf{r})=\sum_p v(\mathbf{r}-[\mathbf{r}(p)+\mathbf{R}(p)]), \qquad (18)$$

in which $v(\mathbf{r})$ is the potential of one of the atoms of the lattice, $\mathbf{r}(p)$ is the positional coordinate of the pth atom of the lattice when the crystal is undeformed and $\mathbf{R}(p)$ is the displacement of the pth atoms, determined from (16) by setting $\mathbf{r}=\mathbf{r}(p)$, would be more accurate for the non-polar insulating atomic substances since the electron cloud is not as highly polarizable in these materials as in metals. However, since the two hypotheses are qualitatively similar, we shall adopt the first, which is simpler.

V. CALCULATION OF THE COLLISION FREQUENCY

The matrix component of (17) connecting the electronic states associated with wave numbers k and k', namely,

$$\int \psi_{\mathbf{k}'}^*\psi_{\mathbf{k}}\mathbf{R}\cdot\operatorname{grad}V_n d\tau, \qquad (19)$$

in which $\psi_{\mathbf{k}}$ and $\psi_{\mathbf{k}'}$ are the electronic wave functions, may readily be placed in the form,

$$\frac{1}{(NM)^{\frac{1}{2}}}a_i(\sigma)\int \chi_{\mathbf{k}'}^*\chi_{\mathbf{k}}\xi_i(\sigma)\cdot\operatorname{grad}V_n e^{-\mathbf{K}\cdot\mathbf{r}}d\tau, \qquad (20)$$

in which $\mathbf{k}$, $\mathbf{k}'$, σ, and $\mathbf{K}$ are related by the equation

$$\mathbf{k}'=\mathbf{k}+\sigma+\mathbf{K}, \qquad (21)$$

and $\chi_{\mathbf{k}}$ and $\chi_{\mathbf{k}'}$ are functions having the periodicity of the lattice which are related to $\psi_{\mathbf{k}}$ and $\psi_{\mathbf{k}'}$ by the equations

$$\begin{aligned}\psi_{\mathbf{k}}&=\chi_{\mathbf{k}}e^{i\mathbf{k}\cdot\mathbf{r}},\\ \psi_{\mathbf{k}'}&=\chi_{\mathbf{k}'}e^{i\mathbf{k}'\cdot\mathbf{r}}.\end{aligned} \qquad (22)$$

In the case in which $\mathbf{K}=0$, the conventional treatment of the matrix components shows that the coefficient of $a_i(\sigma)/(NM)^{\frac{1}{2}}$ in (20) may be reduced to approximately $2iC\sigma/3$ where

$$C=\frac{\hbar^2}{2m}\int|\operatorname{grad}\chi_{\mathbf{k}}|^2 d\tau. \qquad (23)$$

Since we do not have reliable values of $\chi_{\mathbf{k}}$, we shall treat C as an unknown parameter in the following discussion. The analysis leading to (23) also shows that only longitudinally polarized waves are effective in scattering the electron when $\mathbf{K}=0$. It is to be noted that the coefficient of $a_i(\sigma)$ in the matrix component associated with $\mathbf{K}=0$ varies linearly with σ, so that it becomes vanishingly small in the limiting case of very long waves, that is, in the limiting case in which $\mathbf{k}'$ coincides with $\mathbf{k}$. This behavior of the matrix component can be predicted at once from the fact that $\operatorname{grad}V_n$ is an odd function of the electron coordinates.

When $\mathbf{K}$ is not zero, σ, as we have seen previously is very nearly equal to $-\mathbf{K}$, or is close to the origin in the reduced zone scheme as long as $\mathbf{k}$ corresponds to the wave number for a thermal electron. Thus we are interested in values of the matrix component for which $\mathbf{k}$ and $\mathbf{k}'$ differ by small amounts. In the limiting case in which $\mathbf{k}$ and $\mathbf{k}'$ are equal, the integral in (20) becomes

$$\int|\chi_{\mathbf{k}}|^2\xi_i(\sigma)\cdot\operatorname{grad}V_n e^{-i\mathbf{K}\cdot\mathbf{r}}d\tau. \qquad (24)$$

This integral will generally not vanish, although it may do so under conditions of proper symmetry. If it does not vanish, the absolute value of the integral may be written in the form

$$KD_i, \qquad (25)$$

in which K is the absolute value of $\mathbf{K}$ and D_i is a parameter having the dimensions of energy, analogous to the parameter C introduced for the case $\mathbf{K}=0$. We may use (25) for the case in which $\mathbf{k}$ and $\mathbf{k}'$ are not equal since the higher order terms depending on the difference between $\mathbf{k}$ and $\mathbf{k}'$ will be small in comparison with (25), provided the latter is not zero.

When the integral vanishes for the case $\mathbf{K}\neq 0$ because of the symmetry of the functions ap-

[12] J. Bardeen, Phys. Rev. **52**, 688 (1937).
[13] L. W. Nordheim, Ann. d. Physik **9**, 607 (1931).

pearing in the integrand, we may expect the integral in (24) to depend linearly on σ for small values of this vector when expressed in the reduced zone scheme, just as for the case in which $\mathbf{K}=0$. We may treat this case by assuming that the integral has the absolute value

$$\tfrac{2}{3}C'\sigma, \tag{26}$$

in which C' is a parameter analogous to C and σ is the absolute value of σ in the reduced zone scheme.

We shall now calculate the electronic transitions produced by the lattice vibrations. It is convenient to consider separately the effects arising from the acoustical branch, for which $K=0$, and from the other branches since only the acoustical modes will be effective in scattering electrons under the proper circumstances

(1) $\mathbf{K}=0$ (*acoustical modes*).—In this case[14] the quantity $|V_{12}|^2$ appearing in the expression for the transition probability is

$$|V_{12}|^2=\frac{4}{9}C^2\sigma^2\frac{h}{2NM\omega(\sigma)}\begin{Bmatrix}n(\sigma)\\ n(\sigma)+1\end{Bmatrix}. \tag{27}$$

Here the coefficient $4C^2\sigma^2/9$ is the square of the matrix component of $V_p/a_t(\sigma)$ connecting the electronic states associated with k and k' satisfying (21), whereas the remainder of (27) is the square of the matrix component of $a_t(\sigma)$ connecting the state for which the initial vibrational quantum number is $n(\sigma)$ with those for which the quantum numbers are $n-1$ and $n+1$, for which the upper and lower values of the quantity in brackets is to be used, respectively. Since only the longitudinal waves contribute non-vanishing matrix components, the subscript t has been dropped. If the theory of deformable atoms were accurately valid, C would have the value (23).

Using Eqs. (7) and (27) we find that the total differential probability for a transition involving lattice vibrations for which σ lies in a range from θ to $\theta+d\theta$ relative to $\mathbf{k}$ is

$$dP(t,\theta)=\frac{2\pi}{h}t\cdot\frac{2hC^2}{9NM}\int\sigma^4(2n(\sigma)+1)\times\frac{\delta(E_1-E_2)}{\omega(\sigma)}\rho 2\pi\sin\theta d\theta d\sigma \tag{28}$$

provided the second term on the right-hand side of (13) is neglected, which is a permissible approximation for values of $\epsilon(\mathbf{k})$ that are sufficiently large. Here ρ is the density of values of σ in wave number space, namely $V/8\pi^3$, and the integration is to be extended over σ. Using the relation

$$\begin{aligned}E_1-E_2&=\epsilon(k)-\epsilon(k')\pm h\omega(\sigma)\\&=-\frac{h^2}{2m^*}(\sigma^2+2k\sigma\cos\theta)\pm h\omega(\sigma)\\&=-\frac{8h^2}{2m^*}(\sigma^2+2k\sigma\cos\theta),\end{aligned} \tag{29}$$

we find

$$d\sigma=-\frac{m^*}{h^2}\frac{1}{\sigma+k\cos\theta}d(E_1-E_2). \tag{30}$$

Thus the integration over σ may be carried out very simply because of the presence of the delta-function. It follows from (29) that the integrand is finite only when

$$\sigma=-2k\cos\theta. \tag{31}$$

If we replace $n(\sigma)$ by

$$n(\sigma)=k_0T/h\omega(\sigma) \tag{32}$$

to take account of the fact that the modes of vibration with which the electrons react obey classical statistics, we obtain

$$dP(t,\theta)=\frac{8}{9\pi}t\frac{C^2k_0T}{h^2c^2n_0}\frac{m^*}{M}k\cos\theta\sin\theta d\theta, \tag{33}$$

in which θ varies from 90° to 180° and n_0 is the density of unit cells in the lattice.

It is convenient to replace θ by the angle χ through which the electron is deflected. The two angles are related by the equation

$$\cos\theta=\sin(\chi/2), \tag{34}$$

whence

$$\cos\theta\sin\theta d\theta=\sin\chi d\chi/4. \tag{35}$$

[14] The writer is indebted to J. Bardeen for pointing out to him that the case of scattering of free electrons in a semi-conductor by the acoustical modes was treated by A. H. Wilson (*The Theory of Metals*, p. 211), for a simple cubic lattice. The results obtained here reduce to Wilson's when appropriate simplifications are made. It is to be noted that the parameter C employed by Wilson is $\frac{2}{3}$ as large as that employed here.

It follows that the electron has equal probability of being scattered into any element of solid angle, that is, the cross section for scattering is independent of ψ.

If we now integrate over all values of θ or ψ, we obtain for the average collision time τ,

$$\frac{1}{\tau}=\frac{4}{9\pi}\frac{C^2k_0T}{\hbar^3c^2n_0}\frac{m^*}{M}k. \tag{36}$$

Since $\hbar k=m^*v$, where v is the velocity of the electron having wave number k, and $1/\tau=v/\lambda$, where τ is the mean free path for scattering, it follows that λ is independent of v and satisfies the equation,

$$\frac{1}{\lambda}=\frac{4}{9\pi}\frac{C^2k_0T}{\hbar^4c^2n_0}\frac{m^{*2}}{M}. \tag{37}$$

In other words, the conduction electrons satisfy the following three conditions of the elementary theory of transport: (1) The energy of the electrons is essentially conserved during collisions, (2) the scattering is isotropic, and (3) the mean free path is independent of velocity.

The velocity c may be expressed in terms of the characteristic temperature Θ of the crystal with the use of the approximate relation,

$$c=(k_0\Theta/\hbar)(1/(6\pi^2n_0)^{\frac{1}{3}}). \tag{38}$$

In the general case in which it is possible to define a collision frequency, the mobility μ is given by the equation

$$\mu=\frac{2}{3}\frac{e}{m^*}\frac{\langle\epsilon\tau\rangle}{k_0T}, \tag{39a}$$

where $\langle\epsilon\tau\rangle$ is the mean value of $\epsilon\tau(\epsilon)$ averaged over the distribution. This reduces to[15]

$$\mu=\frac{8}{3\pi}\frac{e}{m^*}\frac{\lambda}{\bar{v}} \tag{39b}$$

when λ is independent of energy and the distribution function has the Maxwell-Boltzmann form. Here

$$\bar{v}=4\left(\frac{k_0T}{2\pi m^*}\right)^{\frac{1}{2}} \tag{40}$$

is the average velocity. The final expression for μ is

$$\mu=6\frac{e}{m^*}\frac{ch}{C^2k_0T}\frac{M}{m^{*2}}\frac{n_0}{\bar{v}}, \tag{41a}$$

which, by the use of (38), may be placed in the form

$$\mu=\frac{6}{(6\pi^2)^{\frac{1}{3}}}n_0^{\frac{1}{3}}\frac{e}{m^*}\frac{\hbar^2k_0^2\Theta^2}{C^2k_0T}\frac{M}{m^{*2}}\frac{1}{\bar{v}}. \tag{41b}$$

It is interesting to note at this point that the product of the Hall constant R and the electrical conductivity σ satisfies the relation

$$R\sigma=\frac{e}{m^*c}\frac{\langle\epsilon\tau^2\rangle}{\langle\epsilon\tau\rangle}, \tag{42a}$$

in the general case in which λ depends upon energy, and reduces to

$$R\sigma=\frac{e}{m^*c}\frac{\lambda}{\bar{v}}=\frac{3\pi}{8c}\mu \tag{42b}$$

when λ is constant. This relation, which is commonly used to determine mobilities of semiconductors from experimental measurements of the Hall effect, is only approximately valid when λ is not constant.

According to (41b) the relative mobility of an electron at a given temperature in two different substances, distinguished by subscripts a and b, respectively, for which the only elastic waves causing collisions are those in the acoustical branches, is given by the relation

$$\frac{\mu_a}{\mu_b}=\left(\frac{\Theta_a}{\Theta_b}\right)^2\left(\frac{n_a}{n_b}\right)^{\frac{1}{3}}\left(\frac{C_b}{C_a}\right)^2\left(\frac{M_a}{M_b}\right), \tag{41c}$$

if we assume the effective electron masses are the same.

It is interesting to compute the value of μ for diamond with the use of Eq. (41a). We shall take the density of diamond to be 3.5, take m^* to be the true electronic mass, set $T=300°\text{K}$, and take the velocity of longitudinal waves to be $1.75\cdot10^6$ cm/sec. The last quantity is determined from the equation

$$c_l=(c_{11}/\rho_0)^{\frac{1}{2}}, \tag{43}$$

in which c_{11} is the elastic constant in conven-

[15] See for example, F. Sietz, *Modern Theory of Solids* (McGraw-Hill Book Company, New York, 1941), p. 517.

TABLE I. Evaluation of mobility at room temperature with use of Eqs. (41c) and (44). (The mobilities are given in units of cm²/volt-sec.)

Crystal	Θ(°K)	M	$n\cdot10^{22}$ (cm^{-3})	C(ev)	C^2	$C^2\mu\cdot10^{-5}$	μ(calc.)	μ(obs.)
Diamond	1800	12	17.6	30.6	936	1.46	156	(≅ 100)
Silicon	600	28	5.21	10.2	104	0.253	243	~ 300
Germanium	290	72	4.57	4.9	24.0	0.145	605	~ 130

tional notation and ρ_0 is the density of the crystal. c_{11} is taken to have the value[16] $1.07\cdot10^{13}$ dynes/cm². Using these values, we obtain

$$\mu=\frac{1.46\cdot10^{5}\ \text{cm/sec.}}{C^2}\ \frac{}{\text{volt/cm}} \tag{44}$$

in which C is expressed in units of ev $\bar{v}$, computed with the use of (40) has the value $1.08\cdot10^{7}$ cm/sec. The right-hand side of Eq. (44) should be multiplied by $(m/m^*)^{5/2}$ if m/m^* is not unity.

Given the value of the mobility for diamond, we can determine the mobility for silicon and germanium with the use of Eq. (42). The greatest uncertainty in the numerical evaluation of the mobilities evidently lies in the determination of the values of C and of the effective electron mass. For simplicity we shall assume that m and m^* are equal and that C is given by the equation

$$C(\text{ev})=1.7\cdot10^{-2}\Theta, \tag{45}$$

in which Θ is the characteristic temperature, expressed in degrees Kelvin. This relationship is approximately satisfied in the case of the simpler monovalent metals treated by A. H. Wilson[14] and can be employed here at least to determine orders of magnitude. Table I contains values of the mobility of electrons at room temperature derived with the use of Eqs. (42) and (44). The numerical values of the constants employed in the calculation are also given.

The observed values of the mobilities given in Table I are obtained from several sources.[6] That for diamond is a very rough lower limit estimated by the group at the Bell Laboratories from a study of the pulses observed in crystal counters employing diamond. The value for silicon is obtained by extrapolating to room temperature the mobility observed by the group at the Bell Laboratories in fairly pure samples of n-type silicon at temperatures somewhat above room temperature. The mobility is found to depend upon temperature through a factor $T^{-\frac{1}{2}}$ predicted from (40) in this range. The value for germanium is obtained in a similar way from measurements obtained both at the Bell Laboratories and by Estermann at this laboratory. It is rather surprising that the $T^{-\frac{1}{2}}$ relation predicted from (40) for low temperatures should be observed at temperatures as close to the characteristic temperature as is the case in silicon and germanium. This seems to imply that the electron scattering arising from terms for which $\mathbf{K}\neq0$ is not very strong. This point will be discussed again later in this section.

It may be seen that the agreement between observed and calculated mobilities given in Table I is not very good, only the general order of magnitude being obtained. This is not very surprising in view of the fact that the relation (45) is employed to determine C, that the relative effective electron mass is taken to be unity, and that the fact that the contribution to the scattering from modes of vibration for which $\mathbf{K}\neq0$ has not been separated from the observed values of the mobility of silicon and germanium.

In passing, it may be noted that the value of the characteristic temperature of diamond determined from Eq. (38) with the use of the value of the acoustical velocity obtained from (43), namely $1.75\cdot10^{6}$ cm/sec., is somewhat greater than the observed value (2890°K instead of 1800°) as is usually the case. In deriving μ(calc.) for silicon and germanium it is assumed that the sonic velocities in silicon and germanium bear the same relation to the sonic velocity in diamond that the observed characteristic temperatures of the first two materials do to the characteristic temperature of the latter.

(2) $\mathbf{K}\neq0$ (*non-acoustical modes*).—We shall now consider the contribution to the collision process from the branches of the vibrational spectrum other than the acoustical branch in the case of the non-polar insulators. In the case of polar insulators, the optical branches are of principal importance, provided the temperature is not so low that interaction with the optical modes is forbidden on purely energetic grounds.

We shall proceed in the following manner: First, we shall adopt the reduced zone scheme,

[16] See for example, R. F. S. Hearmon, Rev. Mod. Phys. **18**, 409 (1946).

so that $\omega_i(\sigma)$ is represented by a multivalued function of the range of σ lying in the first Brillouin zone for the lattice. In this case the values of σ of interest for the scattering process are those lying near the origin of $\sigma=0$. Second, we shall assume that $\omega_i(\sigma)$ is a constant for each of the non-acoustical branches in the vicinity of $\sigma=0$. We shall assume that only one mode of vibration is responsible for scattering and drop the subscript on $\omega_i(\sigma)$ describing the direction of polarization, as in the previous case. Since there will generally be more than one non-acoustical branch of waves having given polarization if there are more than two atoms per unit cell, we should introduce an index to indicate to which branch a given value of ω belongs. For convenience we shall assume that there is only one non-acoustical branch since the contribution to scattering from additional branches can be obtained by simple addition of the results derived for one branch.

We must now consider the transition probability in two cases, namely, that in which the absolute value of the integral of (24) has the form

$$KD \quad \text{(Case I)}, \tag{45a}$$

and that in which it has the form

$$\tfrac{3}{5}C'\sigma \quad \text{(Case II)}. \tag{46}$$

In these two situations, the differential transition probability, analogous to (28) is

$$dP(t,\theta)=\frac{2\pi}{\hbar}t\cdot\frac{D^2}{2NM}\frac{\hbar K^2}{\omega}\begin{Bmatrix}n\\ n+1\end{Bmatrix}_\rho \times\int\sigma^2\delta(E_1-E_2)2\pi\sin\theta d\theta d\sigma \quad \text{(I)} \tag{47a}$$

and

$$dP(t,\theta)=\frac{2\pi}{\hbar}t\cdot\frac{2\hbar C'^2}{9NM\omega}\begin{Bmatrix}n\\ n+1\end{Bmatrix}_\rho \times\int\sigma^4\delta(E_1-E_2)2\pi\sin\theta d\theta d\sigma \quad \text{(II)} \tag{47b}$$

in which the integration is to be carried out over the allowed range of σ. In both cases ω is the constant frequency of the modes of vibration with which the electron interacts and n, as previously, is the number of quanta having wave number σ in the branch under consideration. Since n is a function of $\hbar\omega/k_0T$, it can be treated as a constant. The relation between E_1-E_2 and the variables describing the electron and the vibrational waves differs in the case in which the electron receives energy from the lattice and that in which it transmits energy (see Eq. (29)). The relation to be used in the present case is

$$E_1-E_2=-\frac{\hbar^2}{2m}(\sigma^2+2k\sigma\cos\theta)\pm\hbar\omega, \tag{48}$$

in which the upper sign before the last term is associated with transitions in which the electron gains energy, and the lower sign with transitions in which it loses energy. Similarly, the upper value in the expression $\{{}^{n}_{n+1}\}$ before the integrand is to be used with the upper sign and conversely. Since there is a delta function in the integrands appearing in (47a) and (47b), the integrals contribute to dP only for values of σ corresponding to the roots of (48), namely,

$$k[-\cos\theta\pm(\cos^2\theta\pm\hbar\omega/\epsilon)^{\frac{1}{2}}]. \tag{49}$$

The two roots correspond to the two possible signs before the radical (not to the two signs before $\hbar\omega/\epsilon$). As previously, $\epsilon=\hbar^2k^2/2m^*$. Only the positive, real roots are of interest. A simple analysis of the situation shows that the roots are governed by the following rules:

(1) *Electron gains energy* (*positive sign under radical*). In this case there is one positive root for each value of θ between zero and 180°. This root is given by the equation

$$\sigma=k[-\cos\theta+(\cos^2\theta+\hbar\omega/\epsilon)^{\frac{1}{2}}]. \tag{50}$$

(2) *Electron loses energy* (*negative sign under radical*). In this case there are two positive real roots provided θ lies between 90° and 180° and the value for which $\cos\theta=-(\hbar\omega/\epsilon)^{\frac{1}{2}}$. Under these conditions the two roots are

$$k[-\cos\theta\pm(\cos^2\theta-\hbar\omega/\epsilon)^{\frac{1}{2}}]. \tag{51}$$

The corresponding values of the integrals appearing in (47a) and (47b) are $2\pi m^*\sin\theta d\theta/\hbar^2$ times the following quantities.

Case I. (a) Electron gains energy,

$$k\frac{[-\cos\theta\pm(\cos^2\theta+\hbar\omega/\epsilon)^{\frac{1}{2}}]^2}{(\cos^2\theta+\hbar\omega/\epsilon)^{\frac{1}{2}}}. \tag{52}$$

(b) Electron loses energy,

$$-4k\cos\theta. \tag{53}$$

Case II. (a) Electron gains energy,

$$k^3\frac{[-\cos\theta+(\cos^2\theta+\hbar\omega/\epsilon)^{\frac{1}{2}}]^4}{(\cos^2\theta+\hbar\omega/\epsilon)^{\frac{1}{2}}} \tag{54}$$

(b) Electron loses energy,

$$-8k^3\cos\theta(2\cos^2\theta-\hbar\omega/\epsilon). \tag{55}$$

It is evident from these expressions that the angular distribution of scattering is more complex than in the case in which the acoustical waves are responsible for transitions.

As Fröhlich[9] has pointed out, we may obtain the collision frequency of interest for the electrical mobility by taking the integral over-all angles of $dP(\theta,t)/t$ times the quantity

$$-\frac{1}{2}\left(-\frac{\sigma^2}{k^2}\pm\frac{\hbar\omega}{\epsilon}\right). \tag{56}$$

Actually, it is simpler to carry out the integration over σ and θ completely anew, the integration over θ being carried out first. We readily find that the integrals appearing in (46) and (47) have the following values when (56) is included and the operations are carried out over both θ and σ.

Case I:

$$\frac{\pi m^*}{h^2}k^4\left(1\pm\frac{\hbar\omega}{\epsilon}\right)^{\frac{1}{2}}. \tag{57}$$

Case II:

$$\frac{\pi m^*}{h^2}k^3\frac{4}{3}\left(1\pm\frac{\hbar\omega}{\epsilon}\right)^{\frac{1}{2}}\left(8\pm5\frac{\hbar\omega}{\epsilon}\right). \tag{58}$$

The upper sign before $\hbar\omega/\epsilon$ corresponds to the case in which the electron gains energy and the lower sign to that in which it loses energy. The result corresponding to Case I is the same as that which would have been obtained if (56) had been replaced by unity, showing that the scattering behaves as if isotropic as far as the average effect is concerned.

The final values for the collision frequency are as follows.

Case I:

$$\frac{1}{\tau}=\frac{1}{\pi}\frac{D^2\hbar^2K^2/2m^*}{\hbar\omega}\frac{m^{*2}}{M}\frac{k}{\hbar^3n\sigma}\times\begin{Bmatrix}n\\n+1\end{Bmatrix}\left(1\pm\frac{\hbar\omega}{\epsilon}\right)^{\frac{1}{2}}. \tag{59}$$

Case II:

$$\frac{1}{\tau}=\frac{2}{27\pi}\frac{C'^2}{\hbar\omega}\frac{m^*}{M}\frac{1}{h}\frac{k^3}{n_0}\times\begin{Bmatrix}n\\n+1\end{Bmatrix}\left(1\pm\frac{\hbar\omega}{\epsilon}\right)^{\frac{1}{2}}\left(8\pm5\frac{\hbar\omega}{\epsilon}\right). \tag{60}$$

The total collision frequency is obtained by first adding the frequencies for collisions in which the electron gains and loses energy and then combining the result with the expression (36) for the collisions with acoustical waves. It is interesting to note that (59) involves k linearly in the event that $\hbar\omega/\epsilon$ is so small that the factor $(1\pm\hbar\omega/\epsilon)^{\frac{1}{2}}$ can be replaced by unity. In this case, which is not typical of one of the most stable insulators, the mean free path is independent of velocity, provided Case I prevails, even when the non-acoustical vibrations are important. The mean free path will have a complicated dependence upon velocity in Case II if the term (60) is not negligible compared with that arising from the acoustical vibrations.

We shall now compare the ratio of the collision frequencies (59) and (60) to the frequency (36).

Case I.—In this case the ratio is

$$R=\frac{9}{4}\frac{D^2}{C^2}\frac{\hbar^2K^2/2m^*}{k_0T}\frac{m^*c^2}{\hbar\omega}\begin{Bmatrix}n\\n+1\end{Bmatrix}\left(1\pm\frac{\hbar\omega}{\epsilon}\right)^{\frac{1}{2}}. \tag{61}$$

Since D should be of the same order of magnitude as C (if it does not vanish) and since $hKc\sim\hbar\omega$ the ratio has the magnitude

$$R\sim\frac{\hbar\omega}{k_0T}\left(1\pm\frac{\hbar\omega}{\epsilon}\right)^{\frac{1}{2}}\begin{Bmatrix}n\\n+1\end{Bmatrix}. \tag{62}$$

This will be small compared with unity only if $\hbar\omega/k_0T$ is so large that n is very small. Only the positive sign in (62) will then be of interest since ϵ is of the same magnitude as k_0T if the electron is in equilibrium with the lattice. In the case of a material such as diamond for which

the characteristic temperature is in the vicinity of 2000°K, $\hbar\omega/k_0T$ is about 6 at room temperature. Hence n is approximately $2.5\cdot10^{-3}$ and R is a few percent. On the other hand, n should be near unity for a material such as silicon, germanium, or sulfur. In such a case R will not be negligible near room temperature.

Case II. In this case R has the value

$$R=\frac{1}{3}\frac{C'^2}{C^2}\frac{\epsilon}{\hbar\omega}\frac{m^*c^2}{k_0T}\times\begin{Bmatrix}n\\n+1\end{Bmatrix}\left(1\pm\frac{\hbar\omega}{\epsilon}\right)^{\frac{1}{2}}\left(8\pm5\frac{\hbar\omega}{\epsilon}\right). \quad (63)$$

As in Case I, this will be very small if n is very small because $\hbar\omega/k_0T$ is large compared with unity. On the other hand, it may also be quite small if n is near unity, for the factor $C'^2m^*c^2/C^2\hbar\omega$ will be small compared with unity if C' is not substantially larger than C.

In any case, the scattering produced by non-acoustical waves will be negligible if the temperature is sufficiently small that $\hbar\omega/k_0T$ is large compared with unity.

In connection with the discussion of Table I, it was pointed out that the mobilities of relatively pure silicon and germanium seem to obey the $T^{-\frac{1}{2}}$ power law, corresponding to Eq. (41a), at temperatures near their characteristic temperatures. We shall see in the next section that these materials probably belong to Case I described above, so that the expression for the collision frequency of the conduction electrons should contain a term of the type (59) in addition to that arising from the acoustical modes of vibration. If the previous discussion of the influence of the non-acoustical modes is correct, the mobility near the characteristic temperature, for which $\hbar\omega/k_0T$ should be of the order of unity, should be approximately half that which would be observed if only the acoustical modes of vibration were effective, and the temperature dependence should not be exactly $T^{-\frac{1}{2}}$ because the factor

$$\frac{1}{T}\left(1\pm\frac{\hbar\omega}{\epsilon}\right)^{\frac{1}{2}}\begin{Bmatrix}n\\n+1\end{Bmatrix}$$

in (62) will introduce a more complex dependence. We must conclude either that the foregoing estimate of R (Eq. (62)) is too large or that the experiments which seem to support the $T^{-\frac{1}{2}}$ behavior near the characteristic temperature are not sufficiently accurate to separate the deviation which actually exists.

VI. IMPLICATIONS OF CRYSTAL SYMMETRY

It is interesting to consider the question of whether the integral (20) would vanish for diamond. Kimball[17] has investigated the wave functions for diamond and other crystals, such as silicon and germanium, having the same structure, with the use of the cellular approximation. The lattice contains two atoms per unit cell which can be sent into one another with use of a center of symmetry lying at the midpoint of the line joining the two atoms. The two atoms in the cell have the point symmetry of a tetrahedron and the unit cell may be divided into two symmetrically equivalent polyhedra, having tetrahedral symmetry, at whose centers the atoms are situated. Kimball determined the electronic wave functions on the assumption that the portion contained in each polyhedron could be expressed in terms of a single s-function and three p-functions. He found that in this approximation the lowest conduction state possesses a wave function which has tetrahedral symmetry about each atom and has opposite signs in the two polyhedra of a single unit cell. Kimball's wave function is a pure s-function satisfying the equation $s=0$ at the midpoint of four faces of the cellular polyhedron equidistant from the center and possesses an energy that is unreasonably high. The exact wave function having this symmetry[18] would contain spherical harmonics of higher order than the s-function and would undoubtedly have a much lower energy. In fact, it is easy to show with the use of group theory that the next pair of spherical harmonics which would occur are f and g functions having the same angular symmetry as the functions

$$xyz \text{ and } x^2y^2+y^2z^2+z^2x^2-\tfrac{1}{3}(x^4+y^4+z^4). \quad (64)$$

The addition of these functions would lower the the energy of Kimball's solution by replacing the strong curvature in the radial direction with curvature in the angular direction.

[17] G. E. Kimball, J. Chem. Phys. **3**, 560 (1935).

[18] The reasoning employed here is described in the paper by D. H. Ewing and the writer, Phys. Rev. **50**, 760 (1936).

In any case, we shall assume that for small values of $\mathbf{k}$, χ_k has tetrahedral symmetry about each atomic position and that it reverses its sign in passing from one polyhedron of a given cell to the next. According to this assumption, $|\chi_k|^2$ possesses the complete symmetry of the lattice.

Let us now consider the value of the integral (24) for a unit cell of the lattice. We shall assume that one atom is at the origin of coordinates and that the other is at the position $\mathbf{r}_a$ whose components are $(a/2, a/2, a/2)$, where $2a$ is the length of the edge of the unit cubic cell of the crystal. In terms of this notation the allowed values of K are given by the eight vectors,

$$\frac{\pi}{a}\begin{pmatrix}\pm 1\\ \pm 1\\ \pm 1\end{pmatrix}. \tag{65}$$

In the modes of vibration associated with $\sigma = K$, the two atoms in the unit cell move in opposite directions. For those values of $\mathbf{K}$ for which $\mathbf{K}\cdot\mathbf{r}_a$ is equal to $-\pi/2$ or to $3\pi/2$, the displacement of the atoms is expressible in terms of the function

$$R = \xi A[(1-i)e^{i\mathbf{K}\cdot\mathbf{r}} + (1+i)e^{-i\mathbf{K}\cdot\mathbf{r}}], \tag{66}$$

evaluated at the positions of the atom. Here A measures the amplitude of the wave and the vector ξ is the direction of polarization of the atom at the origin. In the four cases in which $\mathbf{K}\cdot\mathbf{r}_a$ is $\pi/2$ or $-3\pi/2$, the corresponding function is

$$R = \xi A[(1+i)e^{i\mathbf{K}\cdot\mathbf{r}} + (1-i)e^{-i\mathbf{K}\cdot\mathbf{r}}]. \tag{67}$$

Equations (66) and (67) can be used to describe modes of vibration for which σ is close to, but not necessarily equal to, $\mathbf{K}$ by replacing $\mathbf{K}$ by σ.

The integral (24) over the unit cell can be broken into two integrals over the polyhedral cells surrounding the two atoms in the unit cell. If the atom in each cell is chosen to be the center of coordinates for the corresponding integral, the sum of the two integrals is

$$\xi\cdot\left[\int_1 |\chi_k|^2 \operatorname{grad} V_n e^{-i\mathbf{K}\cdot\mathbf{r}} d\tau + e^{-i\mathbf{K}\cdot\mathbf{r}_a} \times \int_2 |\chi_k|^2 \operatorname{grad} V_n e^{i\mathbf{K}\cdot\mathbf{r}} d\tau\right], \tag{68}$$

in which the two integrals extend over the two polyhedra. Now the two polyhedra can be brought to congruence after the second has been inverted by reflection in the point at the origin. The same inversion will reverse the sign of the gradient term in the integrand and change the exponential into its complex conjugate. It follows that the second term in brackets in (68) may be transformed to

$$\pm i\int_1 |\chi_k|^2 \operatorname{grad} V_n e^{-i\mathbf{K}\cdot\mathbf{r}} d\tau. \tag{69}$$

The sign before the integral is determined by the sign of $\mathbf{K}\cdot\mathbf{r}_a$ which is equal to $\mp\pi/2$. Thus, if the first integral in (68) is designated by $a = a_r + ia_i$, the second is a^* and the expression in parenthesis in (68) may be written

$$(1\pm i)(a_r \pm a_i). \tag{70}$$

It follows that the integral generally will not vanish so that diamond is a material belonging to the first of the two classes described above. We shall investigate the implications of crystal symmetry on the value of the integral somewhat further.

As we shall see below, even in the case in which χ_k does not have tetrahedral symmetry about each atomic position, $|\chi_k|^2$ will contain a function belonging to the unit irreducible representation of the tetrahedral group. Hence, the conclusion that diamond belongs to the first of the two classes, for which (68) does not vanish, is valid under more general conditions than that in which χ_k has pure tetrahedral symmetry. We may conclude, for example, that the holes produced in the filled band of diamond and in other crystals having the same lattice symmetry will also interact with the non-acoustical modes of vibration in accordance with the first of the two rules of the previous section.

The point symmetry at the position of an atom in the diamond lattice is expressible in terms of a twenty-four element group T_d, which possesses five classes. The five types of element in the classes are as follows:

(1) the unit operator (1 element),
(2) the three-fold rotations about (111) axes (8 elements),

(3) the two-fold rotations about (100) axes (3 elements),
(4) the rotary reflections through 90° about (100) axes (6 elements), and
(5) the reflecting planes passing through (100) axes (6 elements).

The five irreducible representations, which may be designated by Γ_1, Γ_2, Γ_3, Γ_4 and Γ_5 have the following character system

	E	$8C_3$	$3C_2$	$6\delta_4$	6ρ
Γ_1	1	1	1	1	1
Γ_2	1	1	1	−1	−1
Γ_3	2	−1	−2	0	0
Γ_4	3	0	−1	−1	1
Γ_5	3	0	−1	1	−1

in which the columns designate the classes in the order given above. It is readily found that the spherical harmonics decompose in the following manner: s: Γ_1, p: Γ_4, d: $\Gamma_3+\Gamma_4$, f: $\Gamma_1+\Gamma_4+\Gamma_5$, g: $\Gamma_1+\Gamma_3+\Gamma_4+\Gamma_5$, and that the cross products of the representations decompose as follows:

$$\Gamma_1\times\Gamma_j=\Gamma_j,$$
$$\Gamma_2\times\Gamma_3=\Gamma_3,$$
$$\Gamma_2\times\Gamma_4=\Gamma_5,$$
$$\Gamma_2\times\Gamma_5=\Gamma_4,$$
$$\Gamma_3\times\Gamma_4=\Gamma_4+\Gamma_5,$$
$$\Gamma_3\times\Gamma_5=\Gamma_4+\Gamma_5,$$
$$\Gamma_4\times\Gamma_5=\Gamma_1+\Gamma_3+\Gamma_4+\Gamma_5,$$
$$\Gamma_2\times\Gamma_2=\Gamma_1,$$
$$\Gamma_3\times\Gamma_3=2\Gamma_1+\Gamma_2,$$
$$\Gamma_4\times\Gamma_4=\Gamma_1+\Gamma_3+\Gamma_4+\Gamma_5,$$
$$\Gamma_5\times\Gamma_5=\Gamma_1+\Gamma_3+\Gamma_4+\Gamma_5.$$

Since $|\chi_k|^2$ and V_n belong to Γ_1, whereas $\mathbf{R}\cdot\text{grad}$ belongs to Γ_4, it follows that the coefficient of $e^{i\mathbf{K}\cdot\mathbf{r}}$ in the integrand of (24) can be expanded in terms of spherical harmonics having the symmetry of Γ_4, of which the first four are of the type form:

$$x,\ yz,\ x^3-\tfrac{3}{2}x(y^2+z^2),\ \text{and}\ yz(y^2+z^2-6x^2). \quad (71)$$

The first real term in the expansion of $\exp(i\mathbf{K}\cdot\mathbf{r})$ with which any one of these harmonics can possess a non-vanishing integral is $-(\mathbf{K}\cdot\mathbf{r})^2/2$, which, for diamond, may take any one of the four independent values given by the expression

$$(K^2/2)(\pm x\pm y\pm z)^2,$$

where K is the absolute value of $\mathbf{K}$. Two of these functions give non-vanishing integrals when multiplied with xy, a d function belonging to Γ_4.

The first imaginary term in the expansion of $\exp(-iK\cdot r)$ is $-i\mathbf{K}\cdot\mathbf{r}$. This will usually give a non-vanishing integral when multiplied by the first of the four representatives of Γ_4 shown in (71).

It is interesting to observe that D would vanish if $|\chi_k|^2$ and V_n were spherically symmetric about the atom in the polyhedron. It would also vanish if Nordheim's hypothesis of rigid ions were employed, for the use of this procedure would be equivalent to replacing the term $\exp(-i\mathbf{K}\cdot\mathbf{r})$ by unity in the integration over a single polyhedron. The integrand would always be a spherical harmonic belonging to the representation of Γ_4 (if $|\chi_k|^2$ belongs to Γ_1) and the integral would vanish. These results suggest that D will probably be small compared with C in any substance in which the atoms are highly symmetric or highly undeformable. In such a case the ratio (59) might be small so that only the acoustical modes of vibration would scatter electrons at any temperature, as is possibly the case in silicon and germanium.

VII. COMMENT ON CRYSTAL COUNTERS

The preceding discussion shows that the mobility of electrons in the non-polar insulating crystals may be of the order of several hundred cm²/volt-sec. or more even at room temperature. It is interesting to consider the implications of this conclusion in connection with the development of crystal counters. In the conventional arrangements of such counters which are under consideration at the present time, the crystal specimen is of the order of 0.1 cm thick in the direction in which the electric field is applied and across which the charges produced by the ionizing radiation move. The applied electric field are usually somewhat less than 10,000 volts per cm, although a field of this magnitude or greater probably could be obtained without serious difficulty. The time T required for electrons to traverse the specimen under these conditions is given by the equation

$$T=d/\mu E=10^{-5}/\mu \text{ sec.}, \quad (72)$$

where d is the crystal thickness, E is the elec-

tric field intensity, and μ is the mobility expressed in units of cm²/volt-sec. If it is desired that T be 10^{-7} sec. at maximum, it is necessary under the conditions given that μ be at least 100 cm²/volt-sec. Since an energetic charged particle which is either stopped by the crystal or passes through it will produce a sufficient number of electrons and positive holes to be detected if all pass to the electrodes, it would appear that any crystal having sufficiently high mobility should be able to act as a counter.

Actually another important factor will enter into the problem. The careful studies on the alkali halide crystals show that the migrating electrons or holes may be trapped in the interior of the crystal so that they do not necessarily reach the electrodes. Actually, a very small amount of impurity of the kind needed for trapping may suffice to cut the ionization pulses to a negligible value. The experiments on the trapping effect of F- and F'-centers in the alkali halides, that is of halogen ion vacancies and halogen ion vacancies neutralized by an electron, show[19] that the cross section for capture in these cases is of the order of magnitude of 10^{-15} cm².

[19] This result can be obtained from the study of the distances moved by photoelectrons in the colored alkali halides before being trapped (see reference 3). It is assumed that the mobility of the conduction electrons is of the order of 5 cm²/volt-sec. on the basis of the Hall effect measurements of J. Evans, Phys. Rev. **57**, 47 (1940).

If the concentration of trapping centers is n_t and if their cross section for capture is σ_t, the time T_t an electron having velocity v will travel before being trapped is

$$T_t = 1/n_t \sigma_t v. \tag{73}$$

In order that this be at least as large as the 10^{-7} sec. necessary for the electron to travel to the electrodes under the conditions described in the previous paragraph, it is necessary that

$$n_t < 10^7/\sigma_t v. \tag{74}$$

We shall take σ_t to have the value 10^{-15} cm² and v to be 10^7 cm sec., in which case we must have

$$n_t < 10^{15} \text{ atoms per cc.}$$

This condition implies a very high degree of freedom from any kind of contamination which will provide trapping centers, including lattice defects such as vacancies or interstitial atoms. It is not necessary that all types of contamination provide trapping centers, so that it may only be necessary in a given case to free the crystal from certain elements.

The fact that strong pulses have been observed in silver chlorides and diamond by various investigators indicates that the number of trapping centers was very small in the specimens employed in this work.

Disintegration of Positive and Negative Mesotrons in Different Absorbers

NORRIS NERESON*
Department of Physics, University of New Mexico, Albuquerque, New Mexico
(Received December 10, 1947)

The β-decay of positive and negative mesotrons has been studied in the case of boron, carbon, aluminum, and iron absorbers. Positive mesotrons showed a decay process in all of the above four absorbers, while negative mesotrons indicated decay phenomena (having mean lifetimes greater than about 0.6 microsecond) in only the boron and carbon absorbers. Results are in agreement with other similar experiments of this type, showing that for negative mesotrons decay phenomena predominate in absorbers of small atomic number and capture processes are more probable in absorbers of large atomic number.

I. INTRODUCTION

SEVERAL investigators[1] have found a ratio of approximately 0.5 between the number of disintegration electrons and the number of mesotrons of both signs stopped in absorbers of moderately high atomic number ($Z \geqq 13$). A recent similar investigation[2] using an absorber of low atomic number ($Z=4$) showed a value of about one for the above ratio. A more detailed experiment by Conversi, Pancini, and Piccioni[3] investigated the decay of positive and negative mesotrons separately in carbon and iron absorbers and showed that negative mesotrons emitted decay electrons when absorbed in carbon but not when absorbed in iron. The interpretation of these results was that the capture probability of negative mesotrons by nuclei increased with increasing atomic number while positive mesotrons underwent the same decay process in all absorbers. A recent determination[4] of the lifetime of mesotrons of both signs in aluminum ($Z=13$) gives an indication that negative mesotrons undergo a measurable decay process in this element. The investigation described in this paper is similar to the experiment carried out by Conversi and others[3] except in that two additional absorbers were investigated, and a somewhat different experimental arrangement was used.

II. EXPERIMENTAL ARRANGEMENT

The experimental arrangement shown in Fig. 1 was used to study the relative number of disintegration electrons arising from positive and negative mesotrons stopped in different absorbers. The method used to separate the positive and negative mesotrons consisted of using a large piece of magnetized iron to force incoming particles of opposite sign into two well separated directions. The absorber under investigation received two beams of singly charged mesotrons and was surrounded by twelve decay electron counters.

The Geiger-Müller counter tubes used in this experiment were of the all-metal (brass) construction type[5] and were filled with the standard 10 percent ethyl alcohol and argon mixture to a total pressure of 10 cm of mercury. The counters had a central wire of 5 mils, an outside diameter of 2 inches, and a length of 23 inches, with the exception of counters E and X, which had lengths of 27 inches and 36 inches, respectively. The experiment was set up in the basement of a concrete building located at an altitude of 5000 feet and was run continuously over a period of six months.

The four absorbers were alternated every two or three weeks to minimize and average out errors resulting from any slow time changes occurring in the electronic equipment, Geiger-Müller counters, or cosmic-ray intensity. The direction of the magnetic field, which permitted the study of either positive or negative particles, was reversed approximately every 24 hours.

The magnetized iron was arranged in the form

* Now at Los Alamos Scientific Laboratory, Los Alamos, New Mexico.

[1] F. Rosetti, Phys. Rev. 60, 198 (1941); B. Rossi and N. Nereson, Phys. Rev. 62, 417 (1942); M. Conversi and O. Piccioni, Nuovo Cimento 2, 71 (1944); Phys. Rev. 70, 859 (1946).

[2] T. Sigurgeirsson and A. Yamakawa, Phys. Rev. 71, 319 (1947).

[3] M. Conversi, E. Pancini, and O. Piccioni, Phys. Rev. 71, 209 (1947).

[4] H. Ticho, Phys. Rev. 72, 255 (1947).

[5] V. H. Regener, Rev. Sci. Inst. 18, 267 (1947).

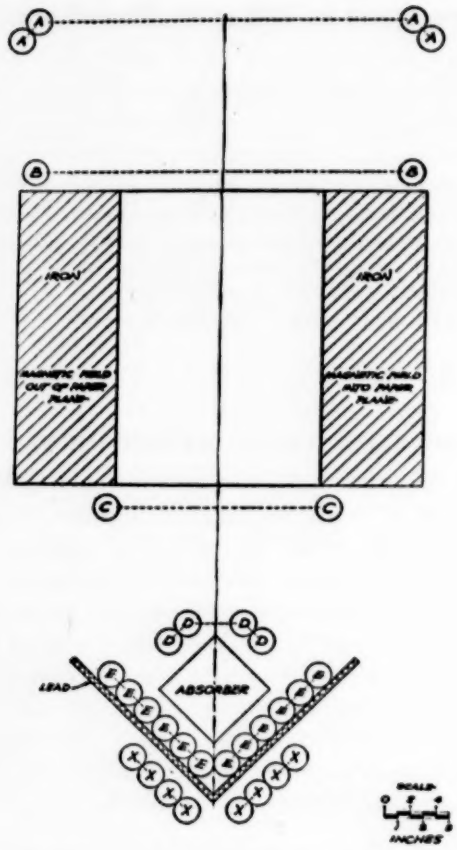

FIG. 1. Experimental arrangement used to investigate decay phenomena of positive and negative mesotrons in different absorbers.

of a square loop, having a width of 8 inches and a height of 24 inches. A coil winding of 4250 ampere turns on two legs of this loop provided an average magnetic induction of 10,000 gauss inside the iron. Counters A and B defined two beams of particles entering the iron piece. Counters C and D defined two beams of mesotrons of the same sign emerging from the iron. The diagram shows the magnetic field so that predominantly negative mesotrons are incident on the absorber.

After plotting the path of mesotrons passing through the magnetized iron, the counters A, B, C, and D were placed along this path so that mesotrons emerging from the iron would have a low momentum value ($p \cong 10^8$ ev/c) and be stopped in the absorber. The path of the mesotrons was determined by a step by step method, taking the energy loss resulting from ionization inside the iron into account. Mesotrons emerging with the above momentum would have to enter the iron piece with a momentum of about 9×10^8 ev/c. If mesotrons entered with momentum values considerably less than 9×10^8 ev/c, they would be stopped in the iron, while mesotrons entering with momentum values considerably greater would miss counters D. The permissible entering mesotron momentum range for the counter path $ABCD$ was estimated to be between 8×10^8 ev/c and 10.5×10^8 ev/c. Mesotrons possessing the upper momentum limit would not be stopped in the absorber, even when using iron as an absorbing material.

Dotted lines between counters indicate a parallel connection. Connecting more than four counters together was avoided because of the slow rise time of the signals arising from such a combination. An electronic mixing system was provided for multiple inputs coming from a set of counters being used for the same purpose. The four counter sets A, B, C, and D were connected into a coincidence unit, and the counters X were connected in anticoincidence with the fourfold coincidence set. The counters E surrounding the absorber were used to detect decay electrons arising from mesotrons stopped in the absorber. A coincidence $ABCD$ usually indicated the passage of a mesotron of one sign through the magnetized iron and into the absorber. An anticoincidence $ABCD-X$ usually indicated that the mesotron had either stopped in the absorber or in the one-half inch lead layer located between E and X. The anticoincidence system was not completely effective in that the X counters did not entirely cover the solid angle subtended by the fourfold coincidence set and in that particles could pass between the X counters. The one-half inch lead layer was placed between the absorber and the X counters to prevent decay electrons from discharging the X counters and thereby nullifying a mesotron anticoincidence $ABCD-X$.

Absorber materials used in the experiment had the following weights and dimensions:

Absorber	*Dimensions*	*Weight*
Boron surrounded by iron container weighing 3600 g	$4\frac{1}{2}''\times6''\times18''$	10,700 g (boron)
Carbon	$6''\times6''\times36''$	42,500 g
Aluminum	$6''\times6''\times30''$	47,700 g
Iron	Six pieces ($\frac{1}{4}''\times6''\times36''$) occupying a space of $6''\times6''\times36''$	41,500 g

III. ELECTRONIC UNITS

A block diagram of the electronic units used in this experiment is shown in Fig. 2. A standard coincidence and anticoincidence unit having a resolving time of 1.5 microseconds was used to furnish signals to drive mechanical registers recording these two events. A coincidence *CD* was used to provide a time signal when the mesotron entered the absorber material. This signal was delayed by about 3 microseconds by a delay line and then made square for a duration of 10 microseconds by a multivibrator before going to one input of a triple coincidence unit. The anticoincidence signal was introduced into a second input of the triple coincidence unit after having been made square for 20 microseconds with a multivibrator. The decay electron pulse from the *E* counters was fed into a third input of the coincidence unit after first having been made square for 20 microseconds and then converted with a blocking oscillator into a signal having a fast rise time and a decay time of about one microsecond.

The purpose of first making the decay electron signal square was to eliminate decay electron counts arising from mesotrons stopped in the lead layer. Thus, a mesotron stopping in this lead layer would almost invariably pass through one of the *E* counters. This would trigger the 20-microsecond multivibrator connected to the *E* counters and make it impossible for any subsequent decay electron pulses occurring in the next 20 microseconds from the *E* counters to be transmitted to the triple coincidence unit. The 20-microsecond square signal produced when any of the *E* counters were discharged also eliminated decay electron counts arising from mesotrons being absorbed in the lower half of the walls of the *E* counters.

The register attached to the triple coincidence unit recorded signals from the *E* counters when they were delayed against a *CD* coincidence in the range from 2.3 to 12.5 microseconds. Furthermore, such signals could be recorded only when an anticoincidence, $ABCD-X$, occurred. Because of natural time lags in the *C* and *D* counters, the *CD* coincidence signal lagged the passage of the mesotron on the average by about 0.3 or 0.4 microsecond. This meant that a decay electron could not be recorded until about 2.6 microseconds, on the average, had elapsed from the passage of the mesotron. The 10-microsecond multivibrator in the *CD* coincidence line determined the time interval in which decay electron pulses could be recorded. The multivibrator in the anticoincidence line was made twice as long as to insure coverage of the *CD* coincidence multivibrator signal.

The purpose of permitting delayed counts from counters *E* to begin recording at the rather large time lag of 2.3 microseconds after the *CD* coincidence was to make very certain that natural time lags from the *E* counters would not enter into the observed delayed count. An additional channel, not shown in Fig. 2, was made to record decay electrons which were delayed within the interval 1.2 to 12.5 microseconds. Natural time lags from the *E* counters were noticed in this interval, and therefore data from this channel are not included in this report. The delay time setting of 2.3 microseconds also aided in giving the anticoincidence signal ample time to reach the triple coincidence unit ahead of the *CD* coincidence signal. Serious disadvantages of this large time delay were to considerably reduce the decay electron counting rate, and to obscure the observation of decay phenomena occurring with

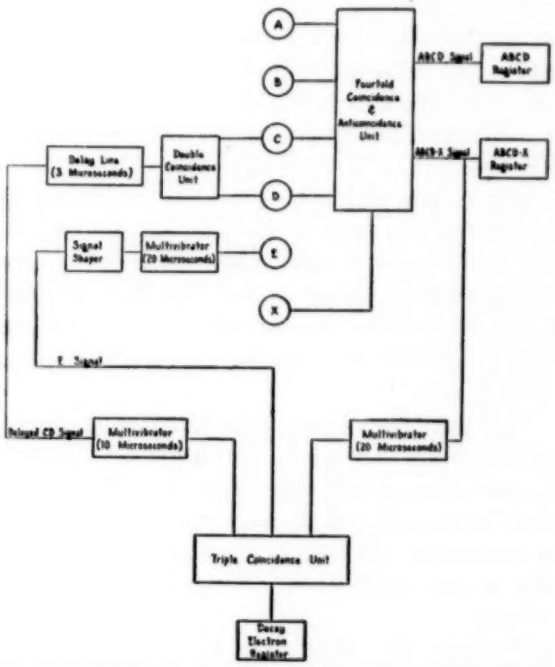

FIG. 2. Block diagram of electronic units connected to experimental arrangement shown in Fig. 1.

TABLE I. Experimental results.

Absorber material	Mesotron sign	Coincidences ($ABCD$) per hour	Ratio of positive to negaive coincidence rate	Anticoincidences ($ABCD-X$) per hour	Ratio positive to negative anticoincidence rate	Total running time for delayed counts	Total delayed counts	Delayed counts per hour	Delayed counting rate corrected for positive mesotron excess
Boron (in iron contiiner)	Positive	46.7 ±0.4	1.10 ±0.01	18.5 ±0.2(5)	1.19 ±0.02	380 hrs.	66	0.17 ±0.02	0.14 ±0.02
	Negative	42.5 ±0.4		15.5 ±0.2(5)		350 hrs.	27	0.08 ±0.01(5)	0.11 ±0.01(5)*
Carbon	Positive	47.5 ±0.4	1.10 ±0.01	19.0 ±0.2(5)	1.16 ±0.02	310 hrs.	53	0.17 ±0.02(5)	0.14(5) ±0.02(5)
	Negative	42.6 ±0.4		16.4 ±0.2(5)		295 hrs.	32	0.11 ±0.02	0.11 ±0.02
	Both signs (no magnetic field)	30.7 ±0.7		10.7 ±0.4		65 hrs.	4	0.06 ±0.03	
Aluminum	Positive	45.2 ±0.4	1.10 ±0.01	20.1 ±0.3	1.17 ±0.03	320 hrs.	64	0.20 ±0.02(5)	0.17 ±0.02(5)
	Negative	41.0 ±0.4		17.2 ±0.3		265 hrs.	6	0.02 ±0.01	0.02 ±0.01
Iron	Positive	47.6 ±0.5	1.09 ±0.02	19.7 ±0.3	1.18 ±0.03	150 hrs.	27	0.18 ±0.03(5)	0.15 ±0.03(5)
	Negative	43.5 ±0.5		16.7 ±0.3		150 hrs.	3	0.02 ±0.01	0.02 ±0.01
	Both signs (no magnetic field)	31.0 ±0.8		11.5 ±0.5		50 hrs.	2	0.04 ±0.03	
None	Positive	47.0 ±0.4	1.11 ±0.01	16.7 ±0.3	1.18 ±0.03	260 hrs.	8	0.03 ±0.01	0.02(5) ±0.01
	Negative	42.5 ±0.4		14.2 ±0.3		240 hrs.	6	0.02(5) ±0.01	0.02(5) ±0.01

* This value is corrected for effect of iron container surrounding boron absorber (see text).

very short periods. Decay processes having mean lifetimes of approximately 0.6 microsecond or less would not be detected in the present experiment.

IV. RESULTS AND DISCUSSION

Results obtained from the experiment are tabulated in Table I. In all cases the standard error is given.

The coincidence rates indicate a positive mesotron excess between 9 and 11 percent, while the anticoincidence rates show a positive mesotron excess between 16 and 19 percent. The anticoincidence figures have been chosen for positive-excess corrections applied to the delayed counting rate since they indicate the excess of positive mesotrons stopped in the absorber producing the decay electrons (and in the ½-inch lead layer). As will be shown later, the result obtained from the anticoincidence rates is less affected by scattering phenomena; furthermore, it agrees better with positive-excess results obtained by other investigators.[6]

The anticoincidence rate does not change greatly from that when no absorber is present to that when an absorber is inserted. This shows that the majority of the anticoincidences are due to mesotrons stopped in the lead absorber and also to the inefficiency of the anticoincidence arrangement. However, the corrected decay electron counting rate from positive mesotrons increases over the background rate by factors between 6 and 7 when an absorber is inserted. Therefore practically all of the observed delayed counts arise from decay processes in the absorber material.

The background effect was taken as the counting rate observed with no absorber in place. The background count observed on the decay electron register was almost entirely due to accidental or chance coincidences occurring between signals from counters E and anticoincidence signals. This fact was checked by carrying out long natural runs with no absorber, as well as by conducting short runs in which artificial anticoincidences were rapidly fed into the circuit while counters E were operating normally. In both cases, one delayed count was recorded for approximately every 700 anticoincidences.

The delayed counting rate from positive mesotrons does not vary greatly for the different absorbers. Undoubtedly, in the case of boron, where not much material was available, the rate was limited by the number of mesotrons stopped in the boron and, in the case of iron, the limiting factor was the short range of the decay electrons compared to the thickness of absorber used. The carbon and iron absorbers were chosen to be of approximately the same total size and weight. The fact that the positive delayed counting rates are the same for both these absorbers indicates

[6] H. Jones, Rev. Mod. Phys. 11, 235 (1939); D. J. Hughes, Phys. Rev. 57, 592 (1940); G. Bernardini, M. Conversi, E. Pancini, E. Scrocco, and G. Wick, Phys. Rev. 68, 109 (1945).

roughly that the decay of positive mesotrons is not affected by atomic number.

In order to compare the delayed counting rates from positive and negative mesotrons, the extreme right column has been corrected for the positive mesotron excess. This positive-excess correction was taken as that determined from the anticoincidence counting rate for each absorber.

The delayed counting rate results obtained from the carbon and iron absorbers agree with the results obtained by other investigators for these absorbers. For carbon, the corrected decay electron counting rates from positive and negative mesotrons are almost equal; considering the attached errors, the rates might be taken as equal. However, for iron, the delayed counting rate from negative mesotrons is the same as the background rate; this indicates that no negative mesotrons, or very few, exist longer than 2.3 microseconds after being stopped in the iron, and that the probability of capture per second greatly exceeds the probability of the normal (positive) decay.

The new absorbers, boron and aluminum, investigated in this experiment show the same results as carbon and iron, respectively. A correction has been applied to the negative delayed counting rate from boron on account of the iron container. The iron container accounted for 25 percent of the total absorber weight, and an estimated correction has been made on this weight basis. It is evident from these results that the transition element or element in which the decay constant (for positive mesotrons) equals the capture probability per second (for negative mesotrons) lies between carbon and aluminum. The transition zone is being investigated in further experiments.

The corrected delayed counting rate for positive mesotrons is observed to be slightly higher than that for negative mesotrons for the boron and carbon absorbers. Because of the large error, it is difficult to tell if this fact is significant or not. It means either that the correction for the positive excess is not large enough or that capture processes occur to a small extent in these light elements.

In order to check scattering phenomena, two short runs were taken in the case of the iron and carbon absorbers with no magnetic field. In order to minimize scattering the counter sets A, B, C, and D were placed so that a particle traveling in a straight line could not possibly pass through all of these counter sets. Considerable scattering is in evidence by the rather high coincidence and anticoincidence rates. However, with magnetic field, there is evidence that practically complete cut-off is obtained for mesotrons of the opposite sign. This is indicated by the fact that the delayed counting rate from negative mesotrons for the aluminum and iron absorbers is the same as that with no absorber. If positive mesotrons were scattered into the above absorbers when the magnetic field was set for negative mesotrons, the delayed counting rate would be expected to be above the background rate. These arguments also indicate that with magnetic field the anticoincidence counting rate is largely due to mesotrons of only one sign.

The author wishes to express his appreciation to the Research Corporation of New York for a research grant-in-aid of this work. The cooperation and assistance of Dr. Darol Froman of the Los Alamos Scientific Laboratory and Dr. V. H. Regener of the University of New Mexico is also gratefully acknowledged.

Transients in Townsend Discharges

ROBERT R. NEWTON
Bell Telephone Laboratories, Murray Hill, New Jersey
(Received November 24, 1947)

An analysis is made of the transients in Townsend discharges for certain stepwise variations in the stimulating photoelectric current from the cathode, while the voltage across the tube is held steady. The method of analysis can be readily generalized to include any type of variation in the photoelectric current. The steady-state current, including the effects of metastable molecules produced in the gas, is also derived; from this result it is shown that the second Townsend coefficient is a function of the electrode spacing. The work also suggests experiments which can separate the radiation, ion, and metastable contributions to the second Townsend coefficient.

I. INTRODUCTION

WE shall consider in this paper only gas discharges between infinite plane-parallel electrodes, operating below breakdown. Under these conditions, the current through the discharge is not self-sustaining, but must be stimulated by a primary current i_0. This primary current is usually obtained by illuminating the cathode with a source of light which is external to the discharge. It is well known that the steady-state current through the discharge, under these conditions, is given approximately by an expression of the form:

$$i=i_0 \exp[\alpha_i(X-x_0)]/ [1-\gamma(\exp[\alpha_i(X-x_0)]-1)]. \quad (1)$$

In this, X is the separation of the electrodes, and α_i, γ, and x_0 are considered to be functions only of the gas pressure and the electric field and are independent of X.

In (1), α_i, called the first Townsend coefficient, is interpreted as the number of ionizing collisions which one electron makes while traveling one cm in the direction of the electric field, and x_0 is interpreted as the distance that an electron must travel before acquiring ionizing energy. γ is interpreted as representing the number of electrons emitted from the cathode under the influence of events which occur in the discharge, as we shall describe more fully below.

Our fundamental picture of a gas discharge will be as follows: An electron which leaves the cathode encounters a certain number of gas molecules while traveling to the anode. If one of these collisions is inelastic, there may be three possible results: (1) the molecule may be ionized, with the simultaneous release of an electron; (2) the molecule may be excited to a level from which it can decay by radiation; (3) the molecule may be excited to a metastable level. Subsequently, electrons may be emitted from the cathode (1) upon impact of a positive ion, (2) when radiation from an excited molecule strikes the cathode, and (3) when a metastable molecule strikes the cathode. (2) above is, of course, an example of photoelectric emission. Processes (1) and (3) have been studied experimentally by Oliphant,[1] and theoretically by Massey[2] and Cobas and Lamb.[3]

As we shall show formally in later sections, this mechanism leads to an expression for γ in Eq. (1), which is the sum of three terms, one each from the electron emission caused by radiation, ions, and metastables. It is of great interest to be able to separate these terms experimentally. This separation cannot be performed accurately by measurements of the steady-state current through a discharge but, as Engstrom and Huxford[4] have pointed out, it can be made by an analysis of the transient currents.

The basis for the separation lies in the different times required for radiation, ions, and metastables to produce effects at the cathode. Suppose that the discharge is initiated by an electron leaving the cathode. At a field of 50 volts/cm, an X of 1 cm, and a pressure of 1 mm, this electron and the ones released by ionization in the gas reach the anode in the order of 10^{-8} sec. The

[1] M. L. E. Oliphant, Proc. Roy. Soc. **A124**, 228 (1929).
[2] H. S. W. Massey, Proc. Camb. Phil. Soc. **26**, 386 (1930); Proc. Camb. Phil. Soc. **27**, 460 (1931).
[3] A. Cobas and W. E. Lamb, Phys. Rev. **65**, 327 (1944).
[4] R. W. Engstrom and W. S. Huxford, Phys. Rev. **58**, 67 (1940).

time required for an excited molecule to radiate, and for the radiation to reach the cathode and produce a photoelectron, is also of the order of 10^{-8} sec. An ion, drifting under the field, does not reach the cathode for about 10^{-6} sec., while a metastable, which must reach the cathode by diffusion, requires the order of 10^{-3} sec. Thus, transients should show three relatively distinct phases, governed by these differences in time required to produce new electrons at the cathode. These three phases are shown schematically in Fig. 1.*

The first phase, of duration about 10^{-8} sec., in which the first electrons are crossing the tube and new photoelectrons are being produced, is probably too short for observation by present techniques. Accordingly, we shall not analyze its form but shall show how to allow for its effect upon other phases.

The second phase, of duration about 10^{-6} sec. and characterized by the first arrival of ions at the cathode, has not previously been analyzed. We shall obtain its form and shall show how, under certain conditions, it contains discontinuities in the current.[5] Observation of these discontinuities may afford a convenient method of measuring α_i and the ion contribution to γ.

The third phase, of duration about 10^{-3} sec. and characterized by the first arrival of metastables at the cathode, has been studied by Engstrom and Huxford.[4] We shall analyze it by a different method and in somewhat greater detail, thus obtaining a different form for the results.

We shall perform the analysis by setting up boundary value problems to be satisfied by the densities of ions and metastables in the gas. Different types of transient are then obtained by solving these problems subject to different initial conditions and to different forms of i_0 as a function of time. Steady-state currents are also found by getting the time-independent solutions of the boundary value problems; from the steady-state currents, we can evaluate γ in (1) above. This process leads to no new results for the contribution of ions to γ, but, for the metastable contribution to γ, shows that γ is not in fact a constant but is dependent upon X.

Sections II through V will be devoted to the formal solution, and Section VI to a discussion of the results. A list of frequently used symbols is given below.

We shall assume that α_i and x_0 are constant from point to point within the discharge. For a discussion of these assumptions and a general survey of the field we refer the reader to Loeb[6] and to Druyvesteyn and Penning.[7] We shall neglect collisions of a molecule with more than one electron, and collisions of ions or excited molecules with each other.

List of Symbols

The following symbols are frequently used throughout this paper. We have not listed symbols which occur infrequently and in only a limited part of the paper.

α_i = number of ions formed per electron per cm; equals first Townsend coefficient.
α_m = number of metastables formed per electron per cm.
α_r = number of radiating molecules formed per electron per cm.

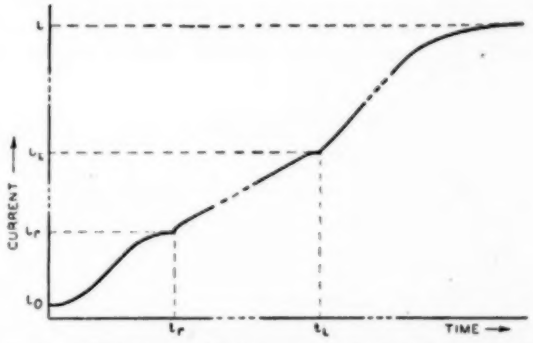

FIG. 1. Sketch of a discharge transient. i_0 = stimulating photo-current. i_r = radiation steady state. i_i = ion steady state. i = true steady state. t_r = duration of radiation transient. t_i = duration of ion transient. The scales are broken in order to display the entire transient.

* *Note added in proof:* In this paper, the phenomenon termed "imprisonment of resonance radiation" has been ignored. The significance of this phenomenon, which was first studied theoretically by K. T. Compton (Phys. Rev. **20**, 283 (1922)) was brought to our attention by T. Holstein (see Phys. Rev. **72**, 1212 (1947)). As a result of this phenomenon, the time required for radiation to reach the cathode, instead of being short, may equal or exceed the transit time of ions. The analysis of this paper is valid whenever the two times are significantly different; if the two times are approximately equal, a more complicated analysis will be necessary.

[5] This part of the present paper was presented before the American Physical Society on May 3, 1945. See Phys. Rev. **72**, 184 (1947).

[6] L. B. Loeb, *Fundamental Processes of Electrical Discharge in Gases* (John Wiley and Sons, Inc., New York, 1939).

[7] M. J. Druyvesteyn and F. M. Penning, Rev. Mod. Phys. **12**, 87 (1940).

$A_i = \alpha_i X$.
$A_m = \alpha_m X M_i M_r$.
γ = parameter occurring in steady state discharge current; very nearly equals second Townsend coefficient divided by α_i.
γ_i = number of electrons released from cathode per positive ion striking.
γ_m = number of electrons released from cathode per metastable striking.
γ_r = number of electrons released from cathode per photon striking.
$\eta = 1 - \xi_0$.
i = current density in electronic charges per cm².
i subscript: denotes a parameter characteristic of positive ions.
i_0 = stimulating photo-current from cathode, in electronic charges per cm².
i_+ = current density carried by ions.
i_- = current density carried by electrons.
κ = square root of diffusion coefficient for metastables.
λ = square root of reciprocal of time constants for metastable decay.
m subscript: denotes a parameter characteristic of metastables.
M_0 = ratio of i_- to current of electrons leaving one cm² of cathode.
M_i = amplification of i_0 resulting from ion effects.
M_m = amplification of i_0 resulting from metastable effects.
M_r = amplification of i_0 resulting from radiation effects.
N, N_a, N_c = parameters occurring in boundary conditions for metastable diffusion.
ρ = density of ions or metastables, as shown by subscript.
P_i = density of ions when expressed in the moving coordinate system y.
r subscript: denotes a parameter characteristic of radiation or radiating molecules.
t = time in sec.
τ = dimensionless time used in ion flow = vt/X.
T = dimensionless time used in metastable flow = $\kappa^2 t/X^2$.
Θ = effective solid angle presented by cathode to radiation from the gas.
v = ion velocity.
x = distance from cathode in cm.
x_0 = distance in cm which an electron must travel to acquire ionizing energy.
X = electrode spacing.
ξ = dimensionless $x = x/X$.
ξ_0 = dimensionless $x_0 = x_0/X$.
y = moving coordinate in ion flow = $x + vt$.

II. AMPLIFICATION BY IONIZATION AND RADIATION

We shall assume that electrons cross the tube in negligible time. As a result of ionizations in the gas, more electrons reach the anode than leave the cathode. Suppose n_0 electrons leave one sq. cm of the cathode at some instant, and let n be the number of electrons per cm² which reach a distance x from the cathode. Then:

$$dn/dx = \alpha_i n,$$
$$n = n_0 \exp \alpha_i (x - x_0), \quad x \geq x_0. \tag{2}$$

For $x < x_0$, $n = n_0$.

Let α_r be the number of excited molecules created per electron per cm. (By excited, we shall mean that the molecules are raised to a level from which they can radiate photons of sufficient energy to eject photoelectrons from the cathode. Thus metastable molecules are not excited in this sense.) The number of excited molecules per cm² created in a distance dx is $\alpha_r n dx$, if x is greater than x_r, the distance an electron must travel to acquire excitation energy, and n is given by (2) above. For brevity, we shall neglect the difference between x_0 and x_r; the difference can readily be included if desired. If x is less than x_r, the number of excited molecules is 0.

Let $\Theta/4\pi$ be the probability that a photon radiated at the distance x will reach the cathode. $\Theta = 2\pi$ if absorption in the gas is negligible. Let γ_r be the number of secondary electrons per photon. Then we have for the number of secondary electrons:

$$\alpha_r \gamma_r n_0 \int_{x_0}^{X} (\Theta/4\pi) \exp[\alpha_i (x - x_0)] dx.$$

However, these secondary electrons can produce more secondary electrons, and so on. We assume that all these secondaries are emitted in negligible time, so that the effect of radiation is to increase the number of electrons leaving the cathode from n_0 to:

$$n_0 \sum_{j=0}^{\infty} \left\{ \alpha_r \gamma_r \int_{x_0}^{X} (\Theta/4\pi) \exp[\alpha_i (x - x_0)] dx \right\}^j$$
$$= n_0 \Big/ \left\{ 1 - \alpha_r \gamma_r \int_{x_0}^{X} (\Theta/4\pi) \times \exp[\alpha_i (x - x_0)] dx \right\}, \tag{3}$$

when the geometric series converges. We shall call the factor by which n_0 is multiplied M_r, the multiplication factor for radiation.

III. EQUATIONS FOR THE ION AND METASTABLE DENSITIES

Let $\rho_i(x, t)$ be the density of ions and $\rho_m(x, t)$ the density of metastables at time t at a distance x from the cathode. We assume that the ions have a uniform velocity v, so that the current of ions per cm² at any point is $-v\rho_i(x, t)$. We assume that the metastables move by diffusion with a coefficient κ^2, so that the current of metastables per cm² is $-\kappa^2(\partial\rho_m/\partial x)$.[8] Thus, the flow equations for ρ_i and ρ_m are:

$$\frac{\partial\rho_i}{\partial t}-\frac{\partial}{\partial x}(v\rho_i)=S_i(x, t),$$

$$\frac{\partial\rho_m}{\partial t}-\frac{\partial}{\partial x}\left(\kappa^2\frac{\partial\rho_m}{\partial x}\right)=S_m(x, t),$$

where S_i and S_m are functions, now to be set up, which give the numbers of ions and metastables created per cm³ per sec.

Let γ_i be the number of electrons liberated per positive ion striking the cathode, and γ_m the number of electrons per metastable. Then the total number of electrons leaving the cathode per cm² per second is:

$$M_r[i_0+\gamma_i v\rho_i(0, t)+\gamma_m\kappa^2\rho_m'(0, t)],$$

in which a prime denotes $\partial/\partial x$, and i_0 is the primary current density measured in electrons per cm² per sec. To get the number of electrons per cm² per sec. at a distance x from the cathode, we multiply by unity for $x\leq x_0$ and by $\exp[\alpha_i(x-x_0)]$ for $x\geq x_0$. If α_i is the number of ions formed per electron per cm, and α_m the number of metastables, we have:

$$\frac{\partial\rho_i}{\partial t}-v\frac{\partial\rho_i}{\partial x}=\begin{cases}0, & x\leq x_0,\\ \alpha_i M_r[i_0+\gamma_i v\rho_i(0, t)\\ \quad+\gamma_m\kappa^2\rho_m'(0, t)]\exp[\alpha_i(x-x_0)], & x\geq x_0.\end{cases}\quad(4)$$

$$\frac{\partial\rho_m}{\partial t}-\kappa^2\frac{\partial^2\rho_m}{\partial x^2}=\begin{cases}0, & x\leq x_0,\\ \alpha_m M_r[i_0+\gamma_i v\rho_i(0, t)\\ \quad+\gamma_m\kappa^2\rho_m'(0, t)]\exp[\alpha_i(x-x_0)], & x\geq x_0.\end{cases}\quad(5)$$

In these, we have taken the minimum distance at which metastables are formed to be the same as that at which ions are first formed, namely, x_0.

As auxiliary conditions to (4) and (5), we must know the forms of $\rho_i(x, t)$ and $\rho_m(x, t)$ when $t=0$. These depend upon the type of transient being studied. In addition, there are certain conditions imposed upon ρ_i and ρ_m at the electrodes. For ρ_i, there is only one condition, which can be derived from the flow conditions at the anode:

$$\rho_i(X, t)=0.\quad(4a)$$

The conditions on ρ_m are more complicated. We expect the boundary conditions to be homogeneous in ρ_m and ρ_m', and hence to be of the form:

$$\begin{aligned}\rho_m(0, t)-N_c X\rho_m'(0, t)&=0,\\ \rho_m(X, t)+N_a X\rho_m'(X, t)&=0,\end{aligned}\quad(5a)$$

which implies a relation between the density and the metastable molecular current at the boundaries. If both electrodes are of the same material, $N_c=N_a=N$. The sign is different in these two conditions because the normals to the two electrodes are oppositely directed.

To evaluate N, we proceed as follows: The number of particles crossing unit area per sec. at any point because of the random thermal motion is $\rho_m(kT/2\pi m)^{\frac{1}{4}}$. Considering also those which cross because of diffusion, the total number crossing unit area per sec. in the negative x direction is $\rho_m(kT/2\pi m)^{\frac{1}{4}}+\frac{1}{2}\kappa^2\rho_m'$. The number crossing in the positive x direction is

$$\rho_m(kT/2\pi m)^{\frac{1}{4}}-\tfrac{1}{2}\kappa^2\rho_m',$$

so that the net flow is $\kappa^2\rho_m'$ in the negative x direction. From continuity, $\kappa^2\rho_m'(0, t)$ must equal the number of metastables destroyed at the cathode per cm² per sec. The work of Oliphant[1] indicates that one electron is emitted for each metastable destroyed, and hence that γ_m is the probability of destruction for a metastable striking the cathode. Therefore:

$$\gamma_m[\rho_m(0, t)(kT/2\pi m)^{\frac{1}{4}}+\tfrac{1}{2}\kappa^2\rho_m'(0, t)]=\kappa^2\rho_m'(0, t).$$

Thus:

$$N=(\kappa^2/X)(2\pi m/kT)^{\frac{1}{4}}(\gamma_m^{-1}-\tfrac{1}{2}).\quad(5b)$$

Using the kinetic theory expression for κ^2, this is approximately

$$N=(4l/3X)(\gamma_m^{-1}-\tfrac{1}{2}),$$

[8] These assumptions require that X equal many mean free paths. If the assumption that α_i is constant is met, we may expect that this is met.

where l is the mean free path of a metastable in an atmosphere of normal molecules. This has two important limiting cases; if $\gamma_m=0$, N is infinite, and we must have $\rho_m'(0,t)=0$. If $l/X\ll\gamma_m$, we have very nearly that $\rho_m(0,t)=0$.

IV. ION TRANSIENT AND STEADY-STATE CURRENTS

In the first several microseconds, ions can cross the tube a number of times before the metastables have moved appreciably. To study the operation of the tube during this interval, we can set $\gamma_m=0$ in Eq. (4). Also, let $\epsilon(w)$ be the step function defined by:

$$\epsilon(w)=\begin{cases}1, & w\leq 0,\\ 0, & w\geq 0.\end{cases}$$

The use of this step function avoids some trouble with limits. (4) now becomes:

$$(\partial\rho_i/\partial t)-v(\partial\rho_i/\partial x)=\alpha_i M_r[i_0+\gamma_i v\rho_i(0,t)]\times\exp[\alpha_i(x-x_0)]\epsilon(x-X)\epsilon(x_0-x). \quad (6)$$

General Solution

For brevity, let

$$\phi(x)=\alpha_i M_r\exp[\alpha_i(x-x_0)]\epsilon(x-X)\epsilon(x_0-x).$$

Also, transform the independent variables from x, t to t and $y=x+vt$, and let $\rho_i(x,t)=P_i(y,t)$. y is obviously a coordinate which moves with the stream of ions. Equation (6) now reads:

$$\partial P_i/\partial t=[i_0+\gamma_i v P_i(vt,t)]\phi(y-vt). \quad (6a)$$

We shall solve (6a) for an arbitrary form of $\phi(x)$, and for any variation of i_0 with t.

Solutions of (6a) which have the proper form at $t=0$ are also solutions of the integral equation:

$$P_i(y,t)=P_i(y,0)+\int_0^t\phi(y-vt')\times[i_0+\gamma_i v P_i(vt',t')]dt'. \quad (7)$$

The current can be calculated once the ion density is known. The current carried by positive ions is:

$$i_+(t)=(v/X)\int_0^X\rho_i(x,t)dx=(v/X)\int_{vt}^{vt+X}P_i(y,t)dy, \quad (8a)$$

in electronic charges per cm² per sec. The number of electrons leaving unit area of the cathode per second is

$$M_r[i_0+\gamma_i v\rho_i(0,t)]=M_r[i_0+\gamma_i v P_i(vt,t)].$$

In addition to these electrons, we have those which are formed in the gas and which do not traverse the entire distance X. Since $\phi(x)/M_r$ is the number of new electrons created per cm per electron leaving the cathode, we get the total current carried by electrons if we multiply the number of electrons leaving the cathode by:

$$M_g=1+\int_0^X[\phi(x)/M_r][(X-x)/X]dx.$$

This weights each electron according to the distance it travels in reaching the anode.[9] The current carried by electrons is therefore:

$$i_-(t)=M_r M_g[i_0+\gamma_i v P_i(vt,t)]. \quad (8b)$$

With the aid of this, we can replace (7) by a simpler equation. Substituting from (8b) for the quantity in square brackets in (7), we have for $y=vt$:

$$P_i(vt,t)=P_i(vt,0)+\int_0^t\phi(vt-vt')[i_-(t')/M_r M_g]dt'.$$

Substituting this back into (8b):

$$i_-(t)=M_r M_g[i_0+\gamma_i v P_i(vt,0)]+\gamma_i v\int_0^t\phi(vt-vt')i_-(t')dt'. \quad (9)$$

This equation can be solved for $i_-(t)$, then $P_i(vt,t)$ can be computed from (8b), and $P_i(y,t)$ and $i_+(t)$ can be computed from (7) and (8a), respectively.

Equation (9) is readily solved by Picard's method. Let:

$$i_-(t)=\sum_{n=0}^{\infty}i_-^{(n)}(t),$$

$$i_-^{(0)}(t)=M_r M_g[i_0+\gamma_i v P_i(vt,0)], \quad (10)$$

$$i_-^{(n+1)}(t)=\gamma_i v\int_0^t\phi(vt-vt')i_-^{(n)}(t')dt', \quad n=0,1,2,\cdots.$$

[9] W. Shockley, J. App. Phys. 9, 635 (1938).

If the sum exists, it is obviously the required solution.

Steady-State Current

Before applying (10) we derive the "steady-state" current. This has significance, in the first place, only if i_0 is constant and in the second place only if the ions can traverse the tube many times before metastables begin to reach the cathode in appreciable numbers. Under these circumstances, this steady-state current will be sensibly reached before the beginning of the metastable transient.

We find the steady state ion density $\rho_i(x, \infty)$ by setting $\partial/\partial t=0$ in Eq. (6) and integrating. The constant of integration is determined by the condition that $\rho_i(X, t)=0$. The result is:

$$\rho_i=(i_0/v)\left[\int_x^X \phi(x')dx'\right]\Big/\left[1-\gamma_i\int_0^X \phi(x')dx'\right].$$

The current is then found by applying formulas (8a) and (8b). If $\phi(x)$ is given by Eq. (6), the current has the well-known form:

$$i_i=i_0M_\tau \exp[\alpha_i(X-x_0)]/(1+\gamma_iM_\tau-\gamma_iM_\tau \times\exp[\alpha_i(X-x_0)]). \quad (11)$$

Pulse Transient

By a pulse transient we mean one resulting from a single pulse of stimulating current occurring at $t=0$. For this transient $i_0=0$ for $t>0$. We assume that n_0 primary electrons are released from the cathode in negligible time at $t=0$ and that these are instantly increased to $M_\tau n_0$, where M_τ is defined below Eq. (3). Then:

$$P_i(y, 0)=n_0\phi(y).$$

We now find P_i and the current by substituting into Eqs. (10), (8a), and (8b).

When we return to our original assumption about the form of $\phi(x)$, that is, to the form of Eq. (6) with a constant α_i, we obtain the following results:

$$\rho_i(x, t)=\alpha_iM_\tau n_0 \exp[A_i(\xi-\xi_0+\tau)] \times\sum_{n=0}^{\infty}(A_iM_\tau\gamma_ie^{-A_i\xi_0})^nI_n(\tau, \xi_0, \xi), \quad (12a)$$

$$i/\alpha_ivM_\tau n_0=(A_i)^{-1}\exp[A_i(\tau-\xi_0)] \times\Big\{\exp[\max A_i(1-\tau), 0] -\exp[\max A_i(\xi_0-\tau), 0] +\sum_{n=1}^{\infty}(A_iM_\tau\gamma_ie^{-A_i\xi_0})^n\int_{\tau-1}^{\tau}I_{n-1}(\tau', \xi_0, 0) \times(\exp[A_i(\tau'-\tau+1)] -\exp[\max A_i(\tau'-\tau+\xi_0), 0])d\tau'\Big\} +M_\tau\gamma_i(A_i)^{-1}\exp[A_i(\tau-\xi_0)] \times(\exp[A_i(1-\xi_0)]+A_i\xi_0-1) \times\sum_{n=0}^{\infty}(A_iM_\tau\gamma_ie^{-A_i\xi_0})^nI_n(\tau, \xi_0, 0). \quad (12b)$$

These are expressed in terms of dimensionless variables $\tau=vt/X$, $\xi=x/X$, $\xi_0=x_0/X$, and $A_i=\alpha_iX$. The symbol $\max A, B$ means that we use the larger of A or B. Also:

$$I_n(\tau, \xi_0, \xi)=\int_{\tau+\xi-1}^{\min(\tau+\xi-\xi_0),\,\tau} I_{n-1}(\tau', \xi_0, 0)d\tau',$$

$$I_0(\tau, \xi_0, \xi)=\epsilon(\xi+\tau-1)\epsilon(\xi_0-\xi-\tau).$$

In order to express the current we need only the $I_n(\tau, \xi_0, 0)$, which are functions of only two variables. The first three of the $I_n(\tau, \xi_0, 0)$ are:

$$I_0(\tau, \xi_0, 0)=1, \qquad \xi_0\le\tau\le 1.$$

$$I_1(\tau, \xi_0, 0)=\begin{cases}\tau-2\xi_0, & 2\xi_0\le\tau\le 1+\xi_0,\\ 2-\tau & 1+\xi_0\le\tau\le 2.\end{cases}$$

$$I_2(\tau, \xi_0, 0)=\begin{cases}\frac{1}{2}(\tau-3\xi_0)^2, & 3\xi_0\le\tau\le 1+2\xi_0,\\ -\frac{1}{2}(\tau-1-2\xi_0)^2-\frac{1}{2}(2+\xi_0-\tau)^2 & \\ \quad+(1-\xi_0)^2, & 1+2\xi_0\le\tau\le 2+\xi_0,\\ \frac{1}{2}(3-\tau)^2, & 2+\xi_0\le\tau\le 3.\end{cases}$$

Others can readily be generated from the definition. The functions are zero outside the given ranges of τ.

The separate terms in (12a) have a simple physical interpretation. The first term, with $n=0$, is just the initial distribution due to the pulse of n_0 electrons. The term with $n=1$ is the distribution set up by the preceding term, and

so on. Each successive term or "wave" begins a time x_0/v later than the preceding one, and lasts a time X/v longer, so that the waves overlap in a complicated fashion.

The integral

$$\int_0^\infty \exp(a\tau) I_n(\tau, \xi_0, 0) d\tau$$

will be useful. With $n=0$, this can be evaluated immediately. The integral with any other value of n can be expressed in terms of the integral with n decreased by unity by means of the definition of I_n. Thus, by induction, we find:

$$\int_0^\infty \exp(a\tau) I_n(\tau, \xi_0, 0) d\tau = (e^a - e^{a\xi_0})^{n+1}/a^{n+1}.$$

For $a=0$, this gives:

$$\int_0^\infty I_n(\tau, \xi_0, 0) d\tau = (1-\xi_0)^{n+1}.$$

With these results, we can readily compute the total number of electrons which leave the cathode and the total charge transferred through the tube. The first quantity is seen to be:

$$n_0 M_r / \{1+\gamma_i M_r - \gamma_i M_r \exp[\alpha_i(X-x_0)]\}.$$

If we let:

$$M_i = \{1+\gamma_i M_r - \gamma_i M_r \exp[\alpha_i(X-x_0)]\}^{-1}, \quad (13)$$

the total number of electrons leaving the cathode is $n_0 M_r M_i$ and the total charge transferred is

$$n_0 M_r M_i \exp[\alpha_i(X-x_0)].$$

In this notation, Eq. (11) becomes

$$i_i = i_0 M_r M_i \exp[\alpha_i(X-x_0)]$$

for the steady-state current, which is seen to be consistent with the value of the total charge transferred as the result of a pulse.

Finally, it should be noted that the product $M_r M_i$ has the form:

$$M_r M_i = \left\{1 - \alpha_r \gamma_r \int_{x_0}^{X} (\Theta/4\pi) \exp[\alpha_i(x-x_0)] dx + \gamma_i - \gamma_i \exp[\alpha_i(X-x_0)]\right\}^{-1}. \quad (13a)$$

Operating Transients

By this term, we mean those transients which occur when i_0 is changed abruptly from zero to a steady value (the rise) or when i_0 is changed abruptly from a steady value to zero (the fall). It is readily shown that the rise and fall have the same shape, so that we shall solve only for the rise.

We can find this transient by integrating the pulse transient over a suitable time variable or by usings Eqs. (10) with $P_i(vt, 0)=0$. The currents carried by ions and by electrons are:

$$i_+(t) = i_0 M_r A_i \int_\tau^{\tau+1} d\xi \int_{\xi-1}^{\xi-\xi_0} e^{A_i(\xi-\xi_0-\tau')} \times \left[\sum_0^\infty (\gamma_i M_r)^n J_n(\tau', \xi_0)\right] d\tau', \quad (14)$$

$$i_-(t) = i_0 M_r M_g \sum_0^\infty (\gamma_i M_r)^n J_n(\tau, \xi_0),$$

and the positive ion density can be found by application of Eqs. (7) and (8b). The $J_n(\tau, \xi_0)$ are given by:

$$J_0(\tau, \xi_0) = \begin{cases} 0, & \tau \le 0, \\ 1, & \tau \ge 0; \end{cases}$$

$$J_n(\tau, \xi_0) = A_i \int_{\tau-1}^{\tau-\xi_0} e^{A_i(\tau-\xi_0-\tau')} J_{n-1}(\tau', \xi_0) d\tau'.$$

As with the pulse transient, the individual terms have a simple interpretation. The first term, with $n=0$, represents the direct effects of the primary current. Ions formed by the primary current release new electrons from the cathode, whose direct effects are given by the second term, and so on. Unlike the terms in the pulse transient, these terms do not rise from zero and fall back to zero but instead rise from zero to a constant value. The nth term starts from zero at $\tau=n\xi_0$ and reaches a constant value at $\tau=n$. It is readily found that the constant value, which we denote by substituting $\tau=\infty$, is:

$$J_n(\infty, \xi_0) = [\exp A_i(1-\xi_0) - 1]^n.$$

The form of Eqs. (14) is not convenient for large values of t or τ. We can find an approxi-

mate form for large τ, however, by making use of the property just mentioned. For τ equal to an integer k all the $J_n(\tau, \xi_0)$ for which $n \leq k$ have attained their limit while the others are still rising. Neglecting the terms which have not attained their limit, the electron current, for example, is:

$$i_-(\tau=k) \approx i_0 M_\tau M_\theta \sum_{n=0}^{k} (\gamma_i M_\tau)^n \times [\exp\alpha_i(X-x_0)-1]^n. \quad (15)$$

Letting $k \to \infty$, we see that this gives the steady-state electron current, provided that we are below breakdown.

Equation (15) can be used to estimate the rise time of the current, that is, the time required for the current to attain some specified fraction of its steady-state value. Since the current estimated by means of Eq. (15) is always too small, the resulting time is always too large.

V. METASTABLE TRANSIENT AND STEADY-STATE CURRENTS

After the metastables begin to move appreciably, we must solve Eqs. (4) and (5) simultaneously. To do this exactly would be a difficult task; we can get a reasonably accurate solution, however, if we assume that, at each instant, the ion density has the steady-state distribution corresponding to the instantaneous value of the electron current leaving the cathode. In other words, we can drop $\rho_i(0, t)$ from the right member of Eq. (5) provided that we multiply what remains by M_i, as defined by Eq. (13). Then, when we have solved for ρ_m the current is given by Eq. (11), with i_0 replaced by the instantaneous value of $i_0+\gamma_m\kappa^2\rho_m'(0, t)$.

We shall solve for the pulse transient and the falling operating transient, for which $i_0=0$ when $t>0$. For these transients Eq. (5) now reads:

$$\frac{\partial\rho_m}{\partial T}-\frac{\partial^2\rho_m}{\partial\xi^2}=\begin{cases}0, & \xi\leq\xi_0,\\ \gamma_m A_m \exp[A_i(\xi-\xi_0)] \times(\partial\rho_m/\partial\xi)_{\xi=0}, & \xi\geq\xi_0,\end{cases} \quad (16)$$

in terms of the dimensionless variables

$$T=(\kappa^2/X^2)t, \quad \xi=x/X,$$

with $\xi_0=x_0/X$, $A_i=\alpha_i X$, and $A_m=M_\tau M_i\alpha_m X$. This is subject to the conditions:

$$\rho_m(0, T)-N(\partial\rho_m/\partial\xi)_{\xi=0} = \rho_m(1, T)+N(\partial\rho_m/\partial\xi)_{\xi=1}=0.$$

For the pulse transient

$$\rho_m(\xi, 0)=n_0(A_m/X)\exp[A_i(\xi-\xi_0)], \quad \xi\geq\xi_0;$$

$\rho_m(\xi, 0)=0$, $\xi\leq\xi_0$. For the falling operating transient $\rho_m(\xi, 0)$ has the steady-state value which we shall derive later. We are taking N to be the same at cathode and anode.

General Solution

We can solve Eq. (16) by separating the variables. We find that

$$\chi_n(\xi)\exp[-\lambda_n^2 T] \quad (17)$$

satisfies (16) and the conditions at $\xi=0$, 1, provided that χ_n is a solution of

$$(d^2\chi/d\xi^2)+\lambda^2\chi = \begin{cases}0, & \xi\leq\xi_0,\\ -\gamma_m A_m \exp[A_i(\xi-\xi_0)](d\chi/d\xi)_{\xi=0}, & \xi\geq\xi_0,\end{cases} \quad (17a)$$

and that χ satisfies the conditions at $\xi=0$, 1. As we shall see, (17a) has an infinite ordered set of eigenvalues λ_n, so that we can write a solution of Eq. (16) in the form:

$$\rho_m(\xi, T)=\sum a_n\chi_n(\xi)\exp[-\lambda_n^2 T]. \quad (18)$$

The coefficients a_n are then chosen so that this reduces to the given form of $\rho_m(\xi, 0)$ when $T=0$.

Equation (17a) can be satisfied by:

$$\chi(\xi)=\begin{cases}c_1(\sin\lambda\xi+N\lambda\cos\lambda\xi), & \xi\leq\xi_0,\\ c_2\sin\lambda(\xi-\xi_0)+c_3\cos\lambda(\xi-\xi_0) +c_4\exp A_i(\xi-\xi_0), & \xi\geq\xi_0.\end{cases} \quad (19)$$

This satisfies the condition on χ at $\xi=0$. There are four other conditions which must be satisfied: χ and its first derivative must be continuous at $\xi=\xi_0$, χ must satisfy the boundary condition at $\xi=1$, and χ must satisfy (17a). These conditions lead to the equations:

$$\begin{aligned} c_1(\sin\lambda\xi_0+N\lambda\cos\lambda\xi_0)-c_3-c_4&=0,\\ c_1\lambda(\cos\lambda\xi_0-N\lambda\sin\lambda\xi_0)-c_2\lambda-c_4A_i&=0,\\ c_2(\sin\eta\lambda+N\lambda\cos\eta\lambda)+c_3(\cos\eta\lambda-N\lambda\sin\eta\lambda) &\\ +c_4e^{\eta A_i}(1+NA_1)&=0,\\ c_1\gamma_m A_m\lambda+c_4(A_i^2+\lambda^2)&=0, \end{aligned} \quad (20)$$

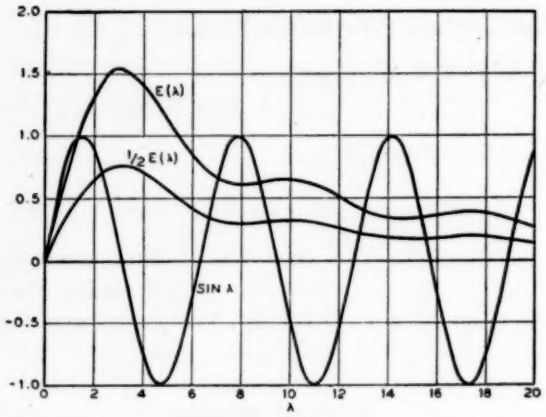

FIG. 2. Functions $\sin\lambda$ and $E(\lambda)$, for $N=0$, $A_i=2$, $\eta=0.9$.

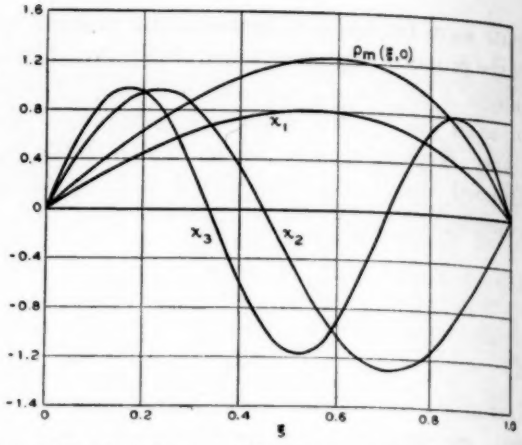

FIG. 3. The first three eigenfunctions, and the steady-state distribution, for $N=0$, $A_i=2$, $\eta=0.9$, $\gamma_m A_m=\frac{1}{2}$.

with $\eta=1-\xi_0$. If these are to have a non-trivial solution for c_1, c_2, c_3, c_4, the determinant of the coefficients must vanish. Multiplied out, this gives for the equation determining the eigenvalues λ:

$$(A_i^2+\lambda^2)[(1-N^2\lambda^2)\sin\lambda+2N\lambda\cos\lambda] = \gamma_m A_m[\lambda(1+NA_i)(e^{\eta A_i}-\cos\eta\lambda) - (A_i-N\lambda^2)\sin\eta\lambda]. \quad (21)$$

Without loss of generality we can take $R(\lambda)\geq 0$.

This has the roots $\lambda=0$, $\pm(-1)^{\frac{1}{2}}A_i$, but these are usually trivial since the values of the c's found for these values of λ give functions which are identically zero. If these roots should happen to be multiple, they become non-trivial.

If $A_m=0$, this reduces to the eigenvalue equation for flow without sources:

$$(1-N^2\lambda^2)\sin\lambda+2N\lambda\cos\lambda=0, \quad (21a)$$

whose roots are all real. The corresponding eigenfunctions are known to form a complete set on the interval $0\leq\xi\leq 1$.

To see the behavior of the eigenvalues when $A_m>0$, we can divide (21) through by $(\lambda^2+A_i^2)$. The behavior of the two members of the resulting equation is shown in Fig. 2, for the numerical values $N=0$, $A_i=2$, and $\eta=0.9$. For $N=0$, we can write (21) in the form:

$$\sin\lambda=\gamma_m A_m E(\lambda), \quad (21b)$$

introducing the function $E(\lambda)$ for brevity. If $N\neq 0$, (21) does not take so simple a form but the spirit of the following remarks about (21b) still holds.

$E(\lambda)$ is a function which rises to a maximum and falls slowly to zero as $\lambda\to\infty$. $E(\lambda)$ has small oscillations, but on the average goes as λ^{-1} for large λ. Thus, no matter how large $\gamma_m A_m$ may be, the right number of the above equation eventually becomes and remains less than unity and the eigenvalues approach the zeros of $\sin\lambda$.

Thus, we see that the eigenvalues of (21b) are continuous functions of $\gamma_m A_m$ and equal the integral multiples of π when $\gamma_m A_m=0$. As $\gamma_m A_m$ increases from zero, we see from Fig. 2 that the root originally at π moves toward the origin. The roots originally at 2π and 3π move toward each other, as do those originally at 4π and 5π, etc.

For some value of $\gamma_m A_m$, the root originally at π reaches the origin. This occurs when the two curves in Fig. 2 become tangent at the origin. $\lambda=0$ is then a double root and is no longer trivial. For still larger values of $\gamma_m A_m$ this eigenvalue becomes imaginary, so that $-\lambda^2$ is positive in Eq. (17) and the current increases without limit. Therefore, the breakdown condition is the condition that the slope of $\gamma_m A_m E(\lambda)$ at $\lambda=0$ be not less than unity. In the general case, with $N\neq 0$, similar remarks hold, and we find that the breakdown condition is that:

$$\gamma_m A_m \geq A_i^2(1+2N)[(1+NA_i) \times(e^{\eta A_i}-1)-\eta A_i]^{-1}. \quad (22)$$

We have seen that, for any value of $\gamma_m A_m$, the eigenvalues of (21) have a one-to-one correspondence to the known set defined by (21a). Further, the eigenvalues and eigenfunctions defined by (21) always approach those defined by (21a) at least as fast as λ^{-1}. Thus, we may

plausibly assume that the set of functions $\chi_n(\xi)$ are complete and, hence, that the expansion of (18) is possible.

Expansion Coefficients and Initial Conditions

Having solved (21) for the eigenvalues, we can readily determine the c's from (20) and any convenient normalizing condition, and are ready to determine the a_n in (18). This determination is more difficult than for a Fourier expansion because the functions χ_n are not orthogonal. Evaluating the a_n is not necessary if we are only interested in the rise or fall time because this time is essentially determined by the smallest value of λ. This value is always less than π while the next value is equal to about 2π, and thus the first term in (18) rapidly becomes dominant.

We determine the coefficients a_n by substituting $T=0$ into Eq. (18), thus:

$$\rho_m(\xi, 0)=\sum a_n\chi_n(\xi).$$

We proceed in the usual fashion to multiply through by $\chi_k(\xi)$ and to integrate over all ξ:

$$\sum a_n(\chi_k\cdot\chi_n)=(\chi_k\cdot\rho_m(\xi, 0)). \tag{23}$$

If the χ_k were orthogonal, this would give a_k immediately. As it is, (23) represents a set of equations to be solved for the a_n.

For the pulse transient, we take:

$$\rho_m(\xi, 0)=\begin{cases}0, & \xi\leq\xi_0,\\ n_0A_m\exp[A_i(\xi-\xi_0)], & \xi\geq\xi_0,\end{cases} \tag{24}$$

expressed in terms of number of metastables per cm² per unit ξ. The current is given by:

$$i=M_rM_ie^{\eta A_i}\gamma_m(\kappa^2/X^2)(\partial\rho_m/\partial\xi)_{\xi=0}. \tag{25}$$

For the falling transient we have everything the same as for the pulse transient, except for the form of $\rho_m(\xi, 0)$. Since the rising transient is the same shape as the falling transient, we know both when we have determined one. For the falling transient we take $\rho_m(\xi, 0)$ to be the steady-state distribution. As we shall show in a minute, this distribution is:

$$\rho_m=(i_0X^2/\kappa^2)M_rM_iM_m(\alpha_m/\alpha_i^2X)$$
$$\times\begin{cases}(\xi+N)(1+2N)^{-1}[(1+NA_i)\\ \qquad\times(e^{\eta A_i}-1)-\eta A_i], & \xi\leq\xi_0,\\ (\xi+N)(1+2N)^{-1}[(1+NA_i)\\ \quad\times(e^{\eta A_i}-1)-\eta A_i]-\exp[A_i(\xi-\xi_0)]\\ \qquad+1+A_i(\xi-\xi_0), & \xi\geq\xi_0,\end{cases} \tag{26}$$

where ρ_m is in number of metastables per cm² per unit ξ, and:

$$M_m^{-1}=1-(\gamma_mM_rM_i\alpha_m/\alpha_i^2X)(1+2N)^{-1}$$
$$\times[(1+NA_i)(e^{\eta A_i}-1)-\eta A_i]. \tag{26a}$$

If we have a problem in which the stimulating current i_0 is an arbitrary function of time, we can proceed by dividing the given function into a set of pulses of infinitesimal duration, finding the pulse transient resulting from each pulse and integrating the result over the set of pulses.

As an example, we have carried through the numerical work for the values $N=0$, $A_i=2$, $\eta=0.9$, and $\gamma_mA_m=\frac{1}{2}$. The eigenvalues are given by the intersections of the $\sin\lambda$ curve in Fig. 2 with the curve $\frac{1}{2}E(\lambda)$ (see (21b)). To four decimal places, the first five eigenvalues are:

$$\lambda_1=2.3392,\quad \lambda_2=6.6487,\quad \lambda_3=9.0955,$$
$$\lambda_4=12.7856,\quad \lambda_5=15.5246.$$

The first three eigenfunctions, normalized by setting $c_1=1$ in Eqs. (20), are shown in Fig. 3. They bear a general resemblance to the trigonometric functions $\sin\pi\xi$, $\sin2\pi\xi$, $\sin3\pi\xi$, but are somewhat distorted. In particular, χ_1 has its maximum at a larger value of ξ than the midpoint. The steady-state density function, indicated by $\rho_m(\xi, 0)$, is also given in Fig. 3 on an arbitrary scale. From it we see that χ_1 is more suitably shaped to be an approximate representation than a symmetrical function would be.

The results of keeping one, two or three terms in Eq. (23) is shown in Fig. 4. We get the fol-

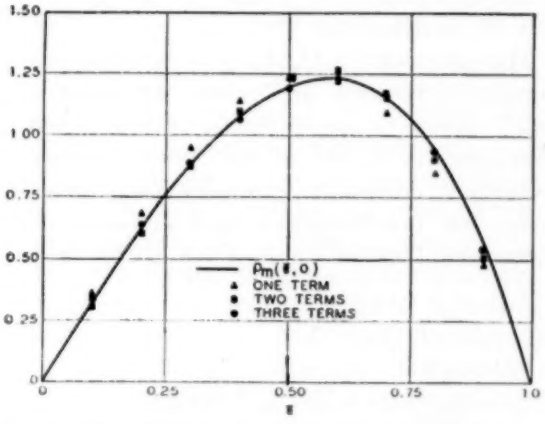

FIG. 4. Successive approximations to $\rho_m(\xi, 0)$.

lowing values of the coefficients:

One term: $a_1=1.5311$.
Two terms: $a_1=1.5013$, $a_2=-0.0668$.
Three terms: $a_1=1.5060$, $a_2=-0.0761$, $a_3=0.0406$.

In this case at least we converge rapidly upon the accurate values of the coefficients. Thus, if we used only a one-term approximation in this case, our accuracy at large T (when only a_1 is important) would be about 2 percent.

We now find the current by substituting the expansion for ρ_m into Eq. (25). From (18) and (19), with the normalizing condition that $c_1=1$, we have:

$$(\partial\rho_m/\partial\xi)_{\xi=0}=\sum a_n\lambda_n\exp[-\lambda_n^2T],$$

and the current is proportional to this quantity. Since λ_2^2 is about eight times λ_1^2, and the other λ^2 are even larger, only the first term is important for T greater than about 0.1.

Steady-State Metastable and Ion Distribution, Steady-State Current

The steady-state densities are found readily by setting $(\partial/\partial t)=0$ in Eqs. (4) and (5), and integrating, subject to the same boundary conditions that we used in finding the time-dependent solutions. The metastable distribution has been given in Eq. (26). The ion distribution and the current are:

$$\rho_i=\frac{i_0X}{v}M_rM_iM_m\begin{cases}e^{\eta A_i}-1, & \xi\leq\xi_0,\\ e^{\eta A_i}-e^{A_i(\xi-\xi_0)}, & \xi\geq\xi_0;\end{cases}\quad(27)$$

$$i=i_0M_rM_iM_me^{A_i(1-\xi_0)},\quad(28)$$

where ρ_i is in number of ions per cm^2 per unit ξ, and M_m is defined in (26a).

The product $M_rM_iM_m$ is a fraction whose numerator is unity and whose denominator is unity minus a sum of terms, each of which is characteristic of one of the three processes of secondary emission: photo-emission, emission under ion bombardment, and emission under metastable bombardment. Thus, if $\Theta=2\pi$:

$$\begin{aligned}(M_rM_iM_m)^{-1}&=1-(\alpha_r\gamma_r/2\alpha_i)\\ &\times[\exp(A_i(1-\xi_0))-1]\\ &-\gamma_i[\exp(A_i(1-\xi_0))-1]\\ &-(\gamma_m\alpha_m/\alpha_i^2X)(1+2N)^{-1}[(1+NA_i)\\ &\times\{\exp(A_i(1-\xi_0))-1\}-A_i(1-\xi_0)].\end{aligned}\quad(29)$$

In the expression for the steady-state current this quantity replaces the denominator in Eq. (1). Thus we see that Eq. (1) is correct, to the accuracy used in this work, only if γ_m is negligible.

Breakdown occurs when $(M_rM_iM_m)^{-1}$ becomes zero or negative. This condition is identical with the condition already given in Eq. (22), as one can see by substituting the values of M_r and M_i into Eq. (22).

Solution by an Integral Equation

Equation (16), like Eq. (6), can be transformed to an integral equation. To effect this transformation, consider first the following method for solving the diffusion equation with sources,

$$(\partial y/\partial T)-(\partial^2y/\partial\xi^2)=S(\xi,T),$$

with y subject to homogeneous boundary conditions, and with $y(\xi,0)$ a given function of ξ.

First, we find a function $y_1(\xi,T)$ which satisfies the homogeneous diffusion equation

$$(\partial y_1/\partial T)-(\partial^2y_1/\partial\xi^2)=0,$$

and which satisfies the same boundary conditions and initial condition as y, so that:

$$y_1(\xi,0)=y(\xi,0).$$

Then we find a function $y_2(\xi,T,T')$, where T' is an as yet undefined parameter, which also satisfies the *homogeneous* diffusion equation, which satisfies the same boundary conditions as y, but which satisfies the initial condition:

$$y_2(\xi,0,T')=S(\xi,T'),$$

which defines the parameter T'. Then one can verify by substitution that the desired solution $y(\xi,T)$ is:

$$y(\xi,T)=y_1(\xi,T)+\int_0^T y_2(\xi,T-T',T')dT',$$

provided that $y_2(\xi,T-T',T')$ can be differentiated under the integral sign.[10]

In other words, we first find the density function which results from the decay of the original distribution without sources. Then we consider that a density distribution equal to $S(\xi,T')dT'$

[10] G. Doetsch, *Laplace Transformation* (Dover Publications, New York, 1943), p. 358.

is set up at $T=T'$ and find the density which results as this decays without further sources. To find the actual density at time T we add up all the contributions from the initial distribution and from the sources which "occur" earlier than time T.

In the present problem, the source function $S(\xi, T)$ is, according to Eq. (16), the product of $(\partial\rho_m\partial\xi)_{\xi=0}$, which is a function only of time, by a function of ξ only. It is then convenient to take the function $y_2(\xi, T, T')$ to be:

$$y_2=(\partial\rho_m/\partial\xi)_{\substack{\xi=0\\T=T'}}\phi(\xi, T), \tag{30a}$$

where $\phi(\xi, T)$ satisfies the homogeneous diffusion equation, and

$$\phi(\xi, 0)=\begin{cases}0, & \xi\leq\xi_0,\\ \gamma_m A_m e^{A_i(\xi-\xi_0)} & \xi\geq\xi_0.\end{cases} \tag{30b}$$

Our method of solution then gives the result:

$$\rho_m(\xi, T)=y_1(\xi, T)+\int_0^T\phi(\xi, T-T')(\partial\rho_m/\partial\xi)_{\substack{\xi=0\\T=T'}}dT'. \tag{31}$$

Operating on both sides with $\partial/\partial\xi$ and evaluating at $\xi=0$, we get an integral equation for the time-dependent variable $(\partial\rho_m/\partial\xi)_{\xi=0}$:

$$(\partial\rho_m/\partial\xi)_{\xi=0}=(\partial y_1/\partial\xi)_{\xi=0}+\int_0^T(\partial/\partial\xi)_{\xi=0}\times\phi(\xi, T-T')(\partial\rho_m/\partial\xi)_{\substack{\xi=0\\T=T'}}dT'. \tag{32}$$

Since the current is proportional to $(\partial\rho_m/\partial\xi)_{\xi=0}$, this equation is analogous to Eq. (9). It is essentially the integral equation which Engstrom and Huxford[4] give for the current.

Equation (32) is identical in form with (9). In both cases, the first term on the right represents the contribution from the initial distribution (there is also an i_0 in (9) which we have taken to be zero in (32)). In both cases, the first factor in the integrand gives the number of electrons leaving the cathode at time T as a result of an electron which left the cathode at time T'.

Equation (32) can be solved by an infinite series, which we know from our study of Eq. (16) to have the form:

$$(\partial\rho_m/\partial\xi)_{\xi=0}=\sum_n a_n\exp(-\lambda_n{}^2T). \tag{33}$$

We also know y_1 and ϕ, and can write:

$$(\partial y_1/\partial\xi)_{\xi=0}=\sum_n b_n\exp[-p_n{}^2T],$$

$$(\partial\phi/\partial\xi)_{\xi=0}=\sum_n c_n\exp[-p_n{}^2T],$$

in which the p_n are the roots of (21a), and b_n and c_n are determined by Eqs. (30a) and (30b). Substituting these into (32), we have:

$$\sum_k c_k/(p_k{}^2-\lambda_n{}^2)=1, \tag{34a}$$

$$b_k-c_k\sum_n a_n/(p_k{}^2-\lambda_n{}^2)=0. \tag{34b}$$

We can determine the λ_n from (34a), and the a_n from (34b) and the values of λ_n.

The roots of (34a) must be identical with the roots of (21). Which of the two equations one uses will probably be determined by the type of information desired.

With either this method or the method presented earlier in this section one can achieve any desired accuracy by retaining a sufficient number of terms, either in series (18) or series (33). It should be noted that the use of, say, two terms of (18) does not give the same approximation as the use of two terms of (33). In the latter case, we approximate to both the eigenvalues (the λ's) and the expansion coefficients. In the former case, we always obtain the accurate eigenvalues from (21), and approximate only to the expansion coefficients.

VI. SOME EXPERIMENTAL APPLICATIONS

In this section, we shall point out some of the consequences of the preceding formal analysis which suggest themselves as bases for experimental measurement of the various parameters which characterize a discharge. We shall not attempt a discussion of the feasibility or accuracy of any experiments.

The parameters which characterize the discharge may be divided into two types: (1) those which determine the "steady-state" currents i_r, i_i, and i (see Fig. 1) and (2) those which deter-

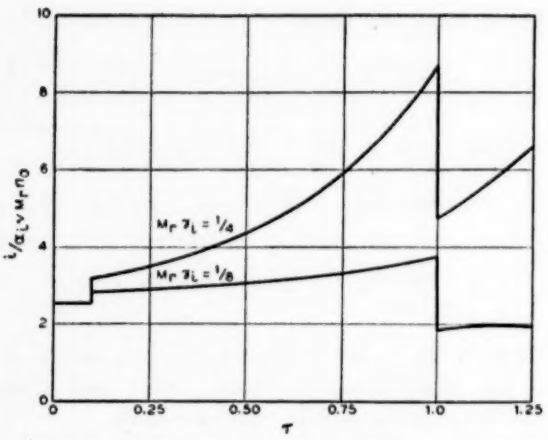

FIG. 5. Initial part of ion transient for $A_i=2$, $\xi_0=0.1$. The curves are only schematic beyond $\tau=1$.

mine the rise times t_r and t_i, and the time constants of the metastable transient.

The steady-state currents are given by:

$$i_r = i_0 M_r \exp[\alpha_i(X-x_0)],$$
$$i_i = i_0 M_r M_i \exp[\alpha_i(X-x_0)],$$
$$i = i_0 M_r M_i M_m \exp[\alpha_i(X-x_0)],$$

where M_r, M_i, and M_m are, respectively, defined below Eq. (3), by Eq. (13), and Eq. (26a). The products M_rM_i and $M_rM_iM_m$ are written out, respectively, in Eqs. (13a) and (29). By referring to these equations, we see that the steady-state currents depend upon the parameters $\alpha_r\gamma_r/\alpha_i$, γ_i, $\alpha_m\gamma_m/\alpha_i$ and α_i. (In addition to these parameters there occur N and ξ_0. We can usually estimate these with sufficient accuracy from other considerations.) Therefore, it is impossible to determine these four parameters from the three steady-state currents at one value of X.

We could overcome this difficulty by performing the classical Townsend experiment, in which the current is measured as a function of X, while keeping the electric field, and hence the α's, constant. The alternative procedure, which Engstrom and Huxford[4] have suggested, is to study the transients. This procedure brings in also the time parameters, namely, the speed v of the ions and the diffusion coefficient κ^2 of the metastables. If we had studied the radiation transient, we should also have a parameter (or parameters) for it.

An analysis of the transients is sufficient, as we shall show explicitly for the ion transient, to yield all the desired parameters. An analysis by this means has two great advantages over the classical method. One is that the parameters are all determined at one geometrical configuration, the second is that measurements can be made beyond the breakdown point, provided that the stimulating current is removed soon enough.

An experimental study of the metastable transient has been given by Engstrom and Huxford.[4] Their method involves measuring the time constants of the exponential decay terms which were discussed in Section V of this paper. Use of these time constants, in general, requires a knowledge of the diffusion coefficient κ^2. They show that, if one uses a one-term approximation in the integral equation method of solution (see Eq. (32) *et. seq.*), λ_1 is determined, to that accuracy, by the ratio i/i_i, without knowing κ^2.

For studying the positive ion transient, we make use of Eq. (12b) for the current following a pulse of stimulating electrons. Figure 5 shows the dimensionless current $(i/\alpha_i v M_r n_0)$ computed from (12b) as a function of the dimensionless time $\tau=vt/X$, for the particular values $A_i=2$, $\xi_0=0.1$, $(M_r\gamma_i)=\frac{1}{8}$ and $\frac{1}{4}$. The latter value is beyond the breakdown value.

The feature of greatest interest in Fig. 5 is that there are two discontinuities in the current, whose origin is not difficult to see. When the initial pulse of electrons passes through the tube, ions are created between $\xi=\xi_0$ and $\xi=1$. This mass of ions moves bodily toward the cathode. At $\tau=\xi_0$, the front wall of the ion distribution strikes the cathode and causes the emission of electrons. The current through the discharge therefore shows a sudden jump. The second discontinuity arises when the ions originally formed near the anode $(\xi=1)$ reach the cathode. The initial density of ions at the anode is much greater than any density formed subsequently, so that after the ions originally at the anode strike the cathode there is a sudden decrease in the number of ions striking the cathode per sec., and therefore a sudden decrease in the current of electrons leaving the cathode.

Mathematically, the discontinuities arise in the first term of the last summation in Eq. (12b), that is, from the term:

$$M_r\gamma_i(A_i)^{-1}\exp[A_i(\tau-\xi_0)]$$
$$\times\{\exp[A_i(1-\xi_0)]+A_i\xi_0-1\}I_0(\tau,\xi_0,0).$$

$I_0(\tau, \xi_0, 0)$ is a function which is unity inside the interval $\xi_0 \leq \tau \leq 1$, and zero outside that interval. Therefore, this term gives discontinuities in the current at $\tau = \xi_0$ and $\tau = 1$, which have the respective magnitudes:

$$M_r\gamma_i(A_i)^{-1}\{\exp[A_i(1-\xi_0)]+A_i\xi_0-1\}$$

and

$$M_r\gamma_i(A_i)^{-1}\exp[A_i(1-\xi_0)] \times\{\exp[A_i(1-\xi_0)]+A_i\xi_0-1\}.$$

Observation of these discontinuities thus allows us to compute $A_i(=\alpha_i X)$, and $M_r\gamma_i$. The combination of these observations with the steady-state currents in Fig. 4 gives one more than the number of relations needed to compute the parameters in the steady-state current.

On a time scale the discontinuities occur at $t = x_0/v$ and $t = X/v$. Therefore, from the times at which they occur, we can compute the ion velocity and hence the mobility.

It should be pointed out that, if metastable activity is significant in the discharge, the coefficient γ in Eq. (1), which is closely related to the second Townsend coefficient, is not independent of the electrode spacing X. Upon comparing (1) with (28) and (29), we see that γ is given by:

$$\gamma = (\alpha_r\gamma_r/2\alpha_i)+\gamma_i+[\gamma_m\alpha_m/\alpha_i(1+2N)] \times\{(1+N\alpha_i X)(\alpha_i X)^{-1} -X^{-1}(X-x_0)[\exp(\alpha_i(X-x_0))-1]^{-1}\}.$$

The radiation and ion contributions to this are constants, but the metastable contribution is a function of X, which varies as $N+(\alpha_i X)^{-1}$ for large X. In other words, if we try to determine a number γ to fit Eq. (1) by varying X, we should find that γ must decrease as X increases.

The reason that the ion and radiation contributions to γ are constant while the metastable contribution is not, is readily seen. Regardless of the value of X, essentially all ions formed in the discharge (if the diameter of the discharge is large compared with its length) reach the cathode. Likewise, one-half of the radiation emitted in the gas reaches the cathode, regardless of X. However, the fraction of the metastables formed which reaches the cathode is not independent of X, even if sidewise diffusion is negligible. As X increases, the distribution of metastables tends to become more concentrated near the anode. Since the metastables move by diffusion, more of the metastables reach the anode and fewer reach the cathode, under these conditions. Therefore, the metastable contribution to γ decreases with increasing X.

The author wishes to express his appreciation to Dr. J. P. Molnar of the Bell Telephone Laboratories, who suggested this investigation of transient currents. He also wishes to acknowledge the critical comment and suggestions of many of his colleagues, particularly Mr. A. H. White, and Drs. W. Shockley, C. Herring, and H. D. Hagstrum.

On the Hyperfine Structure of Gallium†

G. E. BECKER* AND P. KUSCH
Columbia University, New York, New York

(Received December 5, 1947)

The hyperfine structures of the ground $^2P_{\frac{1}{2}}$ and the metastable $^2P_{\frac{3}{2}}$ states of Ga^{69} and Ga^{71} have been determined by the atomic beam magnetic resonance method. The h.f.s. levels for an atom whose nucleus has a magnetic dipole, electric quadrupole, and magnetic octupole moment are given by the formula $W=aC/2+bC(C+1)+c(C^3+4C^2+4C/5)$, where $C=F(F+1)-I(I+1)-J(J+1)$. For the metastable state of gallium, with $I=J=\frac{3}{2}$, there are four levels at zero external magnetic field, corresponding to $F=3$, 2, 1, and 0. The determination of the separations of these levels permits the calculation of the constants a, b, and c in the equation above. It was found that only the first two terms are needed to explain the hyperfine splitting of each Ga isotope, within the precision of these measurements. An upper limit for the value of c is 3×10^{-9} cm^{-1}. Other results are:

Ga^{69}

a: 6.3644×10^{-3} cm^{-1} $=190.790\times10^6$ sec.$^{-1}$
b: 8.6894×10^{-5} cm^{-1} $=2.6049\times10^6$ sec.$^{-1}$
Q: 0.186×10^{-24} cm^2

Ga^{71}

a: 8.0868×10^{-3} cm^{-1} $=242.424\times10^6$ sec.$^{-1}$
b: 5.4759×10^{-5} cm^{-1} $=1.6416\times10^6$ sec.$^{-1}$
Q: 0.117×10^{-24} cm^2

The $\Delta\nu$ of the normal state and the g_I of each isotope have been determined by the use of transitions in which $\Delta m_I=\pm1$, $\Delta m_J=0$ in the Paschen-Back region.

Ga^{69}

$\Delta\nu$: 0.089319 cm^{-1} $=2677.56\times10^6$ sec.$^{-1}$
g_I: $-.0007239$

Ga^{71}

$\Delta\nu$: 0.113488 cm^{-1} $=3402.09\times10^6$ sec.$^{-1}$
g_I: $-.0009218$

The ratio $(\Delta\nu_{71}/\Delta\nu_{69})=1.27059$ is in good agreement with $(a_{71}/a_{69})=1.27063$.

1. INTRODUCTION

THE hyperfine splitting of an atomic energy level is caused chiefly by the interactions of the magnetic field and the gradient of the electric field of the electronic configuration with the nuclear magnetic dipole moment and electric quadrupole moment, respectively. There is also a possibility that higher order nuclear moments may produce measurable effects. Since the magnitude of these interactions depends on the angle between the angular momentum of the nucleus and that of the electrons, states with different values of the total angular momentum, F, will differ in energy.

As has been pointed out previously,[1] the atomic beam magnetic resonance method offers a direct means of determining the hyperfine structure of atomic energy levels. This method has a number of important advantages over optical methods and the atomic beam method of zero moments. The precision is very good because only the measurement of a radio frequency is involved. The resolution is high enough to permit the observation of a clearly resolved Zeeman pattern of a hyperfine structure line in a magnetic field as low as 0.05 gauss. Lastly, the results are easier to interpret than those obtained by optical methods, since only one atomic energy level is involved.

This method has been applied[1,2] to the ground states of a number of atoms. In all these cases, the electronic configuration in the ground state was spherically symmetrical. It is evident that any electrostatic interaction between a nucleus with a quadrupole moment and a spherically symmetrical electronic charge distribution cannot depend on the relative orientations of I and J, and thus on F; therefore the hyperfine splitting is unaffected. The quadrupole interaction is thus zero and no information can be obtained as to the quadrupole moment of the nucleus.

It is possible to produce and detect atomic beams of gallium by the use of well developed experimental techniques.[3] The investigation of the hyperfine structure of gallium is, then, not only possible but also of considerable interest. Gallium exists in two isotopic forms, Ga^{69} (61.5

† Publication assisted by the Ernest Kempton Adams Fund for Physical Research of Columbia University.

* Now at Stanford University.

[1] P. Kusch, S. Millman, and I. I. Rabi, Phys. Rev. **57**, 765 (1940). Hereinafter referred to as KMR.

[2] S. Millman and P. Kusch, Phys. Rev. **58**, 438 (1940).

[3] N. A. Renzetti, Phys. Rev. **57**, 753 (1940).

percent) and Ga^{71} (38.5 percent). In addition, it exists in the ground ($^2P_{\frac{1}{2}}$) state and in the metastable ($^2P_{\frac{3}{2}}$) state, 826 cm^{-1} above the ground state. At the oven temperatures at which beams are produced ($\sim$1600°K) approximately 50 percent of the atoms occur in the metastable state. The lifetime of the state is sufficiently great to permit the propagation of atoms in this state through the length of a molecular beam apparatus. Thus it is possible to determine the quadrupole interaction in the $^2P_{\frac{3}{2}}$ state for each of the two isotopes. A very precise determination of the ratio of the two quadrupole moments is possible, even though the value of neither can be determined with precision from experimental data.

It has been pointed out in earlier papers that the ratio of the $\Delta\nu$'s of two isotopes of an atomic species should be directly determinable from the ratio of the nuclear moments of the two isotopes if only electromagnetic interactions exist between nucleus and electrons. Earlier data indicated that the ratios did, indeed, agree as anticipated. However, the experimental uncertainties were rather large, because of the considerable uncertainty in the determination of nuclear g values from the observations of molecular spectra by the molecular beam magnetic resonance method. In the present case the determination for each of two isotopes and for each of two atomic states of the constants which describe the interaction of the nuclear magnetic dipole moment with the electronic configuration will serve to give a very accurate check of the assumption that electromagnetic interaction alone can account for h.f.s. patterns. This results from the very great precision with which atomic spectra may be observed as compared to unresolved molecular spectra.

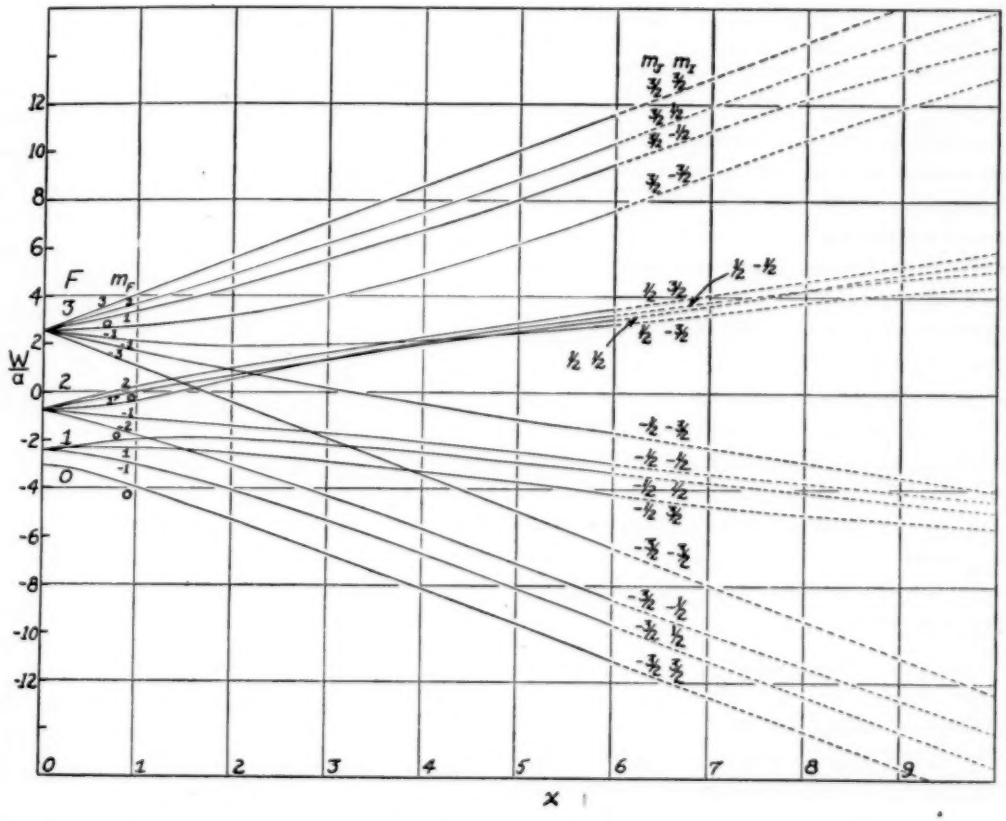

FIG. 1. The variation with magnetic field of the energy levels for Ga^{69} in the $^2P_{3/2}$ state. For values of $x = g_J\mu_0 H/a$ from 0 to 6, the levels have been computed with a Hamiltonian including the magnetic dipole and electric quadrupole interactions. Numerical values for b/a and g_I were taken from Renzetti. At $x = 10$, the calculation was made for a high field approximation, and the dotted curves join the two solutions smoothly.

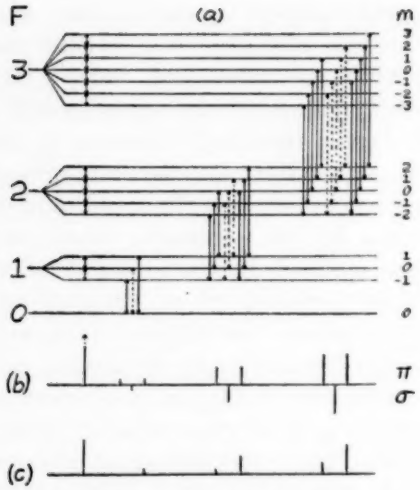

FIG. 2a. A schematic diagram showing the magnetic levels at low field of the hyperfine structure multiplet of a $^2P_{3/2}$ state for a nuclear spin of 3/2, and the allowed transitions between these levels. This diagram shows correctly the relative spacing of the levels for each F-value, but the intervals between F-levels are not drawn to scale. (b) The spectrum resulting from the transitions shown in (a). Again, the diagram shows correctly only the relative spacings of lines for a given transition for which $\Delta F=\pm 1$ or $\Delta F=0$. (c) The spectrum actually observed with the experimental arrangement described in this paper.

The interaction constants of gallium have been measured earlier both by use of optical methods[4] and the atomic beam zero moment method.[3] This present experiment was undertaken to determine these quantities more precisely and to investigate the possibility of the presence of higher order nuclear moments. Theoretical considerations indicate[5] that the ratio between octupole and dipole interactions should be of the order of magnitude (nuclear radius/atomic radius),[2] which would make any octupole effects extremely difficult to measure. However, for the case of iodine, Tolansky[6] reports that a term such as would be produced by an octupole moment is needed for an explanation of the hyperfine structure.

2. THEORY

Aside from constant terms which are independent of F and which, therefore, do not affect the hyperfine splitting, the energy levels of a hyperfine structure multiplet at zero magnetic field are given by the expression[5,7]

$$W=aC/2+bC(C+1)+c(C^3+4C^2+4C/5), \quad (1)$$

where $C=F(F+1)-I(I+1)-J(J+1)$. The three terms in (1) arise from the interaction of the nuclear magnetic dipole moment, nuclear electric quadrupole moment, and nuclear magnetic octupole moment, respectively, with the orbital electrons.

In order to study the behavior of the energy levels in a magnetic field, the octupole interaction will be neglected. The Hamiltonian for the interactions becomes

$$\mathcal{H}=\mu_0 H(g_J J_z+g_I I_z)+a\mathbf{I}\cdot\mathbf{J} +b2\mathbf{I}\cdot\mathbf{J}(2\mathbf{I}\cdot\mathbf{J}+1), \quad (2)$$

where the first two terms on the right are the interaction of the external field, taken in the z-direction, with the electrons and the nucleus. Substitution in the secular equation gives linear, quadratic, cubic, and quartic equations which may be solved for the energies of the states in terms of a, b, g_J, g_I, and H. With Renzetti's[3] values for b/a and g_I, the energy levels are plotted as a function of $x=g_J\mu_0 H/a$ in Fig. 1.

There are four levels at zero external field, corresponding to the four possible values of $F=3$, 2, 1, and 0. If C is evaluated for each F and substituted in (1), there will result an expression for the energy of each F-level in terms of the constants a, b, and c. The frequencies corresponding to the energy differences between these levels are,

$$W_4-W_3\colon f_3=3a+24b+171.3c$$
$$W_3-W_2\colon f_2=2a-24b+54.2c$$
$$W_2-W_1\colon f_1=a-24b+153.1c$$

where a, b, and c are expressed in frequency units. These frequencies for the $^2P_{\frac{3}{2}}$ state of Ga all lie in the range of $100\text{–}800\times 10^6$ sec.$^{-1}$

At very low external magnetic field, the splitting of each F level into $(2F+1)$ levels is adequately described by the Zeeman approximation.

$$W_{(F,m)}=W_F+m\mu H=W_F+mg_F\mu_0 H. \quad (4)$$

[4] H. Schuler and H. Korsching, Zeits. f. Physik **103**, 434 (1936).
[5] H. B. G. Casimir and G. Karreman, Physica **9**, 494 (1942).
[6] S. Tolansky, Proc. Roy. Soc. **A170**, 205 (1939).
[7] H. B. G. Vasimir, *Interaction between atomic nuclei and electrons* (Verh. Teyler's 2e Genootschap, Haarlem, 1937); also: Arch. du Musée Teyler, **III**, 8, 201.

The lines will therefore be found at frequencies

$$\nu=(W_F-W_{F-1})/h+(m_F-m_{F-1})g_F\mu_0H/h, \quad (5)$$

where

$$g_F=g_J\frac{F(F+1)+J(J+1)-I(I+1)}{2F(F+1)}+g_I\frac{F(F+1)-J(J+1)+I(I+1)}{2F(F+1)}.$$

If the term in g_I is neglected, g_F has the value $\frac{2}{3}$ for the $^2P_{\frac{1}{2}}$ state for all values of F. This means that the $(2F+1)$ levels for each F are separated from each other by a constant amount. Figure 2a is a schematic diagram showing the Zeeman splitting in low magnetic field. Figure 2b shows the line pattern derived from an application of the selection rules for magnetic dipole radiation, $\Delta F=0, \pm1$; $\Delta m=0, \pm1$. The π lines, for which $\Delta m=\pm1$, represent transitions caused by the component of the oscillating magnetic field perpendicular to the constant field, H, and the σ lines, for which $\Delta m=0$, arise from the component parallel to H. Note that in low magnetic field all transitions for which $\Delta F=0$ have the same frequency, and that this frequency goes to zero as the magnetic field goes to zero. Moreover, this frequency gives the difference between the frequency of a π line at field H and its frequency at field zero. Note also that the average of the two π lines for a transition $\Delta F=\pm1$ gives directly the frequency at zero field. (If the σ lines were observable, they also would give the frequencies at zero field.) Thus there is a check on the determination of each f for which both π lines are observable. The validity of Eq. (4) as a description for the Zeeman splitting at field strengths actually used in this experiment could be tested simply by using several different field strengths and verifying that the splitting did have the predicted symmetry.

For the normal state, it was found convenient to determine the $\Delta\nu$ by use of a method described in *KMR*, which involves the measurement of the frequencies of the lines resulting from a change in the nuclear magnetic quantum number, m_I, in strong magnetic field. It has been shown that this method yields the value of $\Delta\nu$ with accuracy as good as is obtained by work in low fields. It has the advantage that the frequencies are lower, approaching the value $\Delta\nu/(2I+1)$. This may be seen from the expression[8] for the energies of the states in the Paschen-Back region:

$$W_{m_Im_J}=m_Ig_I\mu_0H+m_Jg_J\mu_0H+[\Delta W/(I+\tfrac{1}{2})]m_Im_J \quad (6)$$

where $\Delta W=h\Delta\nu$. From this equation, with $m_J=\pm\frac{1}{2}$, it is clear that transitions for which $\Delta m_I=\pm1$, $\Delta m_J=0$ give rise to lines whose frequencies approach the limiting value $\Delta\nu/(2I+1)$, since the term $m_Ig_I\mu_0H$ is still relatively small in comparison with the term $[\Delta W/(I+\frac{1}{2})]m_Im_J$ for the highest fields used in this experiment.

The exact expression for the energy of the states of a level with $J=\frac{1}{2}$ is given by the Breit-Rabi formula[9]

$$W_{F,m}=-\frac{\Delta W}{2(2I+1)}+g_Im\mu_0H\pm\frac{\Delta W}{2}\left(1+\frac{4m}{2I+1}x+x^2\right)^{\frac{1}{2}} \quad (7)$$

where $x=(g_J-g_I)\mu_0H/\Delta W$. The frequencies for the $\Delta m_I=\pm1$ transitions as found from Eq. (7) are listed in Table I.

TABLE I. The lines in the spectrum of *Ga* in the $^2P_{\frac{1}{2}}$ state resulting from the transitions $\Delta m_I=\pm1$, $\Delta m_J=0$.

Transitions	Expressions for the frequencies
$(2,2)\leftrightarrow(2,1)$	$\frac{1}{2}\Delta\nu[(1+x)-(1+x+x^2)^{\frac{1}{2}}]+g_I\mu_0H/h$
$(2,1)\leftrightarrow(2,0)$ $(1,1)\leftrightarrow(1,0)$	$\frac{1}{2}\Delta\nu[(1+x+x^2)^{\frac{1}{2}}-(1+x^2)^{\frac{1}{2}}]+g_I\mu_0H/h$ $\frac{1}{2}\Delta\nu[(1+x+x^2)^{\frac{1}{2}}-(1+x^2)^{\frac{1}{2}}]-g_I\mu_0H/h$
$(2,0)\leftrightarrow(2,-1)$ $(1,0)\leftrightarrow(1,-1)$	$\frac{1}{2}\Delta\nu[(1+x^2)^{\frac{1}{2}}-(1-x+x^2)^{\frac{1}{2}}]+g_I\mu_0H/h$ $\frac{1}{2}\Delta\nu[(1+x^2)^{\frac{1}{2}}-(1-x+x^2)^{\frac{1}{2}}]-g_I\mu_0H/h$
$(2,-2)\leftrightarrow(1,-1)$	$\frac{1}{2}\Delta\nu[(1-x)+(1-x+x^2)^{\frac{1}{2}}]-g_I\mu_0H/h$

The determination of these frequencies at constant magnetic field yields the values of $\Delta\nu$, g_I, and H. Furthermore, the field needs to be only approximately constant because the frequencies depend very little on the field in the Paschen-Back region. This is shown in Fig. 3,

[8] E. Back and S. Goudsmit, Zeits. f. Physik **47**, 174 (1928).

[9] S. Millman, I. I. Rabi, and J. R. Zacharias, Phys. Rev. **53**, 384 (1938).

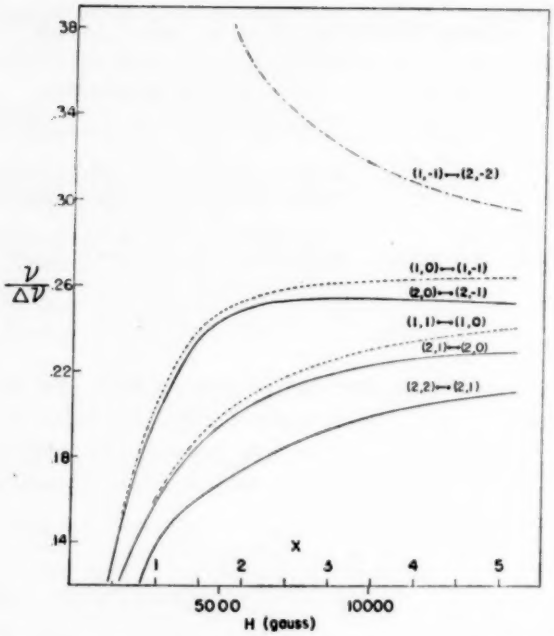

FIG. 3. The field dependence of the frequencies of the lines of Ga^{69} in the $^2P_{\frac{1}{2}}$ state resulting from the transitions $\Delta m_I = \pm 1$, $\Delta m_J = 0$.

a plot of frequency *versus* magnetic field for the transitions $\Delta m_I = \pm 1$, $\Delta m_J = 0$.

3. METHOD

In the magnetic resonance method, the atoms in a beam are first deflected in an inhomogeneous magnetic field, then pass through a homogeneous magnetic field with a weak superimposed radio-frequency oscillating field, and finally are deflected in the opposite direction by a second inhomogeneous field to strike the detecting filament. The net deflection is zero only when the component of the magnetic moment of the atom in the direction of the field is the same in the two deflecting fields. If the frequency of the oscillating field corresponds to the energy difference between two levels in the atom, transitions which are consistent with selection rules will occur. If such a transition produces a change in the magnetic moment of the atom larger than the minimum observable moment change, there will be a drop in the intensity of the beam at the detector. The radiofrequency spectrum of an atom in a given magnetic field is observed simply by the measurement of the intensity of the beam as a function of the applied frequency.

TABLE II.*

Observed frequencies	Mean f_2	Observed f_0	f_2
445.321 445.563	445.442	0.105	445.426 445.458
445.341 445.558	445.450	0.105	445.446 445.453
445.177 445.726	445.452	0.275	445.452 445.451
445.138 445.774	445.456	0.325	445.463 445.449
Mean	445.450		

* Column one gives the observed frequencies of the lines for the transition $(F=2)\leftrightarrow(F=1)$ for the $^2P_{3/2}$ state of Ga^{71}. Column two gives the means of the pairs of π lines for each trial. Column three lists the observed frequencies for the transitions for which $\Delta F=0$, $\Delta m=\pm 1$. Column four gives the values of f_2 found by combining the values of f_0 with the frequencies in column one. The frequencies are in mc/sec.

The magnitude of the inhomogeneous fields is, in general, not critical, but the order of magnitude is dictated by the type of transition being studied and by the dimensions of the apparatus. For a transition for which $\Delta m_I = \pm 1$, the magnetic moment in high fields remains practically unchanged because m_J, and therefore the electronic moment, is the same in both states. Thus, if strong inhomogeneous fields were used in this case, the transition would not be detected. However, if the deflecting field is small ($x<1$), the difference in magnetic moment between the two states is appreciable, and the atoms will miss the detector provided that the deflecting power is great enough for this value of x. This last requirement determines the necessary length and the ratio of gradient to field of the inhomogeneous magnets.

For many of the low field transitions for which $\Delta F = \pm 1$ or $\Delta m = \pm 1$, the change in magnetic moment is appreciable at high fields ($x>1$). Thus, the deflecting fields may be made large, which means that the gradient will be large; in fact, large differential deflections become possible over a large range of x, and the particular values chosen depend on instrumental details. For some of the transitions just mentioned, however, the moment change is not large at large x. The effective magnetic moment in a given state is determined by the slope of the curves in Fig. 1, since $\mu = -\partial W/\partial H$. As an example, reference to Fig. 1 shows that for the transition $(3, -3)\leftrightarrow(2, -2)$, the moment change

at values of $x>1$ is very small. For the $^2P_{\frac{1}{2}}$ state H is about 115 gauss for $x=1$. If the moment change be made large by reducing the inhomogeneous field to this value, the gradient of the field becomes low, and in the apparatus used in this work, the transition is still not observable. With magnets of fixed length and ratio of gradient to field, no point can be found where the product of moment change and gradient is sufficient to permit observation of these lines. With this factor taken into account, the line pattern with the expected relative intensities is given in Fig. 2*c*. The σ lines, which are produced by the component of the oscillating field parallel to the homogeneous field, are not observed, because the oscillating field is designed to be perpendicular to the homogeneous field.

4. APPARATUS

For reasons of intensity and ease of line-up, it is, in general, desirable to have the apparatus as short as possible. The length is determined chiefly by the deflecting power required. As is clear from the discussion in the last section, the deflecting fields for the experiment with the metastable state can be relatively short. The apparatus is modified from that described by Zacharias[10] in his work on K^{40}. The deflecting power of the apparatus has been increased. The present lengths of A and B fields are 10.4 and 16.4 cm, respectively, and the ratio of gradient to field is 3.2. The apparatus functions as described by KMR, that is, the two gradients are oppositely directed and no stop is interposed in the path of the beam. In Zacharias' work, the gradients were in the same direction and refocusing occurred around a stop in the path of the undeflected beam. The oscillating field was produced by the passage of the oscillating current through a $\frac{1}{2}$ by $\frac{1}{16}$-inch copper sheet bent into the form of a vertical hairpin, with a one millimeter gap for the passage of the beam. The oscillating field thus produced was perpendicular to the homogeneous C field. No doubt there was also a small component parallel to the field, but it was not large enough to produce any observable transitions.

The same apparatus would be suited for experiments with the normal $^2P_{\frac{1}{2}}$ state if transitions for which $\Delta F=\pm1$ in low magnetic field were observed. The frequencies required for this are inconveniently high, however, and it was decided to observe the high-field $\Delta m_I=\pm1$ transitions instead. To meet the demands for increased deflecting power, it was necessary to use another apparatus which was designed primarily for work with molecules. Each magnet was 50 cm in length, and the ratio of gradient to field was 8.

The oven design and the temperature of operation were the same as described by Renzetti.[3]

The required frequencies were produced by simple tuned-lines oscillators using WE 316A and 368A tubes. Frequency measurements were made by use of a General Radio heterodyne frequency meter, Type 620A. No attempt was made to determine the shapes of the resonance lines, but the continuously variable oscillator was set at the frequency producing the peak deflection, and the frequency meter was simultaneously tuned to zero beat. The precision for a single setting was about one part in 20,000. The frequency of the quartz crystal against which the wave meter was calibrated was in turn calibrated against a signal from WWV to within one part in a hundred thousand, and therefore introduces no error within the precision of our measurements.

TABLE III. Final mean values of the frequencies of the transitions for which $\Delta F=\pm1$ at zero external field for the metastable state of Ga^{69} and Ga^{71}. The frequencies are given in mc/sec.

	Ga^{69}	Ga^{71}
f_3: $(F=3)\leftrightarrow(F=2)$	634.890±0.020	766.673±0.020
f_2: $(F=2)\leftrightarrow(F=1)$	319.062±0.010	455.450±0.010
f_1: $(F=1)\leftrightarrow(F=0)$	128.274±0.010	203.028±0.010

TABLE IV. Values of the interaction constants a and b for the $^2P_{3/2}$ states of Ga^{69} and Ga^{71}, expressed in sec.$^{-1}$.

	Ga^{69}	Ga^{71}
$a=f_3-f_1$:	$190.788\pm0.014\times10^6$	$242.422\pm0.014\times10^6$
$a=(f_3+f_2)/5$:	190.790 ± 0.005	242.425 ± 0.005
$a=(f_1+f_2)/4$:	190.791 ± 0.006	242.425 ± 0.006
$b=(2f_3-3f_2)/120$:	$2.6050\pm0.0004\times10^6$	$1.6416\pm0.0004\times10^6$
$b=(f_3-3f_1)/96$:	2.6049 ± 0.0004	1.6416 ± 0.0004
$b=(f_2-2f_1)/24$:	2.6048 ± 0.001	1.6414 ± 0.001
Final values a:	$190.790\pm0.005\times10^6$ sec.$^{-1}$	$242.424\pm0.005\times10^6$ sec.$^{-1}$
	$6.3644\pm0.0002\times10^{-3}$ cm^{-1}	$8.0868\pm0.0002\times10^{-3}$ cm^{-1}
b:	$2.6049\pm0.0004\times10^6$ sec.$^{-1}$	$1.6416\pm0.0004\times10^6$ sec.$^{-1}$
	$8.6894\pm0.0013\times10^{-4}$ cm^{-1}	$5.4759\pm0.0013\times10^{-4}$ cm^{-1}

[10] J. R. Zacharias, Phys. Rev. **61**, 270 (1942).

5. RESULTS

$^2P_{3/2}$

The pattern of resonance lines shown in Fig. 2c was observed for both isotopes at values of the homogeneous magnetic field from 0.1 gauss to 0.35 gauss. These values of the field are calculated from the separation of the pairs of π lines for a given $\Delta F=\pm 1$ transition. From the simple theory of the Zeeman pattern given earlier, it may be calculated that each π line moves from the zero-field frequency 0.93 mc/sec. gauss. The zero-field frequency may be determined either by averaging the two π lines, where there are two observed, or by adding to or subtracting from the π lines the frequency for the transition $\Delta F=0$, $\Delta m=\pm 1$. This latter line was used as a kind of calibration line for the homogeneous field. A representative example of the frequency measurements taken is given in Table II for the $(F=2)\leftrightarrow(F=1)$ transition for Ga^{71}. The observations recorded were taken on several separate days, and at least two different harmonics of the wave-meter were used. For the transitions $(F=1)\leftrightarrow(F=0)$, for which only one π line could be observed, about twice the number of separate observations were made to get a better average value. The estimate of the probable limit of error is increased for this line because of the lack of a check. Table III gives the final values of the zero-field frequencies for each isotope.

Assuming $c=0$, f_1 may be calculated from f_2 and f_3 to be 128.272 and 203.025 mc/sec. These values lie well within the limits of error of the observed f_1. If these frequencies are substituted in Eq. (3), the values of c are $c_{69}=c_{71}=6\times10^{-10}$ cm^{-1}. Since these are less than the probable limit of error, 3×10^{-9} cm^{-1}, the value of c is taken to be zero, and the values of a and b thus found are listed in Table IV.

TABLE V. A series of observations of frequencies of lines of the $^2P_{\frac{1}{2}}$ state of Ga^{71} resulting from transitions for which $\Delta m_I=\pm 1$, $\Delta m_J=0$.*

$(1,0)\leftrightarrow(1,-1)$	$(2,0)\leftrightarrow(2,-1)$	$(2,2)\leftrightarrow(2,1)$
808.724	795.539	524.183
808.679	795.580	524.174
808.741	795.543	524.204
Mean 808.715	795.554	524.187

* The sequence of observations is in the order in which the lines are tabulated. The transitions are labelled as in Table I. Frequencies are in mc/sec.

The relation between b and the nuclear quadrupole moment Q as given by Casimir[7] is

$$b=-\frac{e^2}{hc}\left(\left\langle\frac{3\cos^2\theta-1}{r^3}\right\rangle\right)_{JJ}\times\frac{\frac{3}{8}Q}{IJ(2I-1)(2J-1)}\ \text{cm}^{-1},\quad(8)$$

with Q in cm^2 and r in cm. Q is defined as the average of $(3z^2-r^2)$ over the nuclear charge density for the state $m_I=I$. Thus, $eQ=\int\rho(3z^2-r^2)d\tau$, where $\int\rho d\tau=Ze$. The quantity $[(3\cos^2\theta-1)/r^3]$ is averaged over the electronic state $m_J=J$.

For the $^2P_{\frac{1}{2}}$ state, $(\langle 3\cos^2\theta-1\rangle)=-\frac{2}{5}$, and $(\langle 1/r^3\rangle)=[R'ChcZ_i\delta/HZ_i\mu_0^2(2l+1)]$ cm^{-3}. δ is the doublet separation, 826.0 cm^{-1}; R', C, and H are small relativistic correction factors here taken to be 1.028, 1.013, and 1.018, respectively; Z_i is the effective nuclear charge, taken to be 26.4. These are the same numbers used by Renzetti,[3] and discussed in more detail by him. The equation for Q becomes

$$Q=\frac{bZ_iHC}{R'\delta}\frac{\mu_0^2}{e^2}\times 180\quad(9)$$

and the quadrupole moments are

$$Q^{69}=+0.186\times10^{-24}\ \text{cm}^2$$
$$Q^{71}=+0.117\times10^{-24}\ \text{cm}^2.$$

The fact that the values of b calculated from three pairs of frequencies are in good agreement is strong evidence that the departure from the interval rule is due to a nuclear quadrupole moment, and not to some kind of perturbation. Renzetti[3] has given a brief discussion showing that any perturbations from the other term of the fine structure doublet or from states of the same total angular momentum in higher configurations would not be expected to have any appreciable effect on the value of Q.

The ratio of the quadrupole moments is the ratio of the b's and $b^{69}/b^{71}=Q^{69}/Q^{71}=1.5868\pm0.0004$.

$^2P_{1/2}$

As was shown in an earlier section (Table I), there are six resonance lines to be expected for the transitions $\Delta m_I = \pm 1$, $\Delta m_J = 0$. In this experiment, for reasons of convenience, only five of these lines were observed for Ga^{69}, and only three for Ga^{71}. The data for one run with Ga^{71} are shown in Table V. These lines were observed at a field of about 5000 gauss. Figure 3 shows that the lines are field dependent in this region, but the data in Table V show that there was no significant drift in the homogeneous field during the series of measurements.

These lines were sufficient to permit calculation of the deisred constants by use of the equations in Table I. The sets of equations are most simply solved by numerical methods. Since these equations are not linear in x, more than one mathematical solution is possible. However, an approximate knowledge of the field, H, eliminates all but the one correct physical solution. It should be noted that $\Delta\nu$ and x are determined in such a way that the value of $\Delta\nu$ does not depend on an assumed value of g_J. Results are given in Table VI. The values of μ are found by use of the relation $\mu = -Ig_I(1836.6)$ nuclear magnetons. The low precision attached to the value of g_I as compared to that attached to $\Delta\nu$ arises from the fact that the determination of g_I depends on the observation of a small frequency difference between two lines of high frequency.

According to present theory, the $\Delta\nu$-values of the ground states and the a-values determined from experiments with the metastable states depend only on the interaction of the nuclear magnetic dipole moment with the external electrons. Therefore, the ratio of the $\Delta\nu$-values for the two isotopes should be equal to the ratio of the a-values, since the electronic wave functions are the same for both isotopes. Also, these ratios should equal the ratio of the g-factors, since the g-factor is proportional to the nuclear magnetic moment, and the nuclear spins for both isotopes are the same. From Tables IV and VI, these

TABLE VI. Constants derived from the data for the experiments with the ground $^2P_{\frac{1}{2}}$ state of Ga^{69} and Ga^{71}.

	Ga^{69}	Ga^{71}
$\Delta\nu$	$\begin{cases} 2677.56 \pm 0.10 \times 10^6 \text{ sec.}^{-1} \\ 0.089319 \pm 0.000003 \text{ cm}^{-1} \end{cases}$	$\begin{cases} 3402.09 \pm 0.20 \times 10^6 \text{ sec.}^{-1} \\ 0.113488 \pm 0.000006 \text{ cm}^{-1} \end{cases}$
gI	-0.0007239 ± 0.0000015	-0.0009218 ± 0.0000015
μ	1.994 ± 0.005	2.540 ± 0.005

ratios are $(a_{71}/a_{69}) = 1.27063 \pm 0.00006$; $(\Delta\nu_{71}/\Delta\nu_{69}) = 1.27059 \pm 0.00008$; $(g_{71}/g_{69}) = 1.273 \pm 0.05$. The first two ratios are in even better agreement than could have been expected in view of the uncertainties in the values of $\Delta\nu$ and a. The discrepancy in the third ratio is not significant, as it can be explained by the uncertainties in the g-factors. It is probable that the ratios are more accurate than the individual values, because of cancellation of any systematic errors which may be present.

It may be of interest to note the values of the nuclear magnetic moments obtained by use of the Goudsmit[11]-Fermi-Segrè[12] formula for a p-electron:

$$\mu_I = \frac{aIZ_i(l+\frac{1}{2})J(J+1)1836.6\lambda}{\delta l(l+1)x} N.M. \quad (10)$$

λ and x are relativistic correction factors, and the other symbols have the same meaning as above. With the value of $(\Delta\nu/2)$ for the $^2P_{\frac{1}{2}}$ states substituted for a in (10), the moments are $\mu_{69} = 2.09$ and $\mu_{71} = 2.65$. These agree with the values given in Table VI within 5 percent. The values of a from the metastable states give values of μ equal to 1.56 and 1.99, which are too low by about 22 percent. This large discrepancy may be due to a perturbation by a higher configuration with the same value of J, as was discussed by Fermi and Segrè[12] for the case of Thallium.

We wish to acknowledge the help of Miss Zelda Marblestone in numerous calculations associated with this problem.

[11] S. Goudsmit, Phys. Rev. **43**, 636 (1933).
[12] E. Fermi and E. Segrè, Zeits. f. Physik **82**, 729 (1933)

New Experiments Concerning the Surplus Gamma-Radiation from Rocks

VICTOR FRANCIS HESS AND J. DONALD ROLL, S.J.
Fordham University, New York, New York

(Received December 4, 1947)

Previous investigation having shown that certain igneous rocks show a greater gamma-ray intensity than can be explained by their known uranium, thorium, and potassium content, two experiments were devised to determine if this surplus radiation could be due to artificial radioactivity induced within the rocks by cosmic rays, even though this possibility seemed unlikely from a theoretical standpoint.

A. A large sample of crushed dunite, an ultrabasic rock which is practically free of uranium, thorium, and potassium, was placed in an iron house (walls 10 cm thick) surrounding a sensitive ionization meter. It was found that the ionization observed with the dunite in the iron house was the same as with the iron house empty.

B. The experiments were then repeated with the iron house filled with crushed granite, first at Fordham University, and then in an underground station where a thick layer of rock reduced the intensity of cosmic radiation to a few percent of the value at sea level. No difference in the gamma-ray ionization from the granite sample was detected between the two levels. This shows clearly that the surplus gamma-radiation found previously by one of the authors (V.F.H.) cannot be ascribed to the effect of cosmic radiation on the granite.

Recently E. Gleditsch and T. Gráf have published a new determination of the intensity of gamma-radiation from potassium which is considerably higher than the hitherto accepted value of Gray and Tarrant. Since this new value is in sharp disagreement with others found in the literature, further experiments will be necessary before it can be decided definitely whether the surplus radiation is due to the unsuspected intensity of gamma-rays from potassium or to some other source as yet unknown.

IN previous papers[1] one of us has shown that a well-analyzed bulk sample of granite (Quincy, Massachusetts) gives off about twice the amount of penetrating radiation that could be expected from its known content of uranium, thorium, and potassium. This "surplus" of gamma-radiation exceeds by far all possible errors in the determination of the uranium, thorium, and potassium content. It was found[2] that neither the production of photons in transmutations induced by alpha-rays within the granite, nor spontaneous fission of uranium and thorium in the granite by cosmic rays, or by neutrons from cosmic rays, could account for the observed effect.

In order to determine directly whether cosmic rays produce some sort of penetrating and ionizing radiation when they are impinging on rocks, we thought it worth while to perform two decisive experiments:

A. To expose a type of rock almost free of uranium, thorium, and potassium to cosmic radiation and to see if any gamma-radiation is given off, in spite of the absence of radioactive elements in this rock.

B. To take a bulk sample of Quincy granite to a location where cosmic rays are practically absent (underground experiment), and to observe if the ionization produced by the gamma-rays of this sample is the same as was found at the surface of the earth.

It did not seem very likely that these experiments would give a positive result, however, it was necessary to carry them out in order to prove or to exclude the above-mentioned possibilities.

The technique used was the same as before:[1] a very sensitive ionization meter, devised by O. H. Gish, K. L. Sherman, and V. F. Hess, was placed in the center of the hollow interior of a cubical iron house, formed by iron and steel plates (10 cm thick) all around. Thus gamma-rays from the surroundings (local radiation) cannot enter the apparatus. When the space between the inner wall of the iron house and the ionization chamber is filled with about 300 lb. of crushed rock, the gamma-ray effect of this specimen of well defined thickness can be measured with great accuracy. Extrapolation to a layer of infinite thickness allows then a good comparison with the value of ionization computed from the known contents of uranium, thorium, and potassium in the specimen.

[1] V. F. Hess, Trans. Am. Geoph. Union **27**, 670 (1946); Norsk. Geol. Tidskr. **27**, 1 (1947).
[2] V. F. Hess, Phys. Rev. **72**, 609 (1947).

A. THE EXPERIMENT WITH DUNITE

Dunite is a mineral of ultrabasic character. A bulk sample of several hundred pounds of dunite was collected in Addie, North Carolina, by W. D. Urry and G. L. Davis of the Geophysical Laboratory, Carnegie Institution of Washington, D. C., in May 1947. The material was from "fist" to "bead" size. It was crushed by Urry and Davis in a rock crusher reserved for ultrabasic rock only, thus avoiding contamination. The radium content as determined by Davis is 0.007×10^{-12} g Ra per g rock. Therefore the uranium content is about 0.02×10^{-6} g U per g rock. The thorium content is not known exactly, but assuming a ratio Th/U=3, about 0.06×10^{-6} g Th per g dunite is to be expected. The potassium content, also estimated by Urry from a ratio K/U =10,000, would be about 0.0002-g K per g dunite. From these data it is clear that dunite contains less than 1/100 of the uranium, thorium, and potassium found in acidic igneous rocks like granite.

W. D. Urry computed the expected ionization by gamma-rays from an infinite layer of dunite completely surrounding an ionization chamber to be:

	0.0094 I from uranium-radium
	0.0136 I from thorium
	0.0086 I from potassium
Total	0.0316 I (i.e., ion pairs per cm³ per sec.)

Thus the total ionization expected is negligible when compared with the effects observed with granite (4 to 8 I).

The experiments were carried out in a basement laboratory at Fordham University. The ionization meter, an ionization chamber containing 4.9 liters of pure nitrogen at N.T.P., was placed in the center of the iron house previously described. The ionization chamber was also surrounded by a closely fitting lead cylinder and a lead bottom plate 0.98 cm thick. Ionization measurements were taken the first week with the iron house empty. Then 340 lb. of crushed dunite were poured into the hollow space between the cubical iron house and the lead-enclosed ionization chamber. The dunite remained in the house for five weeks, during which time the ionization was measured. Then the dunite was removed, and another background measurement was made. Each value listed below is an average of several days of almost continuous measurements. The observed effect is mainly due to ionization by cosmic rays, which after penetrating through four ceilings and the 10-cm top cover of the iron house have their effect reduced to 1.0 I, plus the residual ionization of the chamber, 1.25 I.

Table I shows that the ionization observed with the dunite around the chamber was, within the limits of experimental error, equal to the ionization observed without the dunite. From this we can conclude that cosmic rays do not excite any gamma-rays from dunite. Since the chemical composition of dunite is not so very different from other basic rocks, it seemed already rather certain that no rock emits more gamma-rays when exposed to cosmic rays than when cosmic rays are absent.

The dunite offered also a good opportunity to check the mass absorption coefficient for gamma-rays from RaC used in our computations. The mean density of the crushed dunite was determined as 1.73 g/cm³, by weighing a known volume. Two sealed radium preparations (30 and 100 micrograms each) were inserted within a thin brass tube at different distances from the center of the ionization chamber, directly within the crushed dunite. The maximum thickness of the absorbing layer of dunite was 21 cm. The value of the mass absorption coefficient of crushed dunite thus obtained was $\mu/\rho=0.0478$ cm²/g which is in good agreement with the accepted value of 0.045 cm²/g for RaC gamma-rays.

B. UNDERGROUND EXPERIMENTS

In order to eliminate completely any influence of cosmic rays the experiments would have to be carried out in a deep mine with several hundred meters of solid rock above the ap-

TABLE I.

1. Iron house empty:		
	Observed ionization	2.45 I before dunite experiment
		2.35 I after dunite experiment
	Mean:	2.40±0.04 I
2. Iron house filled with dunite:		
	Observed ionization	2.26, 2.22, 2.27, 2.53 I
		2.42, 2.29, 2.49, 2.47 I
		2.49, 2.57, 2.27, 2.27 I
	Mean:	2.38±0.02 I

TABLE II.

1. Ionization observed when iron house was empty (average of six days, July 29–August 5)		1.11 *I*
2. Ionization observed when iron house was filled with 350 lb. of granite chips	Aug. 6	3.84 *I*
	Aug. 8	3.69
	Aug. 11	3.84
	Aug. 12	3.96
	Aug. 13	4.01
	Aug. 14	3.89
(averages of about six hours each day)	Aug. 15	3.89
	Aug. 16	3.77
	Aug. 17	3.97
	Aug. 19	4.01
	Aug. 19	3.96
	Aug. 20	4.14
	Aug. 21	3.86
	Average	3.91 *I*
3. Ionization observed with iron house empty (average Aug. 22–26)		1.25 *I*
4. Net effect of gamma-rays from Quincy granite through 1-cm lead shield around ionization chamber		$3.91-1.18 = (2.73\pm0.04)$ *I*

TABLE III.

1. Ionization in empty iron house	2.60 *I*
	2.56
	2.64
	2.63
	2.64
	2.57
Average:	2.60
2. Ionization when iron house was filled with granite	5.35
	5.41
	5.21
	5.46
	5.56
	5.39
Average:	5.39
Net ionization by granite:	2.78 ± 0.06 *I*

paratus. For the present purpose it seemed more convenient and quite sufficient to go to a depth of 120 meters of water equivalent, since at this depth, according to E. Regener, the total intensity (ionization) of cosmic rays is already reduced to about 1 percent of the surface value. Taking the mass absorption coefficient for the hard component as 0.2×10^{-3} cm²/g, a layer of 40 meters of solid rock of density 3 would transmit only 8 percent of the hard mesotron component.

The location chosen for our experiments was a tunnel in the subway system of New York, directly below the hill on which Fort Tryon Park is situated. The Board of Transportation of the City of New York erected a small hut for us on the north end of the platform of the 190th Street station (Washington Heights) of the Independent Subway System. The iron house and all instruments were set up in this hut. Transportation of several thousand pounds of steel and other equipment to this place was not too difficult since there was only one stairway between the entrance and the platform that required unloading and reloading of the wheelbarrows. The experiments were carried out between July 18 and August 30, 1947. Initial difficulties resulting from humidity were soon overcome, and the apparatus was in perfect condition throughout the period mentioned. The results are summarized in Table II.

The net effect of the gamma-rays from the crushed granite as observed in the subway station (2.73 *I*) is approximately the same as was observed under identical conditions in the basement of the Physics Building at Fordham University (2.78 *I*). These latter observations are summarized in Table III.

A comparison of the results in Tables II and III shows that granite produced the same ionization underground as it did at Fordham. It is to be noted that these values have not been corrected for an infinite layer of granite nor for the "open cone," but are for the purpose of relative comparison only. Cosmic rays, therefore, do not produce any secondary effects or artificial radioactivity in the granite. Additional evidence for this is the fact that we did not find any decrease of the gamma-ray activity of the granite during the three weeks that the granite remained underground where the cosmic-ray intensity was only 0.08 of the hard component at sea level.

DISCUSSION

Since a rock like dunite which is practically free of uranium, thorium, and potassium was found to emit no detectable amount of gamma-radiation when exposed to cosmic rays, while, on the other hand, granite, containing well-known amounts of uranium, thorium, and potassium, gives off the same amount of gamma-radiation whether exposed to cosmic rays or protected from them, it is now established by experiment that cosmic rays do not produce detectable amounts of fission or artificial radio-

activity in granite or other rocks, accompanied by gamma-radiation. The surplus radiation observed in the granite, therefore, must either be due to an unknown source contained in the granite, or be connected with its uranium, thorium, and potassium content.

The computation of the ionization effects of the hard gamma-rays from these three components is based upon the use of three values (K_1, K_2, K_3) of Eve's constant for the gamma-rays from RaC, ThC″ and potassium and their mass absorption coefficients. The values for K_1 (for RaC) and K_2 (for ThC″) were directly determined by one of us[1,2] and cannot be off by more than a few percent. The only weak spot in the computation could be the value of K_3 (Eve's constant for potassium) which was taken as 0.07 I per g of potassium per cm per sec., a mean value of two rather divergent determinations of Mühlhoff[3] and Gray and Tarrant.[4] According to the former author the gamma-radiation of 1 g of potassium is equivalent to 3.34×10^{-11} g radium, while according to the latter it is equivalent to 1.6×10^{-11} g radium.

Quite recently E. Gleditsch and T. Gráf[5] published a new determination of the intensity and the absorption coefficient of potassium gamma-rays which leads to considerably higher values. According to them 1-g potassium would be equivalent to $(1.23\pm0.15)\times10^{-10}$ g radium, which would increase the computed effect of the potassium in rocks five times. If this is correct, the computed potassium component of the Quincy granite in our experiments would be brought up from 0.75 to almost 4 I and would exceed the combined effects of uranium and thorium (1.9 I). Thus the total gamma-radiation actually found with granite would be about the same as the one computed using the values of Gleditsch and Gráf. It is obvious that a new and direct determination of the value K_3 of Eve's constant for potassium will show whether or not the surplus radiation of granite can really be ascribed to the potassium gamma-rays. We are planning to do this in the near future.

Several colleagues expressed the opinion that the use of the customary values of the mass absorption coefficients for the gamma-rays from RaC, ThC″ and potassium (0.045 and 0.041 cm²/g) might lead to erroneous values in the computation of the ionization expected when an ionization chamber is completely surrounded with crushed rock, because of the scattering effect. We tested this directly, as pointed out earlier in this paper, and found that the mass absorption coefficient of the gamma-rays from RaC obtained (0.0478) with crushed rock all around the chamber was practically identical with the value used in the computation (0.045).

We acknowledge gratefully the assistance given to us by the Board of Transportation of the City of New York in enabling us to carry out the experiments in the subway station and also the help of the Geophysical Laboratory(Carnegie Institution of Washington) in providing and preparing the bulk sample of dunite, which was furnished through the courtesy of the Harbison-Walker Refractories Company of Pittsburgh. Funds for the experiment were provided by a grant from the American Philosophical Society.

[3] W. Mühlhoff, Ann. d. Physik (5), **7**, 205 (1930).
[4] L. H. Gray and C. T. P. Tarrant, Proc. Roy. Soc. London **A143**, 681 (1934).
[5] E. Gleditsch and T. Gráf, Phys. Rev. **72**, 640 (1947).

Gamma-Radiation from Granite

WILLIAM D. URRY
Geophysical Laboratory, Carnegie Institution of Washington, Washington, D. C.

(Received December 5, 1947)

It has been reported that measurements of the ionization produced by the gamma-rays from Quincy granite are in excess of the ionization computed from the measured uranium, thorium, and potassium content of the rock by a factor of over two. It was concluded that either the measured radioactive contents were much too low or that a hitherto unknown penetrating radiation was given off by the granite.

Measurements of the gamma-radiation from Quincy granite have now been made in such a way that it is unnecessary to *compute* the ionization arising from the reported radioactive contents in order to make the comparison. After the measurements of the ionization produced by the Quincy granite were made, uranium, thorium, and potassium were added in the form of pitchblende, monazite, and potassium carbonate in amounts which would exactly double the reported radioactive contents. The ratio of the measured ionization in the latter case to that in the former was 2.06 ± 0.13. The gamma-ray ionization from the Quincy granite thus seems to be fully accounted for by the measured uranium, thorium, and potassium content.

Now, when the results of the previously reported measurements of the ionization from the Quincy granite and the present measurements are reduced to comparable conditions, the two sets of measurements are in good agreement; therefore, it seems likely that the discrepancy which had indicated a large excess of penetrating radiation, or a large error in the measurement of the radioactive content, may have arisen in the computation of the expected ionization. This conclusion is fully supported by very recent work on the gamma-radiation from potassium which was reported after the preparation of this paper.

1. INTRODUCTION

THE ionization produced by the gamma-rays from Quincy granite according to the measurements made by V. F. Hess[1] exceeded the expected ionization computed from the measurements of the uranium, thorium, and potassium content by a factor of about two. Hess came to the conclusion that either the measured uranium and thorium contents were much too low or that one has to assume that granite, and perhaps most of the other rocks, emits a penetrating radiation of unknown origin. Either conclusion is sufficiently intriguing to warrant further investigation.

It is possible to avoid any computation of the expected ionization in making a comparison of the gamma-ray ionization produced by the granite with that produced by amounts of uranium, thorium, and potassium equal to the reported contents in the rock by adding to the granite amounts of these elements equal to the reported contents. The ionization should be exactly doubled if there exists no unknown radiation from the granite and if the reported contents are correct. An increase in the ionization by only 40 to 50 percent would confirm the result obtained by Hess.

The added uranium and thorium must have all their daughter elements present in equilibrium. Uranium was added in the form of pitchblende from Great Bear Lake. The sample was the remainder of a powder analyzed for uranium. Thorium was added in the form of monazite from Mars Hill, North Carolina, and a part of the same specimen has been analyzed by Marble.[2] Potassium was added as the carbonate.

The principal, if not the only, source of ionization from U and Th in the chamber is the hard gamma-ray from RaC and ThC″, both of which are below radon and thoron in the series. In order to be sure that radon and thoron were not lost from these powdered samples, the materials were bottled and sealed in square-type quart Mason jars. As a further precaution, these jars were stored for 35 days following addition of the internal standards.

A question arises as to whether the background ionization with air surrounding the chamber, which was subtracted in the experiments of Hess from that measured with the granite, might not be lower than the required background be-

[1] V. F. Hess, Trans. Am. Geophys. Union **27**, 670 (1946); Phys. Rev. **72**, 609 (1947).

[2] J. P. Marble, Am. Mineralogist, **21** 456 (1936).

cause of the cosmic-ray transition resulting from the mere presence of the granite. In order to settle this point, several hundred pounds of the ultrabasic rock dunite[3] was collected and sorted at Addie, North Carolina. This rock is practically free of activity. Measurements of the radium content by G. L. Davis at this Laboratory showed 0.007×10^{-12} g Ra per g, which is equivalent to 0.7 percent of the uranium content of the Quincy granite. The potassium content is very small (less than 0.0005 percent), and the thorium content is presumably not very different from that given by the universal ratio of Th/U equal to 3 in rocks. Thus, all of the three elements are present to about the extent of 0.5 to 0.7 percent of the content in Quincy granite. The ionization from the dunite is, therefore, quite negligible. Hess[4] showed with this dunite that any increase in background resulting from cosmic-ray transition in a solid mass surrounding the chamber was quite negligible.

In the experiments of Hess the rock was surrounded by sufficient iron to shield out the gamma-radiation from the walls of the room. In the present experiments, installation of such a shield was not feasible; the true background, therefore, was obtained with a duplicate set of Mason jars filled with dunite.

2. EXPERIMENTAL

The apparatus, primarily designed for the determination of small quantities of radium, has been described.[5] Deflections and hourly calibrations of the Lutz-Edelmann electrometer are recorded on microfile film. As used to determine radium, the apparatus contains a dual system of balancing chambers. In order to measure the gamma-ionization from a source such as granite outside the chamber, the lower chamber was grounded and the upper chamber was surrounded by a circular table, the table top being level with the bottom of the cylindrical chamber.

Without rebuilding the apparatus, it was possible to surround the chamber for an arc of only 194 degrees and for a distance of 45 cm from the axis of the chamber. The upper level of the rock in the Mason jars was approximately level with the top of the chamber.

The most satisfactory arrangement of the 41 bottles on the table to form a closely packed, more or less semicircular mass of rock was established, and positions and bottle numbers were mapped on the table. This "geometry" was rigidly maintained for all the measurements.

For these experiments Dr. Hess kindly lent me 200 lb. of the same Quincy granite that he had used in his measurements. The granite was approximately ½-inch mesh in size. The dunite was crushed and sieved to about the same size. The interstices in this coarse packing of both the granite and the dunite were filled with the same weight of fine dunite (through 32 on 65 mesh). This served the double purpose of increasing the stopping power of the granite-filled bottles to approximately that of the dunite-filled bottles, and of providing a carrier for the internal standards.

Alternate determinations of the ionization with dunite-filled bottles and with the granite-filled bottles were first made. The internal standards were then added to the granite-filled bottles, which were sealed and set aside for 35 days, after which the alternating measurements were repeated. Each determination lasted 16 to 22 hours, the totals being 162 hours for dunite, 66 hours for the granite, and 58 hours for the granite with the internal standards.

All measurements were made with the original filling of nitrogen in the ionization chamber, the density being such that the factor for reduction to 0°C and 760 mm was 1.108. In these experiments the procedure is purely one of comparison, and, therefore, the results were not reduced to N.T.P.

3. RADIOACTIVE CONTENT OF QUINCY GRANITE

Keevil[6] has measured the radium and thorium content of Quincy granite from several quarries —and at several depths in the Swingle quarry, the one from which the material was taken for Hess. Evans and Goodman[7] report a radium and thorium value for the 150-ft. level. The average

[3] The average atomic number of dunite is 10.1, that of Quincy granite 10.2; therefore, there should be no difference in the cosmic-ray transition in the two rocks.

[4] V. F. Hess, Phys. Rev. **72**, 609 (1947).

[5] Wm. D. Urry and C. S. Piggot, Am. J. Sci. **239**, 633 (1941).

[6] N. B. Keevil, Am. J. Sci. **36**, 406 (1938).

[7] R. D. Evans and C. Goodman, Bull. Geol. Soc. Am. **52**, 459 (1941).

TABLE I. The gamma-ray ionization, I, produced by Quincy granite, and Quincy granite to which internal standards of uranium, thorium, and potassium were added to double the reported radioactive content.

Date	Dunite (background)	Quincy granite	Quincy granite with internal standards
June 1947	5.18±0.04[a]	6.22±0.13	
	5.16 0.05	6.02 0.11	
	5.49 0.17	5.96 0.11	
	5.01 0.10	6.29 0.07	
	5.11 0.12		
	5.45 0.04		
Aug. 1947	5.43 0.08		7.28±0.09
	5.07 0.10		7.09 0.06
	5.26 0.08		7.06 0.08
Weighted mean	5.264±0.021	6.165±0.048	7.124±0.042
Weighted(June mean (Aug.	5.26±0.02) 5.28±0.05)		
Quincy granite with internal standards less background			1.86±0.05
Quincy granite less background			0.90±0.05
Ratio of Quincy granite with internal stds/ Quincy granite			2.06±0.13

[a] The root mean square probable error, σ, used to weight the individual determinations by $1/\sigma^2$.

of the results of both investigators for the levels of 12, 120, 150, and 350 feet yields a radium content of 0.99×10^{-12} g per g, with variations from 0.91 to 1.14. The mean thorium content is 8.95×10^{-6} g per g, with variations from 7.0 to 12.4. Dr. L. F. Curtiss of the National Bureau of Standards determined the radium content of the Hess sample to be 1.02×10^{-12} g per g. The radioactive content of the Quincy granite is apparently remarkably uniform. For our purposes we shall take 1.00×10^{-12} g Ra per g and 8.95×10^{-6} g Th per g.

Dr. E. G. Zies of this Laboratory kindly determined the potash content of a quartered sample of the Hess Quincy granite. It contains 4.64 percent K_2O, equivalent to 3.85 percent potassium. This result is in excellent agreement with analyses by Warren[8] on other samples.

4. INTERNAL STANDARDS

The total weight of granite was 51,560 grams, which required the addition of 3508 grams of potassium carbonate to double the potassium content of 3.85 percent. By analysis at this Laboratory, the potassium carbonate contained 0.55×10^{-12} g Ra, equivalent to 0.0055 g U in the total weight to be added.

[8] C. H. Warren, Proc. Am. Acad. 49, 227 (1913).

The monazite contained 5.56 percent Th, which required the addition of 8.299 grams of monazite to double the thorium content, but the monazite also contained 0.0178 percent U, equivalent to 0.00147 g U in the total weight to be added.

The radium content of the granite is equivalent to 2.87×10^{-6} g U per g, which will be doubled by the addition of 0.148 g U, of which 0.007 g will be contributed by the impurities calculated above in the potassium carbonate and monazite, leaving 0.141 g U to be provided by 0.266 g pitchblende containing 53.00 percent U.

In order to insure uniform distribution, the above weights required to double the reported contents were divided by the number of bottles, and the corresponding amounts were added to each bottle. Each bottle contained the same weight of granite. The amount of fine dunite filling the interstices between the granite, with which the internal standards were mixed, was reduced by the weight of the potassium carbonate at this stage.

5. RESULTS

The results are reported in Table I in ion pairs per cc per sec. (designated by I). The accuracy of the absolute values of I is of no importance in this comparison method, but as shown below, the electrostatic capacity has been accurately determined.

Within the narrow limits of the probable error, the ionization produced by the gamma-rays from Quincy granite is just doubled (2.06±0.13) *by adding the amounts of uranium, thorium, and potassium equal to the reported contents.* There is no reason to suspect the reliability of the modern techniques used in the determinations of the small amounts of radium and thorium in rocks, nor to doubt the accuracy of the standards employed in these techniques.

Had the experiment confirmed the result reported by Hess, the measured ratio of the ionizations in the above experiment (if we use his figures[9]) should have been $(9.50+4.12)/9.50 = 1.43$, or, stated another way, a value of only $1.29I$ should have been obtained with the internal standards. Hess employed radium, thorium, and

[9] V. F. Hess, Trans. Am. Geophys. Union 27, 670 (1946). See Table 2.

potassium contents of the Quincy granite, which were somewhat lower than those based here on all the observations in the literature, on a more recent determination by Dr. Curtiss on the sample used by both of us, and on the determination of the potash content at this Laboratory. The effect of using the newer data is to raise the ratio slightly—from 1.43 to 1.49.

At one time it was thought that components of the gamma-radiation softer than those arising from RaC and ThC″ might have caused ionization through the thin wall used by Hess. The softer gamma-rays were neglected in the calculation. Hess[10] has recently repeated the experiments with sufficient lead between the chamber and the granite to absorb any gamma-radiation softer than that arising from RaC, ThC″, and K. The result was essentially the same and equal to 1.55 in terms of the above ratio.

There is, of course, the possibility that an unknown hard gamma-radiation is emitted from the uranium or thorium series or from potassium. Calculation of the expected ionization requires a knowledge of Eve's constant, the number of ion pairs per cc per sec. per gram of uranium (thorium or potassium) at unit distance from the center of the ionization chamber. The only likely source of error, involving an unreported hard gamma-ray among the familiar radioactive elements, is in the value of Eve's constant for potassium. This constant has not been measured. Calculating for the first method employed by Hess, namely, from the three photons emitted for every 100 disintegration electrons, we find that the discrepancy between the computed ionization and the measurements over a flat surface of the Quincy granite would be entirely eliminated if the correct figure were about 15 photons per 100 electrons. One would doubt that Gray and Tarrant[11] could have been in error to this extent.

6. SUPPORTING EXPERIMENTS

A few experiments were performed which support the major results given in Table I.

In one series of measurements on the ionization produced by the Quincy granite with internal standards, the bottles were rearranged in the $(41-n)$ positions. A value of $7.09\pm0.06I$ was obtained, which, compared to $7.16\pm0.06I$ for the measurements in the normal positions of the numbered bottles, demonstrates uniform distribution of the internal standards.

Eve's constant for radium was measured with a 100-microgram radium standard from the National Bureau of Standards, surrounded by 1.50 cm of lead and placed at 50.0 cm from the center of the chamber. With allowance for the absorption in the 0.565-cm brass wall of the chamber (absorption coefficient $\mu=0.370$ cm^{-1}) and in the lead ($\mu=0.531$ cm^{-1}), the value of Eve's constant K at 0°C and 760 mm of nitrogen was found to be $5.64\times10^{9}I$ for a ratio A/W of wall area to volume in the chamber of 0.393. This value can be compared with the plot of K against A/W given by Hess and Balling[12] by dividing by their factors of 1.062 for 20°C and 767.7 mm of nitrogen and 1.097 for the absorption in their brass wall of 0.25-cm thickness. The result is $4.85\times10^{9}I$, which is very close to their curve of K against A/W. Such agreement lends strong support to the conclusion that the measurements are comparable in the two laboratories and indirectly substantiates the correctness of the determination of the electrostatic capacity of the ion-collecting system.

Without moving the radium standard, measurements were made with the dunite and the granite interposed, in turn, between the 100 micrograms of radium and the chamber. The ionization produced by the gamma-rays from the radium was reduced, respectively, to 0.053 and 0.051 of the ionization without absorption in the dunite or in the granite.

It was previously found that the dunite reduced the stray radiation in the room by about $1I$; accordingly, about $0.05I$ is produced by the stray radiation passing through the dunite. From the above absorption experiments, the stopping power of the dunite-filled bottles and of the granite-filled bottles cannot differ by more than 10 percent; hence, the possible error caused by different absorption of the stray radiation in the dunite and in the granite is not over $0.005I$.

From the absorption experiments, one can

[10] V. F. Hess, Phys. Rev. **72**, 609 (1947).
[11] L. H. Gray and G. T. P. Tarrant, Proc. Roy. Soc. London **A143**, 681 (1934).
[12] V. F. Hess and E. Balling, Trans. Am. Geophys. Union **26**, 237 (1945).

compute the absorption coefficients for the rock-filled bottles. With dunite $\mu=0.0837$ cm^{-1} for a bulk density of the bottles in position on the table, $\rho=1.935$-g cm^{-3}. With the granite $\mu=0.0825$ cm^{-1} for $\rho=1.84$-g cm^{-3}. The mass absorption coefficients are thus $\mu/\rho=0.043$-cm^2 g^{-1} and 0.045-cm^2 g^{-1}, respectively, in good agreement with the accepted value of 0.045 for the gamma-rays from RaC, and also with a similar determination by Hess, which is 0.043 for the Quincy granite.

7. COMPARISON OF MEASUREMENTS

The ionization, which would have been produced in the experiments reported here if the whole chamber had been completely surrounded by an infinite thickness of the granite, can be roughly estimated and compared with the same quantity q_∞ determined by Hess.

The thickness of the wall of the chamber used by Hess was 0.25 cm (brass), whereas the thickness of the chamber wall used here was 0.565 cm (also brass). The solid angle subtended by the granite amounted to $4\pi\times0.138$ steradians. Thus, if the present chamber had a wall thickness of 0.25 cm and granite completely surrounded the chamber, q_d would be $(0.90\times1.124)/0.138=7.33I$.

In the present experiments, the chamber was surrounded to a depth of 38 cm, but there was an air gap of 2 cm on the average between the wall of the chamber and the nearest granite. Under these conditions, and taking the absorption coefficient $\mu=0.0825$ cm^{-1} as determined above for RaC (which will be close enough to the mean value for RaC, ThC″, and K in the granite), the value of $q_\infty=7.33/0.804=9.1I$. This is in good agreement with the value of q_∞ of $9.5I$ determined by Hess, particularly in view of the accuracy of such a calculation. There is, thus, no serious disagreement between *measurements* of the ionization produced by the gamma-rays from Quincy granite in the two laboratories.

8. CONCLUSIONS

These experiments show no source of gamma-ray ionization in the Quincy granite other than the reported contents of uranium, thorium, and potassium. The measurements of the ionization produced by the gamma-rays from the Quincy granite are in good agreement with the determinations reported by Hess. Hence, there seems to be only one source of discrepancy between the absence of any extraneous gamma-radiation in the Quincy granite as established by the present experiments and the large excess, reported by Hess, of measured gamma-radiation over that computed from the uranium, thorium and potassium content. The discrepancy apparently lies in the equations for the computation or in the data entered in these equations.

Since this paper was first drafted, Gleditsch and Gráf[13] have reported a value of 3.6 gamma-quanta per second per g K. There are, therefore, 15.7 photons per 100 electrons on the basis of 23 beta-rays per second per g K, the latter figure being that used by Hess. This ratio between the photons and electrons is almost exactly that previously calculated to be necessary in order to remove the discrepancy in the experiments conducted by Hess at the Swingle Quarry (*vide supra*). The value of Eve's constant for potassium can be obtained from that for radium, combined with the value of the equivalency of potassium and radium in gamma-producing capacity determined directly by Gleditsch and Gráf to be 1.23×10^{-10} g Ra. Eve's constant for potassium $=0.590I$ per g K for the chamber used by Hess. This yields a value of $6.34I$ arising from the potassium content (3.85 percent) of Quincy granite or $9.7I$ for U+Th+K for an infinite thickness and 4π steradians. This is in very satisfactory agreement with the measurements in both laboratories.

One may, therefore, conclude that there is no source of extraneous gamma-radiation in Quincy granite and probably not in other rocks. The experiments reported here, taken together with those performed by Hess, strongly support the latest value for the gamma emission of potassium-40 determined by Gleditsch and Gráf.

9. ACKNOWLEDGMENTS

It is a pleasure to acknowledge the continued and kindly cooperation of Dr. V. F. Hess, with whom personal contact was maintained throughout the course of these experiments and during the preparation of this manuscript. To Dr. H.

[13] E. Gleditsch and T. Gráf, Phys. Rev. **72**, 640 (1947).

Yagoda, of the National Institute of Health, the author is indebted for the remainder of a powdered sample of pitchblende that he had analyzed for uranium. The National Museum, Washington, D. C., kindly supplied the sample of monazite through the good offices of Messrs. E. P. Henderson and Wm. F. Foshag, and thanks are due Dr. J. P. Marble for his advice in the choice of a suitable thorium mineral. Dr. E. G. Zies of the Geophysical Laboratory kindly contributed to the problem through his determination of the potash content of the Quincy granite. Dr. Merle A. Tuve of the Department of Terrestrial Magnetism, Carnegie Institution of Washington, was responsible for arousing the author's interest in the problem during the course of an informal discussion concerning the possibility of obtaining for Dr. Hess a rock that would be essentially free of any radioactivity. The Harbison-Walker Refractories Company of Pittsburgh, Pennsylvania, kindly contributed several hundred pounds of such a rock in the form of dunite from their quarry at Addie, North Carolina.

PHYSICAL REVIEW VOLUME 73, NUMBER 6 MARCH 15, 1948

The Beta-Spectra of Cu^{64} as a Test of the Fermi Theory

C. Sharp Cook and Lawrence M. Langer
Indiana University, Bloomington, Indiana

(Received December 10, 1947)

The momentum spectra of the negatrons and positrons emitted by Cu^{64} have been measured with high resolution under such conditions that the usual distortions resulting from source thickness and backing, scattering, and finite counter window are completely negligible for almost the entire range of energies. Whereas the Fermi theory predicts the correct distribution for the high energy region, it is found that there are more negatrons and positrons than are predicted by the theory at low energies. The shapes of the spectra and the fact that no nuclear gamma-rays are observed preclude the possibility that they are complex spectra. Deviation from the Fermi theory occurs for energies below 0.270 Mev for the positrons and for energies below 0.190 Mev for the negatrons.

Incidental to these measurements, the end-point energies have been determined as 0.657 $\pm$0.004 Mev for the positrons and 0.571$\pm$0.002 Mev for the negatrons. The ratio of the total number of electrons to positrons is 2.0.

I. INTRODUCTION

A DETAILED investigation of the momentum distributions of the negatrons and positrons emitted by Cu^{64} has been made in order to test the validity of the Fermi theory of beta-decay.[1] When applied to reliable experimental data, the Fermi theory, using Fermi's original choice of interaction, has been remarkably successful in describing the high energy end of the beta-ray spectrum. The Kurie plot[2] of the experimental data yields a straight line for a large part of the distribution of all allowed and many forbidden transitions and is a valuable tool for accurately determining the end-point energy.

Many experimenters,[3] however, have observed that there are apparently more particles in the low energy region of the distribution than are predicted by the Fermi theory. This deviation from the theory has usually been attributed to distortion resulting from instrumental difficulties such as finite source thickness and backing, absorption in the counter window, and scattering from the walls of the spectrometer. In some cases, the excess at low energies is caused by the fact that the spectrum is complex,

[1] E. Fermi, Zeits. f. Physik **88**, 161 (1934).
[2] Franz N. D. Kurie, J. R. Richardson, and H. C. Paxton, Phys. Rev. **49**, 368 (1936).
[3] A. W. Tyler, Phys. Rev. **56**, 125 (1939). J. L. Lawson, Phys. Rev. **56**, 131 (1939). K. Siegbahn and H. Slatis, Ark. f. Mat., Ast., o Fysik **32A**, No. 9 (1946). A. A. Townsend, Proc. Roy. Soc. **A177**, 357 (1941).

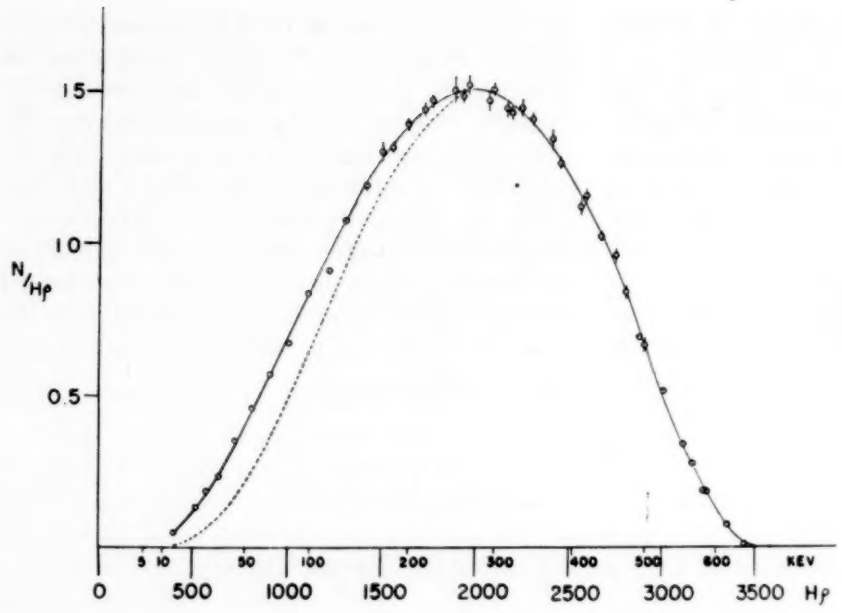

FIG. 1. Momentum spectrum of Cu^{64} positrons. Dashed curve is the distribution according to Fermi theory.

consisting of one or more transitions to excited levels of the product nucleus as well as to the ground state. Such complex spectra should, of course, be accompanied by gamma-radiation corresponding to the difference between the end-point energies.

Recently, Backus[4] measured the energy distribution of the positrons and negatrons from Cu^{64} at low energies, using an extremely thin source and backing and a counter window of negligible thickness. Because of the limitations of the electrostatic spectrometer which was used, he was not able to make measurements above 50 kev. Because of the proximity of the deflecting electrodes to the electron beam and because of the absence of baffles, one might expect a certain amount of scattering, which might or might not be the same for positrons and electrons.

Backus compared his results with the Fermi theory by plotting the log of the ratio of positrons to electrons as a function of the energy. He found a marked disagreement with theory. Lewis and Bohm[5] attempted to account for Backus' results by introducing a linear combination of the possible beta-interactions into the equation for the distribution. From an examination of Backus' data they concluded that the positron distribution was in agreement with the Fermi theory and that the negatron spectrum needed correcting. Since Backus' data cover such a small region of the total distribution, it seems dangerous to rely on deductions from them for the rest of the spectrum. Actually, as is shown below, neither the negatron nor the positron spectrum follows the Fermi theory. Whereas Backus' data for the ratio of positrons to electrons is apparently correct, the explanation offered by Lewis and Bohm is invalid.

In the present experiment, an attempt was made to measure the beta-ray spectra of Cu^{64} over the entire energy range, under such conditions that any possible distortion of the true distribution would be negligible.

Cu^{64} is a particularly suitable element for a test of the Fermi theory. Both beta transitions are allowed and should presumably give straight line Kurie plots. The end points and intensities of both the positrons and negatrons are comparable and so both may be measured under identical conditions. Cu^{64} activates strongly so that extremely thin sources of high specific activity are possible. The 12.8-hr. half-life is convenient so that complete positron and negatron spectra may be obtained from each source which is prepared. Except for an extremely weak radiation of about 1.3 Mev which follows

[4] J. Backus, Phys. Rev. **68**, 59 (1945).
[5] H. Lewis and D. Bohm, Phys. Rev. **69**, 129 (1946).

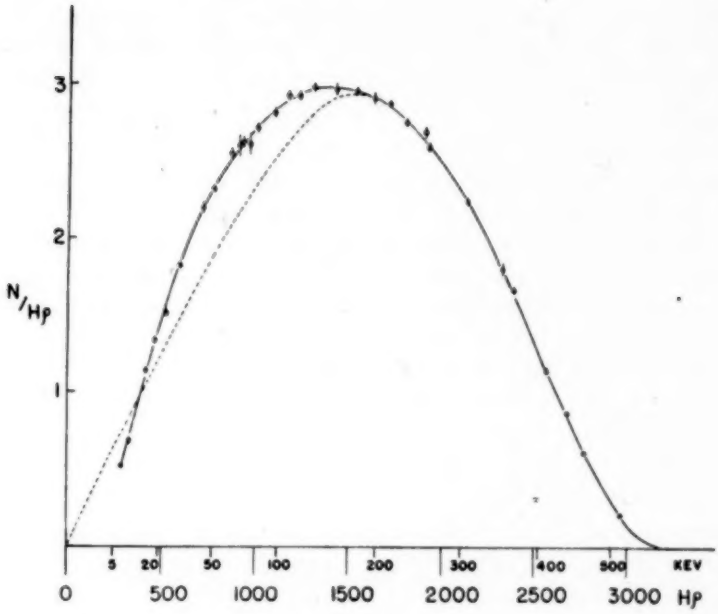

FIG. 2. Momentum spectrum of Cu^{64} negatrons. Dashed curve is the distribution according to the Fermi theory.

a very infrequent transition by K capture,[6] there seem to be no nuclear gamma-rays from Cu^{64} and the spectra are presumably not complex.

II. EXPERIMENTAL METHOD

The measurements on the Cu^{64} spectra have been made with a large, high resolution magnetic spectrometer. This instrument is described in detail in another paper.[7] By using a magnetic field which varies radially in the proper manner, it is possible to obtain high resolution and good intensity in the large instrument. The nominal value of the radius of curvature is 40 cm. Using a source and a counter slit 0.4 cm wide and 2.54 cm high, the measured resolution for an internal conversion line is $\Delta H\rho/H\rho = 0.5$ percent for the full width at half maximum. Under these conditions the transmission is about 0.1 percent of the total solid angle.

Because of the large size and the strategic baffling, background and scattering effects are completely negligible. The source is isolated at a considerable distance from any material which might introduce scattering. The main defining slit, located midway between the source and the counter slit, accepts a 2.54 cm-high beam with a spread of 32 degrees in the plane perpendicular to the magnetic field. The edges of the defining slit are made of Polythene. The inside height of the aluminum vacuum chamber is 2.5 inches giving the beam a $\frac{3}{4}$-inch clearance above and below. Good evidence for the complete lack of scattering in the instrument is the extremely sharp high energy edge obtained for internal conversion and photo-lines and the fact that no counts are observed when the magnetic field is set for an energy lower than the calculated cut-off of the counter window or higher than the end point of a beta-spectrum.

Also because of the large size, it is possible to spread the active material over a larger area so as to minimize the self-absorption and scattering caused by the finite thickness of the source.

The particles are detected by means of an end window G-M counter. For a few preliminary runs, an unsupported mica window of 2.42 mg/cm^2 was used. Such a window has a range of about 35 kev and affects the shape of the electron distribution as high as 150 kev. For the final runs, a very thin Zapon window[7] capable of transmitting electrons having an energy as low as 2.0 kev was used. Such a window should not distort the spectrum above 10 kev (see also reference 4). The supporting grid for the Zapon foil is of sufficient thickness so that trans-

[6] H. Bradt, P. C. Gugelot, O. Huber, H. Medicus, P. Preiswerk, P. Sherrer, and R. Steffen, Helv. Phys. Acta 19, 219 (1946); M. Deutsch, Phys. Rev. 72, 729 (1947).

[7] L. M. Langer and C. S. Cook, Rev. Sci. Inst., in press.

mission by the window is not dependent on energy. This grid is especially designed[7] to avoid partial transmission of rays coming through the window at an angle.

Relative magnetic field measurements were made with a flip coil and ballistic galvanometer. The absolute calibration of the magnetic field is in terms of the photoelectrons ejected by the 0.5108 Mev annihilation radiation. The energizing current for the magnet is stabilized electronically. If about one minute is allowed to elapse after each shift of the energizing current, then the magnetic field remains constant to better than 0.1 percent. At least two ballistic galvanometer readings were taken for each point counted. The calibration of the ballistic galvanometer was checked before and after each run in terms of a standard mutual inductance. In making measurements with a field of less than 20 gauss, care was taken to vary the current according to a prescribed cycle so as to avoid any change in the radial field distribution caused by remanence effects in the iron. This precaution is necessary in order to avoid distortion of the spectrum below about 30 kev.

Counts are recorded by a Higinbotham type scaler.[8] Counting rates are always such that losses are completely negligible.

The general procedure in making runs was to work through a complete spectrum and then put in arbitrary points at various parts of the distribution. It was found that with the preparation of the source described below, all parts of the Cu^{64} spectra decayed with the 12.8-hr half-life.

III. PREPARATION OF SOURCES

Cu^{64} can be prepared by deuteron bombardment of copper or zinc according to the reaction: $Cu^{63}(d, p)$ and $Zn^{66}(d, \alpha)$. Although bombardment of zinc might seem preferable in order to obtain a separated source of high specific activity, it was found that the 11.5-Mev deuterons

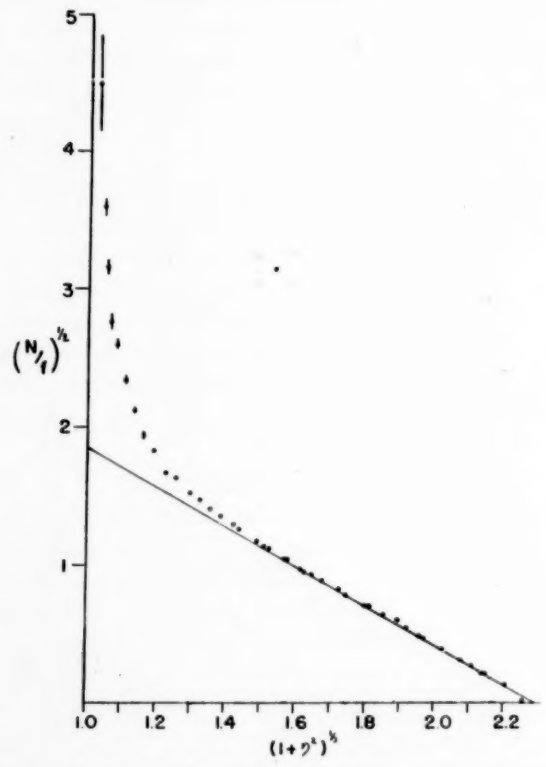

FIG. 3. Fermi plot of Cu^{64} positron spectrum. The extrapolated end point corresponds to 0.657 ± 0.004 Mev. Deviation from the straight line begins at 0.270 Mev.

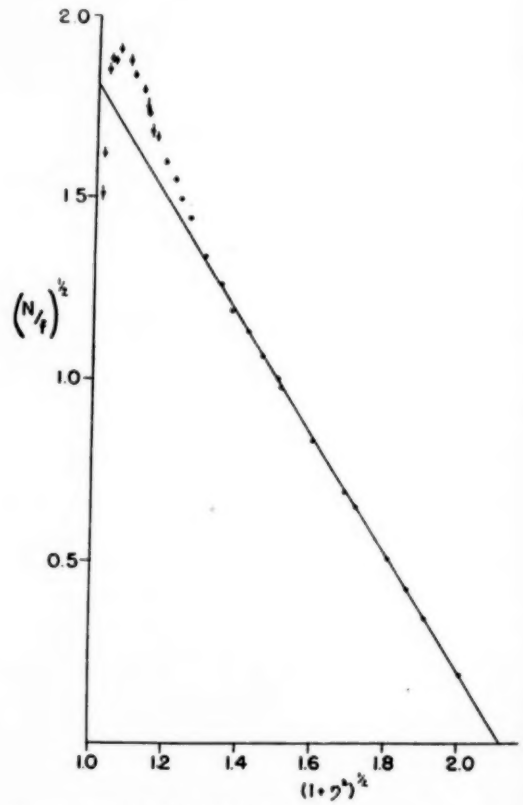

FIG. 4. Fermi plot of Cu^{64} negatron spectrum. The extrapolated end point corresponds to 0.571 ± 0.002 Mev. Deviation from the straight line begins at 0.190 Mev.

[8] W. A. Higinbotham, James Gallagher, and Matthew Sands, Rev. Sci. Inst. 18, 706 (1947).

available at the target chamber of the cyclotron produced a considerable quantity of Cu^{61} of 3.4-hr. half-life according to the reaction Zn^{64}. $(d; \alpha, n)$. The Cu^{61} cannot be chemically separated from the Cu^{64} and its period is sufficiently long so that it interferes with the measurements on Cu^{64}.

The method finally used, therefore, was to bombard copper on a probe. The probe was inserted to a radius which corresponds to 8-Mev deuterons so as to get maximum yield.[9] Bombardments were of from 4 to 8 hours duration with a circulating deuteron beam of several hundred microamperes.

A few flakes were scraped from the most active region of the bombarded target and dissolved in a small amount of nitric acid. To this was added 15 cc of distilled water and 25 cc of concentrated sulphuric acid. The solution was then heated to drive off the excess nitric acid. Copper was then separated from any zinc activities by electroplating onto a rotating tungsten cathode.[10] After plating for about two hours, the cathode was washed with distilled water and the copper deposit dissolved by one or two drops of concentrated nitric acid. The solution was picked up in a micropipette and spread over the surface of the source backing.

Source holders were prepared in the following way. A rectangular hole 2.5 cm by 0.4 cm was cut with a sharp needle in a sheet of mica 0.0005 inch thick. The mica was then cemented onto a Lucite ring 3.3 cm in diameter which mounts on the skeleton framework of the spectrometer source holder. The mica was then covered by two Zapon films each 0.01 mg/cm² thick. These films were made in the same manner as the films used for the counter window.[7] The Zapon sags very slightly into the rectangular opening of the mica. This serves well to confine the active solution to the desired region. The solution was then dried in a separate vacuum system after which it was covered by a single Zapon film 0.01 mg/cm² thick and placed in position in the spectrometer.

After each run, the sources were removed from the spectrometer and immediately weighed. The thinnest source used weighed somewhat less than 0.1 mg/cm². The thickest was 0.35 mg/cm².

[9] E. T. Clarke and J. W. Irvine, Phys. Rev. **69**, 680 (1946).

[10] J. Steigman, Phys. Rev. **53**, 771 (1938),

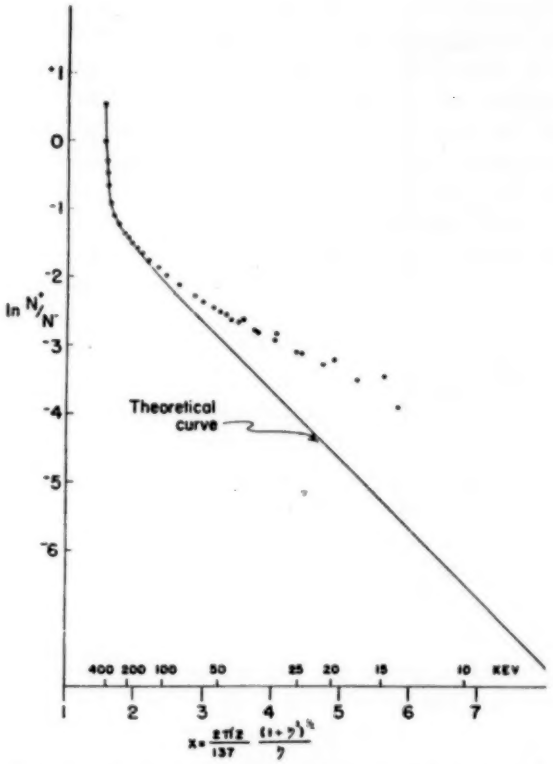

FIG. 5. The ratio of the number of positrons to the number of electrons as a function of the energy. The solid curve is the theoretical curve according to the Fermi theory. The open circles are our experimental data. The solid circles are the data of Backus adjusted to our data at 50 kev.

IV. RESULTS

In all, five sets of data were taken in which the intensity of the source was sufficient to yield good statistics. Three of these runs were made with the extremely thin Zapon counter window. The other two were made using the thicker mica window counter. In addition, several runs were made with much weaker sources yielding poorer statistics.

All the runs show that the momentum distribution is different from that predicted by the Fermi theory. In all cases the deviation from the theory occurs for positrons for energies below 0.270 Mev, while for negatrons the deviations begin for energies below 0.190 Mev.

The runs taken with the thin Zapon window counters have been adjusted to the same intensity and are plotted together.

Figures 1 and 2 show the momentum distributions for the positrons and negatrons. The relative counting rate, divided by the momentum

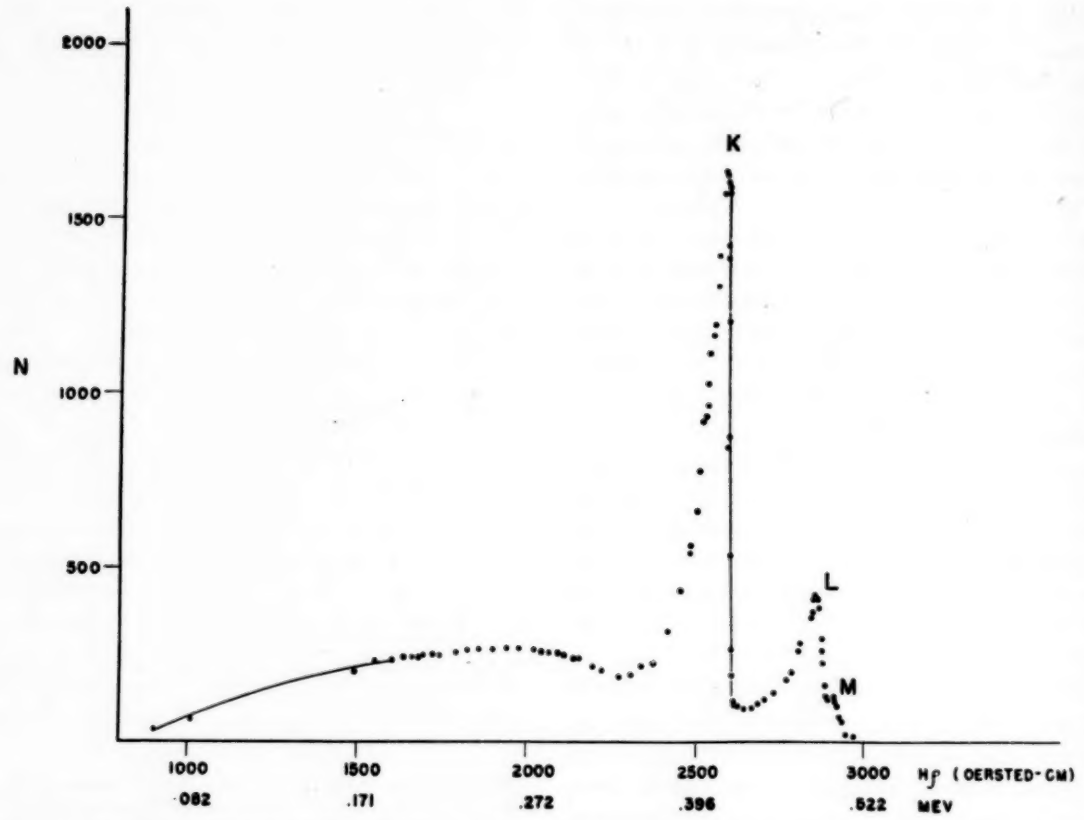

FIG. 6. Compton and photoelectrons ejected from a 0.0263 g/cm² Pb radiator by the 0.511-Mev annihilation radiation of Cu^{64}. The ordinate is the relative number per minute.

is plotted against the momentum in terms of $H\rho$. An energy scale is indicated for convenience. The dashed curves are the distributions predicted by the Fermi theory. Figures 3 and 4 show the Kurie plots of the experimental data. The deviations from the theoretical straight lines occur at a total energy $W=1.53$ mc² for the positrons and 1.37 mc² for the negatrons.

The end-point energies determined from the straight line extrapolation of the Kurie plots are for the positrons 0.657 ± 0.004 Mev and for the negatrons 0.571 ± 0.002 Mev.

By integrating the areas under the experimental distributions, one gets for the ratio of the total number of negatrons to positrons a value of 2.0.

The difference between the experimental and theoretical distribution in Figs. 1 and 2 indicates that there are 9 percent more positrons and 6 percent more negatrons at low energy than is consistent with the theory.

If one uses the low Z approximation[2] for the Fermi coulomb factor, F, one may write for the ratio of the number of positrons to the number of electrons as a function of the energy,

$$N^+/N^-=Ke^{-x}[(W_+-W)^2/(W_--W)^2],$$

where K is a constant, W is the total energy in units of mc², W_+ and W_- are the end-point energies for the positrons and negatrons, respectively, and

$$x=2\pi Z\alpha(W/\eta),$$

where Z is the atomic number, α is the fine structure constant, and $\eta=H\rho/1704$ is the electron momentum in units of mc.

In Fig. 5, $\log N^+/N^-$ is plotted against x. The theoretical curve is shown as a solid line. The open circles are obtained from the experimental data. The solid circles show the data obtained by Backus adjusted to our data at 50 kev.

Our data is in good agreement with the results

of Backus over the region covered by him. Moreover, it is apparent from the curve that the deviation from the theory extends smoothly to the point where the positron spectrum first deviates from the Kurie straight lines, i.e., 270 kev.

If the excess of particles at low energies were due to the spectra being complex, one should expect to find gamma-radiation following the transitions to the excited states of Zn and Ni. The energy available for the gamma-ray turns out to be about the same for the positron and the negatron transitions. One should expect a gamma-ray of 0.387 Mev following 9 percent of the positron transitions and a gamma-ray of 0.381 Mev following 6 percent of the negatron transitions.[11]

A careful search for such radiations was made by examining the photoelectrons ejected from a thin Pb radiator 26.3 mg/cm² thick. Figure 6 shows the lines caused by the electrons ejected from the K, L, and M levels of lead by the 0.511 Mev annihilation radiation from the Cu^{64} positrons. No other gamma-rays were observed of an energy between 0.190 and 0.51 Mev. By comparison with the intensity of the annihilation radiation of which there are two quanta for each positron emitted, one concludes that no nuclear gamma-ray of energy in the neighborhood of 0.38 Mev is emitted with an intensity of as much as 2 percent of the positron emission. If the transition to the ground levels were to proceed by two quanta of lower energy, then, because of the rapid increase in the photoelectric cross section, one should expect lines of even greater intensity. For example, one concludes from the data that no gamma-ray of 0.19 Mev is emitted with an intensity of as much as 0.2 percent of the positron emission.

It should also be noted that the general shapes of the Kurie plots do not readily allow resolution into complex spectra. The manner of deviation is quite different for positrons and negatrons. Whereas the positron distribution deviates more and more from the Fermi straight line at low energies, the negatron intensity first rises to a maximum and then decreases quite rapidly, actually being lower than that given by the Fermi theory for very low energies. Moreover, the decrease in the negatron curve is to be regarded as real since it begins at an energy of about 38 kev which is much higher than the region influenced by the counter window.

[11] Low energy spectra having the abundance of the excess slow particles found here would have to be due to transitions which are allowed as are the high energy spectra. One should then expect only gamma-radiation corresponding to a transition direct to the ground level.

V. CONCLUSIONS

The momentum distributions of the positrons and negatrons of Cu^{64} have been measured with high resolution under such conditions that there is no distortion resulting from scattering, source thickness or backing, and counter window transmission. For both positrons and negatrons, more particles are observed at low energies than are predicted from the Fermi theory. The deviation from the theory begins at 0.270 Mev for positrons and 0.190 Mev for negatrons and is the same for several source thicknesses and two markedly different counter windows. The shapes of the spectra and the fact that no gamma-rays are observed eliminates the possibility that they are complex spectra. The fact that both positrons and electrons are measured under identical conditions and deviate in such different ways gives additional assurance that the effect is real and not instrumental.

One must conclude, therefore, that the Fermi theory does not predict the true distributions for either the negatrons or the positrons. Furthermore, a simple linear combination of the possible beta-interactions, as suggested by Lewis and Bohm, does not account for the experimental results.

It is planned to extend this work to other allowed transitions which can be measured under similar ideal conditions.

We are grateful to Professor E. J. Konopinski for many stimulating discussions.

This work is supported by a grant from the Frederick Gardner Cottrell Fund of the Research Corporation and by the U. S. Navy under Contract N6ori-48, T. O. I.

Wave Transmission and Reflection Phenomena in Liquid Helium II*

JOHN R. PELLAM
Research Laboratory of Electronics, Massachusetts Institute of Technology, Cambridge, Massachusetts

(Received November 24, 1947)

A method is formulated for treating acoustical transmission and boundary value problems in liquid helium II. According to present concepts, He II is a mixture of two fluids obeying a special system of complex hydrodynamics. In particular, this is known to result in two virtually independent modes of sound propagation. Therefore, a reformulation of the intrinsic (or characteristic) acoustical impedance concept is required for which a matrix representation is applicable. By similarly associating a matrix form of impedance with plane-reflecting surfaces, boundary conditions may be imposed. The classical requirements (continuity of pressure and particle velocity at the boundary) are generalized to apply individually to each fluid component in He II. Expressions are obtained for the reflective properties of various types of surfaces. In particular, materials which present unlike boundary conditions to the two fluid components are shown capable of partially converting one mode of sound to the other upon reflection. For example, surfaces of highly porous substances exert unequal viscous forces and should therefore act as such converters (with possible application for extending present frequency ranges of second sound). These properties of reflectors are expressed in terms of *reflectivity arrays*. The array gives direct reflective factors for both types of sound, plus coupling factors between types. Examples are given for several special cases, and a form of reciprocity is shown to exist for the coupling process. The boundary condition is derived for still another type of coupling, due to heat transfer, which occurs at a liquid-vapor interface; a modified form is applicable to the resonance type (Yale) experiment.

I. INTRODUCTION

THE macroscopic hydrodynamic equations of liquid helium II have been developed by Tisza[1,2] and Landau.[3,3a] Whereas these investigators started from different molecular assumptions, most of their macroscopic results were identical. Actually Tisza[2] has recently shown that these results can be obtained from very general assumptions leaving the molecular interpretation open to a large extent. Whatever differences do exist between the two theories are irrelevent for the problems discussed here.

The essence of the complex hydrodynamics of helium II is the presence of two interpenetrating liquids ("normal" and "superfluid") of different densities

$$\rho = \rho_n + \rho_s, \tag{1}$$

velocity fields v_n, v_s, and correspondingly two modes of longitudinal sound propagation. In the first sound (pressure waves) the two liquids move in phase; in the second (temperature waves) the two velocities are out of phase so as to give no net transfer of matter. The first sound can be generated by an ordinary transducer, the second by periodical heating as demonstrated by Peshkov.

The subject of the present paper is to develop a scheme for the solution of boundary value problems in this complex hydrodynamics (reflection, transmission). The interest of this problem lies in the fact that particular boundaries may affect the two fields in a different manner, producing thereby an unbalance, or coupling between the two sound modes.

Generally speaking, there are two reasons for this: (1) heat absorption or rejection by He II is accomplished by the transition $\rho_s \rightarrow \rho_n$, or *vice versa*, (2) the boundary conditions are different for v_n and v_s since the superfluid liquid can slip along solid walls.

(1) has been used to transform second sound generated in the liquid into ordinary sound in the equilibrium vapor phase detectable by a microphone (Yale).[4] (2) could be used to generate second sound mechanically which would be advantageous for high frequencies. The practical application of this principle is not so obvious, since longitudinal waves involve particle motions perpendicular to the plane of a radiating surface, whereas the difference in boundary conditions exists only for the tangential velocity

* This work has been supported in part by the Signal Corps, the Air Materiel Command, and O.N.R.

[1] L. Tisza, J. de phys. et rad. (8) 1, 165 and 350 (1940).
[2] L. Tisza, Phys. Rev. 72, 838 (1947).
[3] L. Landau, J. Phys. U.S.S.R. 5, 71 (1941).
[3a] L. Landau, J. Phys. U.S.S.R. 8, 1 (1944).
[4] C. Lane, H. A. Fairbank, and W. M. Fairbank, Phys. Rev. 71, 600 (1947).

components. An artifice to circumvent this difficulty consists in using surfaces of porous materials, thereby creating a region of helium where the direction *perpendicular* to the radiating surface proper can be considered—from the microscopic point of view—tangential to the walls. (This application is analogous to the possibility examined by Lifshitz[5] of generating second sound by the oscillations of a small sphere, which, however, was shown by him to be inefficient.)

The properties of such surfaces (briefly semi-impervious surfaces) can be conveniently described in terms of an acoustic impedance, which in the complex hydrodynamics of helium II will have the form of a matrix.

Section II will contain the matrix formulation of the general wave propagation in helium II whereby an intrinsic matrix impedance will be defined. Sections III, IV, and V will contain the discussion of transmission and reflection of various surfaces characterized by different impedances.

II. WAVE PROPAGATION IN HELIUM II. INTRINSIC IMPEDANCE

The hydrodynamic equations and in particular the equations of wave propagation in helium II can be described in two different sets of coordinates. In the first set (called briefly the x-scheme), one considers the displacement vectors of the two fluids x_n, x_s and the corresponding velocities $\dot{x}_n$, $\dot{x}_s$. In the second set (briefly the ξ-scheme) one considers "normal coordinates" ξ_1, ξ_2 introduced by Tisza[2] corresponding to the two modes of sound propagation. (Also x_n, x_s are identical to ξ_n, ξ_s in Tisza's notation.) The transformation connecting these schemes is

$$\begin{aligned} x_n &= \xi_1 + \xi_2, & \xi_1 &= (\rho_n x_n + \rho_s x_s)/\rho, \\ x_s &= \xi_1 - (\rho_n/\rho_s)\xi_2, & \xi_2 &= (\rho_s/\rho)(x_n - x_s). \end{aligned} \tag{2}$$

Obviously ξ_1 refers to a "center of mass" motion (first sound) and ξ_2 to a "relative motion" with vanishing net flow (second sound). The general wave motion in the interior of the liquid can most conveniently be described in the ξ-scheme. On the other hand, the boundary conditions, particularly at semi-impervious surfaces can be expressed rather in the x-scheme. Hence the transformations between the two schemes are of interest. These can be represented best in a matrix form. We consider only plane waves traveling in one direction and define the following two component "vectors."

$$\mathbf{X} = \begin{pmatrix} x_n \\ x \end{pmatrix}, \quad \xi = \begin{pmatrix} \xi_1 \\ \xi_2 \end{pmatrix}, \tag{3}$$

and their adjoints

$$\mathbf{X}^* = \overbrace{x_n, x_s}, \quad \xi^* = \overbrace{\xi_1, \xi_2}. \tag{3a}$$

We write (2) in matrix form,

$$\mathbf{X} = \mathbf{S}\xi, \quad \xi = \mathbf{S}^{-1}\mathbf{X}, \tag{4}$$

with

$$\mathbf{S} = \begin{pmatrix} 1 & 1 \\ 1 & -\alpha \end{pmatrix}, \quad \mathbf{S}^{-1} = \frac{1}{1+\alpha}\begin{pmatrix} \alpha & 1 \\ 1 & -1 \end{pmatrix}, \tag{5}$$

where the abbreviation $\alpha = \rho_n/\rho_s$ is used. $\mathbf{S}$ is self-adjoint (does not change if rows and columns are interchanged); hence the adjoint relationships are

$$\mathbf{X}^* = \xi^*\mathbf{S}, \quad \xi^* = \mathbf{X}^*\mathbf{S}^{-1}. \tag{4a}$$

The density of the kinetic energy is

$$W = \tfrac{1}{2}\rho_n\dot{x}_n^2 + \tfrac{1}{2}\rho_s\dot{x}_s^2 = \tfrac{1}{2}\rho\dot{\xi}_1^2 + \tfrac{1}{2}\rho\alpha\dot{\xi}_2^2, \tag{6}$$

where a dot above the symbol indicates the time derivative. The last two terms correspond to the two modes of sound propagations. The total energy flow, or intensity, is obtained by multiplying each energy density of Eq. (6) by its corresponding wave velocity, c_1 and c_2.

$$\gamma = \tfrac{1}{2}\rho c_1\dot{\xi}_1^2 + \tfrac{1}{2}\rho\alpha c_2\dot{\xi}_2^2. \tag{7}$$

This expression suggests the definition of a generalized intrinsic impedance

$$\mathbf{Z}_{0\xi} = \begin{pmatrix} \rho c_1 & 0 \\ 0 & \alpha\rho c_2 \end{pmatrix}, \tag{8}$$

and the intensity appears then as

$$\gamma = \tfrac{1}{2}\dot{\xi}^*\mathbf{Z}_{0\xi}\dot{\xi}, \tag{9}$$

in close analogy with the usual acoustic case. $\mathbf{Z}_{0\xi}$ is a diagonal matrix because we neglect the coupling terms between the two sounds. This coupling term is proportional to the coefficient

[5] E. Lifshitz, J. Phys. U.S.S.R. **8**, 110 (1944).

of thermal expansion and is extremely small (see Lifshitz and Tisza).

Equation (9) suggests the definition of a generalized pressure

$$\mathbf{P}_\xi = \mathbf{Z}_{0\xi}\dot{\boldsymbol{\xi}} = \begin{pmatrix} \rho c_1 \dot{\xi}_1 \\ \alpha \rho c_2 \dot{\xi}_2 \end{pmatrix}. \tag{10}$$

The intensity is then

$$\gamma = \tfrac{1}{2}\dot{\boldsymbol{\xi}}^* \mathbf{P}_\xi = \tfrac{1}{2}\mathbf{P}_\xi^* \dot{\boldsymbol{\xi}}. \tag{9a}$$

The physical meaning of $\mathbf{P}_\xi$ is more apparent from an alternative form which we are now going to derive.

One has for a plane wave of phase velocity c_1

$$\dot{\xi}_1 = -c_1 \nabla \cdot \xi_1 \tag{11}$$

and

$$-\nabla \cdot \xi_1 = \Delta\rho/\rho. \tag{12}$$

Equation (12) is the equation of continuity (compare Tisza) and finally

$$c_1^2 = \Delta P/\Delta\rho, \tag{13}$$

P and ρ are the pressure and density, respectively. From Eqs. (11), (12), and (13) one has

$$\rho c_1 \dot{\xi}_1 = \Delta P.$$

The analagous expressions for second sound are, according to Tisza,[2]

$$\dot{\xi}_2 = -c_2 \nabla \cdot \xi_2, \tag{11a}$$

$$-\nabla \cdot \xi_2 = \Delta\rho_n/\rho_n, \tag{12a}$$

$$c_2^2 = (\Delta P_n/\Delta\rho_n)(\rho_s/\rho) \tag{13a}$$

hence, $\alpha\rho c_2 \dot{\xi}_2 = \Delta P_n$ and

$$\mathbf{P}_\xi = \begin{pmatrix} \Delta P \\ \Delta P_n \end{pmatrix}. \tag{14}$$

Here ΔP_n is the excess of the "osmotic pressure," introduced by Tisza,[1,2] which plays the same role for second sound as the excess of ordinary pressure for first sound.

Although the impedance in the x-scheme is not necessary to the solution of boundary value problems, its formulation does give useful insight to the manner in which the boundary conditions for such problems may be introduced. Since the intensity is invariant, one has

$$\dot{\boldsymbol{\xi}}^* \mathbf{Z}_{0\xi} \dot{\boldsymbol{\xi}} = \dot{\mathbf{X}}^* \mathbf{S}^{-1} \mathbf{Z}_{0\xi} \mathbf{S}^{-1} \dot{\mathbf{X}} = \dot{\mathbf{X}}^* \mathbf{Z}_{0x} \dot{\mathbf{X}},$$

so that

$$\mathbf{Z}_{0x} = \mathbf{S}^{-1} \mathbf{Z}_{0\xi} \mathbf{S}^{-1},$$

and hence

$$\mathbf{Z}_{0x} = (\rho_n\rho_s/\rho) \begin{pmatrix} (\rho_n/\rho_s)c_1 + c_2 & c_1 - c_2 \\ c_1 - c_2 & (\rho_s/\rho_n)c_1 + c_2 \end{pmatrix}. \tag{16}$$

The four-element matrix of (16) bears a close analogy to a four-terminal electrical network in which one set of terminals is considered to correspond to the normal fluid component, the other to the superfluid component. We imagine a geometrical plane passed through a point of observation perpendicular to the direction of wave propagation. Then, for outgoing waves only, $(\rho_n\rho_s/\rho)[(\rho_n/\rho_s)c_1 + c_2]$ is the impedance experienced by normal fluid when motion of superfluid across the plane is prohibited. To extend the analogy, the transfer impedance, $(\rho_n\rho_s/\rho)(c_1 - c_2)$, is the pressure which must be exerted against the superfluid to suppress its motion for unit velocity amplitude of normal fluid (or the reverse for the other off-diagonal element). Similarly $(\rho_n\rho_s/\rho)[(\rho_s/\rho_n)c_1 + c_2]$ is the superfluid input impedance for normal fluid "clamped."

As will become apparent in Section III, the boundary conditions imposed by the porous reflectors mentioned earlier may be introduced most logically in the x-scheme. For example, a thin layer, or region, exhibiting viscous properties serves effectively as a lumped resistance inserted in series between otherwise extended regions possessing intrinsic (or characteristic) impedance $\mathbf{Z}_{0x}$. After expressing in this manner the net resulting x-scheme impedance presented at the layer, conversion is made to the ξ-scheme for application of the boundary conditions derived in Section II.[6]

[6] It is of interest to express the generalized pressure in the x-scheme. One has

$$\dot{\boldsymbol{\xi}}^* \mathbf{P}_\xi = \dot{\mathbf{X}}^* \mathbf{P}_x,$$

and

$$\mathbf{P}_x = \mathbf{S}^{-1}\mathbf{P}_\xi = \begin{pmatrix} p_n \\ p_s \end{pmatrix}.$$

Here p_n and p_s are the excess sound pressures of normal fluid and superfluid considered by Landau.[3a] Accordingly

$$\begin{pmatrix} p_n \\ p_s \end{pmatrix} = \mathbf{P}_x = \frac{1}{1+\alpha} \begin{pmatrix} \alpha\Delta P + \Delta P_n \\ \Delta P - \Delta P_n \end{pmatrix} = \begin{pmatrix} \rho_n c_1 \dot{\xi}_1 + \rho_n c_2 \dot{\xi}_2 \\ \rho_s c_1 \dot{\xi}_1 - \rho_n c_2 \dot{\xi}_2 \end{pmatrix}.$$

The total pressure is the sum of the two components $= \Delta P$. Hence, only the first sound contributes to the total pressure! Ordinary transducers are accordingly incapable of generating or detecting second sound.

III. BOUNDARY CONDITIONS AT A PLANE-REFLECTING SURFACE

We proceed now to derive the boundary conditions which hold at a reflecting surface. In order to keep the problem purely mechanical for the time being, the conditions will be derived first for the case of a boundary which is a perfect heat insulator. That is, no interchange $\rho_s \rightleftarrows \rho_n$ will occur; and any unbalance introduced between the two modes of propagation will be due solely to unequal viscous forces on the two fluid components.

The boundary conditions of classical acoustics are that particle velocity and particle pressure must both be continuous across any interface. (This is equivalent to specifying continuity of velocity and energy flow.) The same is true for the case of He II, except that here both the velocity and the pressure are matrices. Having derived a relationship in the x-scheme in terms of true particle velocities and pressures, we may then transform to ξ-coordinates; the latter system is preferable for dealing with the distribution of energy flow between the two modes of propagation.

Let the incident sound energy of He II travel along the positive y axis and encounter a boundary surface defined by $y=0$ in Fig. 1. In general, there will be some energy reflected back in the negative y direction, and some will continue through the interface (where it may or may not involve two modes, depending upon whether liquid He II is involved for $y>0$).

Let $\dot{\mathbf{X}}_i$ represent the true particle velocity due to incident waves and $\dot{\mathbf{X}}_r$ that due to reflected waves; then the effective velocity experienced by the interface is just the sum of these, or $\dot{\mathbf{X}}_i+\dot{\mathbf{X}}_r$. In order to specify the requirements on pressure, a matrix impedance $\mathbf{Z}_x$ is assigned to the reflecting surface. This matrix determines the reflectivity characteristics. The effective pressure driving the surface then becomes the product of $\mathbf{Z}_x$ times the particle velocity, or $\mathbf{Z}_x(\dot{\mathbf{X}}_i+\dot{\mathbf{X}}_r)$. But the pressure supported by the standing-wave system must be identical with this value, and is given by $\mathbf{Z}_{0x}(\dot{\mathbf{X}}_i-\dot{\mathbf{X}}_r)$. The reversed direction of propagation for the reflected wave accounts for the minus sign. Combining, we have the boundary condition

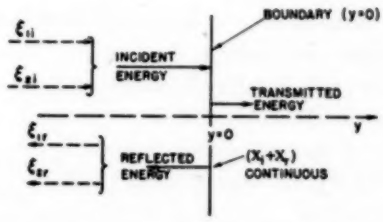

FIG. 1. Reflection of sound in helium II from plane boundary.

$$\mathbf{Z}_{0x}(\dot{\mathbf{X}}_i-\dot{\mathbf{X}}_r)=\mathbf{Z}_x(\dot{\mathbf{X}}_i+\dot{\mathbf{X}}_r) \tag{17}$$

in the x-scheme. Since our concern is primarily with the relative amounts of first and second sound reflected, transformation is made to the ξ-scheme. Employing (4) and (4a), we have

$$\mathbf{Z}_{0\xi}(\dot{\boldsymbol{\xi}}_i-\dot{\boldsymbol{\xi}}_r)=\mathbf{Z}_\xi(\dot{\boldsymbol{\xi}}_i+\dot{\boldsymbol{\xi}}_r), \tag{18}$$

where $\mathbf{Z}_\xi$ is now the characteristic impedance for the surface in the ξ-scheme. The same relationship as used before holds for transforming reflector impedances from one scheme to the other, namely

$$\mathbf{Z}_\xi=\mathbf{S}\mathbf{Z}_x\mathbf{S}. \tag{19}$$

We may solve (18) for the amplitude $\boldsymbol{\xi}_r$ of the reflected waves to obtain the following matrix in terms of the incident waves $\boldsymbol{\xi}_i$

$$\boldsymbol{\xi}_r=(\mathbf{Z}_{0\xi}+\mathbf{Z}_\xi)^{-1}(\mathbf{Z}_{0\xi}-\mathbf{Z}_\xi)\boldsymbol{\xi}_i=\begin{pmatrix}A_{11} & A_{12}\\ A_{21} & A_{22}\end{pmatrix}\boldsymbol{\xi}_i. \tag{20}$$

The diagonal elements A_{11}, A_{22} represent the fractional amounts of incident first- and second-sound amplitudes which are reflected unchanged. Conversely, the diagonal terms A_{12}, A_{21} represent transfer of amplitudes between modes. However, a more significant property of the reflector is the manner in which intensities leaving its surface are divided between first and second sound. For our purposes therefore we allow only one mode of sound at a time to strike the surface and build up a *reflectivity array*. This array, which must not be confused with a matrix, may be written:

$$\text{Reflectivity}=\begin{array}{|c|c|}\hline F_{11}=\gamma_{1r}/\gamma_{1i}=A_{11}^2 & F_{12}=\gamma_{1r}/\gamma_{2i}=(\rho_s c_1/\rho_n c_2)A_{12}^2\\ \hline F_{21}=\gamma_{2r}/\gamma_{1i}=(\rho_n c_2/\rho_s c_1)A_{21}^2 & F_{22}=\gamma_{2r}/\gamma_{2i}=A_{22}^2\\ \hline\end{array}. \tag{21}$$

Thus, if unit intensity of first sound strikes the surface, then intensities $F_{11}=A_{11}^2$ of first sound and $F_{21}=(\rho_n c_2/\rho_s c_1)A_{21}^2$ of second sound will leave the surface. Similarly, for unit incident intensity of second sound, intensities F_{12} of first sound and F_{22} of second sound will be reflected. In this manner, the diagonal elements play the roles of ordinary reflection coefficients, while the off-diagonal elements act as transfer factors. Evaluation of the reflectivity array will be given for specific cases in the following section.

IV. SPECIAL REFLECTING SURFACES

We now turn to the examination of specific cases of reflecting boundaries, still restricting ourselves, however, to the purely mechanical case, i.e., no transition between fluid components. The types of reflectors in which we shall be interested may be divided logically into two main categories; (1) impervious surfaces and (2) semi-impervious surfaces (a third category comprising pervious boundaries[7] will not be considered here).

1. Impervious Surfaces

This category includes any boundary which is permeable to neither normal fluid nor superfluid. As a result the perpendicular component of the internal convection peculiar to second sound is prohibited at the surface (since we have specified infinitely poor heat conductivity). Therefore, ξ_2 is zero at $y=0$, so that all second sound is reflected. We have for the impedance and the reflectivity

$$\mathbf{Z}_\xi=\begin{pmatrix} Z_1 & 0 \\ 0 & 0 \end{pmatrix}; \quad \text{Reflectivity}=\begin{array}{|c|c|}\hline \gamma_{1r}/\gamma_{1i}=\left|\dfrac{\rho c_1-Z_1}{\rho c_1+Z_1}\right|^2 & \gamma_{1r}/\gamma_{2i}=0 \\ \hline \gamma_{2r}/\gamma_{1i}=0 & \gamma_{2r}/\gamma_{2i}=1 \\ \hline \end{array}, \tag{22}$$

where Z_1 is the usual mechanical impedance of the surface to an ordinary acoustic wave (and therefore the impedance experienced by normal sound). For the element γ_{1r}/γ_{1i} the absolute magnitude of the ratio is used, sinze Z_1 may have reactive components. Note the diagonal nature of this reflectivity array, which indicates no coupling between modes of propagation. In particular for a very thin membrane (thin compared to a first-sound quarter wave-length) with low heat conductivity and surrounded by liquid He II, the mechanical impedance will reduce simply to ρc_1. This results in complete transparency to first sound. The array becomes:

$$\text{Reflectivity}=\text{(Membrane)}\begin{array}{|c|c|}\hline 0 & 0 \\ \hline 0 & 1 \\ \hline \end{array}. \tag{23}$$

Its significance is that ideally such a system would constitute a mode filter, transmitting all first sound, but still reflecting all second sound.

2. Semi-Impervious Surfaces

The other case we shall analyze involves reflections from regions of space which present different viscous drag to the two fluid components of He II. We shall consider only the most idealized situations. The unequal viscous drag will be supposed due to the presence of a porous or honeycomb structure through which superfluid may pass unhindered (zero viscosity is one of the properties of superfluid) but which presents ordinary viscous friction to the normal fluid component. Furthermore, the honeycomb will be considered so thin walled that negligible fluid is displaced by its presence, but sufficiently rigid not to participate in the mechanical vibrations. This highly artificial condition may then be represented mathematically by introducing a

[7] Pervious boundaries might constitute such a trite case as a change in cross-sectional area of a narrow duct containing He II and conducting sound. Then the effective impedance presented at the junction would differ from the intrinsic impedance of He II only by a linear scale factor f. The impedance and reflectivity would be, respectively,

$$\mathbf{Z}_\xi=f\mathbf{Z}_{0\xi};$$

$$\text{Reflectivity}=\begin{array}{|c|c|}\hline [(1-f)/(1+f)]^2 & 0 \\ \hline 0 & [(1-f)/(1+f)]^2 \\ \hline \end{array}.$$

normal fluid pressure gradient[8] due to viscous drag throughout all regions occupied by the structure. We shall first examine the case where only a thin layer of space is thus occupied (i.e., a thin porous screen) following which the extension to a semi-infinite space will be given.

Semi-Impervious Rigid Screen

Let the position of the porous screen be represented by a thin layer of thickness Δl at the plane $y=0$. The influence of the layer will be manifest entirely through the viscous drag opposing flow of the normal fluid component. Treating the problem as analogous to a lumped electrical impedance inserted in a continuous transmission line, the effective impedance presented by the screen may be written as

$$\mathbf{Z}_x=\mathbf{Z}_{0x}+\mathbf{R}_x\Delta l. \tag{24}$$

Here the first term is the intrinsic impedance of He II, the second the added series resistance. This series term involves the matrix

$$\mathbf{R}_x=R_0\begin{pmatrix}1 & 0\\ 0 & 0\end{pmatrix}, \tag{25}$$

or in the ξ-scheme

$$\mathbf{R}_\xi=R_0\begin{pmatrix}1 & 1\\ 1 & 1\end{pmatrix}, \tag{26}$$

where the scalar coefficient R_0 is the *flow resistance* for the normal fluid component. Making the simplest assumption that flow resistance behaves in the classical manner with respect to normal fluid, its definition becomes

$$R_0\dot{x}_n=\text{grad}\,p_n=\Delta p_n/\Delta l. \tag{27}$$

R_0 is a real, positive quantity determined entirely by the coefficient of viscosity of normal fluid (essentially equal to that of He I) and the detailed porous structure of the honeycomb. This p_n is the excess pressure of the normal fluid component, as defined in reference 6. Converted to the ξ-scheme, the resultant impedance encountered by incoming waves at the plane $y=0$, becomes

$$\mathbf{Z}_\xi=\mathbf{Z}_{0\xi}+\mathbf{R}_\xi\Delta l=\mathbf{Z}_{0\xi}R_0\begin{pmatrix}1 & 1\\ 1 & 1\end{pmatrix}\Delta l. \tag{28}$$

Applied to (20) the matrix for the reflected waves is

$$\xi_r=\frac{1}{2/R_0\Delta l+(1/\rho c_1+1/\alpha\rho c_2)}\begin{pmatrix}1/\rho c_1 & 1/\rho c_1\\ 1/\alpha\rho c_2 & 1/\alpha\rho c_2\end{pmatrix}\xi_i, \tag{29}$$

all elements of which become maximum for very large values of R_0. The condition for one-half maximum effect is given by

$$R_0=\frac{2/\Delta l}{1/\rho c_1+1/\alpha\rho c_2}. \tag{30}$$

For R_0 greatly in excess of this value, the reflectivity would be

$$(\text{Reflectivity})_{\text{Screen}}=\frac{1}{(1+\rho_s c_1/\rho_n c_2)^2}\cdot\begin{vmatrix}1 & \rho_s c_1/\rho_n c_2\\ \rho_s c_1/\rho_n c_2 & (\rho_s c_1/\rho_n c_2)^2\end{vmatrix}. \tag{31}$$

Because of the extremely low viscosity of even the normal fluid component, porous material fulfilling this condition would be virtually impermeable for ordinary liquids.

Numerical values of the four intensity ratios corresponding to the reflectivity are shown in Fig. 2. Note that the off-diagonal elements represent transfer from one mode to the other upon reflection from the screen. Figure 2 illustrates the interesting fact that the two intensity transfer factors are equal ($F_{12}=F_{21}$), so that the conversion efficiency is the same for either mode of incident sound. This is a type of reciprocity.

[8] The semi-permeable membrane applicable to thermodynamic discussions (see references 1 and 2) represents the extreme case where motion of normal fluid is completely arrested.

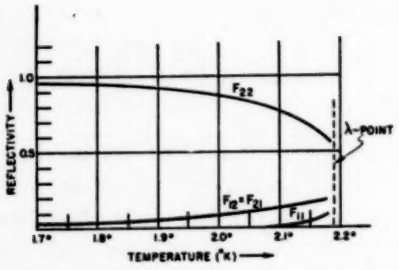

FIG. 2. Reflectivity factors *versus* temperature for thin porous screen.

The viscous properties of the thin porous screen result in a greater impedance mismatch for second sound than for first. Thus the factor F_{22} giving the reflectivity ratio for second sound (the fraction reflected without conversion) greatly exceeds F_{11}. This is a direct consequence of the relatively low wave velocity of second sound ($c_1/c_2 \geq 10$). Thus, from (16), the impedance $(\rho_n\rho_s/\rho)[(\rho_s/\rho_n)c_1+c_2]$ experienced by superfluid at the screen is determined primarily by c_1 and therefore provides a better match for first sound. Of course an actual reflector of this nature would displace an appreciable amount of liquid so that corrections would be necessary for deviation from the idealized situation assumed for deriving the curves of Fig. 2.

Extended Semi-Impervious Region

Perhaps a more practical reflector for converting first sound to second, or the reverse, would be provided by the plane face of an extended porous medium. Thus the interior honeycomb structure of, for example, a sintered material should provide differential viscous drag to the two fluids. For the case of pulsed energy, the structure could be considered infinite in extent (short enough pulses do not detect thickness of a reflector until the reflection process has been completed).

Here again the true situation can be approximated only crudely by visualizing all regions for $y>0$ as endowed with viscous properties (with respect to normal fluid) and determining the resulting characteristic impedance. Space does not permit complete analysis of this case, but it may be shown that in the extreme situation the flow resistance R will be sufficient to suppress virtually all normal fluid vibration. This occurs when $R \gg \omega\rho$.

Under such circumstances the mode corresponding to second sound reduces essentially to vibration of superfluid only, without attenuation, and with effective wave velocity

$$v_2 \rightarrow [(\rho_s c_1^2+\rho_n c_2^2)/\rho]^{\frac{1}{2}}.$$

The mode corresponding to first sound, however, degenerates to an over-damped motion, for which the resistance to normal fluid vibration virtually precludes flow of energy.

Accordingly, this boundary should reflect a greater relative proportion of first sound than did the thin porous screen. Furthermore, the more drastic modifications of the boundary conditions should result in numerically greater coupling factors, F_{12} and F_{21}.

V. PHENOMENA INVOLVING HEAT TRANSFER

Thus far analysis has been simplified by the assumption of zero heat flow between the liquid He II and the reflector. We may now include the effects of such heat interchange. This process occurs for example when the boundary is formed by the liquid surface in equilibrium with its vapor, and is the case investigated experimentally by Lane.[4] Such a liquid-vapor interface provides coupling between the two types of sounds in the liquid and the classical sound in the vapor. For simplicity we consider only perpendicular incidence of sound waves against the free surface.

Coupling takes place due to periodic evaporation and condensation of helium at the surface. The situation for helium differs markedly from that of a classical liquid in equilibrium with its vapor. For ordinary liquids the temperature fluctuations accompanying the evaporation-condensation process occur only at the interface, being thus localized by the condition of adiabaticity. However, in He II an adiabatic means for heat transfer is provided by second sound. In this manner, temperature fluctuations occuring at the surface may be detected at (or, reciprocally, generated from) well submerged positions. We show, in fact, that the impedance encountered at the surface by incident waves of either first sound, second sound, or the vapor mode involves all three modes. This has a direct bearing on acoustical resonance methods such as employed by Lane.

To establish the boundary conditions existing at the interface it is necessary to consider both the temperature fluctuation and the heat flow inherent in second sound. Variations in temperature are produced by the varying relative concentration of normal fluid according to an empirical relationship deduced from experiment

$$\Delta\rho_n/\rho_n = r\Delta T/T. \tag{32}$$

The factor r has been evaluated numerically as about 5.5. Equation (12a) relates this concentration to incident and reflected waves so that

$$\Delta\rho_n/\rho_n = -\nabla\cdot\xi_2 = 1/c_2(\dot{\xi}_{2i}-\dot{\xi}_{2r}) = r\Delta T/T \tag{33}$$

(where the sign has been reversed for the reflected wave velocity). For purposes of computation we now make the assumption that the vapor pressure fluctuations which occur at the surface are given directly in terms of $\Delta T/T$ by means of the Clausius-Clapyron equation. Although this is probably not the physical situation[9] the assumption suffices for specifying conditions of resonance. Hence the vapor pressure p_g is

$$p_g = \{\rho\rho_g/(\rho-\rho_g)\}L\Delta T/T$$
$$= (L/rc_2^2)\{\rho_g/(\rho-\rho_g)\}\rho c_2(\dot{\xi}_{2i}-\dot{\xi}_{2r}), \tag{34}$$

where L is the latent heat of vaporization at the ambient temperature, and ρ_g the vapor density. The boundary requirement that pressure be continuous across the interface results in

$$(L/rc_2^2)\{\rho_g/(\rho-\rho_g)\}\rho c_2(\dot{\xi}_{2i}-\dot{\xi}_{2r})$$
$$= \rho c_1(\dot{\xi}_{1i}-\dot{\xi}_{1r}) = -\rho_g c_g(\dot{x}_{gi}-\dot{x}_{gr}), \tag{35}$$

where $\dot{x}_g$ and c_g represent particle velocity and wave velocity, respectively, for the vapor. This states that the pressure associated with the interaction between second sound and the surface must support (and therefore equal) both first sound pressure in He II and classical sound pressure in the vapor. The minus sign preceding the last term accounts for the reversed sense of incidence for sound in the vapor.

The boundary condition for particle velocity at the surface is a statement of the equation of continuity. This must take into account the alternate changes in material volume due to the periodic interchange between liquid and vapor. The evaporation rate is fixed by the heat transfer characteristics of second sound in He II according to a relationship given by Tisza.[2] Therefore we have

$$\text{heat flow} = \rho_g L v_g = sT(\dot{\xi}_{2i}+\dot{\xi}_{2r}), \tag{36}$$

where s is now the specific entropy and v_g the vapor particle velocity. Note that since the wave velocity c_2 does not enter explicitly into (36) there is no change in sign for the reflected wave. We may now express our condition of continuity

$$(sT/\rho_g L)(\dot{\xi}_{2i}+\dot{\xi}_{2r})+(\dot{\xi}_{1i}+\dot{\xi}_{1r})$$
$$-(\dot{x}_{gi}+\dot{x}_{gr}) = 0. \tag{37}$$

The first term represents source (or sink) of volume due to second sound; the latter two constitute ordinary particle flow due to He II first sound and classical sound in the vapor. Finally, by combining (35) and (37) and eliminating the time derivative, we obtain

$$(1/\beta\rho c_2)\left(\frac{\xi_{2i}+\xi_{2r}}{\xi_{2i}-\xi_{2r}}\right)+(1/\rho c_1)\left(\frac{\xi_{1i}+\xi_{1r}}{\xi_{1i}-\xi_{1r}}\right)$$
$$+(1/\rho_g c_g)\left(\frac{x_{gi}+x_{gr}}{x_{gi}-x_{gr}}\right) = 0, \tag{38}$$

where the quantity β, occuring in the term for second sound, is given by

$$\beta = (\rho_g L)^2/(\rho-\rho_g)rc_2^2 sT.$$

Expression (38) establishes the relationship between the two types of sound in the liquid and the sound in the vapor. This is applicable either to a situation involving acoustical resonance (Yale experiment) or to the case of short pulses where the geometry of the equipment does not enter. Note that the above result (38) is completely analogous to an electric situation involving two different transmission lines in parallel with a third at a common junction; each line has a different characteristic impedance. In this respect $\beta\rho c_2$ enters as an effective characteristic impedance for second sound insofar as interactions with the other types are concerned.

[9] It has recently been learned from Dr. Onsager that a dissipative process occurs at the surface which could be taken into account by the insertion of a complex factor in (34). This would lead to expressions for the heights and widths of resonance peaks in the Lane experiment.

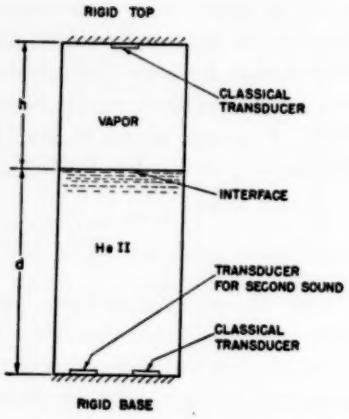

FIG. 3. Coupling due to liquid-vapor interface (idealized Yale resonance experiment).

The Experiment of Lane and Collaborators

Condition (38) is directly applicable to the resonance experiments conducted at Yale.[4] The physical situation is idealized in Fig. 3. Here is shown a vertical column of liquid He II of depth d, beneath a column of helium vapor of height h. Classical transducers, for ordinary sound in the vapor and first sound in the liquid, are provided both at the extreme top and extreme bottom of the containers. In addition, a second sound transducer is located at the bottom. Measurements consist, in general, of activating the second sound transducer and detecting a signal with one of the classical transducers, or the reverse. As either the frequency or the height of the liquid is altered, a succession of resonance peaks is observed.

The precise conditions of resonance depend upon a variety of factors, such as the top and bottom impedance of the container and the internal impedances of the transducers. Only the simplified situation of completely rigid container ends and infinite internal impedance for all transducers need be considered here. (That is, classical transducers of the pressure type; and second-second transducers of the temperature—i.e., low heat flow—type.) Also it is considered that for the steady state, the waves become one-dimensional and plane.

Under such conditions (not necessarily the experimental ones) maximum energy would be fed to the system for resonance conditions, i.e., matched to infinite impedance. This condition is specified by modifying (38) for infinite top and bottom impedances. Accordingly,

$$(1/\rho c_1)\tan(2\pi\nu d/c_1)+(1/\beta\rho c_2)\tan(2\pi\nu d/c_2)+(1/\rho_0 c_0)\tan(2\pi\nu h/c_0)=0 \quad (39)$$

gives the requirement for resonance, where ν is the frequency. This condition holds for any of the transmitter-receiver combinations.

Additional factors, such as dissipative effects occuring at the surface, would have to be introduced for computing heights and widths of resonance peaks. Furthermore, non-infinite impedances would alter the conditions of resonance (39), by modifying the effective depth d or height h. For example, a "low impedance" type of second sound generator (i.e., ratio of temperature fluctuation to heat flow, small) would result in the replacement of the *tan* of the second term by *cotan*. Similar alterations in (39) would occur for other modifications in the equipment.

Note that for this particular situation involving resonance, no recourse is made to the matrix method. For less specialized cases, however, such as reflection of short pulses from the surface, the previously derived matrix formulation would be used.

VI. CONCLUSIONS

The transmission and reflection of sound in He II is formulated on the basis of a matrix representation. A system of generalized coordinates (ξ-scheme) is used for expressing energy flow, whereas true coordinates (x-scheme) are used for setting up boundary conditions at the surface of a reflector. The reflectivity conditions for the case of normal incidence are expressed by means of transformations between these two systems. Distinction is made between reflectors (1) for which heat exchange with the liquid helium plays a basic role, and (2) those for which no heat transfer takes place. Concerning (2), it is shown that impervious (or impenetrable) surfaces reflect all incident second sound. Coupling between first and second sound occurs only for semi-impervious surfaces for which the superfluid component experiences less viscous retardation than does the normal fluid. Reflectivity curves are given for the case of a thin, semi-impervious screen, for which transfer of intensity between

modes may reach 15 percent. That the coupling factor for such a surface is identical for either type of incident sound constitutes a type of reciprocity. Concerning (1), the boundary condition governing reflection of acoustic energy from a liquid-vapor interface is given. Special modifications for the case of resonance are applicable to the Yale type of experiment.

ACKNOWLEDGMENTS

The author is indebted to Dr. C. Kittel, formerly of the Research Laboratory of Electronics, for the suggestion that matrix methods be applied to this analysis. Special acknowledgment is due Professor L. Tisza for many helpful suggestions and for his advice and guidance in the preparation of the manuscript.

PHYSICAL REVIEW VOLUME 73, NUMBER 6 MARCH 15, 1948

The Electromagnetic Shift of Energy Levels

F. J. Dyson
Cornell University, Ithaca, New York

(Received December 8, 1947)

The displacement between the $2s$ and $2p_{\frac{1}{2}}$ levels of hydrogen is calculated on the assumption that it is caused by interaction with the radiation field; the calculation is relativistic, but the spin of the electron is neglected. The theory gives a finite result, agreeing closely with the experimental value.

I. INTRODUCTION

BETHE[1] has proposed a method of calculating theoretically the observed[2] displacements of the hydrogen fine structure levels from the positions predicted by the Dirac theory. The displacements are attributed to interaction between the electron and the radiation field, and are to be calculated by the usual perturbation method of calculating electromagnetic self-energies. Since it is presumed that the measured mass of an electron already includes the electromagnetic self-energy, the level shifts are found by subtracting from the calculated self-energy of the bound electron the self-energy calculated for a "suitable" free electron. Bethe observed that the difference between these two divergent expressions should be finite and of the correct magnitude. Unfortunately, the non-relativistic approximation which he used in his preliminary calculation[1] is not good enough for an exact test of the theory, since in this approximation the formula for the shift is still divergent after the subtraction. An exact calculation, based on the Dirac electron theory, presents formidable, though not fundamental, difficulties.

The present paper outlines a calculation undertaken as an interim program while the exact calculation is in progress; relativistic theory is used throughout, only the effects of spin are ignored. Specifically, the level shift is determined for an "atom" consisting of a proton and a particle of electronic mass and charge and zero spin. The light particle, which will be referred to as "scalar particle," satisfies the Klein-Gordon wave equation and obeys Bose statistics. Since the system thus defined is at least conceptually a physical system (which a non-relativistic system is not), it is satisfactory to find that the theory gives a convergent expression for the level shift. Further, the values obtained are very close to the non-relativistic approximations and to the observed shifts.

From the theoretical standpoint, the convergence of the present calculation is noteworthy and somewhat unexpected. The non-relativistic theory, in which the self-energy before subtraction diverges linearly, gives a logarithmically divergent level shift; and it was to be expected that the Dirac hole theory, in which the self-energy is only logarithmically divergent, would give a convergent level shift. In the case of the scalar particle the self-energy itself is quadratically divergent, and after the subtraction the

[1] H. A. Bethe, Phys. Rev. **72**, 339 (1947).
[2] W. E. Lamb and R. C. Retherford, Phys. Rev. **72**, 241 (1947).

transverse and longitudinal self-energies are still logarithmically divergent; the level shift finally converges only by an almost exact cancellation of the transverse and longitudinal contributions. The underlying significance of this cancellation is still obscure, but it certainly argues in favor of the general correctness of Bethe's interpretation of the self-energies.

II. THEORETICAL FRAMEWORK

The system to be investigated consists of a quantized scalar field interacting with a static Coulomb potential (proton field) and with a quantized electromagnetic field. The scalar field is complex, representing both positive and negative charges, and is denoted by ψ. The electromagnetic potentials are $(V+\phi, \mathbf{A})$, where V is the static potential representing the proton field. The momenta conjugate to ψ and ψ^* are, respectively,

$$\pi=\psi^*-i\frac{e}{\hbar}(V+\phi)\psi^*, \quad \pi^*=\psi+i\frac{e}{\hbar}(V+\phi)\psi, \tag{2.1}$$

and the charge-current 4-vector is

$$\rho=\frac{e}{\hbar}i(\pi^*\psi^*-\pi\psi),$$
$$\mathbf{s}=i\frac{e}{\hbar}c^2(\nabla\psi^*\cdot\psi-\nabla\psi\cdot\psi^*)-2\frac{e^2}{\hbar^2}c\mathbf{A}\psi^*\psi. \tag{2.2}$$

The complete Hamiltonian of the system is[3]

$$H=H_1+H_2+H_3+H_4.$$

Here

$$H_1=\int\left\{\pi\pi^*+c^2(\nabla\psi^*\cdot\nabla\psi)+\frac{m^2c^4}{\hbar^2}\psi^*\psi\right\}d\tau \tag{2.3}$$

is the Hamiltonian of the scalar field in vacuum, H_2 that of the electromagnetic radiation field, and

$$H_3=\int V\rho d\tau,$$
$$H_4=\int\left\{\phi\rho-\frac{1}{c}\mathbf{A}\cdot\mathbf{s}-\frac{e^2}{\hbar^2}\psi^*\psi\mathbf{A}^2\right\}d\tau \tag{2.4}$$

are the interactions of the scalar field with the static field and with the radiation field. The Hamiltonian

$$H_0=H_1+H_2+H_3$$

defines an unperturbed system in which the energy levels will be given by the usual theory of the hydrogen atom. The level shifts will be found by calculating the expectation values of the perturbing Hamiltonian H_4 in the stationary states of the unperturbed system.

In order to use perturbation theory, it is necessary to reduce ψ to the form

$$\psi=\sum_s a(S)\psi_s, \tag{2.5}$$

where the ψ_s are functions of the space coordinates satisfying the stationary Klein-Gordon equation

$$\left\{(E_s+\frac{e}{\hbar}V)^2+c^2\nabla^2-\frac{m^2c^4}{\hbar^2}\right\}\psi_s=0, \tag{2.6}$$

and the $a(S)$ are time-dependent emission and absorbtion operators with the commutation relations

$$[a(S), a(T)]=[a^*(S), a^*(T)]=0,$$
$$[a(S), a^*(T)]=\epsilon_s\delta(S, T). \tag{2.7}$$

Here ϵ_s denotes $+1$ or -1 according as ψ_s represents a state of negative or positive charge, and the energy of the state is

$$F_s=\hbar|E_s|=-\hbar\epsilon_sE_s. \tag{2.8}$$

Note that E_s has the dimensions of a frequency, not an energy; likewise V has the dimensions of a scalar potential and not of a potential energy.

The difficulty now arises that the wave functions ψ_s are not orthogonal, but satisfy the weaker relations

$$\int\psi_r^*\left(E_r+E_s+2\frac{e}{\hbar}V\right)\psi_s d\tau=-\hbar\epsilon_s\delta(S, T). \tag{2.9}$$

As a consequence of this, the expansion (2.5) together with the relations (2.7) does not lead directly to a correctly quantized relativistic field theory. The way to overcome this difficulty is explained by Snyder and Weinberg[4] and, in a

[3] Wentzel, *Einführung in die Quantentheorie der Wellenfelder* (Edwards Borthers, Inc., Ann Arbor, Michigan, 1946), 64–67.

[4] H. Snyder and J. Weinberg, Phys. Rev. **57**, 307 (1940); J. M. Blatt, Phys. Rev. **72**, 466 (1947), particularly the appendix, p. 476.

rather different context, by Blatt.[4] The essential point is that the ψ_s are twice as numerous as a complete orthogonal set of functions, so that the expansion (2.5) is not sufficient to determine the coefficients $a(S)$. The stationary states must be represented by two-component wave functions,

$$\Psi_s=\begin{pmatrix}\psi_s\\ \pi_s^*\end{pmatrix},\quad \pi_s^*=i\left(E_s+\frac{e}{\hbar}V\right)\psi_s. \tag{2.10}$$

The two-component functions form a complete orthogonal set, in a metric defined by the scalar product

$$(\Psi_1,\Psi_2)=\frac{1}{\hbar}\int\Psi_1^*\gamma\Psi_2 d\tau \tag{2.11}$$

where γ is the Hermitian matrix $\begin{pmatrix}0 & i\\ -i & 0\end{pmatrix}$; and every two-component wave function Ψ has the unique expansion

$$\Psi=\sum_s \epsilon_s(\Psi_s,\Psi)\Psi_s. \tag{2.12}$$

Taking in particular for Ψ a function with one component zero and the other a δ-function, the inverse orthogonality relations,

$$\left.\begin{aligned}&\sum_s \epsilon_s\psi_s^*(x')\psi_s(x)=\sum_s \epsilon_s\pi_s^*(x')\pi_s(x)=0,\\ &\sum_s \epsilon_s\psi_s(x')\pi_s(x)=i\hbar\delta(x-x'),\end{aligned}\right\} \tag{2.13}$$

are obtained. These are fundamental for the calculation of the self-energies. In other respects, the theory of the scalar field as developed by Pauli and Weisskopf[5] applies in the presence of the static potential without serious modification.

The initial state of the unperturbed system is one in which a single negative-charge wave function Ψ_u is occupied by one scalar particle, all other scalar particle states and all electromagnetic oscillator states being unoccupied. The self-energy for this state is calculated by the method used by Weisskopf[6] for the Dirac electron; the appropriate modifications being made for the change from Fermi to Bose statistics. The resulting formulae are: for the first- and second-order contributions to the transverse self-energy,

$$L_{T1}=\frac{e^2c^2}{2\pi^2\hbar}\int\nu^{-1}d\mathbf{k}\int|\psi_u|^2 d\tau, \tag{2.14}$$

$$L_{T2}=-\frac{e^2c^4}{\pi^2\hbar}\int d\mathbf{k}\sum_{\mathbf{e}}\nu^{-1}\sum_s\frac{|\mathbf{e}\cdot\mathbf{t}_{su}(\mathbf{k})|^2}{F_s-\epsilon_sF_u+h\nu}, \tag{2.15}$$

$$\mathbf{t}_{su}(\mathbf{k})=\int e^{i(\mathbf{k}\cdot\mathbf{r})}\psi_s\nabla\psi_u^* d\tau, \tag{2.16}$$

and for the direct and exchange contributions to the longitudinal self-energy

$$\left.\begin{aligned}L_{L1}&=\int\int\rho_0(\mathbf{r}')\rho(\mathbf{r})(|\mathbf{r}-\mathbf{r}'|)^{-1}d\tau d\tau',\\ L_{L2}&=\frac{e^2}{4\pi^2\hbar^2}\int k^{-2}d\mathbf{k}\sum_s\left|\int\psi_s e^{i(\mathbf{k}\cdot\mathbf{r})}\right.\\ &\qquad\left.\times\left(E_s+E_u+2\frac{e}{\hbar}V\right)\psi_u^* d\tau\right|^2.\end{aligned}\right\} \tag{2.17}$$

Here $\mathbf{k}$ is the wave number and ν the frequency of a quantum, and $\mathbf{e}$ its direction of polarization; the contribution of two-quantum emission processes to the transverse self-energy is (as usual) ignored. In L_{L1}, $\rho_0(\mathbf{r}')$ is the expectation value of the charge density operator ρ at the point $\mathbf{r}'$, in the vacuum state when no scalar particles are present; this expectation value is different from zero because the external potential polarizes the vacuum. Since the polarization of the vacuum introduces special difficulties not directly connected with the line shift problem, the consideration of the term L_{L1} will be postponed till Section VI.

For a free particle of momentum $\hbar\mathbf{k}_u$ the self-energies are[7]

$$L_{T10}=\frac{e^2c^2h}{4\pi^2}F_u^{-1}\int\nu^{-1}d\mathbf{k}, \tag{2.18}$$

$$L_{T20}=-\frac{e^2c^4h}{4\pi^2}F_u^{-1}\int d\mathbf{k}\nu^{-1}\left(k_u^2-\frac{(\mathbf{k}_u\cdot\mathbf{k})^2}{k^2}\right)\times\frac{(E_++\nu)}{E_+[(E_++\nu)\nu+c^2\mathbf{k}_u\cdot\mathbf{k}]}, \tag{2.19}$$

[4] Pauli and Weisskopf, Helv. Phys. Acta **7**, 709 (1934).
[5] V. F. Weisskopf, Zeits. f. Physik **89**, 27 (1934).

[7] V. F. Weisskopf, Phys. Rev. **56**, 72 (1939); Weisskopf gives (on pp. 82, 83) formulae for the self-energies of a free scalar particle at rest, differing from the results of this paper by constant numerical factors. Weisskopf informs me that these discrepancies are caused by an error in his paper.

$$L_{L10}=0,$$

$$L_{L20}=\frac{e^2\hbar}{8\pi^2}F_u^{-1}\int k^{-2}d\mathbf{k}[E_+ +(F_u^2/\hbar^2E_+)], \quad (2.20)$$

$$E_+=E_{\mathbf{k}+\mathbf{k}_u}, \quad E_{\mathbf{k}}=E_k=(m^2c^4/\hbar^2+c^2k^2)^{\frac{1}{2}}. \quad (2.21)$$

These expressions can be formally expanded in powers of k_u and give a total free particle self-energy

$$L_0=\frac{e^2}{2\pi\hbar c}F_u^{-1}\times\left[m^2c^4\int(2x+(1+2x^2)/(1+x^2)^{\frac{1}{2}})dx-\tfrac{1}{6}\hbar^2c^2k_u^2+O(k_u^6)\right]. \quad (2.22)$$

The remainder term here is not only of order k_u^6 but involves exclusively convergent integrals.

III. THE SUBTRACTION PRESCRIPTION

It is important to define as clearly as possible the assumptions on which the line shift calculations are based. Only thereby can a limit be set to the degree of arbitrariness involved in the subtraction prescription.

It is assumed, first, that in a correct electrodynamics the self-energies L_0 and

$$L=L_{T1}+L_{T2}+L_L \quad (3.1)$$

would be made convergent, but would not be seriously altered in form except for the contributions from very high energy quanta. Secondly, that the use of a conventional cut-off at high quantum energies in place of the unknown correct convergence factor would introduce only small inaccuracies, and that these would be in the same direction for the bound and free particle. Thirdly, that in a correct theory the self-energies would be treated on an equal footing with other forms of energy.

In the case of a free particle, it follows from the principle of relativity that the self-energy can manifest itself physically only as an addition to the rest mass of the particle; if the "true" rest mass is m_0 we may write

$$H_5=\delta\int\psi^*\psi d\tau, \quad \delta=\frac{m^2c^4}{\hbar^2}-\frac{m_0^2c^4}{\hbar^2}, \quad (3.2)$$

and the effect of the self-energy will be completely described by the inclusion of H_5 in the part H_1 of the unperturbed Hamiltonian H_0. For a bound particle, the Hamiltonian H_0 of the usual hydrogen atom theory will not be exactly equivalent to the true Hamiltonian

$$H'=H-H_5. \quad (3.3)$$

The level shift caused by this discrepancy will be equal to the expectation value of the perturbing energy (H_4-H_5) evaluated for a stationary state of the approximate Hamiltonian H_0 (it is to be noted that the unperturbed Hamiltonian must be H_0 and not (H_0-H_5) so that the perturbation is really a small effect). The level shift is thus

$$LS=L-\delta\int|\psi_u|^2d\tau. \quad (3.4)$$

To eliminate the unknown δ, we use the fact that the level shift for a free particle is zero; since (3.4) holds equally for a free particle, we should have

$$L_0=\delta\left[\int|\psi_u|^2d\tau\right]_{\text{Free}}=\delta\tfrac{1}{2}\hbar^2F_u^{-1}, \quad (3.5)$$

$$LS=L-L_0\left[\int|\psi_u|^2d\tau\right]\Big/\left[\int|\psi_u|^2d\tau\right]_{\text{Free}}. \quad (3.6)$$

Unfortunately, it is clear from (2.22) that (3.5) cannot hold exactly for all free particles; while the divergent part of (2.22) is of the correct form (3.5), the finite term in k_u^2 in (2.22) is not, so that L_0 has not exactly the correct dependence on k_u. The discrepancy must be attributed to our ignorance of the correct method of evaluating the divergent parts of L and L_0. When L_0 is written in the form (2.22), it is tacitly assumed that the divergent integrals should be made convergent by a convergence factor depending only on the quantum wave number $\mathbf{k}$ and not on the state of the particle; such a convergence factor cannot be more than approximately correct. The best that can be hoped is that by a suitable choice of free particle the errors in the formulae for L and L_0 will largely cancel out in (3.6); how this shall best be arranged must be partly a matter of guess work.

In order to show the order of magnitude of the arbitrariness introduced by this choice, we shall calculate the level shift with two possible pre-

scriptions. The first ("single particle prescription") is to choose the free particle to be such that

$$\left[\int|\psi_u|^2d\tau\right]_{\text{Free}}=\int|\psi_u|^2d\tau, \tag{3.7}$$

so that the level shift is simply

$$LS=L-L_0. \tag{3.8}$$

The free particle has, in this case, the same kinetic energy as the bound particle, so that the meaning of (3.8) is physically perspicuous. The second ("wave packet prescription") is to analyze the bound particle wave function into a packet of free particle wave functions, and to replace the subtracted term in (3.6) by a weighted average, each free particle being given the same weight as its wave function occupies in the packet. The second prescription is designed to give as detailed as possible a cancellation of errors between the two terms of (3.6), and is the prescription suggested by Weisskopf. The averaging process is very simple, and leads again to the result (3.8), but with k_u^2 replaced by an average in the definition of L_0. Instead of (2.22), we must now take

$$L_0=\frac{e^2}{\pi\hbar^3c}\int|\psi_u|^2d\tau \left[m^2c^4\int(2x+(1+2x^2)/(1+x^2)^{\frac{1}{2}})dx -\tfrac{1}{6}\hbar^2c^2(\nabla\Psi_u\cdot,\nabla\Psi_u)\right], \tag{3.9}$$

the scalar product being defined by (2.11).

It will be found that the difference between the results according to these two prescriptions is small but not negligible in comparison with the total line shift.

IV. OUTLINE OF THE CALCULATIONS

The practical difficulties of the line shift calculation arise from the summations over scalar particle states in L_{T2} and L_L. The only tool we have for performing these summations is (2.13), and before this tool can be used the expressions must be expanded in powers of the potential V. The line shift itself is of the second order in V, and all convergent expressions of higher order than this will be neglected. The expansion is best carried out in momentum space, and accordingly we set

$$\left.\begin{aligned}\psi_s&=\int e^{-i\mathbf{k}\cdot\mathbf{r}}A_s(\mathbf{k})d\mathbf{k},\\ V\psi_s&=\int e^{-i\mathbf{k}\cdot\mathbf{r}}B_s(\mathbf{k})d\mathbf{k},\\ V^2\psi_s&=\int e^{-i\mathbf{k}\cdot\mathbf{r}}C_s(\mathbf{k})d\mathbf{k}.\end{aligned}\right\} \tag{4.1}$$

The wave equation (2.6) in momentum space is

$$(E_s^2-E_k^2)A_s(\mathbf{k})+2\frac{e}{h}E_sB_s(\mathbf{k})+\frac{e^2}{\hbar^2}C_s(\mathbf{k})=0,$$

$$E_k^2=\frac{m^2c^4}{\hbar^2}+c^2k^2. \tag{4.2}$$

Further, the orthogonality conditions (2.13) become

$$\left.\begin{aligned}\sum_s\epsilon_s\psi_s^*A_s(\mathbf{k})&=0,\\ \sum_s F_s\psi_s^*A_s(\mathbf{k})&=\hbar^2(2\pi)^{-3}e^{i\mathbf{k}\cdot\mathbf{r}},\\ \sum_s\epsilon_s\psi_s^*B_s(\mathbf{k})&=0,\\ \sum_s F_s\psi_s^*B_s(\mathbf{k})&=\hbar^2(2\pi)^{-3}Ve^{i\mathbf{k}\cdot\mathbf{r}}.\end{aligned}\right\} \tag{4.3}$$

Now consider L_{T2}. This may be written

$$L_{T2}=-\frac{e^2c^4}{\pi^2\hbar}\int d\mathbf{k}\sum_{\mathbf{e}}\nu^{-1}\int d\tau'\mathbf{e}\cdot\nabla\psi_u(\mathbf{r}')e^{-i\mathbf{k}\cdot\mathbf{r}'} \times\int d\mathbf{k}'(i\mathbf{e}\cdot\mathbf{k}')A_u^*(\mathbf{k}')Q(\mathbf{k}+\mathbf{k}'), \tag{4.4}$$

where

$$Q(\mathbf{k}_1)=\sum_s\frac{1}{F_s-\epsilon_sF_u+\hbar\nu}(2\pi)^3A_s(\mathbf{k}_1)\psi_s^*(\mathbf{r}'). \tag{4.5}$$

We write $F_k=\hbar E_k$. It is clear from (4.2) that F_s may be replaced by F_{k_1} in $Q(\mathbf{k}_1)$ with an error of higher order in V. Thus, neglecting the term in $C_s(\mathbf{k}_1)$,

$$\frac{1}{F_s-\epsilon_sF_u+\hbar\nu}A_s(\mathbf{k}_1) =[(F_{k1}+\epsilon_sF_u+\hbar\nu)/((F_{k1}+\hbar\nu)^2-F_u^2)]A_s(\mathbf{k}_1) +\frac{2e\hbar}{F_s+F_{k_1}}[(1/(F_s-\epsilon_sF_u+\hbar\nu)(F_{k1}-\epsilon_sF_u+\hbar\nu))] \times E_sB_s(\mathbf{k}_1),$$

and after some rearrangements this becomes

$$\frac{F_{k_1}+\hbar\nu}{F_{k_1}[(F_{k_1}+\hbar\nu)^2-F_u^2]}F_sA_s(\mathbf{k}_1)$$
$$-2e\frac{F_u}{F_{k_1}}\frac{F_{k_1}+\hbar\nu}{[(F_{k_1}+\hbar\nu)^2-F_u^2]^2}F_sB_s(\mathbf{k}_1)$$
$$+\text{terms in } \epsilon_sA_s(\mathbf{k}_1) \text{ and } \epsilon_sB_s(\mathbf{k}_1).$$

The relations (4.3) can now be used and give

$$Q(\mathbf{k}_1)=\frac{F_{k_1}+\hbar\nu}{F_{k_1}[(F_{k_1}+\hbar\nu)^2-F_u^2]}\hbar^2e^{i\mathbf{k}_1\cdot\mathbf{r}'}$$
$$\times\left[1-2e\frac{F_u}{[(F_{k_1}+\hbar\nu)^2-F_u^2]}V(\mathbf{r}')\right]. \quad (4.6)$$

When (4.6) is substituted into (4.4), the integration over $\mathbf{k}'$ cannot be carried out owing to the appearance of the quantity $F_{k+k'}$. However, $A_u^*(\mathbf{k}')$ is appreciable only when $\mathbf{k}'$ is small, and therefore $F_{k+k'}$ may be expanded in powers of $\mathbf{k}'$. As the first approximation to $F_{k+k'}$ it is convenient to use

$$F_{ku}=(F_u^2+c^2\hbar^2k^2)^{\frac{1}{2}}=((mc^2-D_u)^2+c^2\hbar^2k^2)^{\frac{1}{2}}, \quad (4.7)$$

so that

$$(F_{ku}+\hbar\nu)^2-F_u^2=2\hbar\nu(F_{ku}+\hbar\nu). \quad (4.8)$$

Then the expansion of $F_{k+k'}$ is to the required order

$$F_{k+k'}=F_{ku}+\frac{c^2\hbar^2\mathbf{k}\cdot\mathbf{k}'}{F_{ku}}$$
$$+\frac{2F_uD_u+c^2\hbar^2k'^2}{2F_{ku}}-\frac{c^4\hbar^4(\mathbf{k}\cdot\mathbf{k}')^2}{2F_{ku}^3}. \quad (4.9)$$

This expansion has to be substituted into (4.6) and the result expanded again; the integration over $\mathbf{k}'$ in (4.4) can then be carried out and gives

$$L_{T2}=-\frac{e^2c^4}{\pi^2\hbar}\int d\mathbf{k}\sum_{\mathbf{e}}\nu^{-1}\int d\tau\mathbf{e}\cdot\nabla\psi_u\hbar^2$$
$$\times\left[\frac{1}{2\hbar\nu F_{ku}}-\frac{eF_uV}{2\hbar^2\nu^2F_{ku}(F_{ku}+\hbar\nu)}\right.$$
$$-\frac{F_{ku}^2+F_{ku}\hbar\nu+\hbar^2\nu^2}{2\hbar^2\nu^2F_{ku}^2(F_{ku}+\hbar\nu)}\times\left\{\frac{F_uD_u}{F_{ku}}-\frac{c^2\hbar^2}{2F_{ku}}\nabla^2\right.$$
$$\left.\left.+\frac{c^4\hbar^4}{2F_{ku}^3}(\mathbf{k}\cdot\nabla)^2\right\}\right]\mathbf{e}\cdot\nabla\psi_u^*. \quad (4.10)$$

Now if $\mathbf{a}$, $\mathbf{b}$, $\mathbf{c}$ are any three vectors, and averages are taken over all directions of the perpendicular pair of vectors $\mathbf{k}$ and $\mathbf{e}$,

$$\text{Av}(\mathbf{e}\cdot\mathbf{ae}\cdot\mathbf{b})=\tfrac{1}{3}\mathbf{a}\cdot\mathbf{b}, \quad \text{Av}(\mathbf{e}\cdot\mathbf{ae}\cdot\mathbf{b}(\mathbf{k}\cdot\mathbf{c})^2)$$
$$=\frac{1}{15}k^2(2c^2\mathbf{a}\cdot\mathbf{b}-\mathbf{a}\cdot\mathbf{cb}\cdot\mathbf{c}).$$

This enables the integration over the direction of $\mathbf{k}$ to be carried out at once. Transforming to the dimensionless variable

$$x=\hbar ck/F_u, \quad (4.11)$$

and using the wave equation (2.6) for ψ_u^*,

$$L_{T2}=-\frac{4}{3\pi}\frac{e^2c}{\hbar}\left[\int|\nabla\psi_u|^2d\tau\int(x^2+1)^{-\frac{1}{2}}dx\right.$$
$$-\tfrac{1}{2}eF_u^{-1}\int|\psi_u|^2\nabla^2Vd\tau$$
$$\times\int[x^{-1}-x^2(x^2+1)^{-1}]dx$$
$$+eF_u^{-1}\int|\nabla\psi_u|^2Vd\tau\int(x^2+1)^{-\frac{1}{2}}dx$$
$$+\tfrac{1}{10}\hbar^2c^2F_u^{-2}\int|\nabla^2\psi_u|^2d\tau$$
$$\left.\times\int[x(x^2+1)^{-1}-x^4(x^2+1)^{-5/2}]dx\right]. \quad (4.12)$$

It will be seen that the first integral over x diverges at infinity, and must be cancelled by a similar term in the free particle energy; the second integral, however, diverges at zero, and this is a more serious matter.

In fact the expansion of (4.5) in powers of the potential is only valid if the energy difference (F_s-F_{ku}) is small compared with the quantum energy $\hbar\nu$ for the important intermediate states. This energy difference will be of the order of a few Rydbergs (in view of Bethe's analysis,[1] it will sometimes be a rather large number of Rydbergs), but it can be verified that the expansion gives negligible error for quantum energies greater than 2×137 Rydbergs. Hence, we shall cut off the integrals in (4.12) at $x=\alpha=e^2/\hbar c$, and evaluate the low energy part of L_{T2} separately.

From the low energy part of L_{T2} we subtract the (negative) corresponding part of the first integral on the right of (4.10), and obtain

$$R=\frac{e^2c^4}{\pi^2\hbar}\int d\mathbf{k}\sum_{\mathbf{e}}\nu^{-1}\sum_{s}\left|\int e^{i(\mathbf{k}\cdot\mathbf{r})}\psi_s\mathbf{e}\cdot\nabla\psi_u^*d\tau\right|^2 \times\left\{\frac{F_s}{2\hbar\nu F_{ku}}-\frac{1}{F_s-\epsilon_sF_u+\hbar\nu}\right\}. \quad (4.13)$$

This first integral in (4.10), which reappears as the first integral on the right of (4.12), is subtracted in order to obtain an expression which shall be directly comparable with the corresponding expression in Bethe's non-relativistic calculation.[1] We may neglect in R all terms which are of second order in the potential and at the same time convergent at $k=0$, for in view of the small range of integration such terms will be a factor α smaller than the terms retained in (4.12). To this accuracy we may replace

$$F_s/(2\hbar\nu F_{ku}) \quad \text{by} \quad 1/(2\hbar\nu)$$

in (4.13), both F_s and F_{ku} being close to mc^2 at low energies; then, adding a multiple of ϵ_s which does not alter the value of the whole expression and using (4.8), this is replaced in turn by

$$1/(F_{ku}-\epsilon_sF_u+\hbar\nu).$$

Therefore

$$R=\frac{e^2c^4}{\pi^2\hbar}\int d\mathbf{k}\sum_{\mathbf{e}}\nu^{-1}\sum_{s}\left|\int e^{i(\mathbf{k}\cdot\mathbf{r})}\psi_s\mathbf{e}\cdot\nabla\psi_u^*d\tau\right|^2 \times\{(F_s-F_{ku})/((F_{ku}-\epsilon_sF_u+\hbar\nu)(F_s-\epsilon_sF_u+\hbar\nu))\}.$$

In this form, it is easy to see that the whole contribution of positive-charge states is negligible. Also, the negative-charge states in this energy range may be replaced with negligible error by the states of a non-relativistic particle. Hence, denoting the non-relativistic wave functions by ϕ_s and taking account of their different normalization,

$$R=\frac{e^2c^4\hbar^3}{4\pi^2}\int d\mathbf{k}\sum_{\mathbf{e}}\nu^{-1}\sum_{s}\left|\int e^{i(\mathbf{k}\cdot\mathbf{r})}\phi_s\mathbf{e}\cdot\nabla\phi_u^*d\tau\right|^2 \times\{(F_s-F_{ku})/(F_uF_s(F_{ku}-F_u+\hbar\nu) \times(F_s-F_u+\hbar\nu))\}.$$

This is simply the formula for the line shift of a non-relativistic particle as given by Bethe, but including the effect of retardation. As remarked by Bethe, the retardation makes a negligible difference at low energies, and therefore R may be equated to Bethe's non-retarded expression (W' in his notation), cut off at αmc^2 instead of at mc^2. Since W' was exactly computed for the $2s$ and $2p$ states of hydrogen by Bethe, it is convenient to write $R=W'-(W'-R)$, with

$$W'-R=\frac{e^2c^2\hbar^2}{6\pi^2F_u^2}\int d\mathbf{k}k^{-2}\sum_{s}\left|\int\phi_s\nabla\phi_u^*d\tau\right|^2 \times(F_s-F_u)/(F_s-F_u+\hbar\nu),$$

the integration extending over quanta with energies between αmc^2 and mc^2. In this energy-range it is allowable to expand in powers of the potential, and this gives the result

$$R=W'-\frac{e^2\hbar c}{3\pi F_u^2}\int|\phi_u|^2\nabla^2Vd\tau\int_{\alpha}^{1}x^{-1}dx. \quad (4.14)$$

The final formula for L_{T2} is obtained by collecting (4.12) and (4.14). The first integral over x in (4.12) must be continued down to $x=0$, because of the subtracted term in the definition of R; the remaining integrals may be continued down to $x=0$ without appreciable effect, with the exception of the integral of x^{-1}; the integral of x^{-1} appears with the same coefficient and opposite sign in (4.12) and (4.14), and is therefore continued only down to $x=1$ in the sum. Inserting numerical values for the convergent integrals, we obtain

$$L_{T2}=-\frac{4}{3\pi}\frac{e^2c}{\hbar}\Big[\int|\nabla\psi_u|^2d\tau\int(x^2+1)^{-\frac{1}{2}}dx -\tfrac{1}{2}eF_u^{-1}(1-\log 2)\int|\psi_u|^2\nabla^2Vd\tau +eF_u^{-1}\int|\nabla\psi_u|^2Vd\tau+\tfrac{1}{10}\hbar^2c^2F_u^{-2} \times\left(\frac{4}{3}-\log 2\right)\int|\nabla^2\psi_u|^2d\tau\Big]+W'. \quad (4.15)$$

Next we must evaluate L_{L2}. Expanding (2.17) and using (2.6) to eliminate the terms in E_s^2 and

E_u^2, we obtain in analogy with (4.4)

$$L_{L2}=\frac{e^2}{4\pi^2\hbar^2}\int k^{-2}d\mathbf{k}\int d\tau' e^{-i\mathbf{k}\cdot\mathbf{r}'}\times\int d\mathbf{k}'[\{A_u^*(\mathbf{k}')(E_k^2+(m^2c^4/\hbar^2)+2(e/\hbar)E_uV(\mathbf{r}')-2(e/\hbar)^2V^2(\mathbf{r}')+2c^2i\mathbf{k}\cdot\nabla-2c^2\nabla^2)\psi_u(\mathbf{r}')+4(e/\hbar)^2B_u^*(\mathbf{k}')V(\mathbf{r}')\psi_u(\mathbf{r}')\}Q_1(\mathbf{k}+\mathbf{k}')+2A_u^*(\mathbf{k}')(E_u+(e/\hbar)V(\mathbf{r}'))\times\psi_u(\mathbf{r}')Q_2(\mathbf{k}+\mathbf{k}')], \quad (4.16)$$

where

$$\left.\begin{aligned}Q_1(\mathbf{k}_1)&=\sum_s (2\pi)^3A_s(\mathbf{k}_1)\psi_s^*(\mathbf{r}'),\\ Q_2(\mathbf{k}_1)&=\sum_s (2\pi)^3E_sA_s(\mathbf{k}_1)\psi_s^*(\mathbf{r}').\end{aligned}\right\} \quad (4.17)$$

As far as order of magnitude is concerned, the square of a gradient operator operating on ψ_u is equivalent, by virtue of the wave equation (2.6), to a single power of V. Since the gradient operator appearing in (2.16) is absent in (2.17), it is necessary to retain terms of order V^2 in (4.16) and (4.17). To this order, using (4.3) as before,

$$\left.\begin{aligned}Q_1(\mathbf{k}_1)&=\hbar^2e^{i\mathbf{k}_1\cdot\mathbf{r}'}F_{k_1}{}^{-1},\\ Q_2(\mathbf{k}_1)&=-e\hbar e^{i\mathbf{k}_1\cdot\mathbf{r}'}F_{k_1}{}^{-1}\{V(\mathbf{r}')\\ &\quad+(c^2\hbar^2/4F_{k_1}{}^2)(2i\mathbf{k}_1\cdot\nabla+\nabla^2)V(\mathbf{r}')\\ &\quad-(c^4\hbar^4/2F_{k_1}{}^4)(\mathbf{k}_1\cdot\nabla)^2V(\mathbf{r}')\}.\end{aligned}\right\} \quad (4.18)$$

When (4.18) is substituted into (4.16), the quantity $F_{k+k'}$ must be expanded to terms of order k'^4. However, there is now no difficulty due to lack of convergence at $k=0$, and the reduction of (4.16) is entirely straightforward. Introducing the dimensionless variable

$$x=\hbar ck/mc^2, \quad (4.19)$$

and evaluating the convergent integrals in finite terms, there results

$$L_{L2}=\frac{e^2c}{\pi\hbar}\left[\frac{m^2c^2}{\hbar^2}\int|\psi_u|^2d\tau\int((1+2x^2)/(1+x^2)^{\frac{1}{2}})dx+\frac{4}{3}\int|\nabla\psi_u|^2d\tau\int(x^2+1)^{-\frac{1}{2}}dx-\frac{1}{6}\int|\nabla\psi_u|^2d\tau-\frac{1}{18}eF_u{}^{-1}\int|\psi_u|^2\nabla^2Vd\tau-\frac{4}{15}\hbar^2c^2F_u{}^{-2}\int|\nabla^2\psi_u|^2d\tau\right]. \quad (4.20)$$

Finally, (2.14) gives

$$L_{T1}=2\frac{e^2c}{\pi\hbar}\frac{m^2c^2}{\hbar^2}\int_0|\psi_u|^2d\tau\int xdx. \quad (4.21)$$

The level shift according to the wave packet prescription is given by (3.8), (3.9), (4.15), (4.20), and (4.21); all the divergent integrals cancel out, and after making allowance for the fact that x given by (4.19) tends to infinity slightly slower than x given by (4.11),

$$LS=W'+\frac{e^2c}{\pi\hbar}\left[\frac{1}{6}\int|\psi_u|^2d\tau(\nabla\Psi_u{}^*,\nabla\Psi_u)-\frac{1}{6}\int|\nabla\psi_u|^2d\tau-eF_u{}^{-1}\left(\frac{1}{18}+\frac{2}{3}\log 2\right)\times\int|\psi_u|^2\nabla^2Vd\tau+\hbar^2c^2F_u{}^{-2}\times\left(\frac{2}{9}+\frac{2}{15}\log 2\right)\int|\nabla^2\psi_u|^2d\tau\right]. \quad (4.22)$$

Evaluation of the scalar product by (2.11) gives

$$\int|\psi_u|^2d\tau(\nabla\Psi_u{}^*,\nabla\Psi_u)-\int|\nabla\psi_u|^2d\tau=2\frac{e^2}{\hbar^2c^2}\left[\int V^2|\psi_u|^2d\tau-\left(\int V|\psi_u|^2d\tau\right)^2\Big/\left(\int|\psi_u|^2d\tau\right)\right]. \quad (4.23)$$

For the one-particle prescription the same quantity (4.23) appears but with the coefficient $+2$ replaced by -1; to avoid repetition this coefficient ($+2$ or -1) will be denoted in what follows by ϵ.

V. DETAILED RESULTS

All terms in (4.22) after substitution from (4.23) are of the same order of magnitude as the line shift; hence, the relativistic wave function ψ_u

may be replaced by a non-relativistic wave function ϕ with negligible error. Allowing for the change in normalization, the final formula for the line shift is

$$LS=\frac{e^3h}{3\pi m^2c^3}\Big[\tfrac{1}{4}\epsilon\frac{me}{h^2}\times\Big\{\int V^2|\phi|^2d\tau-\Big(\int V|\phi|^2d\tau\Big)^2\Big\}-\Big(\frac{1}{12}+\log 2\Big)\int|\phi|^2\nabla^2Vd\tau+\frac{h^2}{me}(\tfrac{1}{3}+\tfrac{1}{5}\log 2)\int|\nabla^2\phi|^2d\tau\Big]+W', \quad (5.1)$$

where W' is Bethe's non-relativistic expression[1] with the cut-off energy at exactly mc^2.

For a coulomb potential, $V=-Ze^{-1}$, the correction terms to be added to W' in (5.1) can be evaluated in finite terms. If the electron is in a state with quantum numbers n and l, the line shift is

$$LS=\frac{8}{3\pi}\frac{Z^4}{n^3}\alpha^3Ry\Big[\text{"log"}-\eta\Big(\log 2+\frac{1}{12}\Big)+(\tfrac{1}{3}+\tfrac{1}{5}\log 2)\Big(\frac{1}{l+\frac{1}{2}}-\frac{3}{4n}\Big)+\frac{1}{16}\epsilon\Big(\frac{1}{l+\frac{1}{2}}-\frac{1}{n}\Big)\Big], \quad (5.2)$$

where $\eta=1$ for S states and $\eta=0$ otherwise; "log" is the logarithm occurring in the non-relativistic calculation and is very small for all except S states. The displacement of a $2s$ state relative to a $2p$ state becomes

$$D=\frac{1}{3\pi}Z^4\alpha^3Ry\Big[\text{"log"}+\frac{13}{36}-\frac{11}{15}\log 2+\frac{1}{12}\epsilon\Big], \quad (5.3)$$

where "log," according to Bethe,[1] is to be given the value 7.63 for the $2s$-$2p$ displacement of hydrogen. Inserting numerical values, we find for hydrogen

$$D=1037 \quad \text{and} \quad 1003 \text{ megaycles} \quad (5.4)$$

with the wave packet and single-particle subtraction prescriptions, respectively. The difference between these two figures in a rough measure of the uncertainty involved in the calculations.

According to (5.2), the relativistic theory predicts a displacement of an np level relative to an nd level; this displacement is small compared to the ns-np displacement, but large compared to the np-nd displacement given by the non-relativistic theory of Bethe.[1] Unfortunately the natural widths of the levels concerned are approximately twice as large as the predicted displacement, so that an observational test of these relativistic effects is hardly to be expected.

The experimental separation[2] of the $2s$ and $2p_{\frac{1}{2}}$ levels of hydrogen is 1000 megacycles, and agrees very closely with (5.4). The agreement is not, however, of much significance; in the first place, the measurements are not yet sufficiently accurate; in the second place, the spin of the electron is likely to modify the calculated values by amounts which, while small compared to the total separation, are of the order of magnitude of the relativistic terms in (5.2).

VI. THE POLARIZATION OF THE VACUUM

In the preceding sections the energy L_{L1} given by (2.17) has been simply ignored. In order to take it into account, it is necessary to use the theory of the polarization of the vacuum as developed[8] by Dirac and Heisenberg. This was done in detail for the hydrogen atom (including electron spin) by Uehling,[9] who found that this term leads to a $2s-2p_{\frac{1}{2}}$ separation of about 25 megacycles in the wrong direction.

In the framework of the present paper, the term L_{L1} has a particularly direct interpretation, and its effect can be calculated by a far simpler method than that used by Uehling. For this reason, and not because the numerical result has any significance, an exact evaluation of the term L_{L1} for spin-zero particles is here given.

Going back to (2.2) and (2.5), the vacuum charge-density is

$$\rho_0=-\frac{e}{h}\sum_s\Big(E_s+\frac{e}{h}V\Big)\psi_s\psi_s^*. \quad (6.1)$$

[8] V. F. Weisskopf, Kgl. Danske Vid. Sels., Math.-Fys. Medd. **144**, 6 (1936).
[9] E. A. Uehling, Phys. Rev. **48**, 55 (1935).

If in this expression ψ_s is replaced by its Fourier transform according to (4.1), there result sums of the type (4.17), which can be evaluated as in (4.18). We have now to retain terms up to the orders V^3, $V\nabla^2 V$ and $\nabla^4 V$, but it is found that only terms in $\nabla^2 V$ and $\nabla^4 V$ appear in the result. Performing the integration over $\mathbf{k}_1$, ρ_0 takes the simple form

$$\rho_0 = \frac{1}{24\pi^2}\frac{e^2}{\hbar c}\left\{\int x^4 dx/(1+x^2)^{5/2}\right\}\nabla^2 V + \frac{e^2\hbar}{480\pi^2 m^2 c^3}\nabla^4 V. \quad (6.2)$$

Therefore L_{L1} can be written

$$L_{L1} = \int V'(\mathbf{r})\rho(\mathbf{r})d\tau, \quad (6.3)$$

where V' is the potential of the charges induced in the vacuum by the potential V, and is given by

$$V' = -\frac{1}{6\pi}\frac{e^2}{\hbar c}\left\{\int x^4 dx/(1+x^2)^{5/2}\right\}V - \frac{e^2\hbar}{120\pi m^2 c^3}\nabla^2 V. \quad (6.4)$$

The first term in V' contains a divergent integral, but this whole term can be eliminated by the same arguments which were used in Section III to deal with the other divergent expressions. In fact, this term represents the potential of an induced charge distribution strictly proportional to the inducing charge distribution; such an induced charge distribution would reveal itself physically only by the fact that every measurement of the charge of any particle would give a value less by a constant factor than the "true" charge. Now if the first term of V' were to be included in the energy L_{L1}, the part H_3 of the original Hamiltonian (2.4) would have to be defined with V the potential generated by the "true" external charges. In fact, however, V is defined to be the potential of the measured external charges, and this means that the actual H_3 is the sum of the "true" H_3 and the first term in L_{L1}. The second term in L_{L1} corresponds to a distribution of charge whose integral over space is zero, and is therefore not included in H_3. Introducing the non-relativistic wave function ϕ of the scalar particle, the surviving part of L_{L1} becomes

$$L_{L1} = -\frac{e^2\hbar}{120\pi m^2 c^3}\int |\phi|^2 \nabla^2 V d\tau. \quad (6.5)$$

This should be added as a correction to (5.1). For a coulomb potential, the correction to (5.2) is

$$-\frac{1}{15\pi}\frac{Z^4}{n^3}\alpha^3\eta Ry, \quad (6.6)$$

and for the $2s$-$2p$ displacement the correction is

$$-\frac{1}{120\pi}Z^4\alpha^3 Ry. \quad (6.7)$$

This would diminish the level shift for hydrogen by 3 megacycles, an utterly insignificant effect.

The calculations here described were carried out at the suggestion of Professor Bethe, to whom the author's thanks are due for much helpful advice and discussion. Thanks are due also to Professor Weisskopf for some useful suggestions and to the Commonwealth Fund for financial support.

Second-Order Corrections to Quadrupole Effects in Molecules

J. BARDEEN AND C. H. TOWNES
Bell Telephone Laboratories, Murray Hill, New Jersey
February 3, 1948

ROTATIONAL lines of the molecules BrCN, ICl, and ICN occur at frequencies near 25,000 mc. Splittings of these lines due to nuclear quadrupole effects have been measured to an accuracy of about 0.1 mc, which is a considerable improvement on previous measurements[1] of BrCN and ICN. The rotational levels of these molecules are split by electrostatic quadrupole interactions between the nuclear and molecular charges. While the positions of the lines are in general agreement with the predictions of Casimir's formula,[2] small differences have been found which require the consideration of second-order effects.

The discrepancies are shown most clearly in the case of ICN. The spectrum is not complicated, as is that of ICl, by a second quadrupole interaction (the splitting due to N is of the order of 0.1 mc), and the splitting due to the halide quadrupole is larger in ICN than in BrCN. The energy levels are characterized by the total angular momentum, $\mathbf{F}=\mathbf{J}+\mathbf{I}$, obtained by combining the molecular rotation with the iodine nuclear spin. Absorption lines observed in ICN connect the rotational levels $J=3$ and $J=4$. We designate the lines by the F-values of the two levels, that for $J=3$ coming first. The first column of Table I gives the measured frequencies relative to that of the strongest line at 25,823.1 mc which results from the transition $J=3$, $F=11/2$ to $J=4$, $F=13/2$. Corresponding theoretical values from Casimir's formula with an interaction constant $eqQ=-2420$ mc are given in the second column. Here Q is the usual quadrupole moment of the nucleus, and q is defined as the gradient of the electric field at the nucleus, $\partial^2 V/\partial Z^2$. Differences between the experimental values and those of the first-order theory are listed in the third column. It has been found that these differences are adequately accounted for by second-order effects arising from matrix elements of the quadrupole interaction connecting different rotational levels.

Non-vanishing matrix elements connect states with the same F, M_F, but with different values of the rotational quantum number, J. They may be designated

$$(IJFM_F|H_Q|IJ'FM_F),$$

where H_Q is the quadrupole interaction. The second-order energy correction is given by the square of the matrix element divided by the energy difference between the rotational levels, summed over the various J' which connect with the given rotational level J. If this second-order effect is considered, the angular momentum due to molecular rotation is not a constant of the motion.

The required matrix elements applying to linear and symmetric top molecules have been evaluated by a method devised by Racah.[3] The quadrupole interaction contains as the pertinent factor $P_2(\cos\omega)$, where ω is the angle between a nuclear charge and a molecular charge, the angle being measured from the centroid of the nuclear charge. By the addition theorem, $P_2(\cos\omega)$ can be expressed as a scalar product of two spherical harmonics of the second order involving separately the nuclear and molecular coordinates. Racah has given a general formula[4] for the matrix element of the scalar product of two tensors which has been found convenient to use for this problem. The matrix element vanishes if J' differs from J by more than two. We need to give the formulas for $J'=J+1$ and $J'=J+2$ only, as the matrix element is symmetric in J

[1] Townes, Holden, and Merritt, Phys. Rev. **71**, 64 (1947); Gordy, Smith, Smith, and Ring, Phys. Rev. **72**, 259 (1947).
[2] H. B. G. Casimir, *On the Interaction Between Atomic Nuclei and Electrons* (E. F. Bohn, Haarlem, 1936).
[3] G. Racah, Phys. Rev. **62**, 438 (1942).
[4] Reference 3, Eq. (38).

and J'. The squares of the matrix elements are:

$$(IJFM_F|H_Q|IJ+1FM_F)^2$$

$$=\left(\frac{3eqQK}{8I(I-1)J(J+2)}\right)^2\left(1-\frac{K^2}{(J+1)^2}\right)$$

$$\times\left(\frac{F(F+1)-I(I+1)-J(J+2)}{(2J+1)(2J+3)}\right)^2$$

$$\times(I+J+F+2)(J+F-I+1)$$

$$\times(I+F-J)(J+I-F+1). \quad (1)$$

$$(IJFM_F|H_Q|IJ+2FM_F)^2$$

$$=\left(\frac{3eqQ}{16I(2I-1)(2J+3)}\right)^2\left(1-\frac{K^2}{(J+1)^2}\right)$$

$$\times\left(1-\frac{K^2}{(J+2)^2}\right)\frac{1}{(2J+1)(2J+3)}$$

$$\times(F+I+J+3)(F+I+J+2)(J+I-F+2)$$

$$\times(J+I-F+1)(J+F-I+2)(J+F-I+1)$$

$$\times(I+F-J)(I+F-J-1). \quad (2)$$

If any of the last four factors of (1) or of the last eight factors of (2) is negative, the corresponding matrix element is zero. The quantum number K refers to the spin about the molecular axis, either caused by rotation in a symmetric top molecule or by a transverse vibration in a linear molecule. In the latter case, $K=0$ for the lowest vibrational state. The matrix element with $J'=J+1$ vanishes when $K=0$, so only states for which J' differs from J by two need to be considered.

The lines of ICN listed in Table I refer to the lowest vibrational state, so we set $K=0$. Theoretical values of the second-order corrections to the lines are listed in column 4 of the table. It is seen that these corrections are in good agreement with the differences between the observed values and those derived from Casimir's first-order formula. Similar differences in ICl and smaller differences observed in BrCN are also accounted for very satisfactorily by these second-order corrections.

Lines produced by ICN molecules excited in the bending mode, for which $K=1$, have also been found and compared with theory. The observed positions, relative the the ground state transition $F=11/2\rightarrow13/2$, are listed in the first column of Table II. The lines are split by l-type doubling[1] into two components separated by about 21.5 mc. The upper lines for the transitions $F=5/2\rightarrow7/2$ and $3/2\rightarrow5/2$ were not observed, because both fall near strong lines of the ground state transitions. The first-order quadrupole frequencies, as calculated from the symmetric top formula[5] with $eqQ=-2420$ mc, are listed in the

TABLE I. Quadrupole splitting of $J=3\rightarrow4$ line of ICN in ground vibrational state. Frequencies are given in megacycles relative to the strongest line, $F=11/2\rightarrow13/2$.

Transition	Experimental	First-order theory	Experiment minus first-order theory	Second-order theory
11/2→13/2	0	0	0	0
9/2→11/2	14.56	14.69	−0.13	−0.06
7/2→9/2	− 39.58	− 37.17	−2.41	−2.35
5/2→7/2	− 94.31	− 93.31	−1.00	−1.04
3/2→5/2	−111.58	−111.65	+0.07	+0.10
1/2→3/2	− 70.43	− 70.17	−0.26	−0.18
11/2→11/2	−429.25	−428.98	−0.27	−0.45
9/2→9/2	− 33.23	− 37.17	+3.94	+3.97
7/2→7/2	131.28	132.54	−1.26	−1.38
5/2→5/2	168.84	170.68	−1.84	−2.18
3/2→3/2	146.50	147.62	−1.12	−1.15

TABLE II. Quadrupole splitting of $J=3\rightarrow4$ line of ICN in first vibrational state, $K=1$. Frequencies are given in megacycles relative to the strongest line, $F=11/2\rightarrow13/2$ of the ground vibrational state. Each line is split by l-type doubling into two components.

Transition	1 Experimental	2 First-order quadrupole effect	3 Theory plus freq. shift	4 Experiment minus first-order theory	5 Second-order theory
11/2→13/2	104.58	35.75	103.65	+0.93	+1.06
	83.20		82.15	+1.05	+1.06
9/2→11/2	70.69	3.85	71.75	−1.10	−1.27
	49.16		50.25	−1.09	−1.27
7/2→9/2	27.70	−40.23	27.67	+0.03	−0.27
	6.23		6.17	+0.06	−0.27
5/2→7/2	—	−65.36	2.54		
	−20.13		−18.96	−1.17	−0.75
3/2→5/2	—	−52.73	17.17		
	− 7.54		− 6.33	−1.21	−1.00

[5] J. H. Van Vleck, Phys. Rev. **71**, 468 (1947); D. K. Coles and W. E. Good, Phys. Rev. **70**, 949 (1946).

second column of Table II. Empirical shifts of 67.9 mc for the upper component and of 46.4 mc for the lower component give the theoretical first-order frequencies relative to the ground state line $F=11/2\rightarrow13/2$ listed in the third column. Differences between the observed positions and those predicted by the first-order theory are given in the fourth column. These values are in fair agreement with the second-order corrections, as calculated from Eqs. (1) and (2) with $K=1$, given in the fifth column. Matrix elements for $\Delta J=\pm1$ as well as for $\Delta J=\pm2$ contribute to the second-order energies.

The residual discrepancies, the differences between columns four and five of Table II, are larger than those for the ground state. The average is about 0.2 mc. The excited state lines are weaker than the ground state lines, and are thus subject to larger observational errors. The discrepancies are, however, somewhat larger than expected from experimental uncertainties, and may be real.

Letters to the Editor

PUBLICATION of brief reports of important discoveries in physics may be secured by addressing them to this department. The closing date for this department is five weeks prior to the date of issue. No proof will be sent to the authors. The Board of Editors does not hold itself responsible for the opinions expressed by the correspondents. Communications should not exceed 600 words in length.

Considerations on the Existence of Element 61 in Nature

N. E. BALLOU
Radiation Laboratory, University of California, Berkeley, California
February 2, 1948

IN the light of the present controversy[1] over the possibility of existence in nature and the naming of element 61, some calculations on the stability toward beta-decay of isotopes of that element have been made by use of the Bohr-Wheeler theory.[2] This theory gives beta-disintegration energies that agree fairly well in most cases with those obtained by direct observation.

The radioactive isotopes of element 61 which have been definitely assigned have the mass numbers 147, 148, 149.[3–5] They are all beta-radioactive with half-lives so short as to preclude their independent existence in nature, the longest-lived one being at mass 147 and having a half-life of only about four years. Other isotopes which warrant consideration in an examination for possible stable or long-lived isotopes of element 61 are those of masses 143, 144, 145, 146, 150, and 151. Calculating the relative stabilities of these by means of the Bohr-Wheeler theory, we find that all of these isotopes except 145 should be unstable by at least one Mev to beta-decay (or its equivalent). For mass 145 the theory indicates essentially no energy difference between Nd^{145} and 61^{145}. Consequently, if element 61 does exist in nature, it is probably the isotope of mass 145.

Pertinent to these considerations are the reported weak beta-rays found in neodymium by Libby.[6] In this work the radiation was shown to be composed of negative beta-particles of about 11-kev energy. No harder radiations were found with them.

Consequently, it is possible that Nd^{145} is beta-active and forms element 61 as its product. Then this latter isotope may be a fairly long-lived alpha-emitter, explaining the very low abundance or non-existence of element 61 in nature. Alpha-emission is not an unlikely occurrence here since samarium has been reported to be alpha-active;[6,7] this indicates that an event such as a marked change in nuclear radii is perhaps occurring in this region. Since tracer activity of element 61 was available, a verification of the assignment of the alpha-activity to samarium (and not to element 61) was made. The separations of samarium from four-year tracer 61 were performed using the sodium amalgam technique.[8] After each of three such separations the specific alpha-activity of samarium was measured and found to remain constant. (The half-life corresponding to the specific activity obtained is 1×10^{11} years.) Only ten percent of element 61 followed the samarium in each of the separations. Thus, the alpha-activity found in samarium samples has conclusively been shown to be due to samarium and not to element 61.

The existence of an unassigned alpha-ray with a range of 1.8 cm of air should be pointed out. Henderson has examined and discussed its occurrence as a pleochroic halo in several micas.[9]

If the neodymium used by Libby had a few tenths percent of impurity of element 61, it is possible that his observed radiation could be due to element 61, the negative particles being Auger electrons or electrons from internal conversion of a low energy gamma-ray.

It should also be pointed out that there is a possibility of beta-emitting, long-lived independent isomers of element 61 at masses with known shorter-lived periods. For example, the Bohr-Wheeler theory predicts essentially no energy difference between the ground states of the 61 and samarium isotopes of mass 147.

Experiments are in progress to prepare isotope 61^{145} and to examine its radiations. This is being done by irradiating highly purified samarium with slow neutrons. Sm^{145} is formed and decays to 61^{145}; this latter isotope, the only 61 isotope formed as a result of neutron capture in samarium, is obtained pure by removing all the samarium activities by the sodium amalgam method.

This paper is based on work performed under Contract No. W-7405-eng-48 with the Manhattan District in connection with the Radiation Laboratory of the University of California.

[1] R. F. Gould, Chem. Eng. News **25**, 2555 (1947); Staff Report, Chem. Eng. News **25**, 2889 (1947); J. H. Harris, L. F. Yntema, and B. S. Hopkins, Nature **117**, 792 (1926).
[2] N. Bohr, and J. A. Wheeler, Phys. Rev. **56**, 426 (1939).
[3] J. M. Siegel, "Plutonium project," J. Am. Chem. Soc. **68**, 2411 (1946).
[4] G. W. Parker, P. M. Lantz, M. G. Inghram, D. C. Hess, Jr., and R. J. Hayden, Phys. Rev. **72**, 85 (1947).
[5] M. G. Inghram, D. C. Hess, Jr., R. J. Hayden, and G. W. Parker, Phys. Rev. **71**, 743 (1947).
[6] W. F. Libby, Phys. Rev. **45**, 845 (1934); *ibid.* **46**, 196 (1934).
[7] G. Hevesy and M. Pahl, Nature **130**, 846 (1932).
[8] J. K. Marsh, J. Chem. Soc. 523 (1942).
[9] G. H. Henderson, Proc. Roy. Soc. London **A145**, 582 (1934); *ibid.* **A173**, 250 (1939).

Erratum: Remarks on H. W. Lewis' Paper "On the Reactive Terms in Quantum Electrodynamics"

[Phys. Rev. **73**, 177 (1948)]
SAUL T. EPSTEIN
The Institute for Advanced Study, Princeton, New Jersey

A TYPOGRAPHICAL error was made in the above Letter. All φ's should be replaced by a derivative symbol d.

Remarks on Diamond Crystal Counters

ROBERT HOFSTADTER
Palmer Physical Laboratory, Princeton University, Princeton, New Jersey
. February 5, 1948

IN a recent interesting publication, Friedman, Birks, and Gauvin[1] have indicated that "gamma-ray counting" diamonds are of the ultraviolet transparent variety, Type II, in the notation of Robertson, Fox, and Martin.[2] Attention may profitably be called to the considerable research performed in recent years on the ultraviolet and infra-red absorption, photo-conductivity, luminescence, birefringence, and x-ray studies of a large number of diamonds. This work has been published by C. V. Raman and his school and is collected in two symposia on the "Structure and Properties of Diamond."[3]

Many facts are reported in these extensive studies, some of which may have direct bearing on the work of Friedman, *et al.* Raman's group has found that Type II ultraviolet and infra-red transparent, highly photo-conductive diamonds show a laminated structure. The other diamond variant, Type I, is ultraviolet opaque and exhibits a uniform isotropic structure on macroscopic examination, although often it is spotted with random inclusions of laminated or Type II material. The x-ray studies of Krishnan[4] and Ramachandran[5] indicate that the ultraviolet opaque material (Type I) is probably a microcrystalline mosaic structure consisting of two similar forms of diamond (see below).

If we assume that Type I is a mosaic and Type II a laminated structure, it may be possible to understand why the Type I, ultraviolet opaque diamond will not count as well as the Type II, ultraviolet transparent variety. For the ability of a material to count depends, among other things, on the range of an electron freed by an ionizing particle in the diamond. It may be expected, although such has not yet been proved, that the range of a secondary electron will be terminated at the boundary of a lamination. In Type II material, the range may be large, particularly if the electric field is parallel to the laminations. Such diamonds can count, and indeed all the better, if the electric field direction is parallel to the laminations. On the other hand, in a mosaic structure, it is likely that electron traps exist at the boundaries of the microcrystals and, hence, that the range is very small. On this theory, it may then be expected that with present amplifier technique, Type I diamonds, having mosaic structure, will not count individual gamma-rays or beta-particles. At best they should show only feeble pulses above amplifier noise. However, pulses due to alpha-particles, protons, or deuterons of energy larger than a few Mev, may be visible over the noise since such heavy ionizing particles will give up all their energy to the crystal, even in very small diamonds. Such is not the case with beta-particles or Compton electrons whose range is larger than the crystal thickness. In Type I diamonds it may be possible to observe integrated effects under strong irradiation by many beta-particles or gamma-quanta.

From the above discussion it appears possible that a change of pulse size per unit electric field intensity may accompany a reorientation of the diamond with respect to the electric field in a "good" specimen of the Type II or gamma-ray counting diamond. By "good" is meant a diamond showing preferably only one set of parallel laminations. A diamond with several crisscrossing sets of laminations should not show such an effect to any marked degree. The laminations in Type II diamonds are not, in general, perpendicular to the face of a cleavage plate. The laminae seem to have thicknesses between 10 and 100 microns.[6]

It may be that the differences between Curtiss' diamond and NRL diamonds[1] are caused by an orientation effect, but it is more probable that the various diamonds studied by Friedman, *et al.* are different mixtures of Types I and II material. Perfect examples of Types I and II seem to be rare. On the other hand, mixtures occur together quite often.[5] This point should be emphasized. Such mixtures can be partially ultraviolet transparent.

The experimental results of Raman's group also suggest that the best gamma-ray counting diamonds should be non-luminescent under ultraviolet excitation and colored when examined in visible light between crossed Nicols. Poorer counting diamonds should show blue luminescence, or possibly yellow or greenish luminescence, and little or no birefringence. Such criteria may be useful in sorting diamonds as crystal counters. Probably such rules will not be found to hold rigidly because mixed samples are so common. A rough criterion might be that diamonds which luminesce brightly will be poor counters or will not count at all.

It was kindly pointed out to the author by Professor Frederick Seitz that the difference in properties between Types I and II might be due to impurities. This view has been considered by Raman[7] and is thought not to be the differentiating principle between Types I and II diamonds. It is interesting that the reorientation test, proposed above, may satisfactorily provide a decision between these two views and, in fact, a test of the theory presented here.

Raman[7] has proposed a theory for the structure of diamond which indicates the existence of two similar tetrahedral forms of diamond (Type I) and two distinct octahedral forms (Type II). The latter two, although distinct, coexist side by side in a strained laminar condition. Thus, according to this theory, there appear to be four types of diamond. It is quite probable that further research on diamond crystal counters will provide new tests or verifications of Raman's theory.

I wish to thank Dr. R. C. Herman for providing me with a copy of Symposium II. I am very grateful for stimulating discussions with Professor Frederick Seitz and Dr. K. G. McKay.

[1] H. Friedman, L. S. Birks, and H. P. Gauvin, Phys. Rev. **73**, 186 (1948).
[2] R. Robertson, T. J. Fox, and A. E. Martin, Phil. Trans. Roy. Soc. London **463**, 232(A) (1934).
[3] C. V. Raman, *et al.*, Proc. Ind. Acad. Sci., Symposium I **19A**, 189 (1944); Symposium II **24A**, 1 (1946).
[4] R. S. Krishnan, Proc. Ind. Acad. Sci., Symposium I, 298 (1944).
[5] G. N. Ramachandran, Proc. Ind. Acad. Sci., Symposium I, 280 (1944); *ibid.*, Symposium II, 95, (1946).
[6] G. N. Ramachandran, Proc. Ind. Acad. Sci., Symposium II, 65 (1946).
[7] C. V. Raman, Proc. Ind. Acad. Sci., Symposium I, 189, 199 (1944).

Altitude Dependence of High Energy Atmospheric Showers*

HENRY L. KRAYBILL
Department of Physics, University of Chicago, Chicago, Illinois
January 26, 1948

RECENT coincidence counter measurements in a B-29 airplane have extended the known altitude dependence of high energy atmospheric showers up to an elevation of 40,000 feet. The counter geometry used is shown in Fig. 1.

Each counter had a sensitive area of 1 inch by 13 inches. Besides the four threefold circuits shown in Fig. 1, a fifth circuit was connected to counters numbered 6 and 8 and to a third counter which was well separated from the other counters, giving a total spread of 42 feet. The coincidence counts of all five circuits were registered as marks upon a photographic film so that simultaneous discharge of the various circuits could be observed.

In Table I data are compared for the altitudes of 31,100 feet and 37,200 feet. All of the time at 37,200 feet was spent near Inyokern, California (41° north geomagnetic latitude). The data at 31,100 feet were collected between 53° and 35° north geomagnetic latitude.

The threefold coincidence counters with 13.5-foot separations were discharged nearly as frequently as the counters having 9-foot separations. The 42-foot coincidences occurred about two-thirds as often as the 9-foot coincidences.

The simultaneous discharge of circuits 1 and 2 or of circuits 3 and 4, shown on the photographic film, enabled fourfold coincidences to be observed. From the ratio of fourfold to threefold coincidences, a rough approximation to the average density of the showers selected by the threefold counters can be computed,[1] if one assumes that a Poisson distribution is approximately valid for the spatial distribution of the shower particles. The density values thus obtained at 31,100 feet and at 37,200 feet are approximately three-fourths of a particle per counter.

It is of interest that the ratio of the counting rate at 37,200 feet to that at 31,100 feet is not greatly different for 42-foot showers than for 9-foot and 13.5-foot showers.

Figure 2 shows the altitude dependence of atmospheric showers measured by the four threefold coincidence circuits shown in Fig. 1. The ordinate denotes the number of independent showers which discharged any one of the circuits 1, 2, 3, and 4 or any combination of them simultaneously. Data from previously reported measurements[2] at Wright Field, Ohio and from Hilberry's measurements[3] at lower altitudes were also plotted in order to obtain a complete altitude curve up to 40,000 feet. The Wright Field data were multiplied by a conversion factor obtained by comparing counting rates at 31,000 feet. Hilberry's data were multiplied by a factor obtained by comparing counting rates near sea level. It was then possible to draw a smooth curve which fitted the data within experimental error. This altitude dependence curve shows a definite maximum which has been drawn near 27,000 feet, but which may be a few thousand feet above or below that altitude.

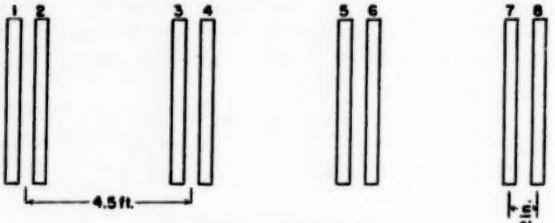

Circuit	Counters
1	1, 5, 7
2	3, 5, 7
3	2, 6, 8
4	4, 6, 8

FIG. 1. Coincidence counter arrangement.

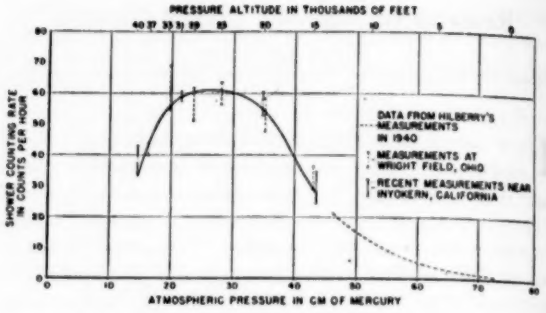
PRESSURE ALTITUDE IN THOUSANDS OF FEET
SHOWER COUNTING RATE IN COUNTS PER HOUR
ATMOSPHERIC PRESSURE IN CM OF MERCURY
DATA FROM HILBERRY'S MEASUREMENTS IN 1940
MEASUREMENTS AT WRIGHT FIELD, OHIO
RECENT MEASUREMENTS NEAR INYOKERN, CALIFORNIA

FIG. 2. Altitude dependence of atmospheric showers.

TABLE I. Comparison of shower data at 37,200 and 31,100 feet.

	31,100 ft.	37,200 ft.	Ratio of rate at 37,200 to rate at 31,100 feet
Time at altitude	1474 min.	556 min.	—
Total counts, circuit 1	592	156	0.70
Total counts, circuit 2	618	141	0.61
Total counts, circuit 3	576	138	0.65
Total counts, circuit 4	610	150	0.65
Total counts, circuit 5	348*	102	0.70
Total number of independent showers discharging any one of circuits 1, 2, 3, or 4	1457	385	0.70
Ratio of 13.5-ft. coincidences to 9-ft. coincidences	0.95	1.01	—
Ratio of 42-ft. coincidences to 9-ft. coincidences	0.63	0.70	—
Combined counting rate per hour of 9-ft. and 13.5-ft. coincidences	24.3	15.7	0.65
Counting rate per hour of 42-ft. coincidences	15.8	11.0	0.70
Counting rate per hour of independent showers discharging any one of circuits 1, 2, 3, or 4	59.3	41.5	0.70

* Based on a total time of 1323 minutes.

* This work was supported in part by U. S. Navy Contract N6ori-20, *T.O.* XVIII.

[1] G. Cocconi, A. Loverdo, and V. Tongiorgi, Phys. Rev. **70**, 841 (1946).
[2] H. Kraybill and P. J. Ovrebo, Phys. Rev. **72**, 351 (1947).
[3] N. Hilberry, Phys. Rev. **60**, 1 (1941).

Nuclear Quadrupole Coupling of Nitrogen in ICN and N_2O*

A. G. SMITH, HAROLD RING,** W. V. SMITH, AND WALTER GORDY
Department of Physics, Duke University, Durham, North Carolina
January 28, 1948

WE have extended our measurements on $IC^{12}N^{14}$ to include the fourth rotational line ($J=3\rightarrow4$) in the 1.18-cm region and have resolved the hyperfine structure caused by the nitrogen nucleus which is essentially superimposed upon that of the iodine nucleus. In our earlier observations which were made on the fifth rotational transition occurring in the millimeter region, only the hyperfine structure resulting from the I nucleus was resolved. A study of the nitrogen quadrupole coupling in $N^{14}N^{14}O$ has also been made.

Townes and his co-workers[2] in their study of BrCN and ClCN have observed quadrupole coupling for two nuclei in the same molecule. The theory of these rather complex spectra has been developed by Bardeen and Townes.[3] We have used this theory in our interpretation of the spectrum of ICN and N_2O.

Figure 1 shows some components of the $J=3\rightarrow4$ transition of ICN at lower pressures, where the structure caused by nitrogen nucleus is evident. Since the N interaction is

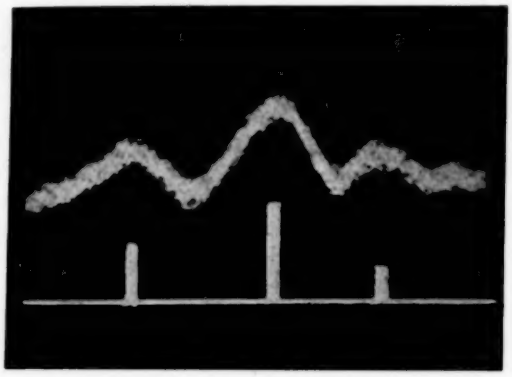

a

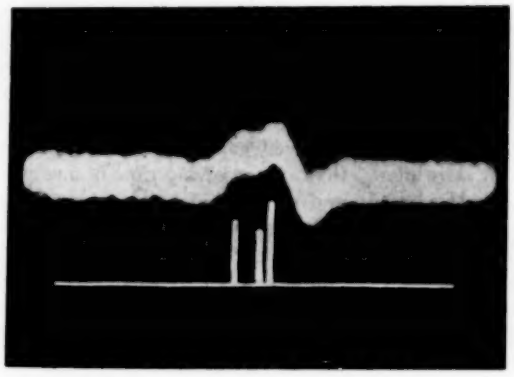

b

FIG. 1. Theoretical and observed nitrogen splitting of the $J=3\rightarrow4$ rotational transition of ICN. a—$F_1=\frac{1}{2}\rightarrow\frac{3}{2}$ transition. Separation of outside peaks is 1290 *kc/s*. b—$F_1=\frac{11}{2}\rightarrow\frac{13}{2}$ transition. Separation of outside peaks is 74 *kc/s*.

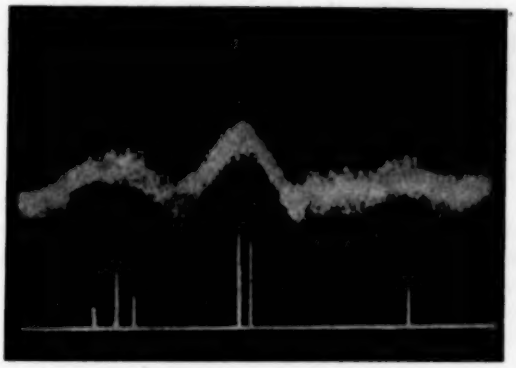

FIG. 2. Theoretical and observed nitrogen splitting of the $J=0\rightarrow1$ transition of $N^{14}N^{14}O$. Separation of two outside peaks is 765 *kc/s*.

small compared to that of the I, the first-order theory developed by Bardeen and Townes[3] provides an adequate interpretation of the spectrum. From the measurements on these lines the nuclear quadrupole coupling of the nitrogen is determined as -3.80 mc, which is close to -3.66 mc, the value[2] obtained for ClCN, but significantly smaller than -4.67 mc, the value[4] for CH_3CN. It is of interest that the N coupling in N_2O[5] and in CH_3NC[4] is considerably smaller. The measurements on the $J=3\rightarrow4$ transition yield a value of -2540 ± 25 mc for the nuclear quadrupole coupling of the iodine if the formula for the quadrupole coupling of a single nucleus as stated by Bardeen and Townes[3] is employed. This value is in satisfactory agreement with the value previously determined for the $J=4\rightarrow5$ rotational transition, if the latter is multiplied by a factor of 5/4 to convert it to the same units.[4,6]

The $J=0\rightarrow1$ rotational transition of N_2O has recently been studied by Coles, Elyash, and Gorman,[5] who obtained a quadrupole coupling for N^{14} in the central position as -0.27 mc and in the end position as -0.84 mc. The first value was determined from $N^{15}N^{14}O$. The latter was obtained from $N^{14}N^{14}O$ by neglecting the effects of the central N^{14}. In the calculated spectrum of $N^{14}N^{14}O$ shown in Fig. 2 we have taken into account the effects of both the central and end nitrogens. In these calculations we have used the value -0.27 mc for the central N^{14} mentioned above and have chosen the quadrupole coupling for the end N^{14} so as to give the best agreement with our own measurements. The value obtained in this way for the nuclear quadrupole coupling of N^{14} in the end position of N_2O is -1.03 ± 0.10 mc.

We wish to thank J. Bardeen and C. H. Townes for sending us a prepublication copy of their paper on the calculation of nuclear quadrupole effects.

* This research was supported by Contract No. W-28-099-ac-125 with the Army Air Forces, Watson Laboratories, Air Materiel Command and by a grant-in-aid from the Research Corporation of New York.
** Frederick Gardner Cottrell Fellow.

[1] W. Gordy, W. V. Smith, A. G. Smith, and H. Ring, Phys. Rev. 72, 259 (1947).
[2] C. H. Townes, A. N. Holden, J. Bardeen, and F. R. Merritt, Phys. Rev. 71, 664 (1947).
[3] J. Bardeen and C. H. Townes, Phys. Rev. 73, 97 (1948).
[4] H. Ring, H. Edwards, M. Kessler, and W. Gordy, Phys. Rev. (in press).
[5] D. K. Coles, E. S. Elyash, and J. G. Gorman, Phys. Rev. 72, 971 (1947).
[6] B. T. Feld, Phys. Rev. 72, 1116 (1947).

Background Eradication of Nuclear Emulsions by Accelerated Fading of the Latent Image

HERMAN YAGODA AND NATHAN KAPLAN
National Institute of Health, Laboratory of Physical Biology, Bethesda, Maryland
February 2, 1948

IN a continuation of our studies[1] on the fading of the latent image of alpha-particle tracks we have observed that conditions of temperature, humidity, and the presence of hydrogen peroxide have a pronounced effect on the rate. As shown in Fig. 1, the normal fading over a period of 20 days can be duplicated in the course of several hours by maintaining the exposed emulsion in an atmosphere saturated with water at 35°C. Storage *in freshly distilled water* does not destroy the latent image. The destruction of the latent image is further accelerated by augmenting the H_2O_2 concentration of the atmosphere in which the plates are stored. After exposure to 10^7 α-particles from RaF, the latent image is completely obliterated by keeping the emulsion *over* 3 percent hydrogen peroxide at 25°C for 4 hours. After 1–2 hour desiccation of the eradicated emulsion over $CaCl_2$, sensitivity is restored and tracks develop from new exposures with normal mean grain spacings.

This phenomenon permits the eradication of the accumulated latent images of the alpha-tracks and stars produced by traces of Ra and Th normally present as impurities in the emulsion. By continuing the exposure of the dry eradicated plate the rate of track growth can be studied accurately. Quantitative recording, without apparent fading of the track structures, can be maintained for periods exceeding 2 months. Under these conditions single α-tracks accumulate at a rate of 8–100/cm²/day, depending on emulsion purity and thickness. Low energy α-ray stars originating from decay of Rd Th in the emulsion layer generate ~0.3 multiple events/cm²/day. Near sea level, the controlled exposure indicates a daily rate of long proton and meson tracks of 0.03–0.06/cm²; and a population of 0.0005/cm² nuclear evaporations induced by cosmic radiation.

This method is applicable only to fine-grained nuclear type emulsions as Eastman NTA and Ilford Conc. With coarse-grained, light-sensitive emulsions as x-ray films and process plates the H_2O_2 vapor produces the well-known pseudophotographic effects.[2] Loading fine-grained emulsions with borax and lithium sulfate inhibits the destructive action of H_2O_2 on the latent image. Background eradication must therefore precede loading. Details of the method and a mechanism for spontaneous fading based on *in situ* H_2O_2 generation by the action of densely ionizing radiations on water in the gelatin will be reported on in the future.

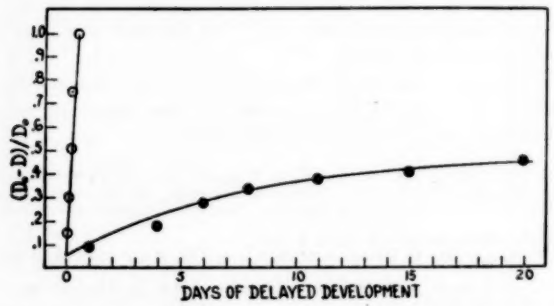

FIG. 1. Rate of latent image fading under differing storage conditions. ● ambient conditions, 25°C, low humidity; ○ eradication conditions, 35°C, saturation humidity.

[1] H. Yagoda and N. Kaplan, Phys. Rev. **71**, 910 (1947).
[2] H. Yagoda, Am. Mineralogist **31**, 87 (1946).

Coincidence Study of Gold[198]*

C. E. MANDEVILLE AND M. V. SCHERB
Bartol Research Foundation of the Franklin Institute, Swarthmore, Pennsylvania
January 29, 1948

THE radiations from Au^{198} have been studied by many investigators.[1–5] Some experiments[2] have purported to show effects from only one gamma-ray of energy 0.4 Mev. On the other hand, considerable evidence[1] has been compiled which would indicate that more than one quantum per disintegration is emitted in the de-excitation of Hg^{198}, the residual nucleus. Results of gamma-gamma coincidence experiments have also been at variance. Norling[3] and Jurney and Keck[3] of the Indiana University group have found no gamma-gamma coincidences in the disintegration of Au^{198}. These results would support the view that only a single gamma-ray is present. Other investigations[4] have shown genuine gamma-gamma coincidences to exist.

In order to reinvestigate the radiations from Au^{198} by coincidence techniques, metallic gold was irradiated by slow neutrons in the Clinton pile. Chemical purification was carried out to remove possible impurities of calcium, iron, phosphorous, and platinum.

Using two matched G-M counters in a coincidence circuit with a resolving time of 0.10 microsecond,[6] gamma-gamma coincidences were measured in Au^{198}. The gamma-gamma coincidence rate was found to be $(0.103\pm0.007)\times10^{-3}$ gamma-gamma coincidence per gamma-ray recorded in the gamma-ray counter. This result should be particularly reliable, since, owing to the short resolving time, the background of accidental counts was virtually negligible for counting rates of 10,000 singles per minute in either counter. Cascade emission of gamma-rays in Au^{198} is thus established. For the same single counting rate and from the observed gamma-gamma coincidence rate, it is estimated that at a resolving time of one microsecond, the background of accidental coincidences would be approximately four times the number of geniune coincidences recorded in any particular period of time. This ratio emphasizes the importance of short resolving times.

The beta-gamma coincidence rate of Au^{198} was measured as 0.19×10^{-3} coincidence per beta-ray recorded in the beta-ray counter and was independent of the beta-ray energy. A delay of a few tenths of a microsecond has been reported in the emission of the 0.4-Mev gamma-ray which follows beta-emission.[6] In the course of measuring beta-gamma coincidences in the present experiment, the re-

solving time of the coincidence circuit was varied from 1.0 microsecond to 0.035±0.002 microsecond. No loss in the genuine beta-gamma coincidence rate was observed down to the shortest resolving time employed. This result must be regarded as evidence against the existence of a short-lived metastable state in Hg^{198}.

* Assisted by the Office of Naval Research.

[1] J. R. Richardson, Phys. Rev. **53**, 942 (1938); *ibid.* **55**, 609 (1939); G. J. Sizoo and C. Eijkman, Physica **6**, 332 (1939); J. L. Lawson and J. M. Cork, Phys. Rev. **58**, 580 (1940); E. H. Plesset, Phys. Rev. **62**, 181 (1942); N. Feather and J. Dainty, Proc. Camb. Phil. Soc. **40**, 57 (1944); M. L. Wiedenbeck and K. Y. Chu, Phys. Rev. **72**, 1171 (1947); P. W. Levy and E. Greuling, Phys. Rev. **73**, 83 (1948).
[2] Kai Siegbahn, Proc. Roy. Soc. **A189**, 527 (1947); J. M. Cork, Phys. Rev. **72**, 581 (1947).
[3] F. Norling, Arkiv f. Mat. Astr. O. Fys. **B(27)** 3, 9 (1941); E. T. Jurney and M. R. Keck, Bull. Am. Phys. Soc. **22**, No. 6, 6 (1947).
[4] A. F. Clark, Phys. Rev. **61**, 242 (1942); N. Feather and J. Dainty, Proc. Camb. Phil. Soc. **40**, 57 (1947); M. L. Wiedenbeck and K. Y. Chu, Phys. Rev. **72**, 1171 (1947).
[5] C. E. Mandeville and M. V. Scherb, Phys. Rev. **73**, 90 (1948).
[6] L. Madansky and M. L. Wiedenbeck, Phys. Rev. **72**, 185 (1947).

Anomalies in the Hyperfine Structure of CH_3I and ICN*

O. R. Gilliam, H. D. Edwards, and Walter Gordy
Department of Physics, Duke University, Durham, North Carolina
January 28, 1948

SIMMONS and Gordy[1] have found that the usual formula for calculating nuclear quadrupole interaction in symmetric top molecules does not agree exactly with the experimentally observed values for the hyperfine structure of ammonia. We have found somewhat larger deviations from this theory in the hyperfine structure of methyl iodide. Certain hyperfine levels have been found to deviate from their theoretically predicted positions by the order of 1 to 3 megacycles. The disagreement with theory is most strikingly illustrated in the cases where theory predicts that because of degeneracy, certain lines in the hyperfine spectrum should fall at the same frequency. Some of these lines are separated by a few megacycles, as may be seen by examination of Fig. 1. Brackets are placed over those lines which, though predicted to fall at the same frequency, are completely resolved. For the $J=3$, $K=2$ rotational term there is, according to theory, no nuclear quadrupole coupling energy because of the vanishing of the factor $(3K^2/J(J+1)-1)$. Our observations, however, show that there is appreciable nuclear interaction for this case.

Deviations from theory in the hyperfine structure of the linear molecule ICN have also been noted. Table I gives a comparison of the nuclear quadrupole coupling of iodine determined by measurements on the different $F_1 \rightarrow F_1+1$ lines of the eighth rotational transition occurring in the region of 5.9 mm.

The nitrogen nuclear quadrupole effects, which for this transition are too small to be resolved, do not appear to

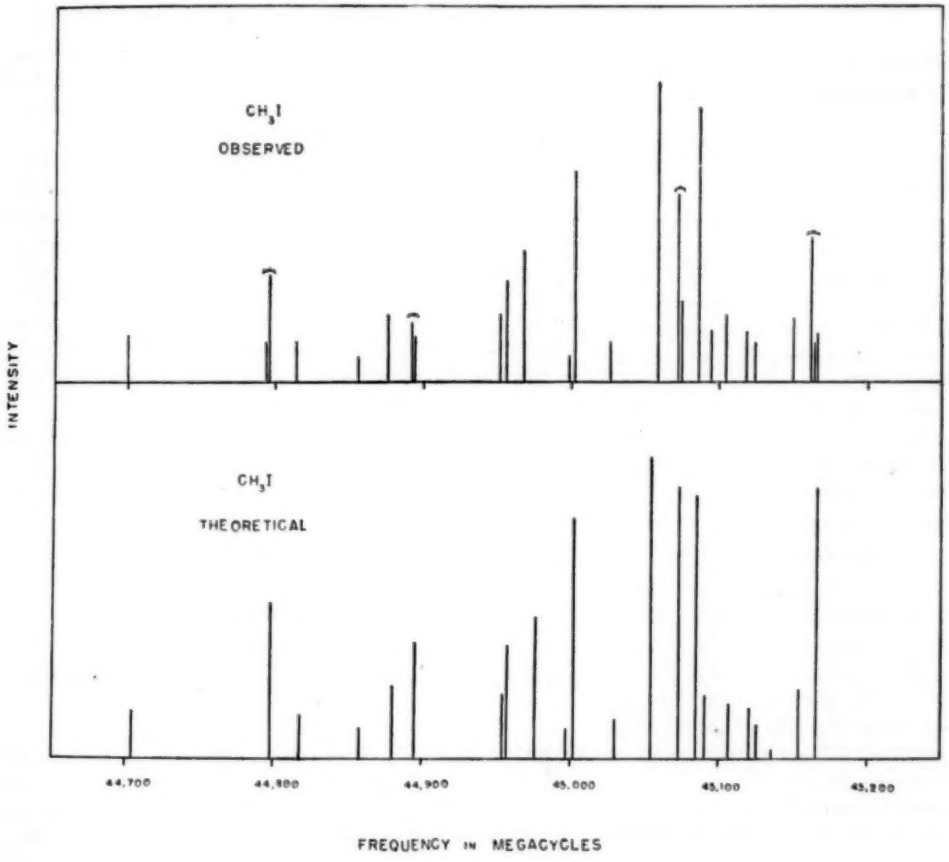

FIG. 1. Hyperfine structure of the $J=2 \rightarrow 3$ rotational transition of CH_3I.

TABLE I. Nuclear quadrupole coupling of iodine in ICN determined from the $F_1 \rightarrow F_1+1$ transitions of the eighth rotational line, $(J=7\rightarrow 8)$. Here $F_1 = J+I_1, J+I_1-1, \cdots |J-I_1|$, where I_1 is 5/2, the nuclear spin of iodine.

$F_1 \rightarrow F_1+1$	Separation from $\frac{15}{2}\rightarrow\frac{17}{2}$ line $\Delta\nu$ in mc	Nuclear quadrupole coupling in mc $eQ\frac{\partial^2 V}{\partial z^2}$
$\frac{9}{2}\rightarrow\frac{11}{2}$	−9.98	−2388
$\frac{11}{2}\rightarrow\frac{13}{2}$	−17.46	−2401
$\frac{13}{2}\rightarrow\frac{15}{2}$	−11.98	−2430
$\frac{15}{2}\rightarrow\frac{17}{2}$	—	—
$\frac{17}{2}\rightarrow\frac{19}{2}$	+9.58	−2488
$\frac{19}{2}\rightarrow\frac{21}{2}$	+5.10	−2563

cause the observed variations in the coupling coefficients listed in Table I. The probable error in the measurements is less than 1 percent.

Further studies of these effects are being made.

* This research was supported by Contract No. W-28-099-ac-125 with the Army Air Forces, Watson Laboratories, Air Materiel Command.

[1] J. W. Simmons and W. Gordy, Phys. Rev. (in press).

Delayed Neutrons from U^{235} After Short Irradiation

F. DE HOFFMANN,* B. T. FELD,** AND P. R. STEIN*
University of California, Los Alamos Scientific Laboratory, Los Alamos, New Mexico
February 6, 1948

DURING the spring of 1945 we investigated the delayed neutrons from U^{235} after very short neutron irradiation of about 10-millisecond duration. The decay curve of the delayed neutrons, from 0.2 second to 10 minutes after irradiation, could be resolved into 5 periods and the relative initial activities of these 5 groups of delayed neutrons determined. When these activities are extrapolated, in the conventional manner, to the case of infinite irradiation time, the rate of delayed neutron emission (on the basis of unit initial activity) is given by the following formula,[1] where t is in seconds:

$$N(t)=0.076e^{-t/0.52}+0.279e^{-t/2.8}+0.297e^{-t/7.9}+0.294e^{-t/32.4}+0.054e^{-t/79.9}.$$

By following the neutron activity during the irradiation and for a period of about 50 milliseconds thereafter we obtained indications of a delayed neutron period of approximately 6 milliseconds. This 6-millisecond period delayed neutron group accounts for only 2 percent of the total yield of delayed neutrons, when the U^{235} is irradiated to saturation. We hope to publish a full account of the above measurements in this journal in the near future.

This letter is based on work performed at the Los Alamos Scientific Laboratory of the University of California under Government Contract No. W-7405-eng-36, and the information contained therein will appear in Division V of the National Nuclear Energy Series (Manhatten Project Technical Section) as part of the contribution of the Los Alamos Laboratory.

* Now at Harvard University, Cambridge, Massachusetts.
** Now at Massachusetts Institute of Technology, Cambridge, Massachusetts.

[1] When these results are compared with the work of Hughes, Dobbs, Cohn, and Hall, Phys. Rev. 73, 111 (1948), there is substantial agreement in the delayed neutron periods. There are, however, discrepancies in the relative intensities which may be due to the fact that our results are not corrected for the varying efficiency of our neutron counters with the various energies of the different delayed neutron groups.

Perturbation of Steady Uniform Flow by Localized Sources of Heat*

BRUCE L. HICKS
Ballistic Research Laboratories, Aberdeen Proving Ground, Aberdeen, Maryland
January 29, 1948

THE configuration of steady diabatic flow is affected by heat addition in ignition and combustion. For the one-dimensional approximation these effects have been described in the literature.[1] For uniplanar flow a study of diabatic inviscid patterns can be based in the incompressible approximation on the previously developed equations,[2]

$$\nabla^2\varphi=q, \quad \nabla^2\psi=-\omega, \quad u=\varphi_x+\psi_y, \quad v=\varphi_y-\psi_x$$

where

$$\bar{W}=\bar{V}/V_i=u\bar{i}+v\bar{j}, \quad \omega=|\nabla x\bar{W}|, \quad q=Q/V_i^2,$$

Q is heat added per unit mass and time, and V_i = limiting velocity (local value). We consider here uniform flow $\bar{W}=u_0\bar{L}$ slightly perturbed by a localized heat source q which is coupled to ω through the equation $q_y=\omega_x$.

Solutions of these equations will be discussed for various simple heat source functions, $q(x, y)$. Upon the characteristics of $q(x, y)$ depend the continuity of the perturbation field $\bar{W}'$ and the distribution of vorticity produced. It appears that sources of heat are inherently more complicated in their structure and effects than sources of fluid. In general, a localized heat source will produce an accelerated jet of fluid downstream of the source, and more or less sharply defined regions of vorticity trail downstream from the edges of the source.

* This communication was submitted to the American Physical Society as an abstract for the New York meeting, but because of an oversight it was not included in the bulletin for that meeting.

[1] B. L. Hicks, D. J. Montgomery, and R. H. Wasserman, J. App. Phys. 18, 891 (1947).

[2] Article accepted for publication in Quart. App. Math.

Excited States of B^{10}

T. LAURITSEN, W. A. FOWLER, C. C. LAURITSEN, AND V. K. RASMUSSEN
W. K. Kellogg Radiation Laboratory, California Institute of Technology, Pasadena, California
February 2, 1948

THE neutron spectrum from the reaction $Be^9(d, n)B^{10}$ has been studied by Bonner and Brubaker,[1] Staub and Stephens,[2] and Powell and Fertel,[3] all of whom observed transitions to states in B^{10} at 0.6, 2.0, and 3.5 Mev,

in addition to the ground state. The accompanying γ-radiation has been measured by Crane, Halpern, and Oleson[4] as consisting of a line at 3.45 Mev and one or more below 1 Mev. Kruger, Stallman, and Shoupp,[5] on the other hand, report 31 γ-ray lines attributed to this reaction. In work on the reaction $Li^7(\alpha, n)B^{10}$, Haxel and Stuhlinger[6] found evidence for levels at $\sim$0.8, 1.3, and 2.1 Mev. (The energy available in their experiment was not sufficient to excite higher levels.) Cascade transition in the capture radiation from $Be^9(p, \gamma)B^{10}$ through a level at $\sim$0.8 Mev has been reported by Fowler, Lauritsen, and Lauritsen.[7] In the latter work it was found that the radiation emitted from the 4-kev wide state which occurs at a proton energy of 1.077 Mev is appreciably softer than that from the 94-kev wide resonance at 0.988 Mev, and the existence of additional radiation of 0.8 Mev from the higher level was indicated.

Using a large aperture magnetic lens spectrometer, we have studied the γ-radiation from several reactions leading to states in B^{10}. Figure 1 shows the result of measurements made on the $Be^9(p, \gamma)B^{10}$ radiation from a 12-kev target bombarded by 1.08-Mev protons (at the narrow resonance) and from a thick target with 1.04-Mev protons (just below the narrow resonance). The curves indicate the number of photo and Compton electrons from a thick lead converter as a function of momentum. Because of the low intensity of the radiation, it was necessary to utilize a large solid angle in the spectrometer, with considerable sacrifice in resolution. Nevertheless, it is clear that a component at 0.72 ± 0.1 Mev exists at the higher resonance, which does not appear at the lower bombarding voltage. By comparison with the distribution of electrons from the 0.511-Mev annihilation radiation from N^{13}, taken with the same geometry, one can make a reasonable fit to the observed curve by superposition of K, L, and Compton electron distributions. The general background is due to Compton electrons from the higher energy radiation (6.7 Mev from the narrow resonance; 7.4 Mev from the broad resonance).

In the study of the γ-radiation from the reaction $Be^9(d, n)B^{10}$, it was possible to use much improved resolution, and the several lines can be clearly resolved into K, L, and Compton components (Fig. 2). The targets in this

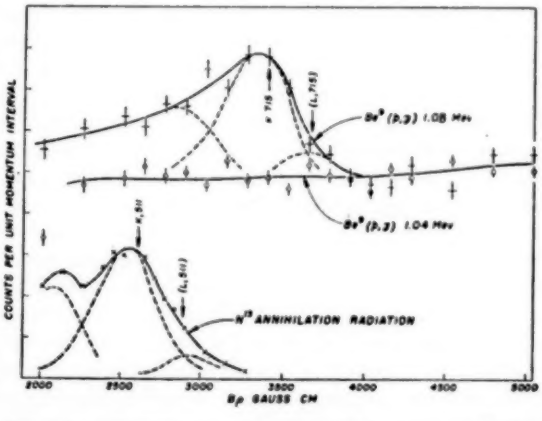

FIG. 1. Secondary electron spectra from Be^9+p gamma-radiation.

case were suspended inside the spectrometer and were bombarded by 0.840-Mev deuterons. To distinguish between Compton and photoelectrons, runs were made with various converters. The location of K and L electron lines for each γ-ray energy is indicated by arrows: a correction of 10 kev has been made for the shift in peak due to the converter thickness. The γ-ray energies are (in kev) 420 ± 10, 480 ± 10, 715 ± 10, 1025 ± 20, 1460 ± 30. Higher

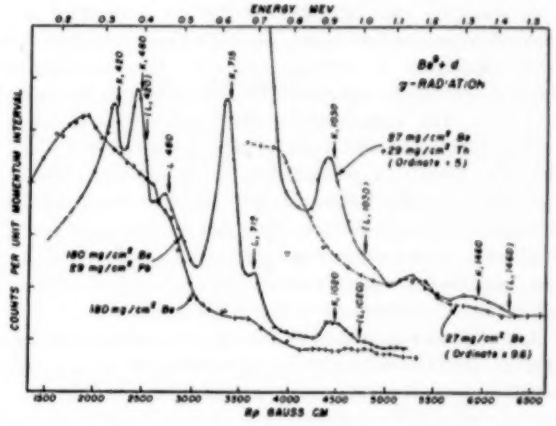

FIG. 2. Secondary electron spectrum from Be^9+d gamma-radiation.

energy lines exist, but could not be reached with the present spectrometer.

The radiation at 0.715 Mev is identical with that observed in the $Be^9(p, \gamma)B^{10}$ reaction and hence is clearly to be associated with a level at 0.715 Mev above the ground state. It is suggested that the lines at 0.420, 1.025, and 1.46 indicate levels at 0.420 and 1.46 Mev, with the 1.025-Mev radiation arising from cascade transitions from the upper level. That the line at 0.480 Mev is due to $Be^9(d, \alpha)Li^{7*}$ was ascertained by a direct comparison with the radiation from $Li^7(p, p')Li^{7*}$, using the same geometry.

In a search for non-capture radiation we have bombarded B^{10} in the form of isotopically enriched B_2O_3(B^{10}:B^{11} = 24:1)* with protons. Radiation at 0.420 Mev was observed with a bombarding energy of 0.9 Mev, with a sharply rising yield, suggesting a threshold process, to 1.4 Mev. No evidence of the expected 0.715-Mev radiation was found at 1.4 Mev. It seems reasonably clear that the 0.420-Mev radiation arises from non-capture excitation of the lowest level in B^{10}; the absence, or low probability of excitation of the next level, may indicate that this level differs radically in character from the ground state, as is also suggested by its behavior in the $Be^9(p, \gamma)B^{10}$ reaction.

This work was assisted by the Office of Naval Research.

* Our thanks are due the Atomic Energy Commission for a supply of $B^{10}F_3$·CaF_2 and to Professor D. M. Yost for the conversion to B_2O_3.

[1] T. W. Bonner and W. M. Brubaker, Phys. Rev. **50**, 308 (1936).
[2] H. Staub and W. E. Stephens, Phys. Rev. **55**, 131 (1939).
[3] Powell and Fertel, Nature **144**, 115 (1939).
[4] Crane, Halpern, and Oleson, Phys. Rev. **57**, 13 (1940).
[5] Kruger, Stallman, and Shoupp, Phys. Rev. **56**, 297 (1939).
[6] Haxel and Stuhlinger, Zeits. f. Physik **114**, 178 (1939).
[7] Fowler, Lauritsen, and Lauritsen, Phys. Rev. **73**, 181 (1948).

A New Isotopic Effect in Liquid Helium*

J. G. DAUNT, R. E. PROBST, AND H. L. JOHNSTON
The Cryogenic Laboratory, Department of Chemistry and Department of Physics, The Ohio State University, Columbus, Ohio
February 2, 1948

IN continuing experiments[1,2] on the behavior of the rare isotope He^3 in the liquid phase, gas containing varying initial concentrations of He^3 has been employed and a new effect found, a preliminary notice of which may be of interest.

In effecting the filtration of He^3 by superfluid flow through supra-surface films, an isothermal technique has been employed in addition to the thermomechanical method previously reported.[1] This technique is illustrated in Fig. 1. The apparatus consisted essentially of an inverted U-tube, in one limb of which was placed a constriction, namely, a ground-glass plug, serving to prohibit the flow of vapor while allowing the free flow of liquid through the supra-surface film. At the bottom of each limb copper end caps were attached at "*s-s*," through which gas could be introduced via the tubes *a* and *b*. This whole apparatus was immersed in liquid helium II.

In a typical run helium gas[3] having an initial concentration of $He^3/He^4 = 2.4\times10^{-5}$ was condensed in the right-hand limb at 1.57°K. After a period of waiting, liquid flowed through the supra-surface film past the constriction into the left-hand limb isothermally and equilibrium was finally reached with the right-hand level remaining 2.1 mm above the left-hand level.

In order to decide whether this difference in levels constituted a real effect, rather than being due to temperature inhomogeneity (the mechano-caloric effects in liquid helium II being very large[4]) the experiments were repeated using "gas-well" helium under otherwise identical conditions. The known concentration[5] of He^3/He^4 in gas-well helium is 1.6×10^{-7}; and with this *no* equilibrium difference in levels was observed.

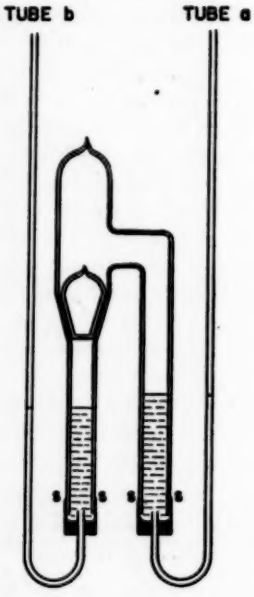

FIG. 1.

Assuming the flow through a supra-surface film prohibits the passage of He^3,[1] the differences in the levels observed in these experiments with the higher concentrations could be explained as the manifestation of an osmotic pressure of He^3, the supra-surface film acting as a semi-permeable membrane. Considerable care, however, must be taken in this interpretation, since as yet no satisfactory measurements of the relative concentration of He^3 (using initial concentrations of the order of 3×10^{-5}) in the vapor phase above liquid helium II are available. Such experiments are now being carried out. A discussion of the complete behavior of solutions of He^3 in He^4 is therefore postponed until this information is obtained.

* This work was supported in part by the Office of Naval Research under a contract with The Ohio State University Research Foundation.
[1] J. G. Daunt, R. E. Probst, J. L. Johnston, L. T. Aldrich, and A. O. Nier, Phys. Rev. **72**, 502 (1947).
[2] J. G. Daunt, R. E. Probst, and H. L. Johnston, J. Chem. Phys. **15**, 759 (1947).
[3] We wish to express our thanks to Professor A. O. Nier for the enriched samples used in these experiments.
[4] J. G. Daunt and K. Mendelssohn, Nature **143**, 719 (1939); P. L. Kapitza, J. Phys. U.S.S.R. **5**, 59 (1941); W. H. Keesom and G. Duyckaerts, Physica **13**, 153 (1947); J. H. Mellink, Physica **13**, 180 (1947); L. Meyer and J. H. Mellink, Physica **13**, 197 (1947).
[5] L. T. Aldrich and A. O. Nier, Phys. Rev. **70**, 983 (1946).

Interconversion of *Ortho-* and *Para*-Deuterium Due to the Deuteron Quadrupole Moment

MORTON HAMERMESH
New York University, New York, New York
January 6, 1948

THE interaction of the quadrupole moment of the deuteron with an inhomogeneous electric field will result in interconversion of *ortho-* and *para*-D_2.[1] In materials like H_2O which have a permanent electric moment but no atomic magnetic moments, this process can compete with the magnetic conversion due to interaction of the deuteron's magnetic moment with the spin and rotational moments in the molecule.

Casimir[2] has given a theoretical estimate of the relative efficiency of the two interactions in producing conversion. Uncertainties concerning the wave functions of the colliding particles are eliminated by replacing the electric dipole by an "equivalent" charge, which results in both interactions having the same spatial dependence. Using the accepted value for the quadrupole moment,[3] Casimir found a total conversion rate in H_2O of 2.3×10^{-5} l mole^{-1} min.$^{-1}$, in reasonably good agreement with the experimental value, 2.6×10^{-5}.[4] Unfortunately, there is an error in the evaluation of the diagonal sums which occur in the calculation. After the corrections are made, the reaction rate caused by the quadrupole moment is reduced by a factor of five, so that the calculated total rate is only 1×10^{-5}. This could be reconciled with the experimental result by the expedient of doubling the equivalent charge. It is, however, apparent that a detailed calculation is necessary.

If the qualitative picture of the process is correct, the conversion of D_2 by diamagnetic materials is caused mainly by the quadrupole moment. This could be tested experimentally as follows:

(a) Measure conversion of D_2 by D_2O. From the experimental data of Farkas and Sandler[4] the rate for this process should be $\sim 2.2\times 10^{-5}$ l mole^{-1} min.$^{-1}$.

(b) Measure conversion of D_2 by various molecules having permanent electric moments. The conversion rates should depend quadratically on the moment of the catalyzing molecule.

[1] F. Kalckar and E. Teller, Proc. Roy. Soc. **150**, 520 (1935).
[2] H. B. G. Casimir, Physica **7**, 169 (1940).
[3] J. M. B. Kellogg, I. I. Rabi, N. F. Ramsey, and J. R. Zacharias, Phys. Rev. **57**, 677 (1940); A. Nordsieck, Phys. Rev. **58**, 310 (1940).
[4] L. Farkas and A. Sandler, Trans. Faraday Soc. **35**, 337 (1939).

Structure of the Ionized Helium Line λ1640

G. R. Fowles
Department of Physics, University of California, Berkeley, California
February 3, 1948

THE ionized helium line at 1640.4A, which corresponds to H_α, has been photographed in the first order of a three-meter vacuum spectrograph, using a grating of 30,000 lines/inch. Three lines are resolved, and the measured peak-to-peak separation of the two strongest is 5.154 ± 0.024 cm^{-1}. The Dirac theory predicts a doublet separation of 5.314 cm^{-1}, whereas the $2^2S_{\frac{1}{2}}$ level shift of 0.442 cm^{-1} calculated by Bethe[1] would modify the structure of the line so as to produce a separation in ionized helium of 5.165 cm^{-1} under the conditions of this experiment. The accuracy of the measurement is sufficient to establish definitely the existence of a shift in the $2^2S_{\frac{1}{2}}$ level much larger than that previously found in the $3^2S_{\frac{1}{2}}$ level by Mack and Austern.[2] The accuracy as a test of Bethe's hypothesis, however, leaves something to be desired.

In the photographs thus far taken the weak center component $2^2S_{\frac{1}{2}}-3^2P_{\frac{1}{2}}$ appears clearly, but the dispersion is too small to locate its position accurately. Work is under way to obtain the line in a higher order of the grating.

[1] H. A. Bethe, Phys. Rev. **72**, 339 (1947).
[2] J. E. Mack and N. Austern, Phys. Rev. **72**, 972 (1947).

Erratum: On the Resolving Time and Genuine Coincidence Loss for Geiger-Mueller Counters

[Phys. Rev. **73**, 90 (1948)]
C. E. Mandeville and Morris V. Scherb
Bartol Research Foundation of the Franklin Institute, Swarthmore, Pennsylvania

THE pressure of the gas in the counters was given inadvertently as 12-cm Hg rather than 7-cm Hg as was actually the case. The ratio of the partial pressures of the argon-ether mixture was 17:3.

The short resolving time was determined by counting random coincidences in separated counters and not from merely a consideration of circuit parameters. The writers have recently become aware of the work of two members of the Zürich group,[1] wherein the successful use of resolving times as low as 0.15 microsecond without genuine coincidence loss was reported.

[1] H. Bradt and P. Scherrer, Helv. Phys. Acta **19**, 251 (1943).

Spin of C^{14}

F. A. Jenkins
Department of Physics, University of California, Berkeley, California
February 9, 1948

THE procedures previously used[1] in determining the spin of C^{13} by the alternation of intensities in the band lines of the C_2 molecule have been successfully applied to radiocarbon. Spectrum tubes have been prepared from which the relative intensity of the bands indicates a concentration up to 30 percent of C^{14}. Some of the enriched samples were prepared by Mr. L. D. Norris of the Clinton Laboratories[2] and others by Dr. W. L. Whitson of the University of California Radiation Laboratory. The former samples were milligram amounts of $BaCO_3$ made available through the Isotopes Division, Atomic Energy Commission, while the latter were microgram amounts of carbon separated in the mass spectrograph, starting with material of lower concentration also obtained from the Isotopes Division.

The lines due to $C^{14}C^{14}$ appear plainly on the grating spectrograms, and most of them are entirely free from confusion by background lines of extraneous origin. Furthermore, the Λ-type doublets of both the R_3 and R_1 lines are resolved in the $C^{13}C^{14}$ band. In spite of this, all lines of $C^{14}C^{14}$ appear as strictly single lines, with an alternate displacement or "staggering" similar to the well-known effect in $C^{13}C^{13}$. This can only mean that alternate lines are completely missing and that therefore the nuclear spin is zero. The missing lines are those one would expect for nuclei obeying the Bose-Einstein statistics. It is worth mentioning that the next higher value of the spin that is possible, $I=1$, would give an intensity ratio of 2:1 and that the presence of the weaker components could not possibly have been overlooked.

This result is surprising in view of the exceptionally long half-life of C^{14}, which, coupled with the relatively high energy of the beta-rays, would seem to require a large spin change in the decay. The product nucleus, N^{14}, has a spin of unity, so that the change is not large. On the other hand, a spin of zero is consistent with the value always observed for stable isotopes of even charge and mass. The details of this work will appear in The Physical Review, including a summary of the work on both C^{13} and C^{14}.

[1] F. A. Jenkins, Phys. Rev. **72**, 169 (1947).
[2] The writer is indebted to Dr. A. H. Snell for calling his attention to the availability of this material.

Incipient Superconductivity in Titanium

ROBERT T. WEBBER AND J. M. REYNOLDS
Sloane Physics Laboratory, Yale University, New Haven, Connecticut*
February 7, 1948

ACCORDING to the measurements of Meissner and his co-workers[1,2] and of de Haas and van Alphen,[3] wires of titanium undergo a transition into superconductivity at either 1.3° or 1.78°K. Shoenberg,[4] on the other hand, using a permeability measurement, found that down to 1.0°K only a very small fraction of the metal appeared to become superconducting.

The specimens in all measurements referred to above were prepared in the Philips Laboratory at Eindhoven by means of thermal decomposition of the vapor of titanium iodide, causing the metal to precipitate on a hot tungsten wire.[5] More recently, the U. S. Bureau of Mines[6,7] has developed methods for comparatively large scale production of ductile titanium using the method of Kroll[8] in which the chloride of titanium is reduced with magnesium at about 1000°C in the presence of pure argon.

The Bureau of Mines has kindly supplied us with a wire of this material, 0.055 inch in diameter and containing the following impurities: magnesium, 0.25 percent; silicon, 0.02 percent; iron, 0.03 percent; hydrogen, less than 0.01 percent.

The ends of this wire were copperplated and potential and current leads attached. The specimen was placed vertically in direct contact with liquid helium which allowed resistance measurements to be made at temperatures between 1.1°K and 4.23°K. The current and potential were determined with a Leeds and Northrup Type K potentiometer and the resistance was calculated differentially to minimize error due to thermal e.m.f.

Figure 1 shows the ratio of the resistance, R, to the resistance at room temperature, R_t. From this figure it is seen that the resistance stayed effectively constant in the region 4.2° to 3.2°K. Between 3.2° and 1.5° the resistance dropped sharply to about half its value at 4.2°K. At 1.1°K, the lowest temperature obtainable with our apparatus, the resistance appeared to be leveling off again.

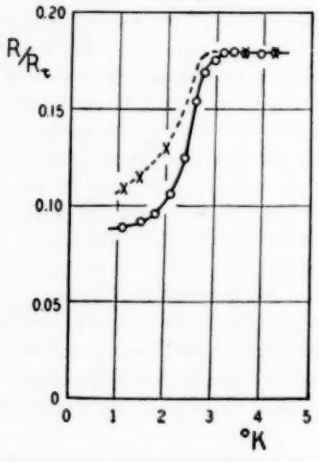

FIG. 1. The resistance of the titanium wire from 1.1 to 4.2°K in zero magnetic field (solid curve) and in a logitudinal magnetic field of 1200 gauss (broken curve).

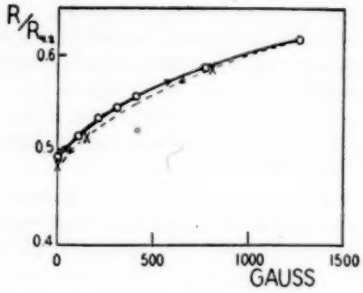

FIG. 2. Dependence of the resistance on logitudinal magnetic field at 1.1°K.

No trace of the transitions into superconductivity previously observed at 1.8° and 1.3°[1,2,3] was evident in our specimen.

The effect on the resistance of longitudinal magnetic fields of intensity up to 1400 gauss was determined. At temperatures above 3.2°K, the effect was negligible. Below 3.2°K the resistance became strongly sensitive to magnetic field, establishing the theory that the drop in resistance was due to incipient superconductivity. The dotted curve in Fig. 1 gives the resistance of the wire in a field of 1200 gauss. Figure 2 shows the resistance of the specimen as a function of magnetic field at 1.1°K. The hysteresis appearing in this figure also appeared at 1.4°K and, to a lesser extent, at 2.0°K.**

As only a small part of the metal need be superconducting to short circuit the remainder and give a zero resistance, it seems reasonable to conclude that the incipient superconductivity observed in these measurements is due to an impurity—probably an alloy of titanium with magnesium or iron. The superconductivity observed by Meissner[1,2] and by de Haas and van Alphen[3] possibly has a similar origin, perhaps an alloy or compound of titanium with tungsten formed at the surface of the hot tungsten wire.

Since titanium appears to have a number of superconducting alloys and since the position on the periodic table and the atomic volume of titanium are favorable,[9] it seems possible that pure titanium may have a transition into superconductivity at some temperature below 1.1°K.

The authors are indebted to the members of the low temperature research group of this laboratory for their assistance in this work. We particularly wish to thank Mr. Charles A. Reynolds for his aid in the collection of data.

* Assisted by the Office of Naval Research under Contract N6ori-44, Task Order 3.

[1] W. Meissner and B. Voigt, Ann. d. Physik **7**, 892 (1930).
[2] W. Meissner, H. Franz, and H. Westerhoff, Ann. d. Physik **13**, 555 (1932).
[3] W. J. de Haas and P. M. van Alphen, Leiden Communication 212e (1931).
[4] D. Shoenberg, Proc. Camb. Phil. Soc. **36**, 84 (1940).
[5] A. E. van Arkel and J. H. de Boer, Zeits. f. anorg. allgen. Chemie **148**, 345 (1925).
[6] R. S. Dean, J. R. Long, F. S. Wartman, and E. L. Anderson, Metals Technology, Feb. 1946.
[7] R. S. Dean and B. Silkes, Bureau of Mines Information Cicular No. 7381 (November, 1946).
[8] W. Kroll, Trans. Am. Electrochem. Soc. **78**, 35–47 (1940).
** A similar hysteresis has been observed by us in measurements on the alternating field permeability of superconducting vanadium. Further details will be given in a future publication.
[9] E. F. Burton, H. Grayson-Smith, and J. O. Wilhelm, *Phenomena at the Temperature of Liquid Helium* (Reinhold Publishing Corporation, New York, 1940), pp. 92–94.

On a Different Form for the Interaction Between Dirac's Electron Field (ψ) and Maxwell's Electromagnetic Field (Φ, $\mathbf{A}$)

FREDERICK J. BELINFANTE
Department of Physics, University of British Columbia, Vancouver, B.C., Canada
November 18, 1947

THERE is little doubt about the validity of Dirac's equation for the wave function of a free electron

$$i\hbar\partial\psi/\partial t = H_{op}\psi \equiv (mc^2\beta - ihc\boldsymbol{\alpha}\cdot\boldsymbol{\nabla})\psi \quad (1)$$

within the limits of special relativity and present wave-mechanical principles. The recent experiments of Lamb and Retherford[1] do not shatter our believe in this equation. There is even hope that the newly discovered shift of the $2S_{\frac{1}{2}}$ level may be explained within the framework of Dirac's equation for the wave function of an electron in a Maxwell field

$$i\hbar\partial\psi/\partial t = H_{op}\psi = H_{op}{}^{0}\psi + (-e)(\Phi - \mathbf{A}\cdot\boldsymbol{\alpha})\psi, \quad (2)$$

if due attention is paid to the term with $\mathbf{A}$, that is, to the interaction with the radiation field.[2]

It might be interesting, though, to check that no form of interaction with the Maxwell field different from (2) is capable of explaining the experimental data. A well-known attempt of introducing such an interaction within the framework of special relativity is presented, for instance, by the formula

$$\{(\boldsymbol{\nabla} - [e/ihc]\mathbf{A})^2 - (\partial/c\partial t + [e/ihc]\Phi)^2\}\psi = (mc/\hbar)^2\psi, \quad (3)$$

which is obtained by replacing E by $E_{\text{total}} - E_{\text{pot}}$, etc., in the Gordon-Klein equation rather than in the Dirac equation (1). It can easily be shown that this is equivalent to denying the existence of the spin magnetic moment of the electron while retaining its spin mechanical moment of momentum $\frac{1}{2}\hbar$. It has been demonstrated[3] that this formula (3) leads for the hydrogen atom to levels approximately given by

$$E_{nl} \approx mc^2 - \frac{R}{n^2} + R\alpha^2\left(\frac{3}{4n^4} - \frac{1}{n^3(l+\frac{1}{2})}\right) + \cdots \quad (4)$$

with $n-l-1=$integer, so that in first approximation we obtain the correct Bohr levels, if (the orbital quantum number) l is integer. ($R = e^4m/2\hbar^2$ and $\alpha = e^2/\hbar c \approx 1/137$.)

On the other hand, Dirac's equation (2) yields

$$E_{nj} \approx mc^2 - \frac{R}{n^2} + R\alpha^2\left(\frac{3}{4n^4} - \frac{1}{n^3(j+\frac{1}{2})}\right) + \cdots \quad (5)$$

with $n-j-\frac{1}{2}=$integer, which is correct in first approximation with the quantum number of total angular momentum j half odd. As this formula (5) is in better agreement with experimental data on the fine structure than (4), one assumes that (3) cannot be correct.

Equations (2) and (3), though, are not the only two hypotheses possible for a relativistic equation for ψ in interaction with Φ and $\mathbf{A}$. This is easily seen as follows:

Dirac's equation (2) can be obtained from a variational principle, in which

$$\rho = (-e)\psi^{\dagger}\psi \quad \text{and} \quad \mathbf{i} = (-e)\psi^{\dagger}\boldsymbol{\alpha}\psi \quad (6)$$

are considered as the charge density (in e.s.u.) and current density (in e.m.u.). A different equation now could be found, in perfect agreement with the principle of special relativity, if we would replace (6) in the variational principle by the almost identical expressions[4]

$$\left.\begin{aligned}\rho &= Re\{(e\hbar/imc^2)\psi^{\dagger}\beta\partial\psi/\partial t\},\\ \mathbf{i} &= Re\{(ei\hbar/mc)\psi^{\dagger}\beta\boldsymbol{\nabla}\psi\},\end{aligned}\right\} \quad (7)$$

where Re means the real part. The Dirac equation is then replaced by

$$i\hbar\partial\psi/\partial t = H_{op}{}^{0}\psi - i(e\hbar/mc)\beta\{\mathbf{A}\cdot\boldsymbol{\nabla} + \phi\partial/c\partial t\}\psi. \quad (8)$$

Maxwell's equations, following from the same variational principle, will ensure the validity of the continuity equation for ρ and $\mathbf{i}$.

From (8), the corresponding levels for a hydrogen atom can be found by putting $\phi = e/r$, $\mathbf{A}=0$, and $i\hbar\partial/\partial t = E$. The result of the calculation is that $\kappa = E_{nj}/mc^2$ is a root of the equation

$$\alpha\kappa = [n' + [(j+\tfrac{1}{2})^2 + \alpha^2\kappa^2]^{\frac{1}{2}}]\cdot(1-\kappa^2)^{\frac{1}{2}}, \quad (9)$$

so that, by successive approximations, we find

$$E_{nj} \approx mc^2 - \frac{R}{n^2} + R\alpha^2\left(\frac{3}{4n^4} + \frac{1}{n^3(j+\frac{1}{2})}\right) + \cdots. \quad (10)$$

Here, like in (5), $n' = n-j-\frac{1}{2}=$integer.

Comparing (10) with Sommerfeld-Dirac's formula (5) we see that again we get the correct Bohr levels, but that the fine structure given by the j-dependent term in (10) lies inverted. Trusting that spectroscopists measuring and checking formula (5) did not interchange both sides of their fine-structure spectra, we must conclude that (10) cannot fit the experimental data, so that the hypotheses (7)–(8) also cannot be correct.

[1] W. E. Lamb and R. C. Retherford, Phys. Rev. **72**, 241 (1947).
[2] H. A. Bethe, Phys. Rev. **72**, 339 (1947).
[3] See, for instance, A. Sommerfeld, *Atombau und Spektrallinien Wellenmechanischer Ergänzungsband* (F. Vieweg und Sohn, Braunschweig, 1929), Kap. I, §9E, pp. 132–138, or the English translation. S. A. Goudsmit, in his doctor's thesis (University of Leiden, 1927), states that W. Pauli was the first to derive (4) from (3).
[4] From a classical point of view, ρ and $\mathbf{i}$ from (6) represent $\psi^{\dagger}\psi$ times $(-e)$ and $(-e)\mathbf{v}/c$, while ρ and $\mathbf{i}$ from (7) represent $\psi^{\dagger}\psi$ times $(-e)(E/mc^2)(1-v^2/c^2)^{\frac{1}{2}}$ and $(-e)(\mathbf{p}/mc)(1-v^2/c^2)^{\frac{1}{2}}$.

Neutron-Proton Scattering at 100 Mev

JULIAN EISENSTEIN AND FRITZ ROHRLICH
Lyman Laboratory, Harvard University, Cambridge 38, Massachusetts
February 7, 1948

A VALUE $0.083\pm0.004\times10^{-24}$ cm^2 for the neutron-proton total cross section at 90 Mev has recently been reported by Cook, McMillan, Peterson, and Sewell.[1]

We have made calculations to determine whether it is possible to fit this value of the cross section if one uses existing phenomenological theories of nuclear forces. The results at 100 Mev for a rectangular well interaction potential are as follows:

1. Central, non-exchange force. Triplet range, 2.80

$\times 10^{-13}$ cm; depth, 21.213 Mev. Singlet range, 2.80×10^{-13} cm; depth 11.904 Mev. Exact cross section, 0.162×10^{-24} cm². Born approximation, 0.169×10^{-24} cm².

Triplet range, 1.80×10^{-13} cm; depth, 43.476 Mev. Singlet range, 2.80×10^{-13} cm; depth 11.904 Mev. Exact cross section, 0.117×10^{-24} cm². Born approximation, 0.123×10^{-24} cm².

2. Central, symmetrical exchange force. Triplet and singlet ranges, 2.80×10^{-13} cm; depths as above. Exact cross section, 0.111×10^{-24} cm². Decreasing the triplet range increases the cross section. In this case the Born approximation to the singlet cross section is too large by a factor of approximately two.

3. Tensor, non-exchange force. Triplet and singlet ranges, 2.80×10^{-13} cm. Rarita and Schwinger[2] constants. Born approximation, 0.205×10^{-24} cm².

4. Tensor, symmetrical exchange force. Ranges, 2.80×10^{-13} cm. Rarita and Schwinger constants. The Born approximation for the triplet cross section and the exact value for the singlet cross section yield a total cross section of 0.113×10^{-24} cm².

Experiments on the angular distribution at 90 Mev were reported by Hadley *et al.*[3] They found 0.3 for the ratio of scattering at 90° to backward scattering in the center of gravity system.

The exact solution at 100 Mev for a central, symmetrical exchange force using the first five phase shifts gives $\sigma(0):\sigma(\pi/2):\sigma(\pi)=2.24:0.062:6.87$. For the tensor, symmetrical theory in the above combination of exact and Born cross sections we obtain $\sigma(0):\sigma(\pi/2):\sigma(\pi)=1.22:0.51:4.03$.

These figures show that only the symmetrical tensor theory is in close enough agreement with experiments so that the remaining discrepancies might be accounted for by relativistic corrections. Comparison of the symmetrical non-tensor theory with the symmetrical tensor theory shows that the tensor force decreases appreciably the forward and backward scattering and accounts for nearly all the scattering at right angles. In the symmetrical tensor theory a reduction of the triplet range increases the tensor part, i.e., the constant[4] γ thus increasing the ratio $\sigma(\pi/2):\sigma(\pi)$ and the total cross section. The same reduction made for the tensor force range rather than the triplet range is more effective in increasing γ and the above ratio.

As an example we used constants calculated by Guindon[5] to fit the epithermal neutron-proton cross section, the binding energy of the deuteron, and the quadrupole and magnetic moments. He assumed an interaction potential which does not contain a spin exchange force ($g=0$),[4] both the non-tensor and tensor parts being rectangular wells of ranges r(non-tensor) $=2.80\times 10^{-13}$ cm and r(tensor) $=2.654\times 10^{-13}$ cm and depths $V_0=11.904$ Mev and γV_0 ($\gamma=1.149$), respectively. With these constants we find for the tensor, symmetrical case $\sigma(0):\sigma(\pi/2):\sigma(\pi)=1.26:0.61:3.44$.

Calculations were also made with Yukawa potentials and a central non-exchange force. They led to considerably lower cross sections. The singlet range 1.8×10^{-13} cm and depth 45.80 Mev found by Hoisington, Share, and Breit[6] in an analysis of proton-proton scattering were used. The triplet range was also taken to be 1.18×10^{-13} cm and the depth interpolated from calculations of Hulthén[7] to be 67.45 Mev. The cross section, in first Born approximation, is 0.111×10^{-24} cm² at 100 Mev. This value is 35 percent below the corresponding value obtained with a rectangular well potential. It is difficult to estimate the cross section on the basis of a symmetrical theory because the Born approximation value of the singlet cross section is so far off. For the range and depth previously used the triplet cross section is 0.093×10^{-24} cm². The singlet cross section will probably be about the same as in the rectangular well case. Consequently, the total cross section will be about 0.11×10^{-24} cm². For a Yukawa potential a symmetrical exchange force therefore apparently does not lead to as strong a reduction in the total cross section as it does for a rectangular well.

Constants for the Yukawa potential in the tensor force case are being calculated.[8] The triplet cross section obtained in the symmetrical tensor case with tentative values of the constants is about 0.09×10^{-24} cm².

A detailed report on these calculations will be presented later.

[1] Leslie J. Cook, Edwin M. McMillan, Jack M. Peterson, and Duane C. Sewell, Phys. Rev. **72**, 1264 (1947).
[2] William Rarita and Julan Schwinger, Phys. Rev. **59**, 436 (1941).
[3] Hadley, Leith, York, Kelly, and Wiegand, Bull. Am. Phys. Soc. **23**, 15 (1948).
[4] For notation see reference 2.
[5] W. Guindon, Theses, Massachusetts Institute of Technolgy.
[6] L. E. Hoisington, S. S. Share, and G. Breit, Phys. Rev. **56**, 884 (1939).
[7] L. Hulthén, Arkiv. mat. astr. fys. **28A**, No. 5 (1942).
[8] Feshbach, Schwinger, and Eisenstein (to be published).

Willard Leslie Severinghaus

H. W. Farwell

WILLARD L. SEVERINGHAUS, the fifth in the line of prominent physicists to serve the American Physical Society as Secretary, died in New York City on August 28, 1947, after a long illness. Professor Severinghaus was born in Terre Haute, Indiana, on January 28, 1882, the youngest son of a Methodist clergyman. As a boy his interest in things scientific was keen and persistent. He received his bachelor's degree from Baldwin-Wallace College, Berea, Ohio, in 1904 and the degree of Doctor of Philosophy from Columbia University in 1914. He was associated with the Phsyics Department at Columbia from 1907, passing from the junior staff to professorial rank in 1919.

Dr. Severinghaus was elected Secretary of the Physical Society in 1929, by this time being well and widely known as a successful and enthusiastic teacher in the sequence of physics courses for pre-engineering students of which he had general charge. He had further become recognized as an authority on measurements of high temperatures.

During his term of service, the membership of the Society increased to such an extent that many changes in office procedure became necessary. In arranging the de-

tails of meetings with crowded programs and simultaneous sessions, with more correspondence, and more insistent demands upon his time from his university obligations, Professor Severinghaus accepted it all cheerfully as being a part of the job and continued to give the Society the wholehearted service so characteristic of him. He really enjoyed the work, not just because it helped him to keep his own horizons broader, but more because it was another of the ways in which to serve the science he loved.

Professor Severinghaus was married in 1920 to Miss Francess Orr, of Piqua, Ohio, who survives him. Many members of the Society recall with pleasure the presence at their meetings of the Secretary and his wife, herself a member in her own right and an interested assistant in the task of making affairs run smoothly.

Perhaps weakened by an extremely severe attack of pneumonia in the early '30s, his physical condition by 1939 began to show the effects of circulatory disturbance. He retired in 1941 to fight a long and losing battle against overwhelming odds. He will be remembered for his wide interests, his personal charm, and his huge store of patience. The Council of this Society recognizes and records here the deep indebtedness of the Society to him for his contribution to its development.

Proceedings of the American Physical Society

Minutes of the Meeting at Houston, Texas November 28–29, 1947

THE 280th meeting of the American Physical Society, the first ever to be held in Texas, took place at Rice Institute in Houston on Friday and Saturday, November 28 and 29, 1947. This was one of our smaller and therefore more agreeable meetings, bringing together about three hundred members and guests. Texas and Louisiana were of course well represented, and there was a group of visitors from Mexico City who contributed to the programme. Homage was paid to the geophysical interests of a large number of our Texan colleagues by a symposium, "Underground Applications of Physics," which was a joint symposium with the Society of Exploration Geophysicists, arranged by L. L. Nettleton. Two other invited papers on geophysical subjects, and several in diverse fields of physics chosen partly to illustrate the researches in progress at Rice Institute and partly to bring distant speakers to Houston, appeared in the general programme. Abstracts of sixty contributed papers are printed below. The rather large proportion "read by title" presumably implies the difficulty of traveling to Texas; it is regrettable that this difficulty could not be more readily surmounted, for the hospitality of Rice Institute and the climate of Houston combined to make this meeting pleasant in every way. The Chairman of the Local Committee was C. W. Heaps, to whom the Society is greatly obligated.

The dinner of the Society was held on Friday evening in Rice Institute Commons, with after-dinner speeches including one by H. A. Wilson and one by M. S. Vallarta who gratified the Society by an enticing invitation to hold one of its future meetings in Mexico City, and culminating in an address by A. H. Compton "The physicists' role in international relations."

The Council met on Friday afternoon, and elected to Fellowship the two candidates and to Membership the 352 candidates whose names are appended.

According to reports reaching the office of the Society, we have lost through death since the June meeting an extraordinary number of our members, including some of the greatest distinction: H. T. Barnes (formerly of McGill), A. P. Carman (formerly of Illinois), J. R. Collins (Cornell), P. Lecomte du Nouy (New York), A. S. Eve (formerly of McGill), A. L. Foley (formerly of Indiana), K. H. Fried (Brooklyn College), Shuichi Kusaka (Princeton), A. L. Longden (Galesburg, Illinois), W. C. Morris (Warrensburg, Missouri), Max Planck (Honorary Member, formerly of Berlin), T. H. Quigley (Holy Cross College), Fernando Sanford (formerly of Stanford), J. E. Shrader (Drexel), George Singer (National Bureau of Standards), L. J. Sivian (Bell Telephone Laboratories), H. W. Smith (Life Member, Tahiti), D. F. Windenburg (David Taylor Model Basin), and B. A. Wooten (Alabama).

Elected to Fellowship: T. A. Read, Abraham Taylor.

Elected to Membership: Robert K. Adair, Harry S. Adams, Mario Ageno, Warren R. Alexander, R. Stanley Alexander, Charles S. Allyn, Alton DeWitt Anderson, Jr., Wilbert Annis, Raymond Sherwin Ashapa, Bruno W. Augenstein, Carl-George Paul Aurell, William H. Avery, William Baer, Carroll K. Bagby, Joe Keagy Bair, William F. Bale, Nathan M. Banks, Charles A. Barnes, William O. Bateson, C. S. Beal, Louis A. Beach, Charles I. Beard, Alan C. Bemis, Evelyn Berezin, G. Bernardini, Ira B. Bernstein, William George Best, Ralph H. Beter, Donald R. Bianco, Daniel Binder, Milton Birnbaum, John A. Bistline, Jr., Charles K. Bockelman, Felix Boehm, C. J. Borkowski, Arthur G. Bousquet, Everett Owen Braaten, Carl F. Brandner, J. Norton Brennan, Douglas Broadbent, Alfred A. Brooks, Ernest Leroy Brown, Robert James Brown, James T. Bull, Elizabeth Thompson Bunce, George G. Bundy III, Hugh W. Byfield, John Williams Calkin, Charles Edgar Campbell, Robert Hodgens Campbell, C. Vernon Cannon, James Alexander Carruthers, Andrew R. Chi, Warren W. Chupp, Brian A. G. Churcher, Chester W. Clark, Eric Norman Clark, Grady W. Clark, Robert Cockburn, Fritz Coester, David S. Cohen, E. Richard Cohen, George Cohen, Robert B. Colten, Donald W. Connor, Stanley Corrsin, Bayard

R. Corson, V. E. Cosslett, Eugene Samuel Cotten, Eugene W. Cowan, Robert D. Cowan, Robert J. Creagan, Marcus O. Creager, Nancy Cross, Charles G. Cruzan, Monarch L. Cutler, Harry Oscar Dagavarian, Milton Danzker, Lee L. Davenport, Richard Harding Davis, John C. Dear, Jack K. Debenham, Jan De Boer, Willy Clement Dekeyser, Emidio Anthony DeLollis, Willard L. Derksen, Ralph Deutsch, John H. DeWitt, Jr., Louis Dick, Zulime Whitney Diehl, Edwin A. Doane, Donald C. Dodder, Donald George Douglas, Eva C. Douglas, William G. Dow, John C. Duecker, G. Wesley Dunlap, Mary Louise Dunham, Roger Lee Easton, E. G. Ebbighausen, Edgar A. Edelsack, H. A. Elliott, H. J. Ettlinger, Leonard Eyges, E. F. Fahy, Henry Faul, Sidney Feldman, Craig Ferris, Reuben E, Fields, James C. Filmer, Rocco Fiore, Harriet H. Forster. Charles P. Foster, Jr., Marvin Fox, Hans Freistadt, John Heaver Fremlin, Anthony Philip French, Sherwood C. Frey, K. Fuchs, Harry W. Fulbright, Andrew J. Galambox, Wray B. Garn, Rev. Alois Gatterer, S.J., Myer M. Geller, Harvey S. Gellman, Millicent Gerson, Barry S. Gourary, Alex E. S. Green, Robert S. Green, Joseph Charles Grosskreutz, Sayed Ramadan Haddara, Nis Hansen, Jr., Richard E. Hartman, Raymond W. Hayward, Marian H. Heineman, William R. Heller, Burton L. Henke, Peter Hidnert, Paul M. Higgs, Landon P. Hill, R. D. Hill, Richard W. Hill, Walter F. Hitschfeld, Gerald Morton Hoffman, Murray Hoffman, John Riley Holt, Gerald J. Holton, Vincent R. Honnold, Oliver W. Hopkinson, Jr., John P. Howe, Hugh K. Howerton, Thomas P. Hubbard, Jr., Oren J. Huber, George E. Hudson, McAllister H. Hull, Jr., Lamek Hulthen, Richard Allan Hunt, Joseph L. Hunter, John B. Hursh, Kitty Iliopoulos, Roy C. Irick, Donald H. Jacobs, Norman L. Irvine, Bernard M. Jaffe, Harry R. James, J. V. Jelley, Rurridge Jennings, James W. Jenson, Harold E. Johns, Peter D. Johnson, Kevin Rice Jones, Robert H. Jones, Stanley Bennett Jones, Kenneth C. Jordan, Surindra Nath Kalra, J. Kastner, Robert E. Katz, K. J. Keller, E. Walter Kellermann, Edward Kelly, David J. Klein, Arthur Kohlenberg, Ignace I. Kolodner, Harwood G. Kolsky, Harold Korbel, Leslie Kovach, Lois Arline Kutz, Anne Yung Kwai, Pablo Daumas Ladouce, Donald Thomas Laird, Victor K. LaMer, George H. Lane, Jr., Neal Lansing, Elisabeth Farber Lanzl, Harold Levenstein, Harold W. Lewis, William Edward Leyshon, John A. Liedtke, David A. Lind, Seymour J. Lindenbaum, Emma Lindsey, George R. Lindsey, Leonard B. Lipson, Robert Loevinger, Ralph A. Logan, Francis E. Low, Ward C. Low, Herman H. Lowell, Robert G. Luce, James Ross Macdonald, D. T. MacRoberts, Dale W. Magnuson, Fred C. Maienschein, Ray C. Makino, Ken M. Manfred, Thurston E. Manning, J. Carson Mark, John H. Marshall, Alex Mayer, C. Keith McLane, Alvin Meckler, Thomas O. Meeks, Donald H. Menzel, Philippe Meyer, W. S. Michel, David Charles Miller, Theodore Miller, Phillip Sidney Mittelman, Dana L. Mock, A. J. Monack, Donald Baker Moore, James F. Moulton, Jr., John E. Nankivell, Jupp Nass, Philip Newman, Robert T. Nieset, Isadore Nimeroff, George M. Nonnemaker, M. G. Nooh, David Okrent, Robert H. Olds, Joseph S. Osoba, Alexander J. Oszy, Ettore Pancini, Earl R. Parker, Homer W. Parker, John R. Parks, Paul Bachtiger, Eric B. Paul, Miles Pennybacker, Julien Peridier, Charles H. Perry, George Claude Pimentel, Jean C. L. Pirenne, Samuel Podgor, Martin F. Popelka, Jr., Alvin Radkowsky, Malcolm Logan Randolph, William A. Reardon, Esther D. Redding, J. Kenneth Richmond, Harold Francis Ring, Alfred E. Roberts, Jr., Harry S. Robertson, Robert C. Rogers, George W. Rollosson, Donald Ross, Jean Rossel, Wilfred Roth, Paul McRae Routly, John W. Rowen, Stanley L. Ruby, Stanley Keith Runcorn, Joseph H. Rush, Arnold Russek, G. A. W. Rutgers, Henry Saltzman, Alfred Sarant, Theodore C. Sargent, Alois Wolfgang Schardt, Morris V. Scherb, Raymond R. Schiff, William G. Schwab, Ralph J. Schwarz, Philip Schwed, G. David Scott, Wayne Max Shaffernocker, David P. Shoemaker, James Wood Simmons, Marcia Anita Simon, Sidney L. Simon, Kurt Sitte, Lawrence R. Sitney, Marvin Slater, David Slepian, Gardner H. Sloan, Murray Slotnick, George A. Snow, Murray J. Stateman, Earl L. Steele, Ellis P. Steinberg, Thomas Edgar Stephenson, Martin O. Stern, David Sternberg, Frank R. Stevens, John M. Stevenson, Hugh B. Stewart, N. Paul Stucky, Martin H. Studier, James A. Suddeth, Andrew W. Sunyar, Conrad D. Swanson, Clifford E. Swartz, Theodore B. Taylor, J. Thewlis, Garland L. Thomas, Harold A. Thomas, Marlin O. Thurston, Charles William Tittle, Cornelius Anthony Tobias, Richard E. Trees, Stanley H. Ungar, Gaston A. J. Vandermeerssche, J. L. Verhaeghe, Robert C. Vernon, Mabel Slattery Vincent, Austin L. Wahrhaftig, M. Carl Walske, Jr., Samuel Abner Ward, John M. Watkins, Jr., Curtis C. Webster, John Wei, Herbert G. Weiss, Richard Jerome Weiss, Joseph Weneser, G. Neilson Whyte, Martin Wiener, John B. Wilcox, Burton J. Wilson, Edward B. Winn, Robert E. Wise, Eligius Jerome Wolicki, John Leonard Yarnell, Carl M. York, Jr., Herbert Frank York, Gregory O. Young, Kenneth L. Yudowitch, Renn Zaphiropoulos, John Robert Zeuschel, Irving Zinnes, Alexander Zucker.

KARL K. DARROW, *Secretary*
American Physical Society
Columbia University
New York 27, New York

Joint Symposium of the American Physical Society and the Society of Exploration Geophysicists

Underground Applications of Physics

Field Equations of the Flow of Liquids through Porous Solids. M. KING HUBBERT, *Shell Oil Company.*

Seismic Travel Paths at Bikini Atoll. R. F. BEERS, *Geotechnical Corporation.*

Physical-Chemical Interpretation of a Geological Problem: Rocks from Sea-Water. PAUL WEAVER, *Gulf Oil Corporation.*

Industrial Applications of Radioactivity. GERHARD HERZOG, *Texas Company.*

Other Invited Papers on Geophysical Topics

Microseisms and Hurricanes. BENNO GUTENBERG, *California Institute of Technology.*

Seismic Measurements in the Antarctic. T. C. POULTER, *Armour Research Foundation.*

Invited Papers from Rice Institute

The Low Temperature Physics Programme at the Rice Institute. C. F. SQUIRE, *Rice Institute.*

Resonances in the Disintegration of Fluorine by Protons. T. W. BONNER, *Rice Institute.*

Normal Vibrations in Crystals. W. V. HOUSTON, *Rice Institute.*

Other Invited Papers

Behavior of Photoelectrons in Silver Chloride Crystals Exhibited by Colloidal Silver Produced at Electron Traps. J. R. HAYNES, *Bell Telephone Laboratories.*

Certain Problems Concerning the Primary Cosmic Radiation. M. S. VALLARTA, *Universidad de Mexico.*

Contributed Papers

A1. Graphical Solution of Non-Linear Simultaneous Equations. JAMES M. SHARP AND S. LEROY BROWN, *University of Texas.**—A pair of non-linear simultaneous equations in two variables, x, y, may be put in polar form by substituting $x=r\cos\theta$, $y=r\sin\theta$. If powers of $r\cos\theta$ and $r\sin\theta$ are expanded into harmonic functions of multiple angles, and any resulting products are expanded into functions of multiple angles, each of the original equations becomes harmonic in form with coefficients containing powers of the modulus r. Assign a value for r, and either harmonic equation may be graphed with a mechanical harmonic synthesizer as θ varies from zero to 2π. The roots from this graph will be points $x(=r\cos\theta)$, $y(=r\sin\theta)$ of the plot of the original equation in the $x-y$ plane. Successively chosen values of r locate other points and, thereby, the original equation is graphed. Each of the pair of equations is plotted in this way, and the intersections of these two curves will indicate the simultaneous values.

* Assisted by the Office of Naval Research.

A2. Graphical Solution for the Real and Complex Roots of Polynomials With a Mechanical Harmonic Synthesizer. ROBERT G. PACKARD AND S. LEROY BROWN, *University of Texas.**—The powers of the variable x in a polynomial may be expressed as harmonic functions of multiple angles by De Moivre's theorem, $x^n=r^n(\cos n\theta+j\sin n\theta)$. After this substitution in the polynomial the real terms give one equation, and the imaginary terms give the second equation of a pair of simultaneous equations with variables r and θ. Eliminate r between these two equations and there results an equation of harmonic terms in multiple angles. This resultant equation may be graphed with a mechanical harmonic synthesizer and its roots determined; that is, values of θ are found that satisfy this equation. These values of θ substituted into either of the simultaneous equations will determine the respective values of the modulus r. Thereby, the real components, $r\cos\theta$, and the imaginary components, $r\sin\theta$, of the roots of the original polynomial are determined.

* Assisted by the Office of Naval Research.

A3. Analytical Solution of Electrical Networks for Resonant and Antiresonant Frequencies. MARY GOWEN FOULKS, *University of Texas.**—Where the circuit constants of a several mesh network are specified, the resonant and antiresonant frequencies can be determined by a mechanical process. If the circuit is non-dissipative, either the resonant or the antiresonant frequencies may be apparent; moreover, the other critical frequencies can be found as the roots of the polynomial obtained by setting either the susceptance or the reactance, depending on the nature of the network, equal to zero. The solution of the polynomial is carried out by making a change of variable, transforming the equation into a function of multiple angles which can be traced with a mechanical harmonic synthesizer. The angles at which the harmonic sum equals the constant term of the transformed equation give the roots of the polynomial. For a dissipative circuit the impedance as a function of the angular velocity is differentiated with respect to argument and the resulting expression equated to zero to calculate the resonant and the antiresonant frequencies; the polynomial is solved mechanically.

* Assisted by the Office of Naval Research.

A4. Graphical Solution of Network Impedances with a Mechanical Harmonic Synthesizer. S. LEROY BROWN, *University of Texas.**—The impedance of an electrical network of specified circuit constants is a complex function of frequency ($\omega=2\pi f$) in the form of a fraction with a real and a pure imaginary term in the numerator, and a common denominator. These terms will be high degree

polynomials in ω. If ω is replaced by a harmonic function such as $r(1-\cos\theta)$, modulus r being chosen so that the desired range in values of ω is obtained as θ varies from zero to π, and if the powers of the new variable are expanded in terms of multiple angles, then the resulting functions can be graphed with a mechanical harmonic synthesizer. For pure reactance networks there will be only one term in the numerator, pure imaginary, and a denominator, but impedances will have both real and imaginary terms in the numerator; therefore, two functions must be plotted to solve non-dissipative networks and three to determine both the resistance and reactance of dissipative networks, these quantities being calculated from the ratios of corresponding ordinates of the graphs.

* Assisted by the Office of Naval Research.

A5. On the Dielectric Wave Guide of Circular Cross Section.* C. W. HORTON, *University of Texas.*—It has been known for a long time that a dielectric rod of circular cross section can be used as a transmission line for electromagnetic waves. When the mathematical theory of such waves is developed, one encounters a characteristic equation[1] of some complexity relating the wave-length in the rod to its radius and dielectric constant. This characteristic equation has been solved numerically for three modes of vibration. These are the transverse electric wave of radial symmetry, the transverse magnetic wave of radial symmetry, and the mode whose angular variation depends on $\sin\theta$. The last case is similar to the $TE_{1,1}$ mode in a circular metallic wave guide. For each of these cases the calculations have been carried out for the first two of the infinitely many branches. The tangential components of the electric and magnetic vectors, over the surface of the dielectric rod, have been computed. These quantities are necessary in order to calculate the radiation patterns of dielectric rods by Schelkunoff's method of equivalent surface currents.

* This work has been done in part under sponsorship of Bureau of Ordnance, Navy Department.

[1] J. A. Stratton, *Electromagnetic Theory*, p. 526, Eq. (9).

A6. Inversion of a Family of Laplace Transforms Associated to the Propagation of Electromagnetic Waves in Cylinders. MANUEL CERRILLO, *Massachusetts Institute of Technology. (Introduced by M. S. Vallarta.)*—In the study of the transient phenomena of the propagation of electromagnetic waves in cylinders, mainly in wave guides, one has to evaluate the inverse of a family of Laplace transforms of the type $F[s, (s^2+b^2)^{\frac{1}{2}}] \exp -a(s^2+b^2)^{\frac{1}{2}}$. In this paper is presented the compact solution in terms of Lommel's functions, as well as the asymptotic expansion and graphical methods to obtain these inverse functions.

A7. Bridged Double T Network. C. H. FAY, *Shell Oil Company.*—For what may be termed a bridged double T, with series impedances numbered Z_1, Z_2, Z_5, shunt impedances Z_3, Z_4, numbering being from the source end, and bridging impedance Z', the condition for zero output voltage is $Z_1[Z_3Z_4+(Z_3+Z_3+Z_4)Z_5]+Z_2[Z_3Z_5+Z_4(Z_1+Z_3+Z_5+Z')]=0$. A special case of interest is $Z_1=Z_3=Z_5=R$, $Z_2=Z_4=(j\omega C)^{-1}$, which for $Z'=12(j\omega C)^{-1}$ has a null at a frequency given by $R\omega C=\sqrt{3}$. The "inverse" case, $Z_1=Z_3=Z_5=(j\omega C)^{-1}$, $Z_2=Z_4=R$, has for $Z'=12R$ a null for $R\omega C=1/\sqrt{3}$. An application to a substitution bridge for measurement of small direct capacitances in the presence of large admittances to ground, with provision for measuring small conductive components, is discussed; it has the advantage that admittances to ground appear only as shunts on source and detector, and thus affect the sensitivity only.

A8. An Electronic Control Device for the Stabilization of a 10,000-Oersted Magnetic Field. D. S. HUGHES, W. L. PONDROM, AND G. B. THURSTON, *University of Texas.*—It was desired to stabilize the magnetic field of a low voltage, high current electromagnet at the University of Texas. The field, to be used in connection with a mass spectrograph, was to be held at 10,000 oersteds$\pm\frac{1}{2}$ oersted for several successive minutes. The device developed is a feed-back control system operating directly from and on the field. An armature located in the field and driven by a synchronous motor yields a 3-phase voltage which is rectified and filtered so that a d.c. voltage is obtained which is directly proportional to the magnetic field with negligible lag. Variations in this d.c. voltage are amplified, the amplified voltage variations controlling the operation of power triodes, which in turn regulate the current in auxiliary coils attached to the pole pieces of the magnet. Thus variations in the magnetic field are amplified and converted into the compensating field of the auxiliary coils on the magnet. Field drifts of $\pm$120 oersteds, and rapid field variations as fast as 0.25 second and as great as 150 oersteds are reduced to $\pm$0.25 oersted, over-all variations being held within $\frac{1}{2}$ oersted for 10-minute intervals.

E1. The Rice Institute Van de Graaff Electrostatic Generator. H. A. WILSON, *Rice Institute.*—This note contains a description of some of the novel features of the Rice Van de Graaff machine, including the electrostatic voltmeter, the flexible joint between the vacuum tube and the end of the tank, and the method of making the aluminum rings.

E2. A Pair Production Spectrometer for Gamma-Rays.* NELSON JAMES TERRELL, JR., *Rice Institute.*—A pair production spectrometer has been designed for the purpose of measuring high gamma-ray energies (3–15 Mev). Electrons and positrons, ejected from a lead radiator, travel in 180° arcs in a uniform magnetic field and are detected by four Geiger counters, two near the focal point of each beam. Electron-positron coincidences are determined as a function of field strength, and the particle energy, E_m, corresponding to the maximum counting rate should determine the gamma-ray energy by the relation $E_\gamma=2E_m+1.02$ Mev. Preliminary tests have been made with

radium as a source of gamma-rays; however, the low energy and complex nature of the radium spectrum make it an unsuitable source for this apparatus. It is planned to extend the tests to ThC″.

* This work was supported by the Office of Naval Research.

E3. Separation of Li Isotopes.* WARD WHALING AND J. E. EVANS, *Rice Institute.*—A mass spectrometer has been constructed in order to collect the isotopes of the light elements in sufficient quantity for nuclear-bombardment experiments. A 30° sector-shaped magnetic field is used to focus a parallel beam of ions emitted from an extended source. Such a lens does not provide theoretically perfect focusing, but the width of the focused image resulting from this imperfection is negligible compared to other factors unavoidable in a high intensity instrument, and its simplicity recommends it. By the use of a heated platinum wire, coated with Amblygonite ($Li\,Al(F, OH)\,PO_4$) as a source of Li ions, satisfactory resolution of the Li isotopes has been attained at low ion currents. Further work is under way to maintain this resolution at the full intensity of which the instrument is capable.

* This work was supported by the Office of Naval Research.

E4. Some Characteristics of Scandium (46).* C. E. MANDEVILLE AND MORRIS V. SCHERB, *Bartol Research Foundation.*—Sc_2O_3 was irradiated by slow neutrons in the Clinton pile. The radioactive material was separated into phosphorous, iron, calcium, and scandium. The beta-rays emitted by the scandium fraction had an end point of 0.076 g/cm² in aluminum. The maximum energy of the gamma-rays was found to be 1.0 Mev by coincidence absorption. The beta-gamma coincidence rate was 1.4×10^{-3} coincidence per beta-particle, and was independent of the beta-ray energy. A gamma-gamma-coincidence rate of $(0.62 \pm 0.06) \times 10^{-3}$ coincidence per gamma-ray was also observed. These coincidence rates suggest that each beta-ray is followed by two gamma-rays. A search was made for the hard beta-rays reported to be emitted by this isotope.[1,2] None were found.

* Supported by the Office of Naval Research.
[1] H. Walke, Phys. Rev. 57, 163 (1940).
[2] Peacock and Wilkinson, Phys. Rev. 72, 251 (1947).

E5. The Thin Target Yield of the Gamma-Rays from the Disintegration of Beryllium by Deuterons.* C. P. SWANN, W. J. SCOTT, E. L. HUDSPETH, AND C. E. MANDEVILLE, *Bartol Research Foundation.*—The bombarding particles were supplied by the 0.4 microampere magnetically analyzed beam of the Van de Graaff generator at the Bartol Research Foundation. The electrostatic voltmeter was calibrated by the 440-kv resonance of the gamma-rays from lithium plus protons. The thin target yield of the gamma-rays emitted in the disintegration of beryllium by deuterons has been investigated for deuteron energies ranging from 150 kev to 750 kev. The yield was found to rise smoothly with increasing bombarding energy, with no evidence for resonance on the voltage interval under study. With the assumption that the gamma-rays are related to the neutrons from this reaction, the curve agrees fairly well with the theoretically calculated yield.[1] The absolute yield at 600 kv from the thin target (stopping power 35 kev) was estimated to be about 7.5×10^{-7} quantum per deuteron.

* Supported by the Office of Naval Research.
[1] H. A. Bethe, Rev. Mod. Phys. 9, 69 (1937).

E6. Gamma-Rays and Neutrons from Beryllium Bombarded by Deuterons. C. W. MALICH* AND J. R. RISSER, *Rice Institute.*—The thin target yields of gamma-rays and of neutrons from beryllium bombarded by deuterons have been determined for bombarding energies from 0.25 Mev to 1.7 Mev. The gamma-rays were detected with a self-quenching Geiger-Mueller counter, and the neutrons with a proportional counter filled with argon at atmospheric pressure. The excitation functions of both the neutrons and the gamma-rays are similar; the yields increase approximately exponentially with bombarding energy up to a deuteron energy of about 1 Mev, and less rapidly at higher energies. No resonances were observed.

* Now at the University of Pennsylvania.

E7. Further Evidence for a $\gamma - p$ Process in Be^9. RICHARD L. CONKLIN* AND WILLIAM OGLE, *Los Alamos Scientific Laboratory.*—A previous paper[1] has reported observation of a $\gamma - p$ process in Be^9. In that work the 12-Mev beta-particles from the decay of Li^8 were observed above the background of 3.7-Mev betas from He^6, also formed during the irradiation by the process $Be^9(n, \alpha)He^6$. Li^8 decays into Be^8,* which promptly breaks up into two alpha-particles. The observation of these alphas should furnish further proof of the presence of Li^8. Such an experiment has been performed, and alpha-particles have been observed from beryllium after irradiation by 20-Mev x-rays. The decay half-life is within experimental error of the 0.88-second half-life of Li^8.

* Now at the University of Illinois, Urbana, Illinois.
[1] Ogle, Brown, and Conklin, Phys. Rev. 71, 378 (1947).

E8. Differential $D(d,n)He^3$ Cross Section for 10-Mev Deuterons. B. R. CURTIS, LOUIS ROSEN, AND J. L. FOWLER, *Los Alamos Scientific Laboratory.*—Deuterons from the Los Alamos cyclotron, focused at the center of a scattering chamber, were used to bombard a thin gas target and the number of He^3 particles observed which were emitted into a known solid angle in a given direction. Several gas targets were used so that, in the laboratory system, all angles from 20 to 42 degrees with the direction of the beam could be measured. The He^3 pulses were recorded by means of a proportional counter and amplifier and were analyzed with a ten-channel amplitude discriminator. The resulting plot of pulses per amplitude interval against amplitude gave a peak well resolved from background. The deuteron current was measured by means of a Faraday cage and current integrator. The value of the deuteron energy determined by magnetic deflection was 10.2 Mev, which value remained constant to about two percent throughout the experiment. From the number of He^3 counts obtained in a given experiment and the integrated current the differential cross sections were calculated. These data indicate that in the

center of mass system the differential cross section for the production of He^3 particles from this reaction is approximately independent of angle from 70 to 130 degrees. The total cross section obtained by extrapolation of the data is 0.04×10^{-24} cm².

E9. The Scattering of Neutrons of Energy Between 12.0 Mev and 13.0 Mev by Protons. J. S. LAUGHLIN AND P. G. KRUGER, *University of Illinois.*—The angular distribution of the recoil protons projected during the scattering of neutrons by protons has been investigated in a methane-filled high pressure cloud chamber. A deuterium gas target bombarded with 10-Mev deuterons provided the high energy neutron source. The spectrum of the neutrons from this source, which entered the cloud chamber through a collimator, was surveyed, and showed a group of high energy neutrons superimposed on a continuous background. Examination of the data with selection criteria to determine those recoils projected by the scattering of neutrons between 12.0 Mev and 13.0 Mev yielded a total of 1573 recoil protons. The azimuthal and recoil angle distributions of these protons have been analyzed. Analysis of the data employing calculated azimuthal-correction factors yielded an angular distribution which agreed satisfactorily with an analysis based on only the 699 recoils which fell in azimuthal zones for which the azimuthal correction factor was unity. A ratio of the differential cross sections for neutron scattering in the backward direction to scattering in a direction perpendicular to that of the incident neutron beam, of unity (spherically symmetric scattering) or slightly greater than unity can be consistent with these data.

E10. The Scattering of Fast Neutrons by Mercury.* G. C. PHILLIPS AND J. C. HARRIS, *Rice Institute.*—The scattering of fast neutrons by mercury has been investigated, using the neutrons from the D^2+D^2 reaction and an ethane- and ethyl alcohol-filled cloud chamber placed at right angles to the deuteron beam. About 4500 stereoscopic photographs were taken, half with a hemispherical mercury scatterer against the target and in the direction of the beam, and half without the scatterer. Two hundred and sixty-three recoil protons, which were directed within 10° of the normal at the target to the incident beam, were measured. The energy distribution of the neutrons scattered from the mercury was calculated from the difference in the energy distributions of the recoil protons, with and without the scatterer. The number *vs.* energy plot for the neutrons indicated an increasing yield in the number inelastically scattered all the way up to 2.0 Mev, and showed no maximum at low energies. Also neutrons were observed at energies almost up to the maximum for the reaction, thus showing that there is considerable backward scattering of the neutrons by mercury.

* This work was supported by the Office of Naval Research.

F1. The 440-Kev Resonance of Li^7+H^1.* J. E. EVANS AND T. W. BONNER, *Rice Institute.*—The gamma-ray resonance at 440 kev for lithium bombarded by protons has been re-examined[1,2] with thin targets and with the high resolution made available by the electronically regulated Rice Institute Van de Graaff generator. The resonance appears to be a singlet whose width at half-intensity is 14 kev. The cross section for the reaction at the peak of the resonance is found to be 7.2×10^{-27} cm². The previously reported [1] asymmetry of the excitation curve for the resonance was confirmed. Attempts to explain the asymmetry on the basis of the barrier penetrabilities have not been successful.

* This work was supported by the Office of Naval Research.
[1] C. M. Hudson, R. G. Herb, and G. J. Plain, Phys. Rev. **57**, 587 (1940).
[2] L. R. Halfstad, N. P. Heydenberg, and M. A. Tuve, Phys. Rev. **50**, 504 (1936).

F2. A Study of the Narrow Resonance at 1430 Kev in the Reaction $C^{12}+H^2$.* J. C. HARRIS, T. W. BONNER, J. E. EVANS, AND G. C. PHILLIPS, *Rice Institute.*—The improved resolution of the Rice Institute pressure Van de Graaff machine has made possible a closer study of the half-width of the gamma-ray resonance in the reaction:

$$C^{12}+H^2\rightarrow{}^*N^{14}\rightarrow{}^*C^{13}+H^1-0.52 \text{ Mev.}^1$$

By the use of a Geiger counter surrounded by lead the half-width was found to be 8 kev for a carbon target 2 kev thick. The cross section at the peak of the resonance was calculated to be 0.08×10^{-24}, using a value of 2 percent as the efficiency of the counter for the 3-Mev radiation. Work is in progress to make sure there are no competing neutrons from the decay of this excited state in N^{14} according to the reaction: $C^{12}+H^2\rightarrow{}^*N^{14}\rightarrow N^{13}+n-0.28$ Mev.

* This work was supported by the Office of Naval Research.
[1] W. E. Bennett, T. W. Bonner, E. Hudspeth, H. T. Richards, and B. E. Watt, Phys. Rev. **59**, 781 (1941).

F3. A Study of the Distribution of Polonium on Thin Silver and Bismuth Films. FRED J. MORRIS AND ARTHUR E. LOCKENVITZ, *University of Texas.*—Thin films of silver and of bismuth were prepared by vaporization in a vacuum. Polonium was deposited on these films by chemical replacement from a solution of RaD with RaE and RaF. The distribution of the polonium on these films was studied by obtaining a pinhole camera photograph of the surfaces by means of the alpha-particles emitted by the polonium. Eastman fine-grain, alpha-particle plates were used. Microphotographs of these plates were made.

F4. Directional Correlation between Successive Beta- and Gamma-Emissions. D. L. FALKOFF AND G. E. UHLENBECK, *University of Michigan.*—The theory of the angular correlation between successive β- and γ-rays has been worked out. The method is analogous to that for $\gamma-\gamma$ angular correlation.* In contrast to the $\gamma-\gamma$ case, the $\beta-\gamma$ angular correlation depends not only on the angular momenta of the nuclear states but also on the upper energy of the β-spectrum, on the nuclear charge, and on the choice of the form of the β-interaction. For example, for a first forbidden scalar or Fermi β-transition followed by a dipole γ-ray, the angular correlation is of the form $1+C\cos^2\theta$, where for a $J-1, J, J$ transition

$$C=\frac{2J+3}{6J-1-10JB(W_0, Z)}.$$

For the scalar interaction and Z small $B=-4/3$ for $W_0 \gg 1$ and $B=(-16/33)$ (W_0-1) for $W_0-1 \ll 1$. For the vector interaction, assuming a relation between nuclear matrix elements, the corresponding values for B are 8/3 and $3/(W_0-1)$. The angular correlation will provide, therefore, a test for the β-interaction. There is no angular correlation for allowed β-transitions.

* D. Hamilton, Phys. Rev. 58, 122 (1940).

F5. Captura de Mesotrones Negativos por Protones. F. E. PRIETO CALDERON, *Universidad de Mexico.* (*Introduced by M. S. Vallarta.*)—Se estudian en este trabajo la posibilidad de que existan átomos de estructura análoga a la del hidrógeno, formados por un protón como núcleo y un mesotrón negativo, y las características de dicho átomo. Suponiendo que el camp de fuerzas entre el protón y el mesotrón es Coulombiano, se resuelve la ecuación de Schrödinger ye se encuentran las funciones de distribución angular y radial así como los valores permitidos de la-energía. Se encuentra que la frecuencia de las radiaciones emitidas es del órden de las de los rayos X.

F6. Electron Showers at 30,000-Foot Elevation.* PAUL E. LLOYD, R. RONALD RAU, CARL D. ANDERSON, AND RAYMOND V. ADAMS, *California Institute of Technology.*—Out of a series of cloud-chamber photographs taken in a B-29 airplane at 30,000-ft. elevation, 1172 have so far been analyzed with respect to the frequency of occurrence of single particles and of electron showers. The magnet cloud chamber is the same as that previously used on Pikes Peak (14,100-ft. elevation) and at Pasadena (800-ft. elevation), and thus a comparison may be made at the three elevations. The cloud chamber is 17 cm in diameter in a magnetic field of 7500 gausses, and is actuated by means of two Geiger counters, one above and one below the cloud chamber. Single tracks were found to occur per unit time 2.7 and 13.3 times as frequently at 14,100 ft. and 30,000 ft., respectively, as at 800-ft. elevation. Corresponding values for electron showers, classified as to size of shower, are given in the table.

No. of particles in shower		2–4	5–10	11–100
Frequency of occurrence per unit time relative to that at 800-ft. elevation	14,100 ft.	9	21	29
	30,000 ft.	85	200	210

* The research described in this abstract was supported in part by the Office of Naval Research.

F7. The Distribution in Energy of Cosmic-Ray Mesotrons and Protons at 30,000-Foot Elevation.* RAYMOND V. ADAMS, PAUL E. LLOYD, R. RONALD RAU, AND CARL D. ANDERSON, *California Institute of Technology.*—The momentum distribution of single cosmic-ray particles has been measured in a 17-cm cloud chamber in a 7500-gauss magnetic field at an altitude of 30,000 ft. The chamber was actuated by Geiger counters, one above and one below the chamber. Only single particles were measured in order to eliminate "shower" electrons. Of a total of 246 tracks measured, 40 could not have actuated both counters and are classified as random tracks, and 31 tracks had momenta greater than 1.5×10^7 gauss-cm and cannot be classified according to sign of charge. For the remaining 175 tracks, in the momentum range 1×10^6 to 1.5×10^7 gauss-cm, the ratio of positive to negative tracks is 2:1, which fact contrasts with the approximately equal numbers of positives and negatives found at sea level. The hypothesis that the excess of positive particles consists almost entirely of protons is supported by the large number of particles among the low energy tracks (including random tracks) which are recognizable as protons, and the fact that the spectrum of the excess positive particles has a sharp cut-off at the lower momentum end at 1.2×10^6 gauss-cm, which is the minimum momentum that a proton must have to penetrate to the bottom counter. Thus, while cosmic-ray protons are relatively scarce at sea level, at 30,000-ft. elevation they constitute about one-third of the single particles in the above momentum range.

* The research described in this abstract was supported in part by the Office of Naval Research.

F8. A Small Radial Cloud Chamber for High Altitude Operation.* R. B. LEIGHTON AND CARL D. ANDERSON, *California Institute of Technology.*—A cloud chamber 10 cm in diameter and 5 cm deep, arranged to compensate automatically for temperature changes over a 20°C range, has been built for operation at high altitudes in free balloon experiments. The cloud chamber, as yet without magnetic field or Geiger-counter control, is expanded regularly every 40 seconds. Power to operate the chamber and the camera is obtained from a small tank of liquid Freon. One 300-volt battery supplies power for the light source and the sweep field. Stereoscopic photographs are made on 35-mm film. The gross weight of the equipment is 20 lb. Out of a total of three flights in September, 120 track photographs were obtained at altitudes up to 80,000 feet above sea level, 55 being at the highest altitude. Numerous cases of electron showers and heavily ionizing particles were observed.

* The research described in this abstract was supported in part by the U. S. Navy.

F9. Photoelectric Effect in a Self-Quenching Geiger-Müller Counter.* M. V. SCHERB, *Bartol Research Foundation.* (*Introduced by W. F. G. Swann.*)—Geiger-Müller photon counters have had limited applications principally because their cathode surfaces have their spectral response in the 2000–3000A region.[1] A method has been discovered for treatment of a G-M photon counter which produces a marked change in the photoelectric properties of the cathode surface. By means of a discharge treatment at liquid-air temperatures of a G-M counter (copper cathode) filled with an argon-butane self-quenching mixture, the following effects have been noted: (1) The spectral response curve has been shifted to the longer wave-lengths—the peak response from 2250A to 3000A and the photoelectric threshold from approximately 2900–3000A to 3500A. (2) The relative increase in sensitivity at the peak response is a factor of at least 15. (3) No long-term fatigue of the photoelectric surface has been observed over a period of months. No changes in the normal properties of the Geiger-Müller counter such as background, useful life, starting voltage, pulse shape, and plateau characteristics have been observed

after treatment. Applications of such sensitized photon counters are being considered, and work is proceeding in the investigation of the phenomena for various gases and cathode surfaces.

* Supported by the Office of Naval Research.
[1] O. S. Duffendack and W. E. Morris, J. Opt. Soc. Am. 32, 8 (1942).

F10. The Effective Path Length through a Vertical Cosmic-Ray Telescope.* ENOS E. WITMER, *University of Pennsylvania*, AND MARTIN A. POMERANTZ, *Bartol Research Foundation*.—In cosmic-ray absorption experiments the separation between extreme counters has usually been taken as the distance traversed through the telescope. For a $\cos^2\theta$ distribution of intensity with zenith angle θ:

$$\frac{\bar{L}}{L}=\frac{\frac{3l}{L}\tan^{-1}\frac{l}{L}}{4\left[1+\left(\frac{l}{L}\right)^2\right]^{\frac{1}{2}}-\frac{2}{\left[1+\left(\frac{l}{L}\right)^2\right]^{\frac{1}{2}}}-2}, \qquad (1)$$

where $\bar{L}$ is the average path length of a cosmic-ray particle through the coincidence counter train, L is the separation between extreme counters, and l is the length of each counter tray. For an isotropic distribution

$$\bar{L}/L=\frac{\frac{l}{L}\tan^{-1}\frac{l}{L}-\frac{1}{2}\log\left[1+\left(\frac{l}{L}\right)^2\right]}{\left[1+\left(\frac{l}{L}\right)^2\right]^{\frac{1}{2}}-1}. \qquad (2)$$

In both cases, if $l/L\equiv u<0.9$,

$$\bar{L}=L\left\{1+\frac{1}{12}u^2-\frac{17}{360}u^4+\frac{25}{756}u^6-\cdots\right\}$$

gives a result accurate to within 1.0 percent. This is of particular significance in connection with Abstract F11.

* This work has been supported in part by the Office of Naval Research.

F11. The Properties of Cosmic-Rays at Very High Altitudes.* MARTIN A. POMERANTZ, *Bartol Research Foundation*.—A series of free balloon flights has provided data regarding the penetrating power of cosmic-ray particles up to altitudes appreciably exceeding those previously attained by balloon-borne equipment. As of October 11, fourteen flights have been conducted in this specific program, utilizing a standardized apparatus which transmits data by radio to the ground station. Several ascents have exceeded 100,000 feet, the remainder generally surpassing 90,000 feet. A confirmed altitude of 129,000 feet ($\sim$2 mm of Hg), establishing a new record for free balloons, was registered in one instance. Intensity *versus* altitude curves have been obtained with identical vertical quadruple coincidence-counter trains containing various thicknesses of Pb up to 7.5 cm, as well as 7.5 cm of C. Absorption curves for cosmic-ray particles at any altitude are thus available from the data. Among the salient features of the results are the following: 1. All of the intensity *versus* altitude curves converge at the top of the atmosphere. 2. The curves display a maximum with interposed absorber thicknesses up to 4 cm, but less than 6 cm of Pb. 3. Curves for the total radiation, and for that penetrating 7.5 cm of Pb, are in good accord with those obtained by others.[1]

* This work has been supported by the Office of Naval Research.
[1] G. Pfotzer, Zeits. f. Physik 102, 23 (1936); M. Schein, W. P. Jesse, and E. O. Wollan, Phys. Rev. 59, 615 (1941).

G1. On the Hypotheses Underlying Any Theory of Gravitation. ALBERTO BARAJAS, *Universidad de Mexico*. (*Introduced by M. S. Vallarta.*)—In this paper we discuss the general form of a theory of gravitation in which the principle of equivalence holds. The trajectories are shown to be paths. The additional conditions are established to obtain Newton's, Einstein's, and Birkhoff's theories of gravitation.

G2. Foundation of Birkhoff's Theory of Gravitation on Particle Mechanics. CARLOS GRAEF FERNANDEZ, *Universidad de Mexico*. (*Introduced by K. K. Darrow.*)—In this paper postulates are set up on which Birkhoff's theory of gravitation can be based. The reference frame used is Minkowski's space-time of Einstein's special relativity. The field is characterized by Birkhoff's gravitational tensor. The velocity of a gravitational perturbation in empty space is assumed to be that of light. The forces acting between particles, at rest in an inertial reference frame, are—supposed to be Newtonian. The field tensor due to a particle at rest is obtained from the postulates with the help of considerations of symmetry. The gravitational field of a particle moving with constant velocity follows therefrom by a Lorentz transformation. For an accelerated particle it is assumed that its field is instantaneously identical with that of a particle of equal rest mass at rest in the instantaneous rest system. The perfect fluid, which Birkhoff originally used to establish his theory, does not appear in the postulates; all conditions refer to fields due to particles. In close analogy with Newton's gravitational theory one can base Birkhoff's theory on particle mechanics.

G3. Motion of a Particle on the Axis of a Rotating Ring in Birkhoff's Theory of Gravitation. FERNANDO ALBA, *Universidad de Mexico*. (*Introduced by M. S. Vallarta.*)—By the use of the potentials given by Birkhoff's theory, the equation of motion of a particle on the axis of a rotating ring can be found. The relativistic mass of the ring is found to be

$$m=m_0\left(1-\frac{3}{2}\frac{v^2}{c^2}\right).$$

The first integral of the equation of motion offers no difficulties, while the second requires series expansions. In this way a good approximate solution is obtained for amplitudes of the motion which are small compared with the radius of the ring. The Newtonian solution of the problem leads to elliptic integrals of the first and third kinds. The solution of this problem in the new theory is the same as the Newtonian solution for small values of the velocity of the particle, as it should be.

G4. Model Solar Atmospheres. GUIDO MUNCH, *Universidad de Mexico*. (*Introduced by M. S. Vallarta.*)—In this paper the model solar atmospheres considered earlier by

Bengt Strömgren (Publikationer og mindre Meddelelser fra Kobenhavns Observatorium, Nr. 138, 1944) have been revised, using the recent determination of the continuous absorption coefficient of the negative ion of hydrogen by Chandrasekhar and Breen (Ap. J. 104, 429 (1946)). The mean absorption coefficients have been obtained in the manner pointed out by Chandrasekhar (Ap. J. 101, 238 (1945)) and with the temperature distribution of a gray atmosphere. The values of the opacity per gram, $\bar{\kappa}$, the total pressure, p, and the electron pressure, p_e, at a number of depths in the range $0.01 \leq q \leq 1.4$ are tabulated for the different values of the hydrogen-metal ratio considered. It is found that the values of p and p_e are systematically lower than those given by Strömgren, while the values of $\bar{\kappa}$ are higher by factors of the order of 1.2 for layers with $q \geq 0.02$. These departures of the parameters that determine the physical structure of a model atmosphere, from those evaluated by Strömgren, are most relevant for the layers on which the Fraunhofer lines arise. As a consequence, it might be important to use these new models when a rediscussion of the chemical composition of the solar atmosphere is undertaken.

G5. A Comparison of the Relative Molecular Stopping Power of $_1H^1$ and of $_1D^2$. ROLAND W. SCHMITT, T. N. HATFIELD, AND ARTHUR E. LOCKENVITZ, *University of Texas.*—The relative molecular stopping power of ordinary hydrogen was compared with that of deuterium, using the apparatus described by Colby and Hatfield.[1] Within the limits of experimental error the stopping power of these two gases is the same.

[1] M. Y. Colby and T. N. Hatfield, Rev. Sci. Inst. 12, 62 (1941).

G6. A Comparison of the Relative Molecular Stopping Power of Some Hydrocarbon Isomers for Alpha-Particles from Polonium. THOMAS E. GIBBS* AND ARTHUR E. LOCKENVITZ, *University of Texas.*—The hydrocarbon isomers, *N*-butane and isobutane, and butene-1, butene-2, and isobutene were used in this study. The specific ionization method, with the apparatus described by Colby and Hatfield,[1] was used for determining the extrapolated ionization range. The relative molecular stopping powers with respect to air at 760 mm and 15°C are:

N-butane	2.905±0.006
isobutane	2.907±0.006
butene-1	2.691±0.006
butene-2	2.690±0.006
isobutene	2.696±0.006

* Now at Louisiana Polytechnic Institute, Rustin, Louisiana.
[1] M. Y. Colby and T. N. Hatfield, Rev. Sci. Inst. 12, 62 (1941).

G7. The Measurement of the Relative Molecular Stopping Power of Gases for Polonium Alphas. T. N. HATFIELD AND M. Y. COLBY, *University of Texas.*—Measurements have been made of the relative molecular stopping power of some twelve gases, using the specific ionization method of Colby and Hatfield.[1] The additive law for atomic stopping powers is found to hold for all gases measured if the stopping powers of the constituents are known. The assumption that the law holds for the other gases measured makes it possible to calculate the relative atomic stopping power of sulfur, carbon, chlorine, and iodine.

[1] M. Y. Colby and T. N. Hatfield, Rev. Sci. Inst. 12, 62 (1941).

G8. Capture of Electrons by Ions. JULIAN K. KNIPP, *Iowa State College.*—The Oppenheimer-Brinkman-Kramers theory of the capture of electrons by alpha-particles in their passage through matter is reformulated in terms of a momentum representation of the electrons. A Thomas-Fermi treatment of the atoms with which the particles collide gives capture cross sections in air in good agreement, except for extreme values of the particle velocity, with cross sections calculated from a Hartree model. Capture into excited electronic states becomes of primary importance for heavy ions carrying a core of electrons. Total cross sections for such ions are estimated assuming hydrogen-like representations for the electron in the captured state and the Thomas-Fermi model for the atom from which capture takes place.

G9. An Electronic Intensity Regulator for a Hydrogen Discharge Tube. W. L. PONDROM AND W. W. ROBERTSON, *University of Texas.*—In absorption spectrophotometry there is considerable need for sources which are accurately constant in intensity and are of reasonably high intensity. However, such sources are difficult to obtain. Experience has shown that commercial regulators of the resonance transformer or saturated core-type are only moderately successful in keeping constant the intensity of a discharge tube. An electronic regulator has been devised in this laboratory to control the intensity of a 2.5-kva Hanovia hydrogen discharge tube used as a source of continuous radiation in the 2500–3000A spectral region. The output of a photo-cell placed at the rear window of the discharge tube controls the value of an impedance in series with the primary of the high voltage transformer in such a manner as to correct for variations in the intensity of the source. Imposed variations in line voltage of ±6 percent cause negligible variations in the intensity as determined spectrophotometrically and also in terms of the output of a photo-cell, the maximum change in the photo-cell current being less than 0.1 percent with the regulator working and about 20 percent without using the regulator.

G10. The Effect of O-Deuteration and Substitution on the Ultraviolet Absorption Spectrum of Phenol. W. W. ROBERTSON, F. A. MATSEN, AND A. J. SERIFF, *University of Texas.*—The substitution of deuterium for the hydrogen atom attached to oxygen in the phenol molecule results in spectroscopic changes that should be functions of the mass change alone, since the force constants and the symmetry of the molecule remain unchanged. The variation in mass affects the ground state and excited state vibrational frequencies and the location of the O—O band, the latter through unequal changes of the zero-point vibrational energies in the ground and excited state. O-deuteration decreases the frequency of the O—O band by 3 cm^{-1}. The vibrational frequencies are decreased on deuteration as expected, although the magnitudes seem anomalous. An

additional anomaly appears in the apparent splitting of the O+783 band of phenol into O+772 and O+789 cm^{-1} in deuterophenol. This splitting occurs also in combinations and indicates that the phenol band at O+563 cm^{-1} (6b in Wilson's notation) was incorrectly assigned as a fundamental and instead should be assigned as O+783−222. O-substitution of $VH_3C_2H_5$, C_3H_7, C_4H_9, or C_6H_5 produces, in addition to the mass effect described above, a modification of the electronic structure of the molecule by inductive and resonance effects. This modification will change the value of the force constants as well as the height of the excited state. The shift in the position of the O−O band appears to be in accord with the known electrical properties of the substituents.

G11. Raman Spectrum of Hexamethylethane. RICHARD W. MITCHELL* AND FORREST F. CLEVELAND,** *Lynchburg College.*—Raman frequencies, relative intensities, and depolarization factors are reported for solutions of hexamethylethane (2,2,3,3, tetramethylbutane) in CCl_4 and in benzine. The exciting frequencies used are those of the 4047A and 4358A lines of mercury. Raman frequencies are measured by comparison with an iron arc spectrum. Relative intensities and depolarization factors are obtained by use of a Gaertner microdensitometer. The technique employed for determining depolarization factors is that developed by Cleveland.[1] The Raman data indicate that the equilibrium configuration for hexamethylethane is D_{3D}. The selection rules for D_{3D}, D_{3H}, and C_{3V} are worked out and discussed.

* Now at A and W College of Texas.
** Now at Illinois Institute of Technology.
[1] Forrest F. Cleveland, J. Chem. Phys. 13, 101 (1945).

G12. Molecular Orbitals for Methane and Ethane. F. A. MATSEN, *University of Texas.*—Molecular orbitals are formed from wave functions described only by the identification of the atoms with which they are associated, valence electrons alone being considered. The irreducible representations are CH_4, T_d: $\Gamma(\psi)=2A_1+2T_1$; C_2H_6, D_{3h}: $\Gamma(\psi)=3A_1'+3A_2''+2E'+2E''$; and C_2H_6, D_{3d}: $\Gamma(\psi)=3A_{1g}+3A_{2u}+2E_g+2E_u$, which factor the eighth- and fourteenth-order secular equations into blocks of two and blocks of two and three, respectively. Certain approximations and expansions yield the energies of the states as sums of interaction integrals between the "atomic" wave functions and the squares of these integrals. The electron configurations for the ground state become CH_4: $(A_1)_1^2(T_1)_1^6$; C_2H_6, D_{3h}: $(A_1')_1^2(A_2'')_1^2(E')_1^4(E'')_1^4(A_1')_2^2$; and C_2H_6, D_{3d}: $(A_{1g})_1^2(A_{2u})_1^2(E_g)_1^4(E_u)_1^4(A_{1g})_2^2$. The ordering of the terms in the ground state cannot be completely justified, but there is no ambiguity in the classication of ground-state and excited-state terms. The rotational barrier and second-order hyperconjugation in ethane will be briefly discussed in terms of these calculations.

H1. X-Ray Determination of Thermal Expansion Coefficients of Crystals. M. Y. COLBY AND L. F. CONNELL, JR., *University of Texas.*—The extremely high resolution which can be obtained from high angle Bragg scattering has been used to measure linear thermal expansion coefficients for a number of substances. Several workers in this field have reported discrepancies between the lattice expansion coefficients as measured by x-ray diffraction and the macroscopic coefficients obtained for large single crystals of the same material; e.g., A. Gott[1] reported a 14 percent discrepancy for melt-grown potassium iodide in the range 20–200°C. Lattice expansion measurements on both melt- and solution-grown crystals of pure sodium chloride have been made in this laboratory in the range 20–300°C; a sensitive dilatometer for determination of the macroscopic expansion over the same range is under construction. The only values available at present for the macroscopic expansion of pure NaCl over a wide range are those of Eucken and Dannohl.[2] Their results for the range 20–300°C are 9 percent larger than the results of the lattice measurements made in this laboratory. This difference appears to support Gott's claim for a discrepancy between lattice and over-all expansion coefficients for alkali halides.

[1] A. Gott, Ann. d. Physik 41, 520 (1942).
[2] A. Eucken and W. Dannohl, Zeits. f. Elektrochemie 40, 814 (1934).

H2. Crystal Structure of Element 43, Technetium. R. C. L. MOONEY, *Argonne National Laboratory.*—The element of nuclear charge 43 may be prepared by deuteron bombardment of molybdenum, and the chemical properties of a sample prepared in this way were studied by C. Perrier and E. Segrè in 1937. The element is also formed by fission. A sample containing the long-lived isotope was kindly prepared for us by Dr. G. W. Parker of the Clinton Laboratory in order to study the crystal structure of the compounds by x-ray analysis. Dr. Sherman Fried prepared several samples in microgram amounts, and one of these proved to be the element itself. The fact that the sample was metallic technetium was shown conclusively by the characteristics of the x-ray pattern itself. Like rhenium, osmium, ruthenium, and a number of other elements, technetium was found to crystallize in the hexagonal close-packed arrangement. The cell, which contains two atoms, has the following dimensions: $a=2.738\pm0.003$A and $c=4.393\pm0.006$A. Each atom has twelve neighbors, six at 2.706A and six at 2.738A. The density, assuming the atomic weight to be 99, is calculated to be 11.46.

H3. Small-Angle Diffraction in Lattices. OTTO HALPERN, *University of Southern California.*—The diffraction of light and material waves under angles which lie close to the direction of the incident beam has been investigated under various assumptions. It can be shown that the effects are independent of the exact angle of incidence but are strongly influenced by the specific nature of the imperfections of the lattice; in both respects the presently studied phenomena differ qualitatively from the diffraction into Laue spots of order larger than zero. The diffraction by a small ideal crystal (extinction neglected) under small angles has an integral cross section proportional to $N^{4/3}$ (N total number of atoms in the ideal microcrystal). An analogous result is obtained in the treatment of a "gas" composed of independent ideal microcrystals if the average

distance between them is comparable with their linear dimensions. In the commonly encountered case of polycrystalline material, on the other hand, the result is radically changed because here the lattice errors are usually of the order of magnitude of the lattice constant; therefore the contributions of neighboring microcrystals to the scattering under small angles possess a large amount of coherence. Experiments, particularly those on electron diffraction by Kikuchi, will be discussed from the point of view here presented.

H4. Propagation of Waves of Finite Amplitude. ANTONIO ROMERO JUAREZ, *Universidad de Mexico.* (*Introduced by M. S. Vallarta.*)—The problem of the propagation of a sound wave is generally solved under the assumption that the amplitude of the wave is infinitely small. Under this assumption the theory of sound is developed. In the present paper some results are given concerning the study of the propagation of a plane wave whose amplitude cannot be considered infinitely small. The medium is assumed to be a gas, and a relation is derived between the velocity of a particle of the medium and the pressure. Both the isothermal and adiabatic cases are considered. A relation is also obtained giving the velocity of the wave at every point in terms of the pressure of the medium at that point.

H5. Ultrasonic Absorption in Water as a Function of Temperature.* MYRON C. SMITH AND ROBERT T. BEYER, *Brown University.*—The absorption of ultrasonic radiation in water has been measured as a function of temperature in the range 0° to 80°C at three frequencies. The balance method of observing the radiation pressure was employed.[1,2] For temperatures above room temperature the measuring tank was placed in an insulated box containing a heating coil, while at values below room temperature a refrigerating unit was employed, with the expansion coil soldered to the outside of the tank. The results are accurate to 10 percent. Measurements are reported at 16.0, 22.5, and 27.3 megacycles. The values of $2\alpha/\nu^2\times10^{17}$ vary from 140 at 0°C to 15 at 80°C. Comparison is made with the theoretical values predicted by Hall[3] on the basis of a lag in the rearrangement of the molecules during a compression, and a rather close agreement is shown.

* The research reported in this abstract was supported in part by the Office of Naval Research.
[1] E. Hsu, J. Acous. Soc. Am. **17**, 127 (1945).
[2] R. T. Beyer and M. C. Smith, J. Acous. Soc. Am. **18**, 424 (1946).
[3] L. Hall, Phys. Rev. **71**, 318 (1947); **72**, 537 (1947).

H6. The Form of the Seismic Disturbance Due to an Explosion. NORMAN RICKER, *Carter Oil Company.*—It has been shown in previous researches that a sudden explosion in a homogeneous and isotropic earth gives rise to a disturbance of a characteristic form, shaped by the earth's absorption, and which has been designated as a *seismic wavelet.* At relatively large distances from the explosion this form has been investigated, and the laws of propagation of the wavelet have been determined theoretically and checked experimentally in work previously published. At these large distances the spectrum of this wavelet lies in a low frequency range where there is no appreciable dispersion, and the wavelet assumes a symmetrical form. Near the explosion, however, the high frequency components of the shot pulse, which have not yet been filtered out by the earth's absorption, introduce an assymmetry to the wavelet form resulting from dispersion among these high frequency components. In the present paper, calculated wavelet forms are given for the displacement and velocity for unit numerical distance.

H7. The Balancing of Sedimentation by Electrophoresis in the Ultracentrifuge. M. L. RANDOLPH, *University of Virginia.** (*Introduced by J. W. Beams.*)—The method of balancing sedimentation in an ultracentrifuge by electrophoresis[1] has been extended and improved. The standard analytical centrifuge cell is adapted as a combination sedimentation and electrophoresis cell. The cell contains two side chambers, each filled with a saline solution in contact with a silver-coated electrode. These side chambers communicate directly with the test solution in the sector-shaped observation cell at its surfaces nearest the axis and periphery, respectively. The test solution is not at the isoelectric point. Thin Lucite partitions, containing many fine holes and covered with thin filter paper, separate the saline and test solutions. This avoids unnecessary mixing and prevents contamination of the test solution by the electrode products. The electrical current passes radially through the spinning sector-shaped observation cell in such a direction that the electrophoresis balances the sedimentation at one radial distance. This arrangement makes possible the separation and study of different molecular species whose mass or charge differ by very small amounts. Also, the homogeneity of various substances can be studied. The results obtained with human hemoglobin will be described.

* National Research Council Predoctoral Fellow at Virginia. Now at Tulane University.
[1] J. W. Beams, *Science in Progress, Second Series* (Yale University Press, New Haven, 1940), p. 258; Phys. Rev. **69**, 546 (1946).

H8. The A.C. Magneto-Resistance of Bismuth. ROBERT F. BLUNT, *Rice Institute.*—Measurements of the magneto-resistance of Bi in a constant magnetic field of 5000 oersteds were made using alternating currents with frequencies up to 3.5 megacycles. No decrease in magneto-resistance was observed as the frequency was increased, and in all cases it was nearly the same as that found with direct current. In the near infra-red it has been shown[1] that the magneto-resistance of Bi probably does not exist, and this experiment constitutes an attempt to find the frequency at which the magneto-resistance either disappears or begins to decrease. The experiment shows that up to 3.5 megacycles the magneto-resistance is normal. A possible reason for the disappearance in the infra-red is that magneto-resistance does not exist on the surface of a conductor. Thus a decrease should be observed when the skin effect becomes sufficiently pronounced. It is planned to make measurements at higher radio frequencies and also perhaps in the far infra-red to determine at what frequency and in what manner the observed magneto-resistance disappears.

[1] C. W. Heaps, Phys. Rev. **27**, 764 (1926). J. C. McLennan, Phil. Mag. **14**, 508 (1932).

H9. Temperature Coefficient of Resistance of Sodium-Ammonia Solutions. ANGUS PEARSON, *Rice Institute.**—The temperature coefficient of resistance of solutions of sodium in liquid ammonia has been measured for various concentrations. The resistance was determined by comparing with a cathode-ray oscilloscope the 500-cycle voltage across a conductivity cell with the voltage across a standard resistance. The concentration of the solution was determined by a titration method. In the region where two liquid phases coexist, the resistance variation as a function of the temperature depends in part on the change with temperature in the composition of the phase being investigated, according to

$$dR/dT=\partial R/\partial T+(\partial R/\partial C)(dC/dT),$$

where R, T, C represent, respectively, resistance, temperature, and concentration. When only one phase is present the second term is zero. It was found that dR/dT was always negative, and its magnitude increased as the temperature decreased.

* This research was financed through a fellowship granted by the Socony-Vacuum Oil Company, Inc.

Supplementary Programme

SP1. The 72-Day Isomer of Titanium (51).* C. E. MANDEVILLE AND MORRIS V. SCHERB, *Bartol Research Foundation.*—Chemically pure TiO_2, irradiated by neutrons in the Clinton pile, was separated into phosphorus, iron, calcium, scandium, and titanium. A weak activity of long half-period was found in the titanium fraction. The half-period of this activity was given as 72 days by Walke *et al.*[1] The end point of the beta-ray spectrum was found to be 0.09 g/cm² as measured by absorption in aluminum, and the maximum gamma-ray energy was found to be 1.02 Mev by coincidence absorption. These values agree well with those reported by Walke *et al.* The beta-gamma coincidence rate was 0.9×10^{-3} coincidence per beta-particle, and was independent of the beta-ray energy, suggesting that the beta-ray spectrum of titanium (51) is simple. A gamma-gamma-coincidence rate of $(0.35\pm0.03)\times10^{-3}$ coincidence per gamma-ray was also observed. Some or all of the excited vanadium (51) residual nuclei then proceed to the ground state with the emission of two gamma-rays in cascade.[2]

* To be called after Session E if time permits.
[1] Walke, Williams, and Evans, Proc. Roy. Soc. **A171**, 360 (1939).
[2] Work supported by the Office of Naval Research.

SP2. The Scattering of Particles by an Attractive Center of Force Varying Inversely as the Cube of the Distance.* H. A. WILSON, *Rice Institute.*—This paper gives a solution of the problem in question which appears to be satisfactory. The usual expression for the asymptotic value of Bessel's function is shown to hold for complex values of the order. The scattering cross section is equal to

$$(\pi/k^2)\sum_{n=0}^{n=\infty}(2n+1)(e^{\pi a_n}+1),$$

where $k=2\pi/\lambda$, λ = de Broglie wave-length of incident particles, $\alpha_n=(4\beta-(2n+1)^2)^{\frac{1}{2}}$, $\beta=8\pi^2my/h^2$, and $-y/r^2$ = potential energy of a particle at distance r from the attracting center.

* To be called after Session E if time permits.

SP3. A Spherical Shell Nuclear Model.* H. A. WILSON, *Rice Institute.*—Experimental results appear to show that many atomic nuclei have a set of nearly equally spaced energy levels with spacings of 0.387 Mev. The liquid drop model does not seem to offer any explanation of these levels. A model consisting of a hollow spherical shell is proposed, and it is shown that such a shell has a series of nearly equally spaced levels with spacings given by a function,[1] with no arbitrary constants, of the atomic number, the mass number, the radius, Planck's constant, and the mass of a nucleon. With spacings 0.387 Mev, this formula gives values of the radii of all nuclei agreeing nearly with those found by other methods. The energy of the shell model is discussed, and the shell is shown to be stable for uniform radial displacements. The root mean square amplitude of radial vibration of the shell caused by the ground-state vibrational energy is found to be about 7/10 of the mean distance between adjacent nucleons in the shell.

* To be called after Session E if time permits.
[1] H. A. Wilson, Phys. Rev. **69**, 538 (1946).

To Be Read by Title

T1. The Second Law of Thermodynamics from the Standpoint of the Equation of State. J. L. FINCK, *J. L. Finck Laboratories.*—In this paper the concepts "equilibrium" and "reversibility" are examined from the standpoint of the number of independent variables which define a thermodynamic system. The endeavor is made to show that the number of independent variables which are selected is crucial to the basic concepts as well as to the second law of thermodynamics. If this number is less than the minimum required to define the system completely, the equation of state for the internal energy will be incomplete. It is our practice to employ incomplete equations of state, and this results in processes which we consider to be irreversible. The Kelvin-Planck and Clausius principles are shown to be somewhat related to the first law of thermodynamics, and their validity arises from the fact that the equations of state which are used are incomplete. If these equations were complete, i.e., if the number of independent variables were not less than the minimum required to describe the system completely, we would have complete conversion of heat into work, as well as work into heat. The difficulties in realizing complete equations are considered. The entropy concept is considered in detail and it is shown that there are serious limitations in its application.

T2. The 54-Minute Isomer of Indium (116).* MORRIS V. SCHERB AND C. E. MANDEVILLE, *Bartol Research Foundation.*—The fifty-four minute activity was induced in indium when a strip of indium metal of thickness 0.018 cm was irradiated by slow neutrons from a radium-

beryllium source of strength 600 mc. The beta-gamma and gamma-gamma coincidence rates were reinvestigated.[1] In observing beta-gamma coincidences, corrections were made for cosmic-ray background, gamma-gamma coincidences, accidentals, and gamma-ray counts in the beta-ray counter. The decay of the source and its effect on the various corrections was taken into account. The beta-gamma coincidence rate was found to be 1.3×10^{-3} coincidence per beta-ray and was independent of the beta-ray energy. This suggests that the beta-ray spectrum is simple. No genuine beta-gamma coincidences were observed for beta-ray energies greater than 0.7 Mev by Feather's more recent equation. The gamma-gamma coincidence rate was $(0.9\pm0.1)\times10^{-3}$ coincidence per gamma-ray recorded in the gamma-ray counter. The coincidence rates suggest that three gamma-rays are emitted per beta-particle in cascade.

* Supported by the Office of Naval Research.
[1] Langer, Mitchell, and McDaniel, Phys. Rev. **56**, 380 (1939).

T3. Properties of Radioactive Tantalum (182).* C. E. MANDEVILLE AND MORRIS V. SCHERB, *Bartol Research Foundation.*—The 100-day activity was induced in tantalum irradiated by slow neutrons in the Clinton pile. Separations were performed to remove phosphorous, calcium, potassium, tungsten, and hafnium as possible contaminants. The beta-rays had an absorption limit of 0.112 g/cm² in aluminum, corresponding to an energy of 0.36 Mev. The maximum gamma-ray energy was found to be 1.16 ± 0.1 Mev by coincidence absorption. No hard beta-rays were observed.[1] The beta-gamma-coincidence rate was 0.93×10^{-3} coincidence per beta-ray, independent of the beta-ray energy. This is consistent with the view that only one beta-ray spectrum is present. The gamma-gamma-coincidence rate was $(0.27\pm0.03)\times10^{-3}$ coincidence per gamma-ray. A comparison of these coincidence rates with those of Sc^{46}, using the same counters and geometry, suggests it to be unlikely that the two high energy gamma-rays of comparable intensity[2] are in cascade.

* Supported by the Office of Naval Research.
[1] Zumstein, Kurbatov, and Pool, Phys. Rev. **63**, 59 (1943).
[2] Rall and Wilkinson, Phys. Rev. **71**, 321 (1947).

T4. The Beta-Rays of Antimony (122).* C. E. MANDEVILLE AND MORRIS V. SCHERB, *Bartol Research Foundation.*—The 2.8-day activity was induced in metallic antimony, irradiated by slow neutrons for about two hours in the Clinton pile. The short exposure time suppressed the 60-day period. Measurements were begun about 20 hours after removal from the pile. The genuine beta-gamma coincidence rate was observed to decrease from an extrapolated value of 0.19×10^{-3} coincidence per beta-ray at zero absorber thickness to zero at 0.487 g/cm² of aluminum. The inner beta-ray group then has an end point at 1.19 Mev by Feather's equation. This group is coupled with gamma-radiation. The beta-ray distribution of higher energy, which leads to the ground state of the residual nucleus, has an absorption limit at 0.806 g/cm² in aluminum, 1.77 Mev by Feather's equation. The energy difference suggests a gamma-ray energy of 0.58 Mev. This value agrees with 0.57 Mev obtained by the thin magnetic lens.[1] The earlier estimate[2] of 0.80 Mev from semicircular focusing is obviously too high.

* Supported by the Office of Naval Research.
[1] Rall and Wilkinson, Phys. Rev. **71**, 321 (1947).
[2] Mandeville and Fulbright, Phys. Rev. **64**, 265 (1943).

T5. Minimization of Some Effects of Scattering in Experimental Determinations of XR for High Energy Particles. F. T. ROGERS, JR., *University of North Carolina.*—This note is in extension of an earlier one[1] upon the same general subject. Its object is to point out that in some instances, and within certain limitations, the configuration of the electrostatic field used in an experimental apparatus may lead to *XR*-determinations in which the subject scattering[1] produces only relatively small disturbing effects. Thus, for example, the cylindrical-electrode electrostatic analyzer has focusing properties[2] which may be used to minimize the effects of thin-window scattering: if the thin window be used as an "object" and if the particle detection be done in the corresponding "image" surface, then the lens-like focusing properties of the field may render the subject scattering unobservable and hence largely insignificant. In the instance of this particular field, however, the focusing properties are, to judge from the literature,[3] still incompletely understood for particles of higher relativistic speeds, although calculations now under way[4] may be expected to clarify them somewhat.

[1] F. T. Rogers, Jr., Phys. Rev. **71**, 833 (1947).
[2] A. J. Dempster, Phys. Rev. **51**, 67 (1937); R. Herzog, Ann. d. Physik **33**, 89 (1938).
[3] F. T. Rogers, Jr. and C. W. Horton, Rev. Sci. Inst. **14**, 216 (1943); Phys. Rev. **69**, 537 (1946).
[4] The author is indebted to Dr. Nathan Rosen for having pointed out valuable approaches to these calculations.

T6. Studies in the Progress of Ductile Fracture in a Notched Steel Bar.* MARGUERITE M. ROGERS AND PAUL E. SHEARIN, *University of North Carolina.*—In order to study the physical behavior of mild steel under conditions causing plastic flow (or brittle failure, if such failure occurs) a technique has been devised whereby the fracture area of a slow-bend test specimen is stained distinguishing colors at successive stages of crack propagation on a given specimen. In this way the crack contour can be ascertained progressively, and for the work involved in the propagation of the crack a given distance can be calculated. Bend specimens both with single notches and with four 15 percent Izod notches have been used. The latter specimen is designed to give a crack, the advancing head of which remains parallel to the rootline of the initiating notch.[1,2] The crack depth has, therefore, an accurately determinable value which can be correlated with many quantities, such as: (1) accumulated work, (2) stored elastic energy, (3) work associated with fracturing unit cross-sectional area, (4) temperature. In an effort to perceive something of the fundamental physical nature of brittle failure, it is desired to compare the relationship between these variables for those specimens which went brittle during the test and those specimens which remained ductile.

* Work supported by Office of Naval Research.
[1] C. Zener and J. H. Holloman, J. App. Phys. **17**, 69 (1946).
[2] P. E. Shearin, Phys. Rev. **71**, 832 (1947).

T7. On the Acceleration of Electrons by Cylindrical Cavities in TM_{01n} Modes. B. L. MILLER AND J. M. WOLF, *Bartol Research Foundation.**—For the acceleration of electrons moving at nearly light speed, the possibility of obtaining the effect of a number of cavities in series by using a single cavity in a TM_{01n} mode was considered. The length is limited by the fact that the electrons must emerge from the cavity before falling too far out of phase with the accelerating wave, the speed of which is greater than c. For a given available power at a definite frequency, the values of n and r are determined for which the electrons gain maximum energy in passing through the axial electric field. The energy gained, ΔE, is

$$\Delta E = 2.9[r/(1+r)]^{\frac{1}{2}} \sin\{\tfrac{1}{2}n\pi[[1+(4.81/n\pi r)^2]^{\frac{1}{2}}-1]\}$$

in Mev per megawatt at 2800 megacycles. The maximum value of ΔE occurs for n equal to one (and $r=0.9$) so that there is no advantage in using a cavity of length greater than one-half guide wave-length in this mode. ΔE_{max} is 2 Mev.

* Work supported by the Office of Naval Research.

Author Index to Abstracts of Papers Presented at the Stanford Meeting

Adams, Raymond V., Paul E. Lloyd, R. Ronald Rau, and Carl D. Anderson—No. F7
Alba, Fernando—No. G3
Barajas, Alberto—No. G1
Blunt, Robert F.—No. H8
Brown, S. Leroy—No. A4
Cerrillo, Manuel—No. A6
Colby, M. Y. and L. F. Connell, Jr.—No. H1
Conklin, Richard L. and William Ogle—No. E7
Curtis, B. R., Louis Rosen, and J. L. Fowler—No. E8
Evans, J. E. and T. W. Bonner—No. F1
Fay, C. H.—No. A7
Falkoff, D. L. and G. E. Uhlenbeck—No. F4
Fernandez, Carlos Graef—No. G2
Finck, J. L.—No. T1
Foulks, Mary Gowen—No. A3
Gibbs, Thomas E. and Arthur E. Lockenvitz—No. G6
Halpern, Otto—No. H3
Harris, J. C., T. W. Bonner, J. E. Evans, and G. C. Phillips—No. F2
Hatfield, T. N. and M. Y. Colby—No. G7
Horton, C. W.—No. A5
Hughes, D. S., W. L. Pondrom, and G. B. Thurston—No. A8
Juarez, Antonio Romero—No. H4
Knipp, Julian K.—No. G8
Laughlin, J. S. and P. G. Kruger—No. E9
Leighton, R. B. and Carl D. Anderson—No. F8
Lloyd, Paul E., R. Ronald Rau, Carl D. Anderson, and Raymond V. Adams—No. F6
Malich, C. W. and J. R. Risser—No. E6
Mandeville, C. E. and Morris V. Scherb—No. E4, No. SP1, No. T3, No. T4
Matsen, F. A.—No. G12
Miller, B. L. and J. M. Wolf—No. T7
Mitchell, Richard W. and Forrest F. Cleveland—No. G11
Mooney, R. C. L.—No. H2
Morris, Fred J. and Arthur E. Lochenvitz—No. F3
Munch, Guido—No. G4
Packard, Robert G. and S. Leroy Brown—No. A2
Pearson, Angus—No. H9
Phillips, G. C. and J. C. Harris—No. E10
Pomerantz, Martin A.—No. F11
Pondrom, W. L. and W. W. Robertson—No. G9
Prieto Calderon, F. E.—No. F5
Randolph, M. L.—No. H7
Ricker, Norman—No. H6
Robertson, W. W., R. A. Matsen, and A. J. Seriff—No. G10
Rogers, F. T., Jr.—No. T5
Rogers, Marguerite M. and Paul E. Shearin—No. T6
Scherb, Morris V.—No. F9
Scherb, Morris V. and C. E. Mandeville—No. T2
Schmitt, Roland W., T. N. Hatfield, and Arthur E. Lockenvitz—No. G5
Sharp, James M. and S. Leroy Brown—No. A1
Smith, Myron C. and Robert T. Beyer—No. H5
Swann, C. P., W. J. Scott, E. L. Hudspeth, and C. E. Mandeville—No. E5
Terrell, Nelson James, Jr.—No. E2
Whaling, Ward and J. E. Evans—No. E3
Wilson, H. A.—No. E1, No. SP2, No. SP3
Witmer, Enos E. and Martin A. Pomerantz—No. F10